PALLADIUM, PLATINUM AND GOLD COMPLEXES: A SYNTHETIC APPROACH TOWARDS THE DISCOVERY OF ANTICANCER AGENTS

FRANKLINE KIPLANGAT KETER

Thesis

submitted in fulfillment of the requirements for the degree

Philosophiae Doctor

in

Chemistry

in the

Faculty of Science

at the

University of Johannesburg

Supervisor: Professor James Darkwa

Co-Supervisor: Professor D. Jasper G. Rees

January 2008

ABSTRACT

Ligands bis(pyrazolyl)acetic acid (**L1**) and bis(3,5-dimethylpyrazolyl)acetic acid (**L2**) were synthesised by reacting pyrazoles and dibromoacetic acid under phase transfer conditions, by using benzyltriethylammonium chloride as the catalyst. Ligands **L1** and **L2** were characterised by a combination of ^{1}H, $^{13}C\{^{1}H\}$ NMR, IR spectroscopy and microanalysis. Esterification of **L1** and **L2** led to formation of bis(pyrazolyl)ethyl acetate (**L3**) and bis(3,5-dimethylpyrazolyl)ethyl acetate (**L4**). Ligands **L3** and **L4** were also characterised by a combination of ^{1}H, $^{13}C\{^{1}H\}$ NMR, IR spectroscopy and microanalysis.

Subsequently, new pyrazolyl palladium(II) and platinum(II) compounds, $[PdCl_2(\mathbf{L1})]$ (**1**), $[PdCl_2(\mathbf{L2})]$ (**2**), $[PtCl_2(\mathbf{L1})]$ (**3a**) and $[PtCl_2(\mathbf{L2})]$ (**4**) were prepared by reacting bis(pyrazolyl)acetic acid ligands (**L1**-**L2**) with $K_2[PdCl_4]$ or $K_2[PtCl_4]$ respectively. The structures of complex **1** and **2** reveal distorted square planar geometries. The bond angles of N-Pd-N, N-Pd-Cl, N-Pd-Cl, for **1** and **2** are between 85.8(3)^{o} and 90.81(4)^{o}). The platinum compound, $K_2[Pt_4Cl_8(\mathbf{L1})_2(\text{deprotonated-}\mathbf{L1})_2].2H_2O$ (**3b**), crystallised from aqueous solutions containing **3a** when such solutions were left to stand overnight. Each platinum coordination environment consists of two *cis*-Cl ligands and one κ^2-N^N$_{(\mathbf{L1})}$ unit (**L1** = bis(pyrazolyl)acetic acid), with two ligand moieties in **3b** that are deprotonated with two K^+ counter ions.

Reaction of bis(pyrazolyl)acetic acid ligands (**L1**-**L2**) with $[HAuCl_4].4H_2O$ gave gold(III) complexes $[AuCl_2(\mathbf{L1})]Cl$ (**5a**) and $[AuCl_2(\mathbf{L2})]Cl$ (**6a**). The spectroscopic, mass spectroscopy and microanalysis data were used to confirm the formation of the desired

complexes. However, attempts to crystallise **5a** and **6a** led to formation of $[AuCl_2(pz)(pzH)]$ (**5b**) and $[AuCl_2(3,5\text{-}Me_2pz)(3,5\text{-}Me_2pzH)]$ (**6b**). This was confirmed by the structural characterisation of **5b**, which has a distorted square-planar geometry.

When complexes **1-6a** were screened for their anti-tumour activity against CHO-22 cells, they showed no appreciable biological activities against CHO-22 cells. Substitution reactions of complexes **1-6a** with L-cysteine performed to probe any relationship between the observed antitumour activities and the rates of ligand substitution of these complexes were inconclusive.

Dithiocarbamate ligands **L5-L8** were synthesised as potassium salts by introducing a CS_2 group in positions 1 of pyrazole, 3,5-dimethylpyrazole, indazole and imidazole. The reaction of **L5-L8** with $[AuCl(PPh_3)]$, $[Au_2Cl_2(dppe)]$, $[Au_2Cl_2(dppp)]$ and $[Au_2Cl_2(dpph)]$, led to isolation of complexes $[Au(\mathbf{L})(PPh_3)]$ (**13-16**), $[Au_2(\mathbf{L})_2(dppe)]$ (**17a-19**), $[Au_2(\mathbf{L})_2(dppp)]$ (**20-22**) and $[Au_2(\mathbf{L})_2(dpph)]$ (**23-25**) (dppe = bis(diphenylphosphino)ethane, dppp = bis(diphenylphosphino)propane, dpph = bis(diphenylphosphino)hexane; **L** = anions of **L5-L8**). The mononuclear molecular structure of **15** features a near linear geometry with a P(1)-Au(1)-S(1) angle of 175.36(2) ^{o}. The binuclear gold(I) complexes **20-22** and **23-25** have two P-Au-S moieties as evident in the solid state structure of **25**. Attempts to crystallise complex **17a** led to the formation of a gold(I) cluster complex $[Au_{18}S_8(dppe)_6]^{2+}$ (**17b**) as confirmed by X-ray crystallography. Cluster **17b** features weak Au···Au interactions (2.9263(7)-3.1395(7) Å).

Complexes **13-16** and **20-25** were tested *in vitro* for anticancer activity on HeLa cells. The activities of gold(I) complexes **13-16** were comparable to that of cisplatin. Dinuclear gold(I) complexes **20-25** also showed appreciable antitumour activity against HeLa cells. However, the dpph gold(I) compounds (**23-25**) were highly active, with **24** showing the highest activity against HeLa cells (IC_{50} = 0.1 μM). The tumour specificity (TS) factors for **23** and **24** were 31.0 and 70.5, respectively.

Excitation measurements of solids and solutions of **13**, **14**, **15**, **17a** and **17b** at room temperature showed weak yellow emissions, whereas **16** showed a light blue emission. Neither solids nor solution of **15** at 77 K luminescenced, but UV-Vis irradiation of complexes **13**, **14**, **16**, **17a** and **17b** at 250-800 nm gave weak visible photoluminescence.

Reaction of ligands **L5-L7** with $K_2[PtCl_4]$ formed bis-chelated complexes $[Pt(\mathbf{L})_2]$ (**31-33**) (**L** = anions of **L5-L7**) with three sulfur and one nitrogen atoms coordinated to the platinum, leaving one uncoordinated sulfur. But when the same ligands were reacted with $[PtCl_2(dppe)]$, complexes of general formula $[Pt(\mathbf{L})_2(dppe)]$ (**26, 28** and **29**) were obtained. The yellow $[Pt(\mathbf{L})_2(dppe)]$ complexes were found to be unstable in solution and transformed to identical green product, $[Pt(S_2CO)(dppe)]$ (**27**). The structure of complex **27** was confirmed by X-ray crystallography.

Ligands **L5-L7** readily oxidises to new bis(dithiocarbamato)disulfide ligands (**L9-L11**). The solid state structures of **L9** and **L10** indicate that the pyrazole rings are connected *via* N(I) and N(1A) by a disulfide bridge and are in perpendicular planes. Whereas ligands

L5-L8 and **L11** showed no inhibition against growth of HeLa cells, **L9** and **L10** showed some activity, with **L9** being the most active (IC_{50} = 3.6 μM, TS = 9.6). Ligands **L9-L11** formed unstable products when reacted with [AuCl(tht)], but gave mixed products when reacted with $[(Ph_3P)Au]^+$ salts.

DECLARATION

I declare that the work "*Palladium, platinum and gold complexes: a synthetic approach towards the discovery of anti-cancer agents*" is my own work, that it has not been submitted for any degree or examination in any other university, and that all the sources I have used or quoted have been indicated and acknowledged by complete references.

FRANKLINE KIPLANGAT KETER

…….. ……

Signature Date

ACKNOWLEDGEMENTS

I wish to express my sincere gratitudes to my principal supervisor Professor James Darkwa for his invaluable support through the period of my PhD studies. I would also wish to acknowledge my co-supervisor Professor Jasper Rees (University of the Western Cape) for his help and advice. I should not forget to thank Dr. Werner (University of Johannesburg) and Dr. Oyetunji (University of Botswana) for all the fruitful discussion we had. Many thanks go to Mrs. Nell of Pharmacology department, Pretoria University, South Africa and Mr. Khanyanda of department of Biotechnology, University of the Western Cape for some assistance in biochemical assays. I would also like to thank Dr. Guzei, Mrs. Spencer of Wisconsin University USA, and Dr. Omondi of University of Johannesburg, South Africa, for having helped in solving the crystal structures reported herein. I would also like to thank Prof. Mohamed and Ms. Sumitra of University of North Texas, USA, for their assistance in acquiring luminescence data. Individual contributions of these people are further acknowledged at the beginning of the respective chapters.

I also take this opportunity to thank the Chemistry department and the University of Johannesburg as a whole for giving an opportunity to pursue my doctoral studies. Many thanks go to Organometallic chemistry research group for the group meetings that were stimulating and informative. I would also like to acknowledge Mintek for the prestigious bursary awarded to me. Finally I would like to sincerely thank my family for their invariable support through the entire period. Thank you for believing in me. This was all possible because of the almighty GOD, and I thank him for his guidance and protection.

DEDICATION

This work is dedicated to my family

LIST OF FIGURES

LIST OF TABLES

ABBREVIATIONS

NMR	Nuclear magnetic resonance
IR	Infra red
ESI-MS	Electrospray ionisation mass spectrometry
UV-Vis	Ultra violet-visible
CHO	Chinese hamster ovary
HeLa	Human cervix epitheloid carcinoma
PBS	Phosphate buffer saline
MTT	3-(4,5-dimethylthiazol-2yl)-2,5-diphenyltetrazolium bromide
MOMP	Mitochondrial outer membrane permeabilisation
Cisplatin	*cis*-dichlorodiammineplatinum(II)
LMCT	Ligand metal charge transfer
ca.	Approximately
DNA	Deoxyribonucleic acid
IC_{50}	Concentration of compound needed to inhibit cell growth by 50% against a single cell line.
TS	Tumour specificity
Nu	Nucleophile
bpza	Bis(pyrazolyl)acetic acid
dtc	Dithiocarbamate
dppe	Bis(diphenylphosphino)ethane
dppp	Bis(diphenylphosphino)propane
dpph	Bis(diphenylphosphino)hexane

Preface

Cancer is one of the diseases that contribute to the overall mortality rate globally and thus has prompted continuous research to develop drugs to curb it. The development of modern medicinal inorganic chemistry, stimulated by the serendipitous discovery of cisplatin, has been facilitated by the inorganic chemist's extensive knowledge of the coordination and redox properties of metal ions. Metal centres being positively charged, are favoured to bind to the negatively charged biomolecules in particular proteins and nucleic acids, which have negative charges. Such interactions could also provide a mechanistic understanding of how the activities of these metal complexes are reduced and is crucial to the rational design of new compounds.

Cisplatin remains the drug of choice for the treatment of testicular, ovarian, bladder, head and neck, lung and cervical cancers. The remarkable success of cisplatin is marred somewhat by several major drawbacks including toxicity, inactivity against certain cancers and resistance. Despite these shortcomings, approximately 50% of all anticancer therapies are platinum-based. Nevertheless, the search for cisplatin analogues with exceptional features remains the subject of intense investigation. Palladium(II) and gold(III) complexes, which are isostructural and isoelectronic with platinum(II) complexes, are also potentially attractive as anticancer agents.

Thus it is with the intention of linking coordination chemistry and biochemistry in their widest sense that this project was envisaged. All the same, this area of research is very broad and thus the main objective for this study was to prepare various palladium(II), platinum(II), gold(I) and gold(III) complexes with a view to test them as anticancer agents; while exploring all chemistry aspects of these complexes.

List of submitted manuscripts and some in preparation

The work in this thesis is based on reports submitted to "Biomedical applications for gold: Stages 9-15", *Mintek Communication (SA)*, **C4050M**,-**C4262M**.

1. Bis(pyrazolyl)Palladium(II), Platinum(II) and Gold(III) Complexes: Syntheses, Molecular Structures and Substitution Reactions with L-cysteine. **Frankline K. Keter**, Stephen O. Ojwach, Olayinka A. Oyetunji Ilia A. Guzei and James Darkwa (*Submitted to Inorganica Chimica Acta, 2008*)

2. Dichloro-bis-(3,5-dimethyl-pyrazolyl)palladium(II) complex. A DMSO-$_{d6}$ solvated complex. **Frankline K. Keter**, Bernard O. Omondi, and James Darkwa. (Submitted to *Journal of Molecular Structures*).

3. The work reported in chapters four and five are currently at various stages of manuscript preparation for publication (Target journals: *Inorganic Chemistry* and *Journal of Inorganic Biochemistry*).

CHAPTER 1

1.0 Introduction

1.1. Overview

Cancer is one of the diseases that contribute to the high mortality rate globally. It was estimated that in 2000, 10 million new cases of cancer were identified; and about 6 million reported deaths were cancer related.[1a,b] In the same year, an estimated 22 million people were living with cancer already diagnosed within the previous five years.[1b] These statistics depicts a 22% increase in cancer incidence and mortality in the world in 2000 compared to 1990.[1,2] The most common types of cancer in 2000 were breast (17.2%), colorectal (10.6%) and prostate (6.9%), and the highest tumour types world-wide were lung (12.3%), breast (10.4%) and colorectal (9.4%) tumours (Fig. 1.1). The estimated and projected numbers of cancer cases over a period of years is shown in Table 1.1. Therefore, there is a need for more efficient drugs to curb this scourge.

[1] [a]Shibuya K., Mathers C. D., Boschi-Pinto C., Lopez A. D., Murray C. J. L., BMC Cancer, 2002, 2, 37; [b]Schwartsmann G., Ratain M. J., Cragg G. M., Wong J. E., Saijo N., Parkinson D. R., Fujiwara Y., Pazdur R., Newman D. J., Dagher R., Di Leone L., *J. Clin. Oncol*. **2002**, *20*, 47.
[2] Parkin D. M., *Lancet Oncol*. **2001**, *2*, 533

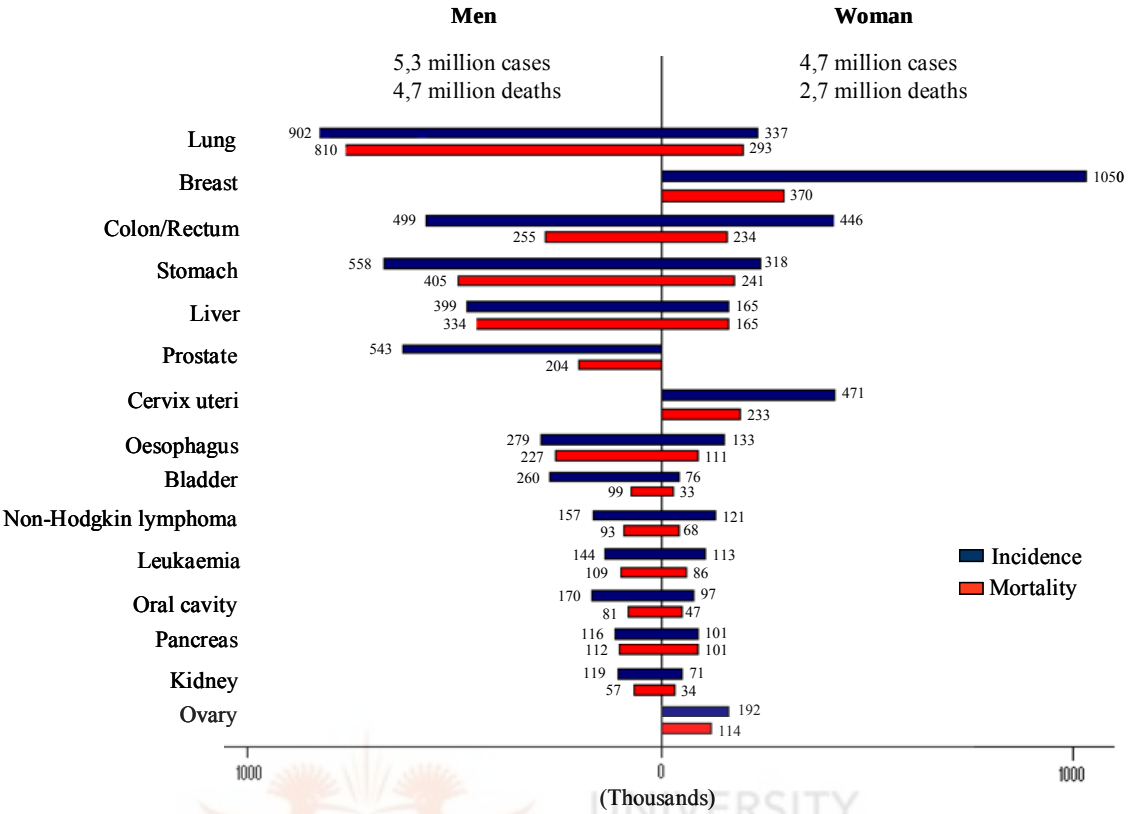

Figure 1.1. Estimated numbers of new cases (incidence) and deaths (mortality), by sex and site. (Taken from ref. 1).

Table 1.1. Estimated and projected numbers of cancer cases. (Taken from ref. 1)

	Years			
Region	**2000**	**2010**	**2022**	**2050**
World	10.06	12.34	15.35	23.83
More developed regions	4.68	5.31	6.03	6.79
Less developed regions	5.38	7.03	9.32	17.04
Africa	0.3	0.79	1.04	2.53
Asia (Japan)	0.52	0.61	0.67	0.65
Asia (Other)	3.94	5.17	6.75	10.74
Europe	2.77	3.06	3.36	3.64
South America	0.83	1.10	1.48	2.88
North America	1.38	1.65	2.03	2.61
Oceania	0.11	0.13	0.16	0.24

NOTE: The number of new cases (millions) of all cancer.

There is no doubt that plants have a long history of use in the treatment of cancer[3a]; though many of the claims for the efficacy of such treatment have been viewed with some skepticism because cancer, as a specific disease, is poorly defined in terms of myths and traditional medicine.[1,3a] Nevertheless, with the current experience in medicinal chemistry and pharmacology, *in vivo* studies done on natural products have resulted in a number of clinically useful drugs that are now available. Examples include, Taxol (Fig. 1.2**a**),[3b] Camptothecin (Fig. 1.2**b**)[3c] and Tamoxifen (Fig. 1.2**c**).[3d] These are all drugs from plant sources, generally known as natural products.

Apart from natural products being directly applied as drugs, there are many others that have served as chemical models or templates for the design and synthesis of other cancer drugs. Despite significant progress being made in tackling cancer with natural products derived drugs, it is still a challenge as some of these drugs have side effects. Thus, efforts to solve this problem continue.

[3] [a]Newman D. J., Cragg G. M., Snader K. M., *Nat. Prod. Rep*. **2000**, *17*, 215; [b]Wani M., Taylor H., Wall M., Coggon P., McPhail A.I, *J. Am. Chem. Soc*., **1971**, *93*, 2325; [c]Wall M. E., Wani M. C., Cook C. E., Palmer K. H., McPhail A. I., Sim G. A., *J. Am. Chem. Soc*., **1966**, *88*, 3888; [d]Jordan V. C., *Br. J. Pharmacol*., **2006**, *147*, S269.

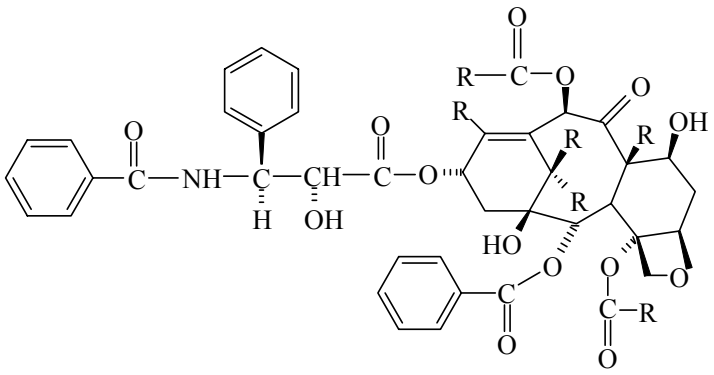

(**a**)

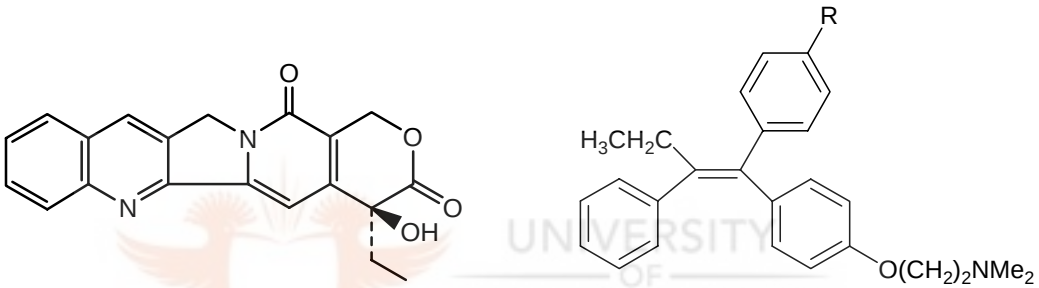

(**b**) (**c**)

Figure 1.2. Structures of (**a**) Taxol, (**b**) Camptothecin, and (**c**) Tamoxifen.

One area that has gained prominence is the use of inorganic compounds as anticancer drugs. Since the serendipitious discovery of *cis*-diamminedichloroplatinum(II) (cisplatin) by Rosenburg and co-workers in 1965,[4] (Fig. 1.3) this compound has become a well established antineoplastic agent. Cisplatin is one of the most effective drugs in the treatment of testicular, ovarian, bladder, head and neck cancers.[5] The chemotherapeutic

[4] Rosenberg B., Van Camp L., Krigas T., *Nature* **1965**, *205*, 698.
[5] Gumus F., Algul O., Eren G., Eroglu H., *Eur. J. Med. Chem* **2003**, *38*, 473

efficacy cisplatin is derived from its ability to bind and cross link deoxyribonucleic acid (DNA); the major adduct from this interaction is the *cis*-Pt-GG intrastrand crosslink.[6]

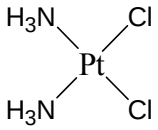

Figure 1.3. Structure of dichlorodiammineplatinum(II) complex (cisplatin).

This discovery has led to the progressive development of cisplatin-like complexes, because of their ability to bind to DNA under physiological conditions. Despite the great success of treating certain kinds of cancers with cisplatin there are several side effects, as well as the occurrence of intrinsic and acquired resistances, which limit the organotropic profile of the drug.[7] Some of the reasons that lead to this acquired resistance include reduced cellular uptake and deactivation of cisplatin by thiol containing biomolecules, such as, glutathione.[8] This has generated continuous interest in the development of not only new platinum complexes but also other platinum group metal-based complexes, which could be less toxic and exhibit no cross-resistance in tumour cells as cisplatin. As a result, this has led to the discovery of interesting second-generation platinum(II) antitumour complexes that carry 'non-leaving' ligands other than ammonia.

[6] Sherman S. E., Lippard S. J., *Chem. Rev*. **1987**, *87*, 1153.
[7] Jamieson E. R., Lippard S. J., *Chem. Rev*. **1999**, *99*, 2467
[8] Wong E., Giandomenico C. M., *Chem Rev*. **1999**, *99*, 2451.

Several platinum complexes with N-heterocyclic ligands such as imidazole, thiazole, benzimidazole, benzoxazole and bezothiazole, have been reported[9] and some of these compounds have shown significant cytotoxicity.[9b,c] This is clear evidence that N-heterocycles impart therapeutic value to platinum complexes in which they feature as ligands. As such, the use of other nitrogen-donor ligands that are more compatible to the human system appears to be another way of producing new cancer drugs.[10,11]

The ability of platinum compounds mentioned above to modulate drug metabolism and target binding through steric and electronic effects, on the substitution mechanism that govern the action of these compounds, is of interest.[12] For this reason, different strategies have been employed in a bid to reduce the systematic toxicities of existing drugs, *viz*. (i) passive tumour targeting based on the enhanced permeability and retention (EPR) effect; (ii) receptor mediated targeting; (iii) enzymatically activated prodrugs; (iv) compounds targeted towards cellular DNA.[13] It should be noted that most of these strategies employ platinum derived complexes because of their ease of syntheses and stabilities. No doubt that the four strategies mentioned above have added value to the drugs, especially platinum. However, the targeted drugs are still far from being used to treat patients as the

[9] [a]He X.-F., Vogels C. M., Decken A., Westcott S. A., *Polyhedron*, **2004**, *23*, 155; [b]Mock C., Puscasu I., Rauterkus M. J., Tallen G., Wolff J. E. A., Krebs B., *Inorg. Chim. Acta*, **2001**, *319*, 109; [c]Bloemink M. J., Engelking H., Karentzopoulos S., Krebs B., Reedijk J., *Inorg. Chem*., **1996**, *35*, 619.
[10] Iakovidis A., Hadjiliadis N., *Coord. Chem. Rev*. **1994**, *135*, 17
[11] Beck, W., Purucker B., Girnth M., Schonenberger H., Seidenberger H., Ruckdeschel G., *Z. Naturforsch* **1976**, *31b*, 832.
[12] Wang K., Lu J., Li R., *Coord. Chem. Rev*. **1996**, *151*, 53.
[13] [a]Gabizon A., Shmeeda H., Barenholz Y., *Clin. Pharmacokinet*., **2003**, *42*, 419; [b]Barnes K. R., Kutikov A., Lippard S. J., *Chem. Biol*., **2004**, *11*, 557; [c]Hanessian S., Wong J. G., *Can. J. Chem. Rev. Can. Chim*., **1993**, *71*, 896; [d]Ren S. M., Cai L. S., Segal B. M., *J. Chem. Soc., Dalton Trans*., **1999**, 1413; [e]Van Zutphen S., Reedijk J., *Coord. Chem. Rev*. **2005**, *249*, 2845.

activities are not enormously different from those of cisplatin. Thus, the fourth strategy remains the most applied at the moment.

1.2. General DNA-metal interactions

DNA is now generally accepted as the target for most anticancer agents. Out of the four strategies mentioned (*vide supra*), it is apparent that synthesising a primary drug targeted towards the DNA is an appropriate route to anticancer drug discovery. Thus, DNA remains an attractive target for the design of antitumour agents.[14] The reactivity of cisplatin and its mimics is dependent not only on physiological conditions but also on structure activity relationships (SARs), *viz.* (i) a *cis* geometry with the general formula *cis*-$[PtX_2(amine)_2]$ for platinum(II) compounds and *cis*-$[PtY_2X_2(amine)_2]$ for platinum(IV) compounds; (ii) the ligand X should be an anion with intermediate binding strength, such as, chloride or oxalate; (iii) the amine ligands should possess at least one NH moiety necessary for hydrogen bonding interactions.[8,15] It should, however, be pointed out that an N-H moiety is not necessarily a requirement when designing anticancer drugs. This is supported by the fact that some compounds without N-H groups have shown antitumour activity.[16,17,18]

Within the extracellular *milieu* the physiological chloride ion concentration is *ca*. 100 mM, while inside cells it is *ca*. 4 mM. These conditions facilitate the aquation of cisplatin

[14] Budzisz E., Graczyk-Wojciechowska J., Zieba R., Nawrot B., *New J. Chem.*, **2002**, *26*, 1799.
[15] Cleare M. J., Hoeschele J. D., *Bioinorg. Chem.*, **1973**, *2*, 187.
[16] Gund A., Keppler B. K., *Angew. Chem., Int. Ed. Engl.*, **1994**, *33*, 186.
[17] Bloemink M. J., Engelking H., Karentzopoulos S., Krebs B., Reedijk J., *Inorg. Chem.*, **1996**, *35*, 619.
[18] Rauterkus M. J., Fakih S., Mock C., Puscasu I., Krebs B., *Inorg. Chim. Acta*, **2003**, *350*, 355.

(Fig. 1.4). The aquated species would then easily react with the target molecule, DNA.[19,20] The binding of metal species to DNA is known to occur in two steps, leading to formation of two forms of adducts; intra-strand and inter-strand cross-links (Fig. 1.4). The formation of these adducts then blocks DNA transcription and replication causing cells to undergo G2 cell-cycle arrest. Under normal circumstances a nucleotide excision repair (NER) pathway would repair DNA damage.[21] However, DNA damage caused by cisplatin adducts is very poorly repaired in cells. This is due to the fact that cisplatin-induced intra-strand cross-links serve as binding targets for high-mobility-group proteins (HMG)[22] because of structural similarity between these intra-strand cross-links and the natural binding sites for HMG. The binding of HMG to cisplatin-DNA adducts cause distortion in DNA structure, hence inhibiting DNA repair.[19,23] The above findings about the biological chemistry of cisplatin are informative in drug research as it helps in the design of new effective metallo-drugs.

[19] Chu G., *J. Biol. Chem*., **1994**, *269*, 787.
[20] Jordan P., Carmo-Fonseca M., *Cell Mol. Life Sci*., **2000**, *57*, 1229.
[21] Zamble D. B., Mu D., Reardon J. T., Sancer A., Lippard S. J., *Biochemistry*, **1996**, *35*, 10004.
[22] HMG are small chromosomal-associated proteins that are involved in gene regulation and maintenance of chromosomal structure.
[23] Zlatanova J., Yaneva J., Leuba S. H., *FASEB J*, **1998**, *12*, 791.

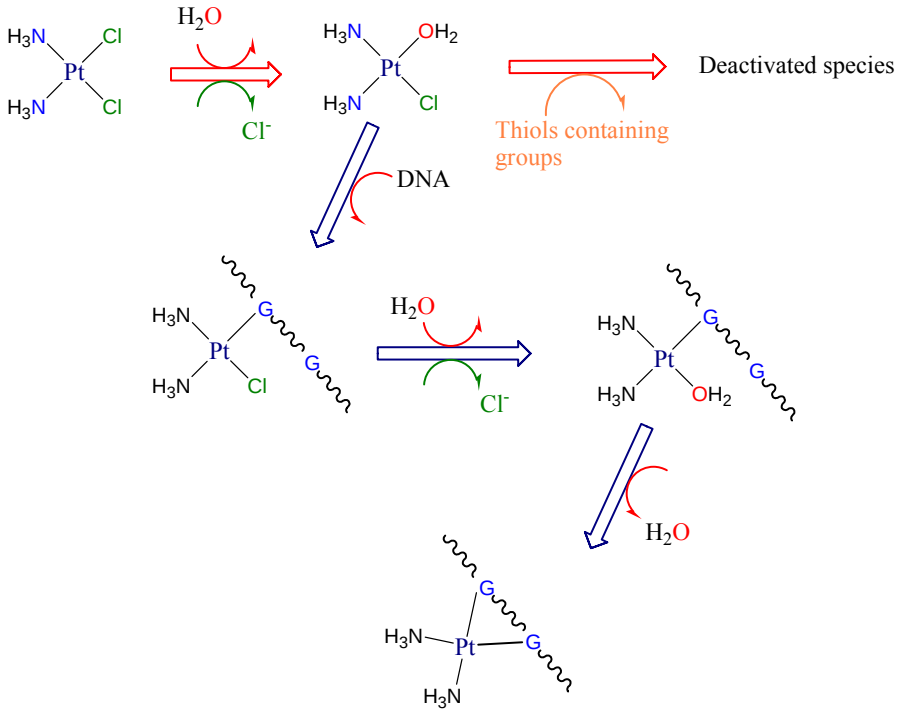

Figure 1.4. A Schematic representation of how cisplatin is activated and subsequently bind to DNA.

More than 3000 platinum analogues of cisplatin have been synthesised and a few have made it to the clinical stages.[24] Examples include carboplatin (Fig. 1.5**a**), AMD-473 (Fig. 1.5**b**) and oxaliplatin (Fig. 1.5**c**). Carboplatin displays similar activities with cisplatin but also exhibits bone-marrow toxicity,[25,26] On the other hand, AMD-473 showed promising *in vitro* activity against cisplatin-resistant A2780cisR cells.[25,27] Despite its low toxicity profile, the activity of AMD-473 is not great. Oxaliplatin, which is a highly sterically hindered complex, has good activity and has been approved for clinical use in Europe, China and United states for colorectal cancer.

[24] Marzano C., Trevisan A., Giovagnini L., Fregona D., *Toxicology in Vitro*, **2002**, *16*, 413.
[25] Kelland L. R., Sharp S. Y., O'Neill C. F., Raynaud F. I., Beale P. J., Judson I. R., *Inorg. Biochem.*, **1999**, *77*, 111.
[26] Cadron I., Leunen K., Amant F., Van Gorp T., Neven P., Vergote I., *Gynecol. Oncol.*, **2007**, *106*, 354.

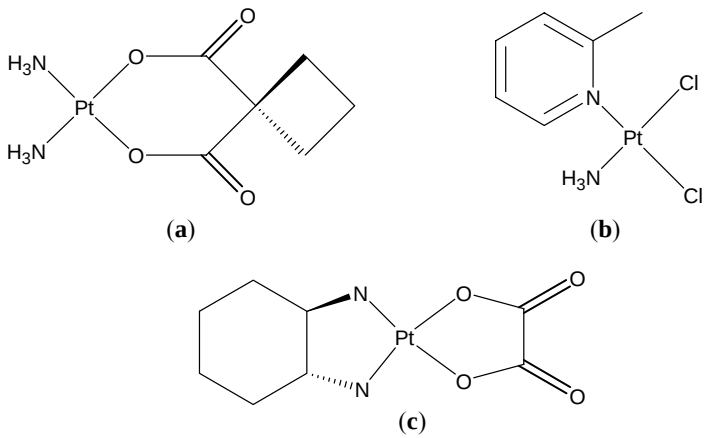

Figure 1.5. Structures of (**a**) carboplatin, (**b**) AMD-473 and (**c**) oxaliplatin.

1.3. Non-platinum metal compounds as anti-cancer therapeutic agents

From the preceding section it would appear that platinum is the only metal that has been used in anticancer therapy. This is far from the truth. The earliest reports on the therapeutic use of metals or metal containing compounds in cancer date back to the sixteenth century. They were forgotten until the 1960s when the antitumour activity of cisplatin was discovered.[4,28] This led to renewed interest in metal-containing cytostatic drugs. It has since been shown that a number of metal complexes exhibit antitumour activities. Some of these compounds are discussed in the subsequent sections in the order of their positions in the periodic table.

---

[27] Holford J. Sharp S. Y., Murrer B. A., Abrams M., Kelland L. R., *Br. J. Cancer*, **1998**, *77*, 366.
[28] Rosenberg B., VanCamp L., Trosco J. E., Mansour V. H., *Nature*, **1969**, *222*, 385.

1.3.1. Titanium and Vanadium compounds

The search for new anticancer agents was extended to titanium compounds after the discovery of cisplatin. Titanium is one of the early transition metal to be investigated for its antitumour properties. Firstly, titanocene dichloride has been investigated for its anti-tumour activity and has reached the end of phase I clinical trials.[29] Seventy-six percent of all titanium compounds that have been screened for their anticancer activity are derivatives of bis(β-diketonate)titanium(IV) complexes.[30] Bis(β-diketonate)titanium(IV) complexes are analogues of the titanium drug budotitane (*cis*-dietoxybis(1-phenylbutane-1,3-dionato)titanium(IV) (Fig. 1.6), which is one of the first non-platinum metal drug to reach phase I clinical trials.[31] The therapeutic target of budotitane derivatives is gastrointestinal tumours, but the mode of action is unknown. However, it has been suggested that complete hydrolysis of the β-diketonato titanium complexes lead to total loss of ligands and formation of the water insoluble titanium dioxide (TiO_2).[32] Interestingly, TiO_2 itself has been shown to have antitumour activity.[33] In a more recent report, iron-derived free radicals (ROS) have been implicated as part of the mechanism of TiO_2-induced mitochondrial membrane potential changes, which in turn result in *alveolar epithelial* cell apoptosis.[34]

[29] Christodoulou C. V., Ferry D. R., Fyfe D. W., *J. Clin. Oncol*., **1998**, *16*, 2761.
[30] Huang R., Wallqvist A., Covell D. G., *Biochem. Pharmacol*., **2005**, *69*, 1009.
[31] Keppler B. K., Friesen C., Vongerichten H., Vogel E., *Met. Complexes Cancer Chemother*., 1993, 297.
[32] Dubler E., Buschmann R., Schmalle H. W., *J. Inorg. Biochem*., **2003**, *95*, 97.
[33] Afaq F., Abidi P., Matin R., Rahman Q., *J. Appl. Toxicol*., **1998**, *18*, 307.
[34] Kamp D. W., Panduri V., Weitzman S. A., Chandel N., *Mol. Cell. Biochem*., **2002**, *234*, 153.

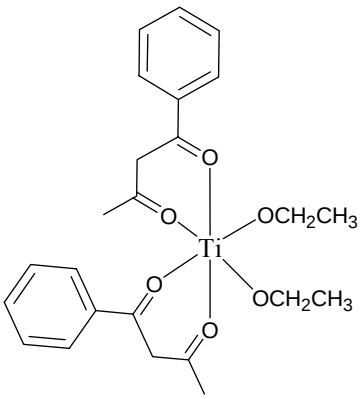

Figure 1.6. Structure of (*cis*-dietoxybis(1-phenylbutane-1,3-dionato)titanium(IV), budotitane.

The potential use of vanadium compounds as antitumour agents also received strong attention after the discovery of cisplatin, even though this speculation has existed since the beginning of the 20th century.[35] Evidence from experimental studies carried out suggests that vanadium could be considered as a representative of a new class of anticancer agents.[36] Various vanadium complexes, such as, the peroxovanadates and vanadocene dichloride (Fig. 1.7**a**)[37] are amongst the active complexes. Literature survey reveals that only two vanadium-L-cysteine or L-cysteine methyl ester complexes (Fig. 1.7) have been isolated and shown to significantly prevent lung metastasis *in vivo*.[38] Studies on various cell lines reveal that vanadium exerts its antitumour activity through inhibition of cellular tyrosine phosphatases and/or activation of tyrosine phosphorylases.[39] Ultimately signal transduction pathways are triggered, hence causing apoptosis and/or activation of tumour suppressor genes. It is clear from what is known

[35] Kieler J., Gromek A., Nissen N. I., *Acta Chir. Scand*., **1965**, *343*, 154.
[36] Evangelou A. M., *Crit. Rev. Oncol./Hematol*., **2002**, *42*, 249.
[37] Toney J. H., Murthy M. S., Marks T. J., *Chem. Biol. Interact*., **1985**, *56*, 45.
[38] Papaioannou A., Manos M., Karkabounas S., Liasko R., Evangelon A. M., Correia I., Kalfakakou V., Pessoa J. C., Kabanos T., *J. Inorg. Biochem*., **2004**, *98*, 959.
[39] Bevan A. P., Drake P. G., Yale J.-F., Shaver A., Posner B. I., *Mol. Cell Biochem*., **1995**, *153*, 49.

about the mode of action for titanium and vanadium anticancer agents that they are different from cisplatin.

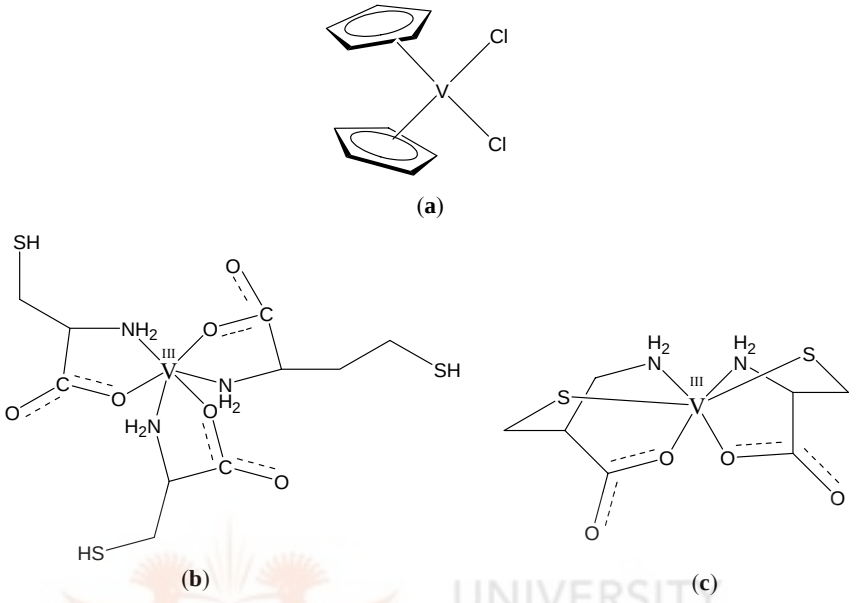

Figure 1.7. Structures of (**a**) vanadocene dichloride, (**b**) vanadium-L-cysteine complex and (**c**) vanadium-L-cysteine methyl ester complex.

1.3.2. Ruthenium compounds

Investigation of ruthenium complexes as anticancer agents was stimulated by the reports of antitumour activity of sodium salt of $[RuCl_4(Im)Me_2SO)]$, generally referred to as NAMI (Fig. 1.8**a**) , which is currently in clinical trials.[40] As a result, many ruthenium complexes have been synthesised and shown to have antitumour activity.[41] Organometallic ruthenium(II) complexes with arene ligands represent another group of ruthenium compounds with antitumour activity. Since the initial discovery that

[40] Sanna B., Debidda M., Pintus G., Tadolini B., Posadino A. M., Bennardini F., Sava G., Ventura C., *Arch. Biochem. Biophys*., **2002**, *403*, 209.
[41] Zhang C. X., Lippard S. J., *Curr. Opin. Chem. Biol*., **2003**, *7*, 481.

$[RuCl_2(\eta^6\text{-}C_6H_6)(DMSO)]$ (Fig. 1.8**b**) can inhibit topoisomerase II activity,[42a] three derivatives have been prepared by replacing the dmso ligand in $[RuCl_2(\eta^6\text{-}C_6H_6)(DMSO)]$ with 3-aminopyridine, p-aminobenzoic acid or aminoguanidine.[42b] These analogues show enhanced efficacy of topoisomerase II inhibition and higher cytotoxicity against breast and colon carcinoma cells. In general, the cytotoxicity of ruthenium complexes, both in 2+ and 3+ oxidation states is related to its ability to bind DNA. For ruthenium(III) complexes its reaction with DNA is preceded by reduction from ruthenium(III) to ruthenium(II).

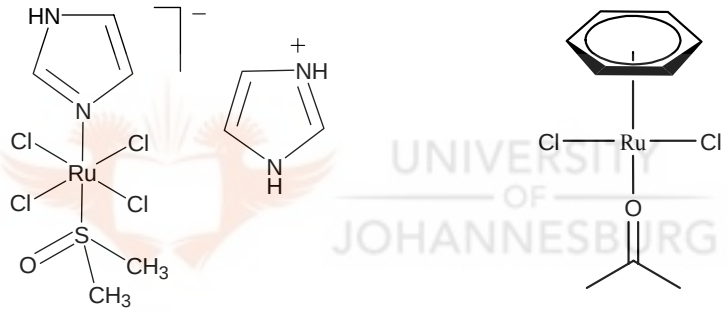

(**a**) (**b**)

Figure 1.8. Structures of (**a**) $[RuCl_4(Im)Me_2SO)]$ (NAMI) and (**b**) $[RuCl_2(\eta^6\text{-}C_6H_6)(DMSO)]$.

Another set of important compounds are the ruthenium(II) arene complexes of the type $[(\eta^6\text{-arene})Ru(II)(en)Cl][PF_6]$ (en = ethylenediamine) reported by Sadler and co-workers.[43] They include, $[(\eta^6\text{-Bip})Ru(II)(en)Cl][PF_6]$ (Bip = biphenyl), $[(\eta^6\text{-THA})Ru(II)(en)Cl][PF_6]$ (THA = 5,8,9,10-tetrahydroanthracene), and $[(\eta^6\text{-DHA})Ru(II)(en)Cl][PF_6]$ (DHA = 9,10-dihydroanthracene) (Fig. 1.9). These complexes

[42] [a]Gopal Y. N. V., Konuru N., Kondapi A. K., *Biochemistry*, **1999**, *38*, 4382; [b]Gopal Y. N. V., Konuru N., Kondapi A. K., *Arch. Biochem. Biophys.*, **2002**, *401*, 53.

[43] Chen H., Parkinson J. A., Parsons S., Goxall R. A., Gould R. O., Sadler S. J., *J. Am. Chem. Soc.*, **2002**, *124*, 3064.

specifically target guanine bases of DNA oligomers and form monofunctional adducts.[44,45] A case in point is where the structures of monofunctional adducts of complexes [(η^6-Bip)Ru(II)(en)Cl][PF_6], [(η^6-THA)Ru(II)(en)Cl][PF_6], and [(η^6-DHA)Ru(II)(en)Cl][PF_6] with guanine, were determined.[43]

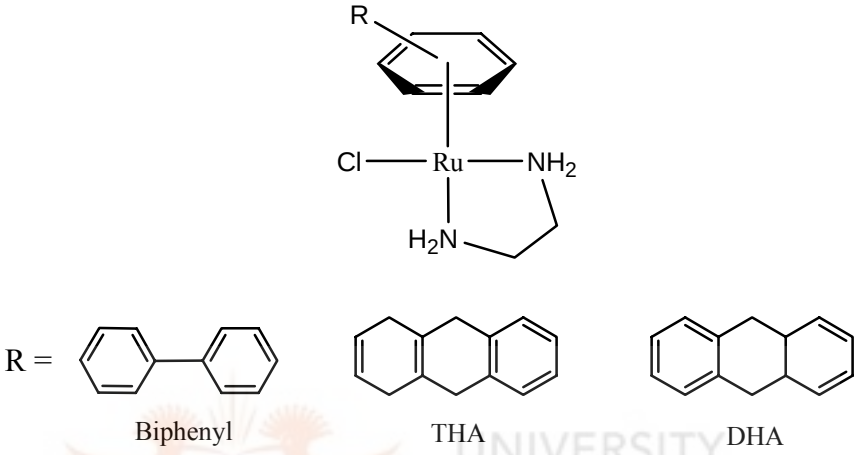

Figure 1.9. Structures of ruthenium complexes with general formula [RuCl(η^6-arene)(en)Cl][PF_6].

The hydrophobic interactions between the arene ligand in [(η^6-arene)Ru(II)(en)Cl]$^+$ and DNA could produce a driving force for DNA binding.[43,46] In addition, the modeling studies performed by Chen *et al*. led them to suggest a new potential DNA-binding mode for ruthenium anticancer drugs. It involves simultaneous intercalation and covalent coordination with DNA.

[44] Morris R. E., Aird R. E., Murdoch P., Chen H., Cummings J, Hughes N. D., Parsons S, Parkin A, Boyd G., Jodrell D. I., Sadler P. J., *J. Med. Chem*. **2001**, *44*, 3616.
[45] Chen H., Parkinson J. A, Morris R. E., Sadler P. J., *J. Am. Chem. Soc.*, **2003**, *125*, 173.
[46] Ren J., Jenkins T. C., Chaires J. B., *Biochemistry*, **2000**, *39*, 8439.

1.3.3. Rhodium compounds

Investigations of the potential of rhodium complexes as anticancer agents mainly stems from rhodium belonging to platinum group metals. However, rhodium compounds that possess significant antitumour properties have been found to be less effective mainly due to their toxic effects.[47] The above notwithstanding, rhodium(II) compounds show anticancer activity. For instance, the dirhodium tetraacetate complex, $[Rh_2(CH_3COO)_4(H_2O)_2]$ (Fig. 1.10**a**), is much more inhibitory towards *Escherichia coli* DNA polymerase I and show good antitumour activity against sarcoma and even melanoma.[48]

Other examples of rhodium complexes include two new rhodium carboxylate sugar derivatives, cyclophosphamide adducts of rhodium(II) keto-gluconate, $[Rh_2(KG)_4]$, and glucuronate compounds $[Rh_2(GU)_4]$ (Fig. 1.11), which have been shown to have *in vitro* activity against the human leukemia cell line, K-562 cells.[49] Trifluoroacetimide dirhodium complexes, such as, $[Rh_2(CF_3CONH)_4]$ (Fig. 1.10**b**), have also shown good antitumour activities.[50] The interesting feature is that this rhodium complex needs lower doses than cisplatin to promote the same inhibitory effects against human leukaemia cells.[50] In addition to rhodium(II) complexes above showing anticancer activities, there are rhodium(I) and rhodium(III) complexes (e.g. $[RhCl(COD)NH_3]$ and $[RhCl_2L_4]Cl$ (L = sulpha-quinoxaline)) that have also been tested and shown to have considerable antitumour activities.[47]

[47] Katsaros N., Anagnostopoulou A., *Crit. Rev. Oncol./Hematol.,* **2002**, *42*, 297.
[48] Hall L. M., Speer R. J., Ridgway H. J., *J. Clin. Hematol. Oncol.,* **1980**, *10*, 25.
[49] Gil E., Gonçalves M. I., Ferreira E. I., Zyngier S. B., Najjar R., *Met. Based Drugs* **1999**, *6*, 19.
[50] Espósito B. P., Zyngier S. B., De Souza A. R., Najjar R., *Met. Based Drugs* **1997**, *4*, 333.

Investigations suggest that rhodium compounds may exert their activity by causing alterations to DNA.[51] But a more likely mechanism of action of rhodium complexes may involve protein binding of rhodium compounds at sulfhydryl sites, thereby inhibiting enzymes essential for DNA synthesis such as DNA polymerase A, and hence inhibit DNA synthesis.[52]

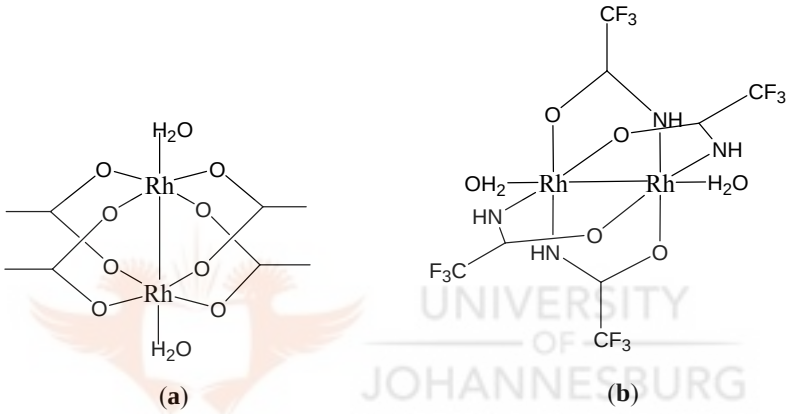

Figure 1.10. The dirhodium tetraacetate complex, (**a**) $[Rh_2(CH_3COO)_4(H_2O)_2]$ and (**b**) $[Rh_2(CF_3CONH)_4]$.

[51] Clarke M. J., Zhu F., Frasca D. R., *Chem. Rev*., **1999**, *99*, 2511.
[52] [a]Howard R. A., Spring T. G., Bear J. L., *Cancer Res*., **1976**, *36*, 4402; [b]Tselepi-Kalouli E., Katsaros N., *J. Inorg. Biochem*. **1990**, *40*, 95.

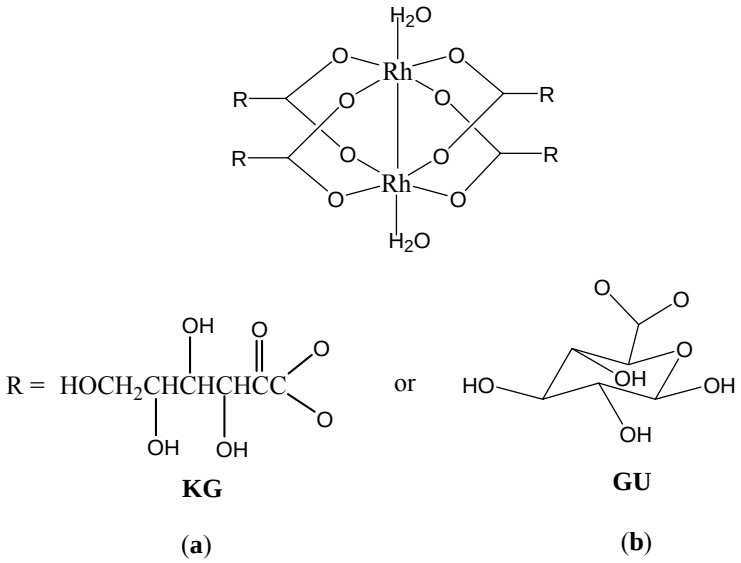

Figure 1.11. Cyclophosphamide adducts of (**a**) rhodium(II) keto-gluconate complex, $[Rh_2(KG)_4]$, and (**b**) rhodium(II) glucuronate complex, $[Rh_2(GU)_4]$.

1.3.4. Palladium complexes

Interest in palladium(II) anticancer agents stems directly from being isoelectronic and structural with platinum(II). Thus, development of palladium(II) as anticancer agents is beginning to gain popularity.[53] Budzisz and co-workers have described the syntheses of palladium(II) complexes based on pyrazole-derived ligands (Fig. 1.12).[54] The dimethoxyphosphonyl and/or methoxy-carbonyl moieties present in these ligands, as well as highly substituted pyrazole ligands confer on these palladium compounds high cytotoxicity and better selectively toward cancer cells as compared to cisplatin. The *trans*-$[Pd(L)_2Cl_2]$ (L = 5-(2-hydroxyphenyl)-1,3-dimethyl-4-methoxycarbonyl-1*H*]-2-pyrazole) complex (Fig. 1.12**b**) exhibited highest toxicity towards HL-60 and NALM-6 cells than its analogue (Fig. 1.12**a**).

[53] Szűčová L., Trávníček Z, Zatloukal M., Popa I., *Bioorg. Med. Chem*., **2006**, *14*, 479.
[54] Budzisz E., Krajewska U., Rozalski M., Szulawska A., Czyz M., Nawrot B., *Eur. J. Pharmacol*., **2004**, *502*, 59.

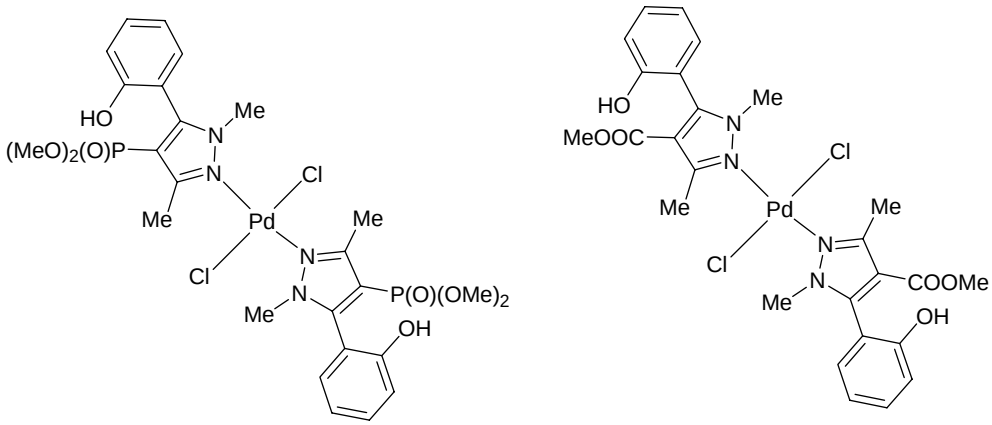

Figure 1.12. The *trans*-[Pd(L)$_2$Cl$_2$] complexes (L = 5-(2-hydroxyphenyl)-1,3-dimethyl-4-methoxycarbonyl-1*H*]-2-pyrazole), 5-(2-hydroxyphenyl)-1,3-dimethyl-4-dimethoxyphosphonite]-2-pyrazole)

Another palladium(II) complex of a ligand obtained from the condensation of 2-(diphenylphosphino)benzaldehyde and ethyl hydrazinoacetate, has been reported (Fig. 1.13).[55,56] Its activity against cisplatin-resistant U2-OS/Pt cells and HeLa cells is attributed to the steric bulkiness of the ligand, and the tridentate nature of the ligand that enforces a *cis*-conformation. The 6-membered ring formed around the palladium centre stabilises the complex, which possibly helps to avoid easy translabilisation in the biological *milieu*.

[55] Bacchi A., Carcelli M., Costa M., Fochi A., Monici C., Pelagatti P., Pelizzi C., Pelizzi G., Roca L. M. S., *J. Organomet. Chem.*, **2000**, *593*, 180.
[56] Radulovic V., Bacchi A., Pelizzi G., Sladic D., Brceski I., Andjelkovic K., *Monatsh. Chem.*, **2006**, *137*, 681.

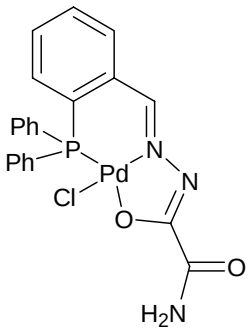

Figure 1.13. A palladium(II) complex utilizing ligand obtained from condensation of 2-(diphenylphosphino)benzaldehyde and ethyl hydrazinoacetate.

1.3.5. Gold compounds

Gold complexes are mainly known for their use in treating rheumatoid arthritis. Interestingly, gold(I) compounds including auranofin (Fig. 1.14**a**), have also been reported to show antitumour activity.[57] For instance, tetrahedral gold(I) complexes of 1,2-bis(diphenylphosphino)ethane ligands (Fig 1.14**b**) display a wide spectrum of antitumour activity *in vivo*, especially in cisplatin-resistant cell lines.[58] Very recently, a hydrophilic tetrakis((tris(hydroxy-methyl))phosphine)gold(I)chloride complex (Fig 1.14**c**) was reported to be cytotoxic to several tumour cell lines, for example HCT-15 cells, which is derived from human colon carcinoma.[59]

[57] McKeage M. J., Maharaj L., Berners-Price S. J., *Coord. Chem. Rev*., **2002**, *232*, 127.
[58] Urig S., Fritz-Wolf K., Réau R., Herold-Monde C., Tóth K., Davioud-Charvet E., Becker K., *Angew. Chem. Int. Ed*., **2006**, *45*, 1881.
[59] Pillarsetty N., Katti K. K., Hoffman T. J., Volkert W. A., Katti K. V., Kamei H., Koide T., *J. Med. Chem*., **2003**, *46*, 1130.

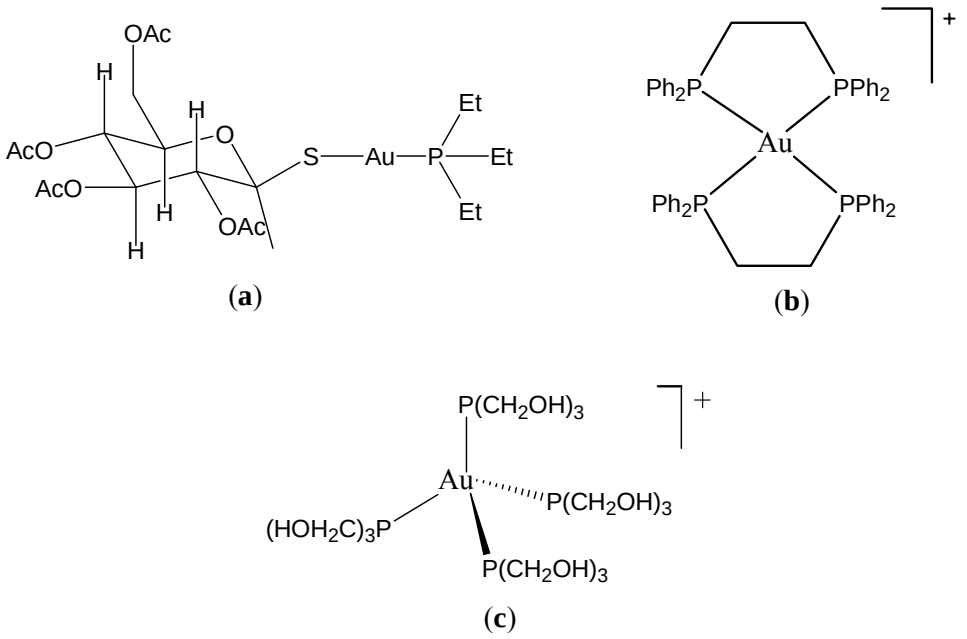

Figure 1.14. Structures of (**a**) auranofin, (**b**) tetrahedral gold(I) complex of 1,2-bis(diphenylphosphino)ethane and (**c**) tetrakis((tris(hydroxy-methyl))phosphine)gold(I) complex.

Mechanistic studies into antitumour activity of auranofin, chloro-(triethylphosphino)gold(I) and bis[1,2-bis(diphenylphosphino)ethane]gold(I) chloride provide evidence that gold(I) compounds affect mitochondrial function and not DNA.[60,61] These studies can be interpreted to be consistent with an antitumour mechanism involving the induction of apoptosis. The apoptosis is suggested to involve selective inhibition of the mitochondrial isoform of thioredoxin reductase, an enzyme which has emerged as a potential new drug target.[62] Thus, gold(I) compounds continue to receive much attention as anticancer agents since it was shown that auranofin induces apoptosis

[60] Rigobello M. P., Scutari G., Folda A., Bindoli A., *Biochem. Pharmacol*., **2004**, *67*, 689.
[61] Dong Y., Berners-Price S. J., Thorburn D. R., Antalis T., Dickinson J., Hurst T., Qui L., Khoo S. K., Parsons P. G., *Biochem. Pharmacol*., **1997**, *53*, 1673.
[62] Barnard P. J., Berners-Price S. J., *Coord. Chem. Rev*., **2007**, *251*, 1889.

by a mechanism involving inhibition of the mitochondrial enzyme thioredoxin reductase.[63,64]

On the other hand, gold(III) could be stabilised through judicious choice of donor atoms that can impart stability to this higher oxidation state of gold. Gold(III) complexes are isoelectronic and isostructural to platinum(II) and are promising candidates as anticancer agents. Gold(III) compounds investigated for potential antitumour activity are inevitably four coordinate and feature square planar geometries as found for cisplatin, thus a similar mechanism of action, i.e. interaction with DNA and disruption of normal cellular processes, may be operative for these gold(III) compounds.[65,66] In this connection, evidence has been provided that some gold(III) species, e.g. $[AuCl(dien)]Cl_2$ (dien = diethylendiamine) (Fig. 1.15), bind DNA.

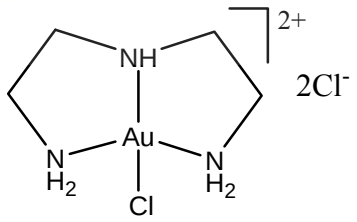

Figure 1.15. The structure of $[AuCl(dien)]Cl_2$.

Several other gold(III) compounds with multidentate ligands such as ethylenediamine, diethylenediamine and *N*-benzyl-*N*,*N*-dimethylamine have also been reported to be active

[63] Gromer S., Arscott L. D., William Jr. C. H., Schirmer R. H., Becker K., *J. Biol. Chem.*, **1998**, *273*, 20096.
[64] Gromer S., Urig S., Becker K., *Med. Res. Rev.*, **2004**, *24*, 40.
[65] Carotti S., Guerri A., Mazzei T., Messori L., Mini E., Orioli P., *Inorg. Chim. Acta*, **1998**, 2*81*, 90.
[66] Carotti S., Marcon G., Marussich M., Mazzei T., Messori L., Mini E., Orioli P., *J.Chem.-Biol. Interact.*, **2000**, *125*, 29.

against human cancer cell lines.[67] A recent *in vitro* cytotoxicity study demonstrated promising activity of two gold(III) complexes (Fig. 1.16) with bispyridyl ligands, $[Au(bipy)(OH)_2]PF_6$ and $[Au(bipy^*\text{-}H)(OH)]PF_6$ (bipy = bispyridyl).[68] Both complexes are quite stable under physiological conditions, with $[Au(bip^*\text{-}H)(OH)]PF_6$ being resistant to sodium ascorbate reduction. From this particular study, and contrary to cisplatin, mechanistic studies indicated that DNA is not the primary cellular target. What is interesting about one of the gold(III) complexes (Fig. 1.16**b**) described above is the stabilisation of the complex by a Au-C bond, thereby prohibiting easy reduction of the complex. The five-membered chelating ring in which the nitrogen of the amino group and the carbon of the aryl ring bond to the metal, stabilizes the complex, hence could possibly prevent translabilisation.[69] Other examples of gold(III) compounds that possess antitumour activities include $[AuCl_2(ppy)]$ (ppy = 2-phenylpyridine)[70] and $[AuCl_3(Hpm)]$ and $[AuCl_2(pm)]$ (Hpm = 2-pyridylmethanol).[71]

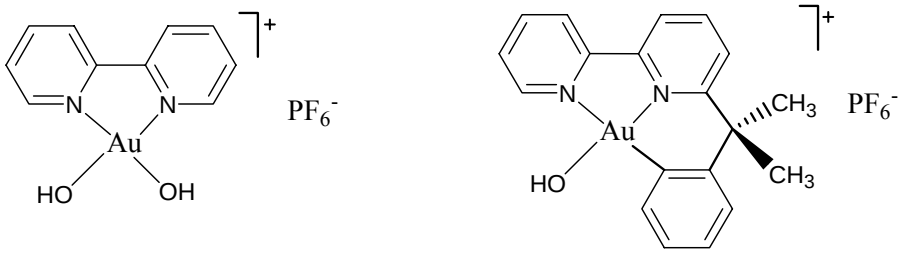

(**a**) (**b**)

Figure 1.16. Structures of (**a**) $[Au(bipy)(OH)_2]PF_6$ and (**b**) $[Au(bipy^*\text{-}H)(OH)]PF_6$.

[67] Messori L., Abbate F., Marcon G., Orioli P., Fontani M., Mini E., Mazzei T., Carotti S., O'Connell T., Zanelo P., *J. Med. Chem*., **2000**, *43*, 3541.
[68] Marcon G., Carotti S., Coronnello M., Messori L., Mini E., Orioli P., Mazzei T., Cinellu M. A., Minghetti G., *J. Med. Chem*., **2002**, *45*, 1672.
[69] Zhu Y., Cameron B. R., Skerlj R. T., *J. Organomet. Chem*., **2003**, *677*, 57.
[70] Fan D., Yang C., Ranford J. D., Lee P. F., Vittal J. J., *Dalton Trans*., **2003**, 2680.
[71] Calamai P., Carotti S., Guerri A., Messori L., Mini E., Orioli P., Paolo G., *J. Inorg. Biochem*., **1997**, *66*,

Judging from the palladium, platinum and gold complexes cited above, it is apparent that N-containing organic compounds are ligands of choice. In particular, the N-donor ligands would stabilise gold in its 3+ oxidation state. Bis(pyrazolyl)alkanes are examples of such N-donor ligands that could be utilised to prepare stable palladium, platinum and gold compounds. However, there is little information on the use of bis(pyrazolyl)alkanes as ligands for preparation of potential metal anticancer agents. Thus, the following section highlights on the preparation of bis(pyrazolyl)alkanes and their derivatives. Subsequently, their ability to form stable metal complexes is also highlighted.

1.4. Bis(pyrazolyl)alkanes and related derivatives

Bis(pyrazolyl)alkanes, $(R_2C)_n(pz^*)_2$, (R = H, Me, ^{t}Bu), can be described as organic compounds constituting pyrazoles as sources of N-donors for coordination to metals (Fig. 1.17). They constitute a family of stable and flexible bidentate ligands, isoelectronic and isosteric with well-known bis(pyrazolyl)borates.[72] Preparation of $H_2C(pz)_2$ was achieved by reaction of pyrazole with CH_2Cl_2 in an autoclave at 150 ^oC. Several other derivatives, $R_2C(pz^*)_2$ (R = H, Me), were also prepared by reacting potassium salts of the pyrazole with methylene iodide.[73] Bis(pyrazolyl)alkanes can also be prepared by way of phase transfer catalysis in dichloromethane (eq. 1.1).[74,75]

103.

[72] Trofimenko S., *J. Am. Chem. Soc*., **1970**, *92*, 5118.
[73] Singh H., Singh P., *Chem. Ind.* (London), **1978**, *4*, 126.
[74] Elguero J., Ochoa C., Julia S., del Mazo J., Sancho M., Fayet J. P., Vertut M. C., *J. Heterocycl. Chem*., **1982**, *19*, 1141.
[75] Claramunt R. M., Hernandez H., Elguero J., Julia S., *Bull. Soc. Chim. Fr*., **1983**, *2*, 5.

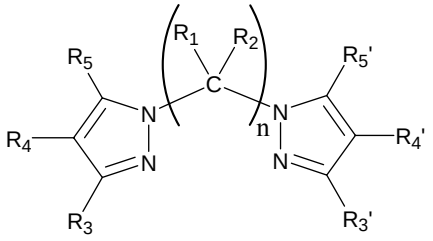

R_1 = H, Me $R_4 = R_{4'}$ = H n = 1, 2

$R_3 = R_{3'}$ = H, Me $R_5 = R_{5'}$ = H, Me

Figure 1.17. General structure of bis(pyrazolyl)alkanes, $(R_2C)n(pz^*)_2$.

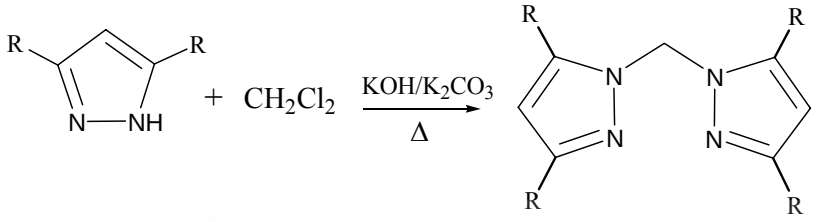

R = H, Me, ^{t}Bu

(**1.1**)

Various substituents may replace each hydrogen atom so that electronic and steric effects can be easily varied (eq. 1.1). These bis(pyrazolyl)alkanes contain pyrazole rings that are generally very stable towards chemical attack, e.g. against both oxidising and reducing agents. They form a variety of coordination compounds with main group such as Li and Na and transition metals including, Zr, V, Cr, Re, Pd, and Pt metals.[76] The coordinating behaviour of $(R_2C)_n(pz^*)_2$ yield stable adducts having six M-N-N-C-N-N and even seven M-N-N-C-C-N-N membered rings (Fig. 1.18). It is for these stability reason that a steady stream of new derivatives of $(R_2C)_n(pz^*)_2$ has been recently of interest.

[76] Pettinari C., Lorenzotti A., Pellei M., Santini C., *Polyhedron*., **1997**, *16*, 3435.

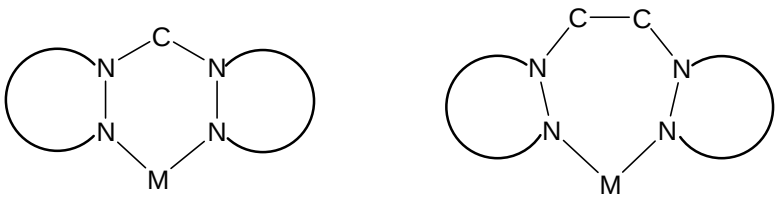

Figure 1.18. Observed coordination with $(R_2C)_n(pz^*)_2$.

Using similar procedures of phase transfer catalysis (*vide supra*), bis(pyrazolyl)ethanes were also isolated.[74,75] This was achieved by reaction of pyrazoles with dibromoethane under phase transfer catalysis conditions. This procedure has since led to the isolation of substituted $(H_2C)_n(pz^X)_2$ compounds (X = substituents on pz = H, NO_2, 4-Br, 4-NO_2, NH_2, 5-NH_2; n = 1, 2).[75,77]

An alternative route to preparation of bis(pyrazolyl)alknes is by lithiating the geminal protons of the alkane linker.[78,79] The resulting carbanions can then be reacted with a range of of electrophiles to get unsymmetrical bis(pyrazolyl)alkanes (eq. 1.2). This has led to the isolation of several unsymmetrical neutral bis(pyrazolyl)alkanes by Otero and co-workers[80] in which a third arm is attached to the bridging CH unit that contains a donor atom (Fig. 1.19).

[77] Julia S., Del Mazo J. M., Avila L., Elguero J., *Org. Prep. Proced. Int*., **1984**, *16*, 299.
[78] Diez-Barra E., de la Hoz A., Sánchez-Migallon A., Tejeda J., *J. Chem Soc., Perkin Trans*., **1993**, *1*, 1079.
[79] Katritzky A. R., Abdel-Rahman A. E., Leahy D. E., Schwarz O. A., *Tetrahedron Lett*., **1983**, *39*, 4133.
[80] Otero A., Fernandez-Baeza J., Antinolo A., Tejeda J., Lara-Sanchez A., Sanchez-Barba L., Sanchez-Molina M., Franco S., Lopez-Solera I., Rodriguez A. M., *Dalton Trans*., **2006**, 4359.

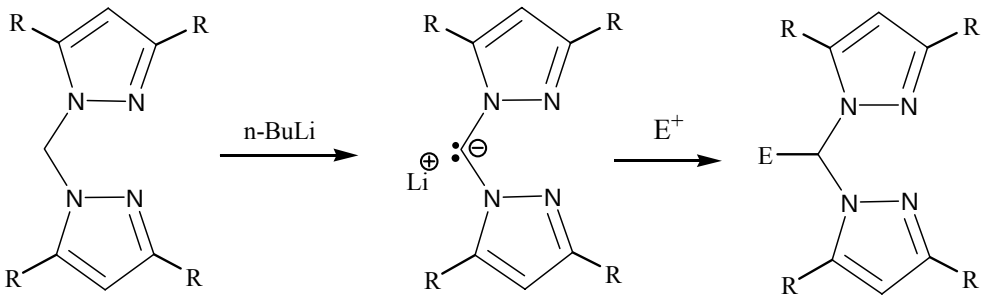

R = H, Me; E = electrophile

(**1.2**)

These unsymmetrical ligands are similar to tris(pyrazolyl)methane ligand, but in this case one of the pyrazole groups is replaced by a carboxylate, dithiocarboxylate, methoxy or pyridine group (Fig. 1.19). The inclusion of a pyridinyl arm in **a** (Fig. 2.19) gives a pyrazolyl ligand that can coordinate to metals not just as in a bidentate fashion but also in a tridentate fashion. An introduction of a methoxy moiety as the third arm of the lithiated bis(pyrazolyl)methane (eq. 1.2) gives **b** (Fig. 1.19), which is an *N*,*N*,*O*- tridentate ligand. Similarly, addition of an acetamide moiety to a lithiated bis(pyrazolyl)methane leads to formation of ligand **c** (Fig. 1.19). The delocalisation of electrons on the acetamide unit would allow the coordination of this ligand in an *N*,*N*,*N*- or *N*,*N*,*O*- tridentate manner.

In order to prepare water-soluble bis(prazolyl) ligands, a new approach to synthesising bis(pyrazolyl)acetic acid (Fig. 1.19**d**) was followed. It involves reacting dibromoacetic acid with two mole equivalents of pyrazole and/or its derivatives to obtain the carboxylate ligand (Fig. 1.19**d**).[81] Ligand **d** binds either in an *N*,*N*- or *N*,*O*- bidentate fashion or *N*,*N*,*O*- tridentate fashion. Ligand **d** is a hard acid donor ligand and thus serves

[81] Burzlaff N., Hegelmann I., Weibert B., *J. Organomet. Chem.*, **2001**, *626*, 16.

to stabilise high oxidation state metals, e.g. gold(III). Similarly, heteroscorpionate ligand **e** (Fig. 1.19) has been synthesised in the same way as **d** by introducing a CS_2H moiety. Ligand **e** is of interest because of its ability to form bidentate and tridentate complexes and also its combination of both hard (N) and soft (S) donor centres. In line with the aims of this project, which were to prepare several water soluble palladium(II), platinum(II) and gold(III) complexes for their application as anticancer agents, ligand **d** and **e** were of interest to this work. Several metal complexes have been isolated using bis(pyrazolyl)methane and its derivatives. The next section highlights on a few selected cases.

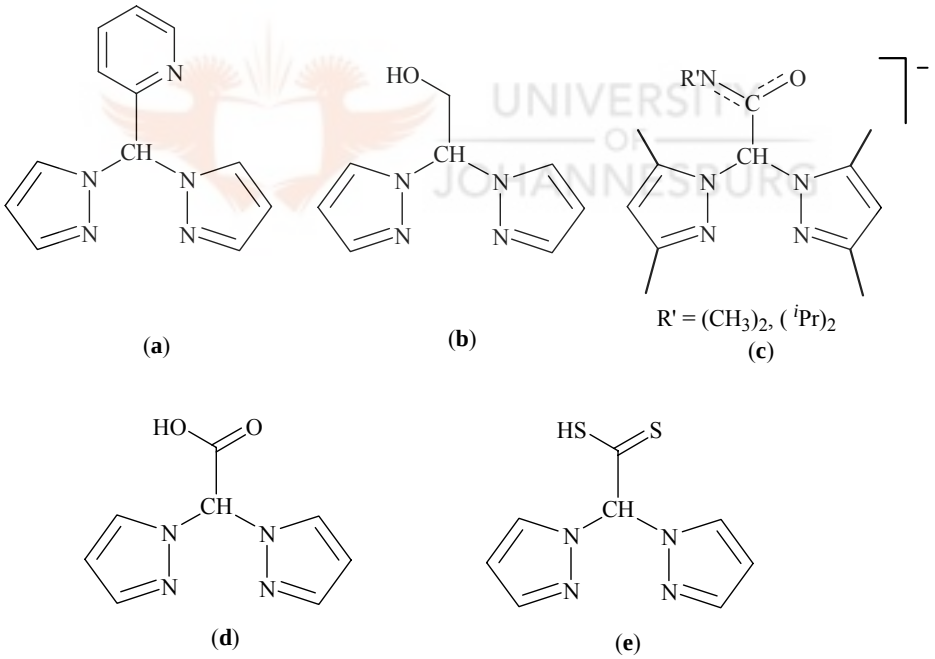

Figure 1.19. Bis(pyrazolyl) ligands. (**a**) (R′)CH(3,5-Me_2pz)$_2$. (**b**) (py)CH(3,5-Me_2pz)$_2$. (**c**) (CH_2OH)CH(3,5-Me_2pz)$_2$. (**d**) (CO_2H)CH(3,5-Me_2pz)$_2$. (**e**) (CS_2H)CH(3,5-Me_2pz)$_2$.

1.5. Metal complexes of bis(pyrazolyl)alkanes and other related ligands

The use of bis(pyrazolyl)alkanes and their derivatives as ligands for preparation of various metal complexes, would give rise to different coordination modes and geometries; partly due to the flexibility of the bis(pyrazolyl)alkanes. The following section highlights on the structural features of a few selected cases of early and late transition metal complexes of bis(pyrazolyl)alkanes in that order.

1.5.1. Niobium(II) complexes

Group 5 metals having bis(pyrazolyl)alkanes as ligands have been prepared and reported.[82,83] For instance, reaction of $H_2C(5\text{-}PPh_2pz)_2$ with $[NbCl_3(dme)]_n$ produce a binuclear complex $[NbCl_3\{H_2C(5\text{-}PPh_2pz)_2\}]_2$ (pz = pyrazolyl) (Fig. 1.20**a**). However, reaction of $H_2C(5\text{-}PPh_2pz)_2$ with the mononuclear species $[NbCl_3(dme)(RC{=}CR')]$ gives the corresponding derivatives $[NbCl_3\{H_2C(5\text{-}PPh_2pz)_2\}(RC{=}CR')]$ (R = R′ = Ph; R = R′ = $SiMe_3$; R = Ph, R′ = Me; R = Ph, R′ = $SiMe_3$) (Fig. 1.20**b**). In general, ligand $(5\text{-}PPh_2pz)_2$ coordinates to niobium in a bidentate *N*,*N*-fashion. In another instance the use of bis(3,5-dimethylpyrazolyl)acetate (bdmpza), which is a water soluble ligand, leads to isolation of the niobium(II) complex $[Nb(NR)Cl_2(\kappa^3\text{-bdmpza})]$ (R = ^{t}Bu, p-tolyl) with bdmpza coordinated to niobium in a *N*,*N*,*O*- tridentate fashion.[84] In spite of the fact that bdmpza is a water soluble ligand the resultant niobium complex is not. Spectroscopic

[82] Antinolo A., Carrillo-Hermosilla F., Diez-Barra E., Fernandez-Baeza J., Fernandez-Lopez M., Lara-Sanchez A., Moreno A., Otero A., Rodriguez A. M., Tejeda J., *J. Chem. Soc., Dalton Trans*., **1998**, 3737.
[83] Fernandez-Baeza J., Jalon F. A., Otero A., Rodrigo-Blanco M. E., *J. Chem. Soc., Dalton Trans*., **1995**, 1015.
[84] Otero A., Fernandez-Baeza J., Antinolo A., Tejeda J., Lara-Sanchez A., Sanchez-Barba L., Rodriquez A.

studies shows that the [Nb(NR)Cl_2(κ^3-bdmpza)] complex is in an asymmetrical structural disposition, thus making niobium a chiral centre (Fig. 1.20**c**). The X-ray structure of the analogous [$NbCl_2$(κ^3-bdmpza)(PhC≡CMe)] complex (Fig. 1.20**d**) is an indirect confirmation of isolation of [Nb(NR)Cl_2(κ^3-bdmpza)].[85] Complex [$NbCl_2$(κ^3-bdmpza)(PhC≡CMe)] (Fig. 1.20**d**) exhibits an octahedral geometry where the two pyrazolyl rings are located in *cis*- and *trans*- positions with respect to the (PhC≡CMe) moiety.

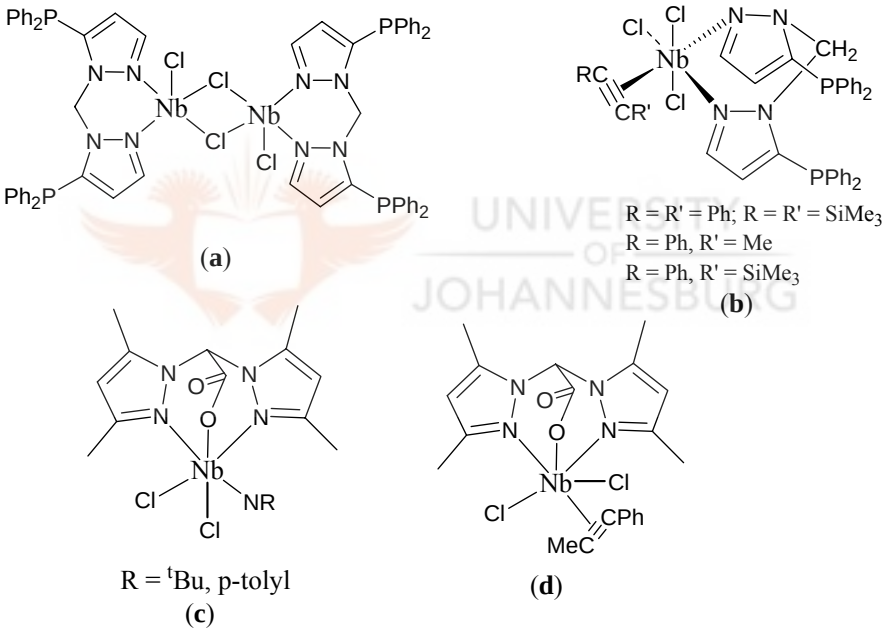

Figure 1.20. Structures of (**a**) [$NbCl_3${H_2C(5-PPh_2pz)$_2$}]$_2$, (**b**) [$NbCl_3${H_2C(5-PPh_2pz)$_2$}(RC=CR′)], (**c**) [Nb(NR)Cl_2(κ^3-bdmpza)], (**d**) [$NbCl_2$(κ^3-bdmpza)(PhC≡CMe)].

M., *Dalton Trans*., **2004**, 3963.

[85] Otero A., Fernandez-Baeza J., Tejeda J., Antinolo A., Carrillo-Hermosilla F., Diez-Barra E., Lara-Sanchez A., Fernandez-Lopez M., Lanfranchi M., Pellinghelli M. A., *J. Chem. Soc., Dalton Trans*., **1999**, 3537.

1.5.2. Manganese(II) and Rhenium(V) complexes

Group 7 metal complexes, having bis(pyrazolyl)alkanes as ligands, have also been reported.[86] The first manganese compound reported in the literature was $[Mn_2\{H_2C(3,5\text{-}Me_2pz)_2\}_4(\mu\text{-}F)_2][BF_4]_2$ in which the two manganese ions are bridged by fluorides (Fig. 1.21**a**). Recently the manganese complex, $[Mn(bdmpza)(CO)_3]$ ((Fig. 1.21**b**), was shown to have a tridentate *N*,*N*,*O*- coordination.[81] In $[Mn(bdmpza)(CO)_3]$, the bond distance of the Mn-CO *trans* to the carboxylic group of the bpzma ligand is relatively short in comparison to the other two Mn-CO distances. This is attributed to the carboxylate group of the ligand exerting less *trans* effect as opposed to the greater *trans* influence of the two pyrazolyl π acceptor groups on the other two metal-carbonyl bonds.

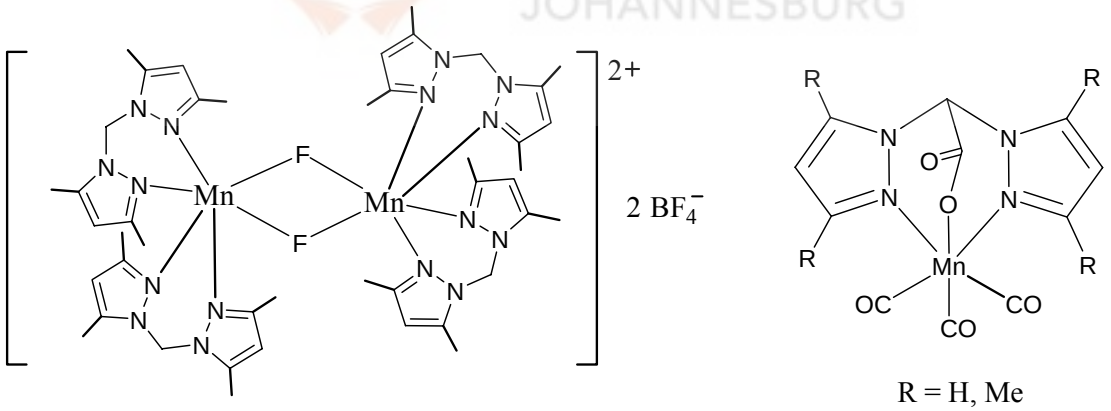

(**a**) (**b**)

Figure 1.21. (**a**) Structure of $[Mn_2\{H_2C(3,5\text{-}Me_2pz)_2\}_4F_2][BF_4]_2$, and (**b**)$[Mn(bdmpza)(CO)_3]$.

[86] Verbiest J., Van Ooijen J. A. C., Reedijk J., *Inorg. Nucl. Chem.*, **1980**, *42*, 971.

The bpzma ligand has also been used to prepare rhenium compounds. Porchia *et al*.[87] reported a new rhenium compound, [(Re(O)(bdmpza)Cl_2] (Fig. 1.22), which contains a stable mono-oxo rhenium core fragment, $[Re(O)(NNO)]^{2+}$. Complexes **a** and **b** (Fig. 1.22) are isomers with **a** having a Cl ion *trans* to the carboxylate moiety of the ligand, while **b** has O (Re=O) *trans* to the carboxylate moiety. The choice of bdmpza is not only because of its ability to stabilise the resultant rhenium complexes but also because it confers water solubility to the complexes. The rhenium complex, [(Re(O)(bdmpza)Cl_2], is of interest due to its possible biological application as a radiopharmaceutical.[88]

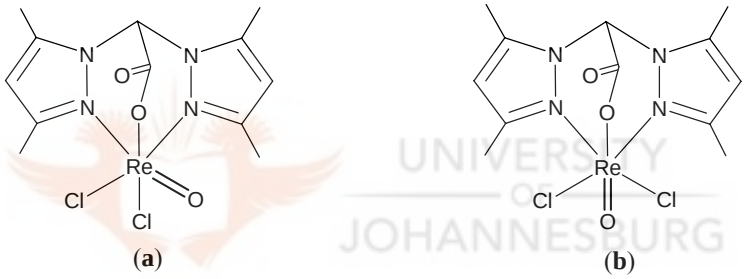

Figure 1.22. Structural isomers of [Re(O)(bdmpza)Cl_2].

1.5.3. Ruthenium complexes

Arene and cyclopentadienyl ruthenium(II) complexes, for example [(P-cymene)RuCl(PPh_3)$_2$] and [Ru(Cp)Cl(PPh_3)$_2$] (Cp = cyclopentadienyl; PPh_3 = triphenylphosphine), have been used for more than thirty years as a versatile starting material in organometallic reactions.[89,9091] Due to the similarity between Cp and

[87] Porchia M., Papini G., Santini C., Lobbia G. G., Pellei M., Tisato F., Bandoli G., Dolmella A., *Inorg. Chim. Acta*, **2006**, *359*, 2501.
[88] Dilworth J., Parrott S., *Chem. Soc. Rev*., **1998**, *27*, 43.
[89] [a]Bozec H. L., Touchard D., Dixneuf P. H., *Adv. Organomet. Chem*., **1989**, *29*, 163; [b]Govindaswamy P.,

hydrotris(pyrazol-1-yl)borato ligand (Tp), the complex [Ru(Tp)Cl(PPh_3)$_2$] has also been isolated.[92] Furthermore, because of the resemblance between Tp and bis(pyrazolyl) acetic acid (bpza), bpza has recently been used to prepare a stable ruthenium(III) complex, [Ru(bpza)(Cl)$_2$(PPh_3)] (Fig. 1.23). The compound exhibits a tridentate *N,N,O* coordination of the ligand, with the PPh_3 being *trans* to one of the pyrazolyl rings. However, there is no information on its application

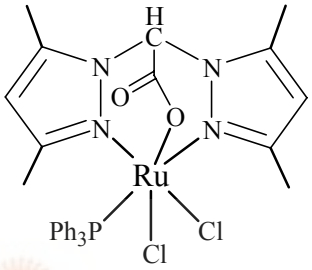

Figure 1.23. Structure of [Ru(bdmpza)Cl$_2$(PPh_3)].

1.5.4. Cobalt complexes

To the best of our knowledge, there are no known examples of cobalt complexes based on bis(pyrazolyl)acetic acid ligands, but a related ligand, tris(pyrazolyl)methane sulfonate ligands (Tpms) (Fig. 1.24**a**), has been used to prepare cobalt complexes as mimics for coenzymes related to vitamin B_{12}.[93] The Tpms ligand has also been used to mimic metalloenzymes called His-1-carboxylate enzymes,[94] which refers to mononuclear non-

---

Mozharivskyj A. Y., Kollipara M. R., *Polyhedron*, **2004**, *23*, 1567; [c]Govindaswamy P., Mozharivskyj A. Y., Kollipara M. R., *Polyhedron*, **2004**, *23*, 3115.

[90] Lopez-Hernandez A., Muller R., Kopf H., Burzlaff N., *Eur. J. Inorg. Chem*., **2002**, 671.

[91] Lopez-Hernandez A., Muller R., Kopf H., Burzlaff N., *Eur. J. Inorg. Chem*., **2002**, 671.

[92] Alcock N. W., Burn I. D., Claire K. S., Hill A. F., *Inorg. Chem*., **1992**, *31*, 2906.

[93] Parkin G., *Chem. Rev*., **2004**, *104*, 699.

[94] Papish E. T., Taylor M. T., Jernigan F. E., Rodig M. J., Shawhan R. R., Yap G. P. A., Jove F. A., *Inorg. Chem*., **2006**, *45*, 2242.

heme iron(II) enzymes responsible for various metabolic process, e.g. biosynthesis of antibiotics.[95] Reactions of Tpms with $Co(NO_3)_2.6H_2O$ gives $[Co(Tpms)_2]$ (Fig. 1.24**a**). Coordination of Tpms to cobalt(II) ion is through *N,N,O*- ligating end to give $[Co(Tpms)_2]$ (Fig. 1.24**b**). Compound $[Co(Tpms)_2]$ shows a distorted octahedral geometry. Other similar cobalt(II) complexes utilising pyrazolyl ligands include $[CoCl_2\mathbf{L}]$ (**L** = bidentate N-donor (2-propargyloxyphenyl)bis(pyrazolyl)methane) (Fig. 1.24**c**).[96] The structure of $[CoCl_2\mathbf{L}]$ is a five-coordinate complex consisting of a chloro-bridged dimer of $[CoCl_2\mathbf{L}]$ units. The coordination around each metal ion is a distorted trigonal bipyramid. While there is no known native occurrence of cobalt(II) enzymes, cobalt has been used for preparation of mimics of several enzymes.[93,94] because of its spectroscopic properties that make it an important structural and functional probe with respect to enzymes functions.[97]

[95] Hegg E. L., Que Jr. L., *Eur. J. Biochem*., **1997**, *250*, 625.
[96] Mohr F., Cerrada E., Laguna M., *Dalton Trans*., **2006**, 5567
[97] Maret W., Vallee B. L., *Methods Enzymol*., **1993**, 226, 52.

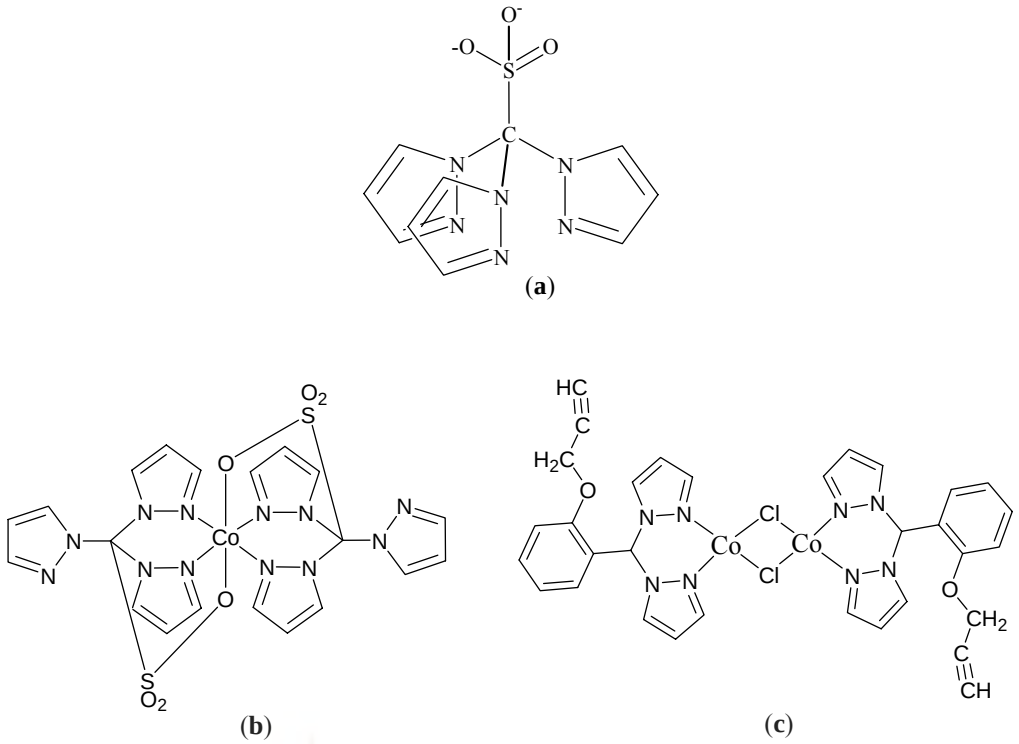

Figure 1.24. (**a**) Tris(pyrazolyl)methane sulfonate (Tpms), (**b**) $[Co(Tpms)_2]$, (**c**) $[CoCl_2\mathbf{L}]$ (**L** = bidentate N-donor (2-propargyloxyphenyl)-bis(pyrazolyl)methane).

1.5.5. Palladium, platinum and gold complexes

For the group 10 and 11 metals, complexes of bis(pyrazolyl)acetic acid ligands did not exist before the work reported in this thesis. Nonetheless, palladium compounds of other bis(pyrazolyl)alkanes ($R_2C(pz)_2$, R = H, Me) have been prepared and investigated as catalysts for polymerization.[98] Coordination of $R_2C(pz)_2$ to palladium leads to formation of stable six-membered metallacycles that adopt a boat conformation such as in $[PdCl_2\{Me_2C(pz)_2\}]$ (Fig. 1.25**a**). The observed agostic interaction further stabilises these palladium complexes. Despite the stability displayed by these pyrazolyl palladium(II) compounds, there are no reports on their biological activities.

[98] Tsuji S., Swenson D. C., Jordan R. F., *Organometallics*, **1999**, *18*, 4758.

Structural studies of neutral $[PdCl_2\{H_2C(pz)_2\}]$, $[PdCl_2\{H_2C(3,5\text{-}Me_2pz)_2\}]$ and $[PdCl_2\{Me_2C(pz)_2\}]$ and the cationic species $[Pd\{H_2C(pz)_2\}_2]^{2+}$, $[Pd\{H_2C(3,5\text{-}Me_2pz)_2\}]^{2+}$ and $[Pd\{Me_2C(pz)_2\}_2]^{2+}$ (Figs. 1.25**b** and **c**) display weak Pd…H-C (agostic) as reported by Minghetti and co-workers.[99] These agostic interactions make the complexes quite stable.

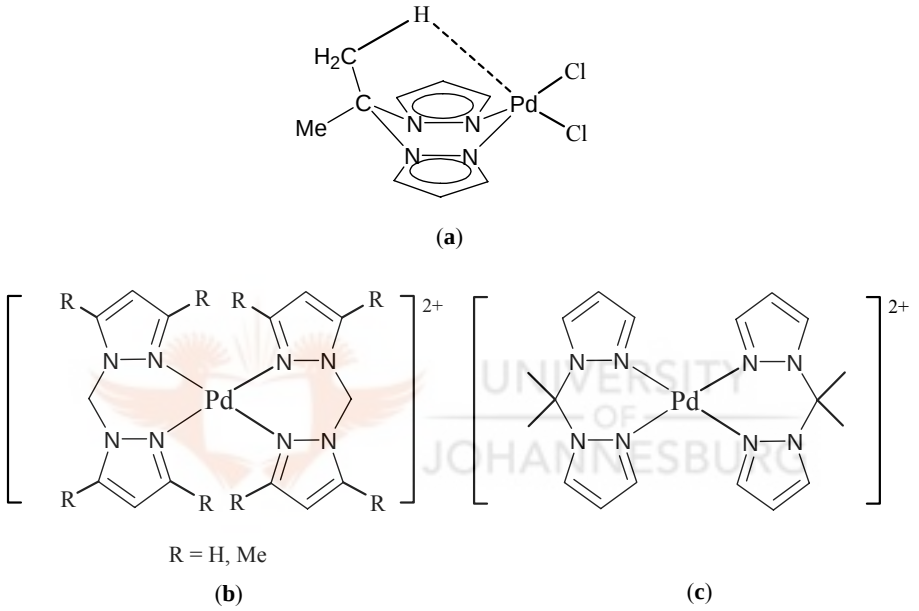

Figure 1.25. (**a**) Six-membered palladacycle $[PdCl_2\{Me_2C(pz)_2\}_2]$, (**b**) $[Pd\{H_2C(3,5\text{-}R_2pz)_2\}_2]^{2+}$, (**c**) $[Pd\{Me_2C(pz)_2\}_2]^{2+}$.

Stable platinum(II) complexes of bis(pyrazolyl)alkanes ligands have also been reported and include the neutral complexes, $[PtCl_2\{H_2C(3,5\text{-}R_2pz)_2\}]$ (R = H, Me) (Fig. 1.26).[99] They have distorted square-planar geometry with the proton (H_{endo}) of the bridging methylene in close proximity to the metal centre with a boat conformation of the

[99] Minghetti G., Cinellu M. A., Bandini A. L., Banditelli G., De Martin F., Manassero M., *J. Organomet. Chem*., **1986**, *315*, 387.

metallacycle. However, there are no reports of the biological activities of these platinum(II) complexes.

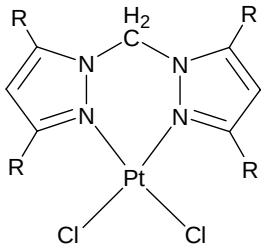

R = H, Me

Figure 1.26. Structure of $[PtCl_2\{H_2C(3,5\text{-}R_2pz)_2\}]$.

Similarly, platinum(IV) complexes of bis(pyrazolyl)alkanes are known.[100] Examples include $[Pt^{(IV)}I_2Me_2(R)HC(pz)_2]$ complexes (R = py, thi; py = pyridine, thi = thiophene) shown in Figure 1.27. It was expected that $[Pt^{(IV)}I_2Me_2(thi)HC(pz)_2]$ would exhibit a tridentate coordination mode because of the sulfur atom in thiophine (Fig 1.27). However, that was not the case as the structural investigations showed that the ligand coordinates to the platinum metal in a bidentate fashion through the *N*,*N*-chelating end.[100] This is possibly due to the S-donor atom having its coordination ability reduced by the π-electron system of the thiophene. Other examples of bis(pyrazolyl)alkane platinum(IV) complexes include $[PtX_2Me_2\{R_2C(pz^*)_2\}]$ (X = I or NO_3; $R_2C(pz^*)_2$ = $H_2C(pz)_2$, $Me_2C(pz)_2$, $H_2C(3,5\text{-}Me_2pz)_2$) (Fig. 1.27) reported by Clark *et al*.[101]

[100] Canty A. J., Honeyman R. T., Skelton B. W., White A. H., *J. Organomet. Chem*., **1990**, *396*, 105.
[101] Clark H. C., Ferguson G., Jain V. K., Parvez M., *J. Organomet. Chem*., **1984**, *270*, 365.

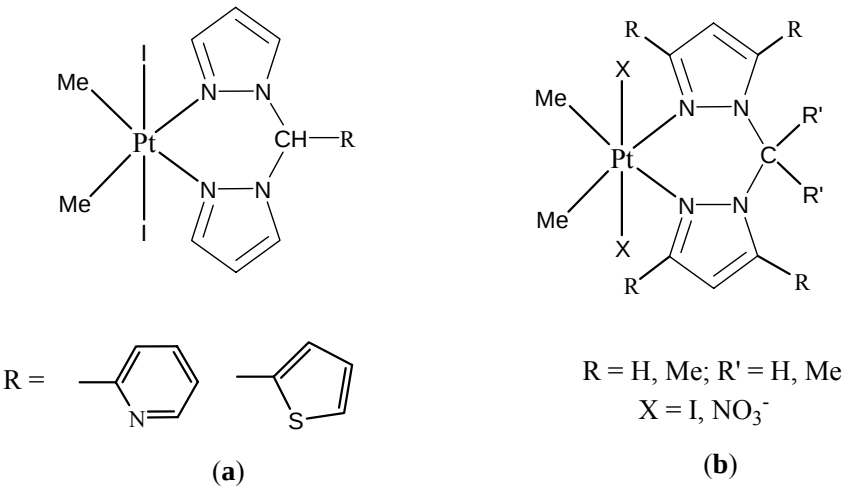

Figure 1.27. Structure of (**a**) $[Pt^{(IV)}I_2Me_2(R)HC(pz)_2]$, (**b**) $[PtX_2Me_2\{R_2C(pz^*)_2\}]$.

As far as group 11 metals are concerned, gold(III) is gaining popularity in cancer research because of its isoelectronic and isostructural similarities to platinum(II) complexes. Gold(III) complexes utilising poly(pyrazolyl)alkanes as ligands are quite rare. In fact the only gold compound described in literature is the cationic $[Au(Me)_2\{H_2C(3,5\text{-}Me_2pz)_2\}][NO_3]$ (Fig. 1.28), which has never been structurally characterised.[102] Its structural proposition is based on the closely related gold(III) analogue utilising tri-pyrazolylmethane (tpzm), which displays a N^N coordination mode to give $[Au(Me)_2(N\text{-}N)]^+$.

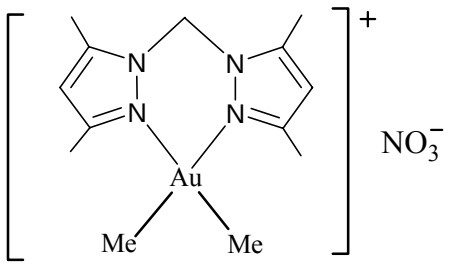

Figure 1.28. Cationic gold(III) complex, $[Au(Me)_2\{H_2C(3,5\text{-}Me_2pz)_2\}][NO_3]$.

[102] Canty A. J., Minchin N. J., Healy P. C., White A. H., *J. Chem. Soc., Dalton Trans.*, **1982**, 1795.

1.6. Aims of this study

From the extensive overview above on bis(pyrazolyl) ligands and their complexation to various transition metals, it is clear that these ligands lead to isolation of stable metal complexes. Owing to the interest in developing new metal compounds as anticancer drugs, the aim was to prepare palladium(II), platinum(II) and gold(III) complexes by utilising bis(pyrazolyl)acetic acid (R_2bpza) compounds as ligands because of their potential water solubility and flexible coordination. In addition, σ-donor ability of such ligands was expected to stabilise gold(III) compounds. The choice of gold(III) emanates from the fact that this ion gives rise to complexes that are isoelectronic and isostructural with those of platinum(II), whose antitumour activity is well established. The expected coordination of the bis(pyrazolyl)acetic acid to palladium(II), platinum(II), and gold(III), would give compounds that are closely related to cisplatin. This is not to insinuate that the biological activities would be the same. It is also worth mentioning that the bis(pyrazolyl)acetic acid gold(III) complexes prepared in this thesis, are the second examples of gold(III) complexes of bis(pyrazolyl)alkanes after $[Au(Me)_2\{H_2C(3,5\text{-}Me_2pz)_2\}][NO_3]$ described earlier (*vide supra*).[102] Furthermore, by using bis(pyrazolyl)acetic acid ligands it is shown that these ligands are able to stabilise both palladium(II) and gold(III) enough to allow the kinetics of their substitution reactions with L-cysteine to be studied.

Owing to the insignificant biological activities observed with the new palladium(II), platinum(II) and gold(III) complexes reported in this thesis, a second initiative involving

the use of bis(pyrazolyl) dithioic acid ligands, was pursued. However, attempts to prepare gold(III) complexes from this type of ligand were unsuccessful as the resultant gold(III) complexes readily decomposed. As a result of this, no further attempts were made to isolate the palladium(II) and platinum(II) analogues either. Nonetheless, further exploration of dithiocarbamate (dtc) as ligands for synthesising gold(I) complexes, was pursued. Bearing in mind that the scope of this thesis included preparation of gold(I) complexes, the use of these dtc ligands led to isolation of several mononuclear and dinuclear gold(I) complexes, which are reported in this thesis.

CHAPTER 2

BIS(PYRAZOLYL)ACETIC ACID COMPLEXES OF PALLADIUM(II), PLATINUM(II) AND GOLD(III)

*X-ray structures **L4**, **1**, **3b**, and **5b** were solved by Dr. Guzei and Mrs. Spencer both of Wisconsin University (USA), whilst X-ray structure of **2** was solved by the candidate and Dr. Omondi (University of Johannesburg). The crystal structure discussions are the sole work of the candidate except for **3b**, where Dr. Guzei helped with the discussion.*

2.0 Introduction

Substituted pyrazoles constitute an important family of heterocyclic compounds that have found use in drug development and catalysis.[1] Thus there is considerable interest in the synthesis of pyrazole-based ligands e.g. bis(pyrazolyl)alkanes. Pyrazole-based ligands are remarkably versatile sources of coordination ligands.[2,3] Research on pyrazole-derived ligands has focused on models of metalloproteins and the applications of pyrazolylborates as ligands in coordination chemistry. The appeal of pyrazole and its derivatives is the opportunity it offers to alter steric, electronic and solubility properties of the resultant complexes. It is for this reason that pyrazoles continue to be an important class of ligands in the syntheses of several metal complexes.

[1] Elguero J., *Comprehensive Hetercyclic Chemistry II: Pyrazoles,* vol. 3, edited by Katrizky A. R., Rees C. W., Scriven E. F. V., **1993**, 1-75.
[2] Trofimenko S., *Chem. Rev*., **1972**, *72*, 492.
[3] Esquius G., Pons J., Yanez R., Ros J., Solans X., Font-Bardia M., *J. Organomet. Chem*., **2000**, *605*, 226.

The ease with which substituted pyrazoles could be achieved is also an added advantage. This is evident from the extensive overview on the bis(pyrazolyl)alkane ligands (Chapter 1). In this study, pyrazole and 3,5-dimethylpyrazole were used to prepare water soluble bis(pyrazolyl)acetic acid (**L1**) and bis(3,5-dimethylpyrazolyl) acetic acid (**L2**) ligands. Subsequently, palladium(II), platinum(II) and gold(III) complexes were prepared by reacting ligands **L1** and **L2** with the respective metal salts. The results are systematically reported in the following sections. Schemes 2.1 and 2.2 below show ligands and various metal complexes reported in this thesis.

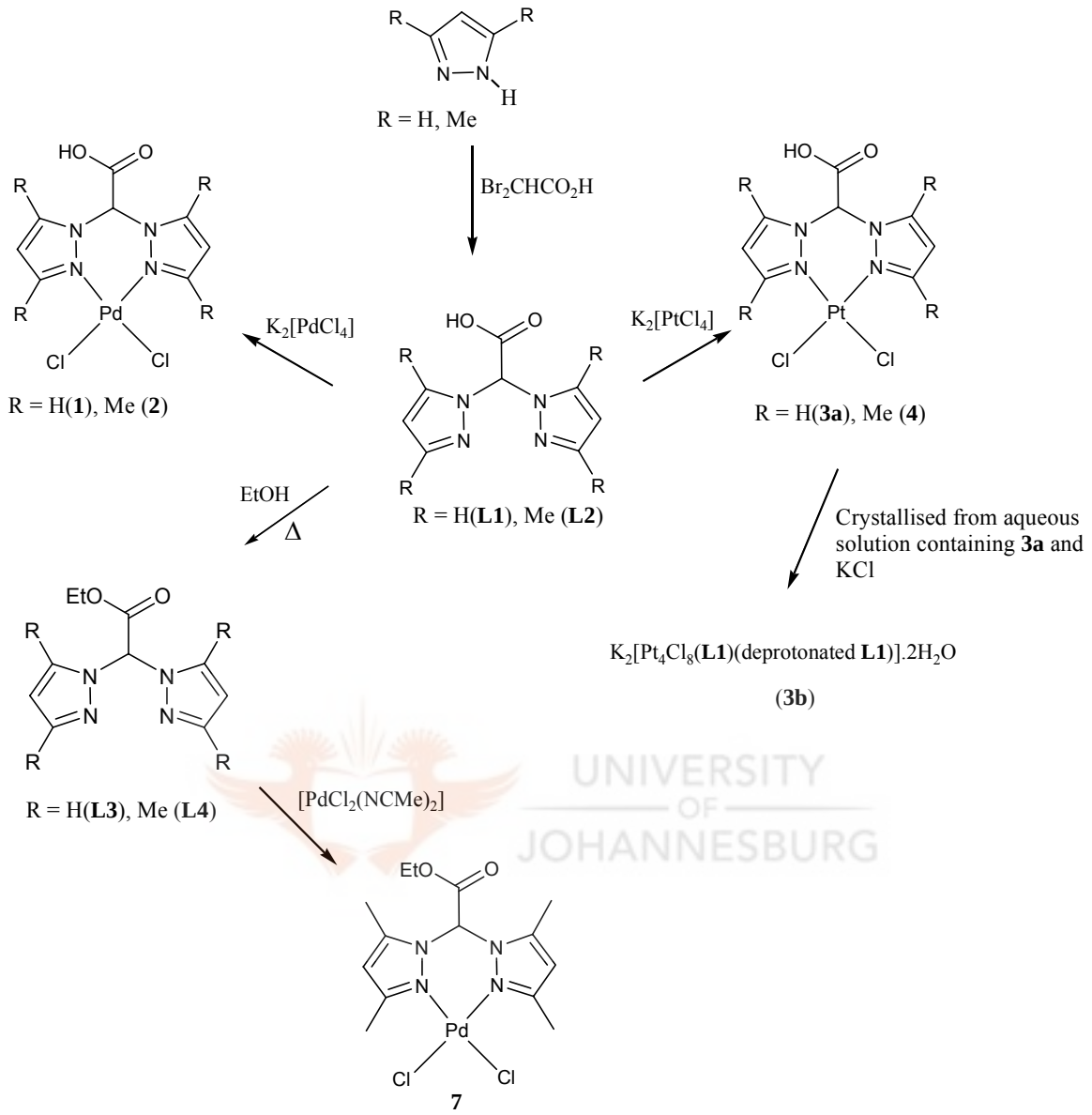

Scheme 2.1. Preparation of palladium(II) and platinum(II) complexes **1**-**4** and **7**.

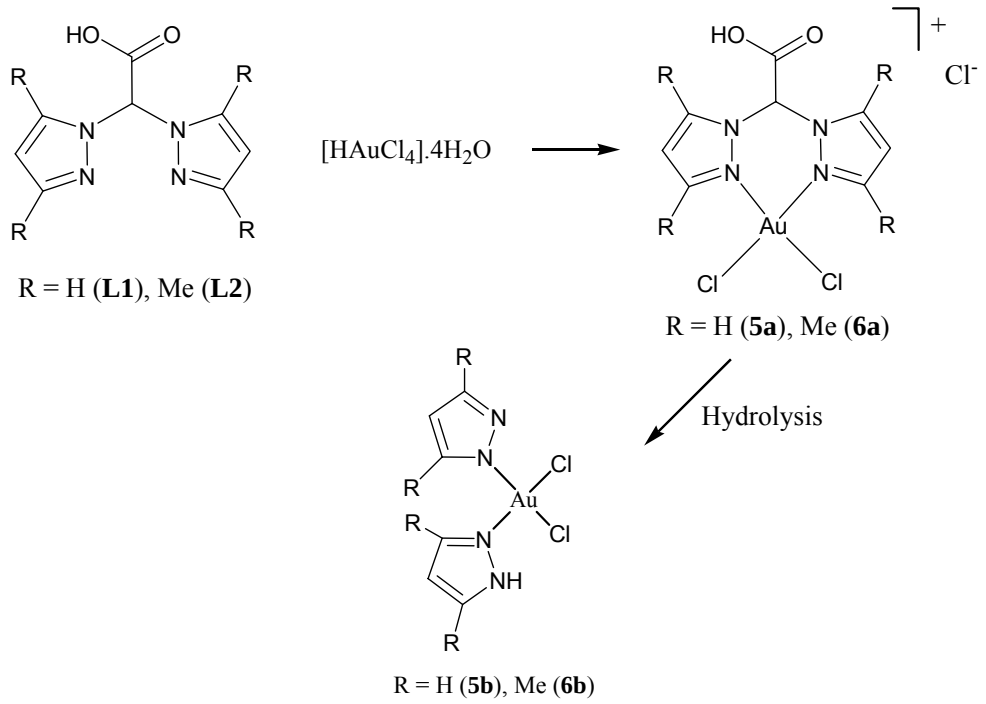

R = H (**L1**), Me (**L2**)

R = H (**5a**), Me (**6a**)

R = H (**5b**), Me (**6b**)

Scheme 2.2. Shows preparation of gold(III) complexes **5a** and **6a** and the hydrolysis products **5b** and **6b**.

2.1. Experimental

2.1.1. Materials and Instrumentation

All commercial chemicals other than those described below were used as received. $K_2[PtCl_4]$, $K_2[PdCl_4]$, pyrazole, 3,5-dimethylpyrazole, KOH, K_2CO_3, $NaHCO_3$, $MgSO_4$, dibromoacetic acid and L-cysteine were purchased from Sigma-Aldrich and used without further purification. Bis(pyrazolyl)acetic acid (**L1**) and bis(3,5-dimethylpyrazolyl)acetic acid (**L2**) were synthesised according to the literature procedures with minor modifications.[4] The palladium and gold starting materials, $[PdCl_2(NCMe)_2]$[5] and

[4] Burzlaff N., Hegelmann I., Weibert B., *J. Organomet. Chem*., **2001**, *626*, 16.
[5] King B. R., Eisch J. J., *Organometallic syntheses*. Elsevier Science Publishers B. V., New York, **1986**, *3*, 324.

$[HAuCl_4].4H_2O$,[6] were synthesised according to the literature procedures. All the solvents were also purchased from Sigma-Aldrich and dried using conventional methods. Tetrahydrofuran (THF) and diethylether (Et_2O) were dried over sodium with sodium benzoate as an indicator, while dichloromethane (CH_2Cl_2) was dried over phosphorous pentoxide with sodium benzoate as an indicator. The water used was double distilled. All manipulations of air-and/or moisture sensitive compounds were performed under dry, deoxygenated nitrogen atmosphere using Schlenk techniques.

IR spectra were recorded as nujol mulls using NaCl cells and some as KBr pellets on a Perkin-Elmer, paragon 1000 PC FTIR spectrophotometer. ^1H and $^{13}C\{^1H\}$ NMR spectra were recorded on a Gemini 2000 instrument (^1H, 200 MHz and ^{13}C, 50.3 MHz) and a Bruker Avance DPX 300 spectrometer (^1H, 300 MHz) in $CDCl_3$ and DMSO-d_6 at room temperature. ^1H and ^{13}C chemical shifts were referenced to the signals of the residual protons of the NMR solvents and are quoted in ppm as follows; (i) $CDCl_3$ at 7.26 and 77.0 ppm for ^1H and ^{13}C respectively and (ii) for DMSO-d_6 at 2.50 and 39.9 ppm for ^1H and ^{13}C respectively. Elemental analyses were performed on a Fisons elemental analyser at the University of Cape Town, South Africa. ESI-MS spectra were recorded on a Waters API Quattro Micro spectrotometer at the University of Stellenbosch, South Africa. The spectra were collected using 3.0 s cyclical scans and applying the sample cone voltage of 15 V at the source block temperature of 100 ^oC. Desolvation temperature was 350 ^oC and desolvation cone gas flow rate 350L/h.

[6] Block B. P., *Inorg. Synth*., **1953**, *4*, 14.

2.1.2. Synthesis of ligands and metal complexes

*2.1.2.1. Bis(pyrazol-1-yl)acetic acid (**L1**)*

To a solution of KOH (1.43 g, 25 mmol) and K_2CO_3 (3.46 g, 25 mmol) in THF (100 mL) was added dibromoacetic acid (1.92 g, 8.81 mmol) and pyrazole (1.20 g, 17 mmol). Benzyltriethylammonium chloride (1.00g, 4.40 mmol) was added to the solution as a phase transfer catalyst and the mixture refluxed for 15 h. The solvent was then removed and the residue re-dissolved in 25 mL of water. The pH of the resultant solution was then adjusted to 7 using conc HCl and unreacted pyrazole removed by extraction with Et_2O (25 mL). The pH of the aqueous phase was further adjusted to 2 and **L1** extracted with Et_2O (25 mL) three times. Subsequently **L1** was recrystallised from Et_2O/acetone mixture. Yield = 1.01 g (60%). ^{1}H NMR (DMSO-d_6, 200 MHz): δ = 7.98 (d, 2H, $^3J_{HH}$ = 2.20 Hz, 5-pz); 7.59 (d, 2H, $^3J_{HH}$ = 2.21 Hz, 3-pz); 7.57(s, 1H, C<u>H</u>CO_2H); 6.35 (s, 2H, 4-pz). $^{13}C\{^1H\}$ NMR (DMSO-d_6, 200 MHz): 166.2 (C(C=O)); 142.3 (C(3-pz); 131.0 (C(4-pz)); 106.1 (C(5-pz)); 73.2 (C(<u>C</u>HCO_2H)). IR (Nujol, cm^{-1}): υ_{O-H} = 3439, $\upsilon_{C=O}$ = 1720, $\upsilon_{C=N}$ = 1509. Anal. Calc. for $C_8H_8N_4O_2$: C, 50.00; H, 4.20; N, 29.15%. Found: C, 49.95; H, 3.94; N, 28.59%.

*2.1.2.2. Bis(3,5-dimethylpyrazol-1-yl)acetic acid (**L2**)*

The synthesis of **L2** was performed in a similar manner as described for **L1** using KOH (1.78 g, 31.26 mmol); K_2CO_3 (4.32 g, 31.26 mmol); dibromoacetic acid (2.27 g, 10.42 mmol); 3,5-dimethylpyrazole (2.00 g, 20.83 mmol); benzyltriethylammonium chloride (1.00g, 4.40 mmol). Yield = 1.83 g (71%). ^{1}H NMR (DMSO- d_6, 200 MHz): δ = 7.13 (s, 1H, C<u>H</u>CO_2H); 5.86 (s, 2H, 4-pz); 2.17 (d, 12H, $^6J_{HH}$ = 20.8 Hz, 5-pz, 3-pz). $^{13}C\{^1H\}$

NMR (DMSO- d_6, 200 MHz): 165.9 (C(C=O)); 146.8 (C(3-pz); 140.5 (C(4-pz)); 106.4 (C(5-pz)); 71.4 (C(CHCO$_2$H)); 13.2 (C(CH$_3$, 5-pz)); 10.8 (C(CH$_3$, 3-pz)). IR (Nujol cm^{-1}): υ_{O-H} = 3402, $\upsilon_{C=O}$ = 1743, $\upsilon_{C=N}$ = 1558. Anal. Calc. for $C_{12}H_{16}N_4O_2$.0.5 H_2O: C, 56.02; H, 6.61; N, 21.78%. Found: C, 55.71; H, 5.75; N, 20.92%.

*2.1.2.3. Bis(pyrazol-1-yl)ethyl acetate (**L3**).*

Compound **L1** (0.50 g, 2.60 mmol) was refluxed in excess ethanol (40 mL) under acidic conditions (HCl, 5 mL) for 18 h. The mixture was cooled to room temperature and 50 mL of deionised water added after which the pH was adjusted to 11 by adding $NaHCO_3$. The product was extracted with dichloromethane (50 mL) and dried over $MgSO_4$. The solvent was then removed *in vacuo* to afford an analytically pure white crystalline **L3**. Yield = 0.33 g (58%). ^{1}H NMR ($CDCl_3$, 200 MHz): δ 7.74 (d, 2H, pz, $^3J_{HH}$ = 2.2 Hz); 7.59 (t, 2H, pz, $^3J_{HH}$ = 1.6 Hz,); 7.10 (s, CH, 1H, pz,); 6.33 (t, 2H, pz $^2J_{HH}$ = 1.8 Hz); 4.34 (q 2H, CH$_2$CH$_3$, $^3J_{HH}$ = 7.4 Hz); 1.26 (t, 3H, CH$_2$CH$_3$, $^3J_{HH}$ = 7.4 Hz). ^{13}C{^{1}H}NMR ($CDCl_3$, 200 MHz): δ 163.8 (C(C=O)); 140.4 (C(5-pz); 129.6 (C(3-pz)); 106.8 (C(4-pz)); 74.1 (C(CHCO$_2$CH$_2$CH$_3$)); 62.7 (C(CH$_2$, CH$_2$CH$_3$)); 13.4 (C(CH$_3$, CH$_2$CH$_3$)). IR (Nujol cm^{-1}): $\upsilon_{C=O}$ = 1750. Anal. Calc. for $C_{10}H_{12}N_4O_2$: C, 54.54; H, 5.49; N, 25.44%. Found: C, 54.36; H, 5.75; N, 25.09%.

*2.1.2.4. Bis(3,5-dimethylpyrazol-1-yl)ethyl acetate (**L4**).*

The synthesis of compound **L4** was performed in a similar manner as described for **L3** using **L2** (1.50 g, 6.05 mmol). Yield = 0.90 g (54%). ^{1}H NMR ($CDCl_3$, 300 MHz): δ 6.91 (s, CH, 1H, pz); 5.84 (s, 1H, pz); 4.36 (q, 2H, CH$_2$CH$_3$, $^3J_{HH}$ = 8.1 Hz); 2.19 (s, 6H, CH$_3$,

5-pz); 2.11 (s, 6H, CH_3, 3-pz); 1.30 (t, 3H, $CH_2C\underline{H}_3$, $^3J_{HH}$ = 7.8 Hz). $^{13}C\{^1H\}$NMR ($CDCl_3$, 200 MHz): δ 166.1 (C(C=O)); 147.0 (C(5-pz); 140.8 (C(3-pz)); 106.6 (C(4-pz)); 71.7 (C($\underline{C}HCO_2CH_2CH_3$)); 63.2 (C($\underline{C}H_2CH_3$)); 13.4 (C($CH_2\underline{C}H_3$)); 12.8 (C($\underline{C}H_3$, 5-pz)); 11.0 (C($\underline{C}H_3$, 3-pz)). IR (Nujol cm^{-1}): $\upsilon_{C=O}$ = 1735. Anal. Calc. for $C_{14}H_{20}N_4O_2$: C, 60.85; H, 7.30; N, 20.28%. Found: C, 60.76; H, 7.55; N, 19.98%.

*2.1.2.5. Dichloro-{bis(pyrazol-1-yl)acetic acid}palladium(II) (**1**).*

To a yellow solution of $K_2[PdCl_4]$ (0.17 g, 0.52 mmol) in distilled water (15 mL), was added **L1** (0.10 g, 0.52 mmol) and the mixture stirred vigorously at room temperature. After 1.5 h, a colour change from a yellow solution to an orange suspension was observed and further stirring for 3 h resulted in the formation of a yellow precipitate. The precipitate was isolated by filtration and washed with ethanol to afford pure **1**. Yield = 0.15 g; (75%). ^1H NMR (DMSO-d_6, 300 MHz): δ 8.29 (d, 2H, $^2J_{HH}$ = 1.8 Hz, 5-pz); 8.14 (s, 1H, C$\underline{H}CO_2H$) 8.02 (d, 2H, $^2J_{HH}$ = 1.8 Hz, 3-pz); 6.63 (t, 2H, $^2J_{HH}$ = 2.6 Hz, 4-pz). $^{13}C\{^1H\}$ NMR (DMSO-d_6, 300 MHz): δ 164.9 (C(C=O)); 144.4 (C(5-pz); 136.9 (C(3-pz)); 108.0 (C(4-pz)); 72.2 (C($\underline{C}HCO_2H$)). IR (Nujol cm^{-1}): υ_{O-H} = 3441, $\upsilon_{C=O}$ = 1738. Anal. Calc. for $C_8H_8Cl_2N_4O_2Pd$: C, 26.00; H, 2.18; N, 15.16%. Found: C, 26.34; H, 2.22; N, 15.20%.

*2.1.2.6. Dichloro-{bis(3,5-dimethylpyrazol-1-yl)acetic acid}palladium(II) (**2**).*

The synthesis of **2** was performed in a similar manner as described for **1** using **L2** (0.10 g, 0.40 mmol) and $K_2[PdCl_4]$ (0.13 g, 0.40 mmol). Yield = 0.10 g; (63%). ^1H NMR (DMSO-d_6, 300 MHz): δ 7.59 (s, 1H, C$\underline{H}CO_2H$); 6.23 (s, 2H, 4-pz); 2.58 (s, 6H, 5-pz);

2.51 (s, 6H, 3-pz). $^{13}C\{^{1}H\}$ NMR (DMSO-d_6, 300 MHz): δ 165.3 (C(C=O)); 149.2 (C(5-pz); 145.7 (C(3-pz)); 106.2 (C(4-pz)); 72.6 (C($\underline{C}HCO_2H$)); 13.6 (C(3-CH_3)); 12.9 (C(5-CH_3)). IR (Nujol cm^{-1}): υ_{O-H} = 3410, $\upsilon_{C=O}$ = 1756. Anal. Calc. for $C_{12}H_{16}Cl_2N_4O_2Pd.0.5CH_2Cl_2$: C, 32.25; H, 3.23; N, 12.04%. Found: C, 32.27; H, 3.41; N, 12.25%.

*2.1.2.7. Dichloro-{bis(pyrazol-1-yl)acetic acid}platinum(II) (**3a**)*

To a red solution of $K_2[PtCl_4]$ (0.43 g, 1.00 mmol) in distilled water (15 mL), was added **L1** (0.20 g, 1.00 mmol) and the mixture stirred vigorously at room temperature. After 2 h a colour change from red solution to orange suspension was observed and further stirring resulted in the formation of a yellow precipitate. The precipitate was isolated by filtration as pure **3a**. The filtrate left to stand for 1 day upon which golden yellow single crystals of **3b** suitable for X-ray analysis were formed. Yield: **3a** = 0.25 g (52%). ^{1}H NMR (DMSO - d_6, 300 MHz): δ 8.34 (d, 2H, $^{3}J_{HH}$ = 2.20 Hz, 5-pz); 8.12 (d, 2H, $^{3}J_{HH}$ = 4.80 Hz, 3-pz); 7.96 (s, 1H, C$\underline{H}CO_2H$); 6.65 (s, 2H, 4-pz). $^{13}C\{^{1}H\}$ NMR (DMSO-d_6, 300 MHz): δ 166.8 (C(C=O)); 140.1 (C(5-pz); 132.1 (C(3-pz)); 106.5 (C(4-pz)); 73.9 (C($\underline{C}HCO_2H$)). IR (Nujol, cm^{-1}): υ_{O-H} = 3460, $\upsilon_{C=O}$ = 1763, $\upsilon_{C=N}$ = 1517. ESI-MS: m/z 457 (10%) $[PtCl_2(bpza)]^+$ (10%), m/z 490 $[PtCl_2(bpza)+Na]^+$ (20%). Anal. Calc. for **3a**, $C_8H_8Cl_2N_4O_2Pt$: C, 20.97; H, 1.76; N, 12.23%. Found: C, 20.67; H, 1.60; N, 12.29%.

*2.1.2.8. $K_2[Pt_4Cl_8$(**L1**)$_2$(deprotonated **L1**)$_2$].2H_2O (**3b**)*

After isolation of **3a**, the filtrate was left to stand for 1 day upon which golden yellow single crystals of **3b** suitable for X-ray analysis were formed. Yield: = 0.05 g (11%).

Anal. Calc. for **3b,** $K_2[C_{32}H_{34}Cl_8N_{16}O_{10}Pt_4]$: C, 19.76; H, 1.76; N, 11.52%. Found: C, 19.68; H, 1.65; N, 11.89%.

*2.1.2.9. Dichloro-{bis(3,5-dimethylpyrazol-1-yl)acetic acid}platinum(II) (**4**).*

The synthesis of **4** was performed in a similar manner as described for **3**, but reaction time was longer (15 h). $K_2[PtCl_4]$ (0.37 g, 0.81 mmol) and bis(3,5-dimethylpyrazol-1-yl)acetic acid (0.20g, 0.81 mmol). Yield: 0.38 g (75%). ^{1}H NMR (DMSO-d_6, 300 MHz): δ 7.13 (s, 1H, C<u>H</u>CO_2H); 5.86 (s, 2H, 4-pz); 2.17 (s, 6H, 5-pz); 2.07 (s, 6H, 3-pz). ^{13}C{^{1}H} NMR (DMSO-d_6, 300 MHz): δ 165.9 (C(C=O)); 146.8 (C(5-pz); 140.5 (C(3-pz)); 106.4 (C(4-pz)); 71.4 (C(<u>C</u>HCO_2H)); 13.2 (C(3-CH_3)); 10.8 (C(5-CH_3)). IR (Nujol cm^{-1}): υ_{O-H} = 3439, $\upsilon_{C=O}$ = 1743, $\upsilon_{C=N}$ = 1560. ESI-MS: m/z 519 [$PtCl_2$(3,5-Me_2bpza)]$^+$ (10%). Anal. Calc. for $C_{12}H_{14}Cl_2N_4O_2Pt$: C, 28.03; H, 3.14; N, 10.89%. Found: C, 27.72; H, 3.25; N, 10.80%.

*2.1.2.10. Dichloro-{bis(pyrazol-1-yl)acetic acid}gold(III) chloride (**5a**).*

To a solution of $[HAuCl_4].4H_2O$ (0.18 g, 0.52 mmol) in distilled water (10 mL) was added **L1** (0.10 g, 0.52 mmol) resulting in the immediate formation of a yellow precipitate. The reaction mixture was stirred for 45 min at room temperature. The product was isolated by filtration and dried *in vacuo*. Yield: 0.15 g (63%). ^{1}H NMR (DMSO-d_6, 300 MHz): δ 8.47 (m, 4H, 3-pz,5-pz); 8.11 (1H, C<u>H</u>CO_2H); 6.95 (m, 2H, 4-pz). ^{13}C{^{1}H} NMR (DMSO-d_6, 300 MHz): 174.3 (C(C=O)); 149.4 (C(5-pz); 140.2 (C(3-pz)); 115.9 (C(4-pz)); 83.2 (C(<u>C</u>HCO_2H)). IR (KBr, cm^{-1}): υ_{O-H} = 3492, $\upsilon_{C=O}$ = 1761, $\upsilon_{C=N}$ = 1509.

ESI-MS: m/z 463 $[AuCl_2(bpza)]^+$ (5%). Anal. Calc. for $C_8H_8Cl_3N_4O_2Au$: C, 24.39; H, 2.52; N, 9.42 %. Found: C, 24.53; H, 2.87; N, 9.53 %.

*2.1.2.11. Dichloro-{bis(3,5-dimethylpyrazolyl)acetic acid}gold(III) chloride (**6a**).*

The synthesis of **6a** was performed in a similar manner as described for **5a** using $[HAuCl_4].4H_2O$ (0.10 g, 0.30 mmol) and bis(3,5-dimethylpyrazol-1-yl)acetic acid (0.07 g, 0.30 mmol). Yield: 0.09 g (59%). ^{1}H NMR (DMSO-d_6, 300 MHz): δ 7.15 (s, 1H, C<u>H</u>CO_2H); 5.88 (s, 2H, 4-pz); 2.18 (s, 6H, 5-pz); 2.08(s, 6H, 3-pz). $^{13}C\{^1H\}$ NMR (DMSO-d_6, 300 MHz): 165.8 (C(C=O)); 146.9 (C(3-pz); 140.6 (C(4-pz)); 106.4 (C(5-pz)); 71.1 (C(<u>C</u>HCO$_2$H)); 13.1 (C(3-CH_3)); 10.7 (C(5-CH_3)). IR (KBr cm^{-1}): υ_{O-H} = 3451, $\upsilon_{C=O}$ = 1765, $\upsilon_{C=N}$ = 1518. ESI-MS: m/z 519 $[AuCl_2(3,5Me_2bpza)]^+$ (5%). Anal. Calc. for $C_{12}H_{14}Cl_3N_4O_2Au$: C, 26.13; H, 2.92; N, 10.16%. Found: C, 25.70; H, 3.06; N, 9.99%.

*2.1.2.12. Dichloro-{bis(3,5-dimethylpyrazol-1-yl)ethyl acetate}palladium(II) (**7**).*

Compound **7** was prepared by suspending **L4** (0.51 g, 1.80 mmol) in CH_2Cl_2 (20 mL) for 3 min after which it dissolved. $[PdCl_2(NCMe)_2]$ (0.47 g, 1.80 mmol) was then added and the mixture stirred for 6 h upon which a yellow precipitate was formed. The precipitate was filtered, washed with minimum amount of ethanol and the solid dried to afford an analytically pure complex. Yield = 0.42 g (51%). ^{1}H NMR ($CDCl_3$, 200 MHz): δ 1.35 (t, 3H, $CH_2C\underline{H}_3$, $^2J_{HH}$ = 7.4 Hz); 2.25 (s, 6H, CH_3, pz); 2.47 (s, 6H, CH_3, pz); 4.31 (q 2H, $C\underline{H}_2CH_3$, $^2J_{HH}$ = 7.4 Hz); 5.90 (s, 1H, pz); 7.22 (S, CH, 1H, pz). $^{13}C\{^1H\}$NMR ($CDCl_3$, 200 MHz): δ 168.5 (C(C=O)); 145.7 (C(5-pz); 141.5 (C(3-pz)); 107.1 (C(4-pz)); 70.9 (C($CHCO_2CH_2CH_3$)); 62.4 (C(CH_2)); 13.6 (C(CH_3))13.4 (C(3-CH_3)); 10.0 (C(5-CH_3)).

IR (Nujol cm^{-1}): $\upsilon_{C=O}$ = 1741. Anal. Calc. for $C_{14}H_{20}Cl_2N_4O_2Pd$: C, 37.07; H, 4.44; N, 12.35%. Found: C, 37.48; H, 4.05; N, 12.62%.

2.1.3. X-ray crystallography

2.1.3.1. Data collection

An orange crystal of [$PdCl_2$(**L1**)] (**1**) with approximate dimensions 0.45 x 0.33 x 0.21 mm^3 was selected under oil under ambient conditions and attached to the tip of a Micromount©. The crystal was mounted in a stream of cold nitrogen at 105(2) K and centreed in the X-ray beam by using a video camera. The crystal evaluation and data collection were performed on a Bruker CCD-1000 diffractometer with Mo K_α (λ = 0.71073 Å) radiation and the diffractometer to crystal distance of 4.9 cm.

The initial cell constants were obtained from three series of ω scans at different starting angles. Each series consisted of 20 frames collected at intervals of 0.3º in a 6º range about ω with the exposure time of 10 seconds per frame. A total of 131 reflections were obtained. The reflections were successfully indexed by an automated indexing routine built in the SMART program. The final cell constants were calculated from a set of 12116 strong reflections from the actual data collection.

The data were collected by using the full sphere data collection routine to survey the reciprocal space to the extent of a full sphere to a resolution of 0.80 Å. A total of 20998 data were harvested by collecting four sets of frames with 0.4º scans in ω and one set of frames with 0.5º scan in φ. These highly redundant datasets were corrected for Lorentz

and polarisation effects. The absorption correction was based on fitting a function to the empirical transmission surface as sampled by multiple equivalent measurements.[7]

2.4.3.2. Structure solution and refinement

The systematic absences in the diffraction data were uniquely consistent for the space group $P2_1/n$ that yielded chemically reasonable and computationally stable results of refinement. A successful solution by the direct methods provided most non-hydrogen atoms from the *E*-map. The remaining non-hydrogen atoms were located in an alternating series of least-squares cycles and difference Fourier maps. All non-hydrogen atoms were refined with anisotropic displacement coefficients. All hydrogen atoms except those on the water molecule were included in the structure factor calculation at idealised positions and were allowed to ride on the neighbouring atoms with relative isotropic displacement coefficients. There is also one solvated water molecule per Pd complex in the unit cell. The water molecules were refined with restraints. The final least-squares refinement of 172 parameters against 3166 data resulted in residuals *R* (based on F^2 for $I \geq 2\sigma$) and *wR* (based on F^2 for all data) of 0.0180 and 0.0504, respectively. The final difference Fourier map was featureless. The molecular diagram is drawn with 50% probability ellipsoids.

The solid state structures of $[PdCl_2(\mathbf{L2})]$ (**2**), $K_2[Pt_4Cl_8(\mathbf{L1})_2$(deprotonated $\mathbf{L1})_2].2H_2O$ (**3b**), $[AuCl_2(pz)(pzH]$ (**5b**), and **L4** were determined in a similar manner such as described above for **1**.

[7] Bruker-AXS. (**2000**-**2003**) SADABS V.2.05, SAINT V.6.22, SHELXTL V.6.10 & SMART 5.622 Software Reference Manuals. Bruker-AXS, Madison, Wisconsin, USA.

2.2. Results and discussion

2.2.1. Synthesis of ligands

Ligands **L1** and **L2** were synthesised by reacting pyrazoles and dibromoacetic acid under phase transfer conditions, by using benzyltriethylammonium chloride as the catalyst (eq. 2.1). Minor modifications to the literature procedure included using NaOH instead of KOH and the reaction time increased to 15 h from 5 h, which led to improved yields as compared to those in the literature. All the ligands were characterised by a combination of IR, NMR spectroscopy, microanalysis and in selected cases mass spectrometry and X-ray crystallography.

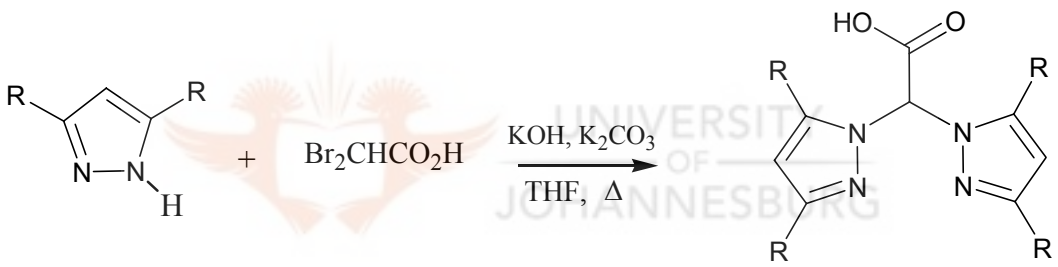

R = H (**L1**), Me (**L2**)

(**2.1**)

Ligands **L1** and **L2** were isolated as white solids in good yields at pH 2. The ^{1}H and $^{13}C\{^{1}H\}$ NMR spectra of **L1** and **L2** are indicative of their isolation. For instance the ^{1}H NMR spectrum of **L1** showed peaks due to the protons of the pyrazolyl rings and the sp^3 CH linker at 7.98 ppm (5H, 5′H; pz), 7.59 ppm (3H, 3′H; pz), 7.57 ppm (sp^3 CH linker proton (CHCOOH)) and 6.35 ppm (4H, 4′H; pz). The peaks at 7.98 ppm (5H, 5′H) and 7.59 ppm (3H, 3′H) resonated as doublets as a direct consequence of their coupling with the protons on the fourth positions of the pyrazole (4H, 4′H). The coupling constants are

ca. 2.2 Hz. Pyrazolyl protons appeared downfield as a result of the aromaticity invoked by the π electron system of the pyrazolyl rings. Despite the fact that the CH linker proton is an sp^3 proton and that would normally appear upfield,[8] that was not the case for **L1** as the sp^3 proton appeared downfield (7.57 ppm). This is attributed to the fact that the sp^3 proton is also de-shielded due to a less electron density chemical environment created by the π- systems of the pyrazolyl rings. Similarly, the spectrum of **L2** showed the same pattern as that of **L1**. The only difference was the presence of methyl groups in **L2**, which appear upfield at 2.17 and 2.27 ppm for 3-pz and 5-pz, respectively.

Subsequently the $^{13}C\{^1H\}$ NMR of **L1** showed five distinctive peaks that were characteristic of five carbons of **L1**. The peak at 166.2 ppm in the $^{13}C\{^1H\}$ NMR of **L1** was characteristic of carbonyl carbon ($CH\underline{C}O_2H$) of **L1**, whereas the peaks at 140.1, 131.0 and 106.5 ppm were due to pyrazolyl ring carbons, C-5pz, C-3pz and C-4pz, respectively. The carbonyl carbon appears downfield at 166.2 due to its de-shielded environment as a result of the carboxylic moiety. The carboxylic moiety has delocalisation of electrons around O=C-OH bonds, which leads to reduced electron density around the carbonyl carbon; thus leading to it appearing downfield at 166.2 ppm. Generally the pyrazolyl ring carbons also appeared downfield (C-5pz = 140.1 ppm, C-3pz = 131.0 ppm and C-4pz = 106.5 ppm) as a result of the de-shielding effect brought about by the π electron system of the pyrazolyl rings. The sp^3 CH linker carbon ($\underline{C}HCO_2H$) appears at 73.9 ppm. This is in agreement with the fact that aliphatic carbons are more

[8] Morrison R. T., Boyd R. N., *Organic Chemistry* 6th Ed, **1994**, Prentice-Hall International inc., New Delhi India, pp. 604-639.

shielded as a result of increased electron density around them and thus would appear upfield. Similar spectral patterns were observed for **L2**, with sp^3 CH linker carbon ($\underline{C}HCO_2H$) and carbonyl carbon ($CH\underline{C}O_2H$) appearing at 71.4 and 165.9 ppm, respectively.

Infrared spectroscopy was further used to characterise the ligands especially because of its usefulness in identifying functional groups present on the compounds. The ligands were run as nujol mulls between NaCl plates and IR spectra acquired. For **L1** and **L2**, the most important stretching frequencies were those of C=O and O-H, which appeared at 3439 cm^{-1} υ(O-H), 1720 cm^{-1} υ(C=O) for **L1** and at 3402 cm^{-1} υ(O-H), 1743 cm^{-1} υ(C=O) for **L2**. These frequencies were indicative of the incorporation of carboxylic moiety in the CH linker of pyrazolyl ligands (eq. 2.1). Microanalysis data for **L1** were in agreement with literature values, whilst that of **L2** suggests the presence of 0.5 moles of water.

The acetic acid ligands, **L1** and **L2**, behave like any classical carboxylic acid and have the propensity to ionise in an aqueous medium. Ligands **L1** and **L2** could therefore undergo classical esterification to produce new bis(pyrazolyl)ethyl acetate (**L3**) and bis(3,5-dimethylpyrazolyl)ethyl acetate (**L4**), respectively (Scheme 2.1). Thus **L3** and **L4** were synthesised by reacting **L1** and **L2** with excess ethanol under acidic conditions and isolated in moderate yields. In the ^1H NMR spectrum of **L4** (Fig. 2.1), the additional peaks to those of **L2** is a triplet at 1.30 ppm and a quartet at 4.36 ppm, which are characteristic of the methylene and methyl protons of the ethyl moiety, respectively. The

peak at 1.64 ppm is due to traces of water in the NMR solvent. The $^{13}C\{^{1}H\}$ NMR spectrum of **L4** showed peaks at 63.2 and 13.4 ppm assignable to methylene and methyl carbons for the ethyl alcohol moiety ($CHCO_2\underline{C}H_2\underline{C}H_3$). The carbonyl carbon ($\underline{C}$=O) of **L4** appeared at 166.1 ppm compared to that of the starting material, **L2** (165.9 ppm), signifying the formation of **L4**. Ligand **L3** display similar spectral patterns with the carbonyl carbon ($\underline{C}$=O) resonating at 163.8 ppm in the $^{13}C\{^{1}H\}$ NMR spectrum.

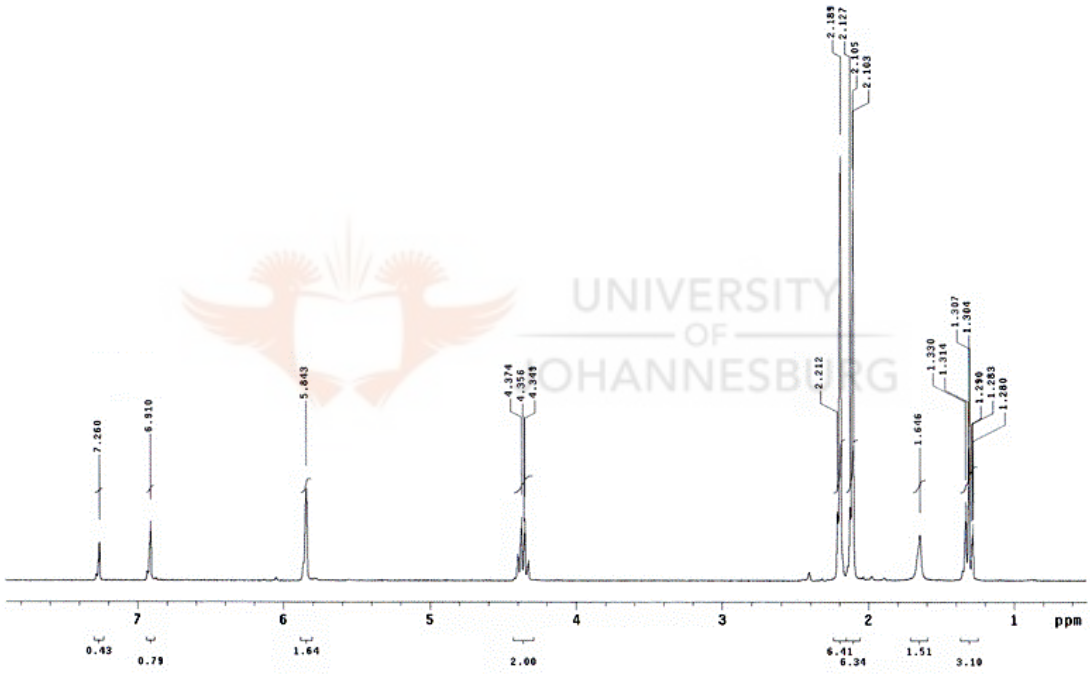

Figure 2.1. The ^{1}H NMR spectrum of **L4**.

To further characterise **L3** and **L4**, their infrared spectra were acquired. Contrary to the IR spectrum of **L1**, the IR spectrum of **L3** showed that the υ(O-H) band at 3439 cm^{-1} was absent, thus signifying the conversion of OH moiety in **L1** to OCH_2CH_3 in **L3**. Similar observations were made for **L4**. In addition, the microanalysis data acquired for **L3** and **L4** were in agreement with the formulation of the new ligands.

The isolation of **L4** was further diagnostic evidence that the R_2bpza ligands do undergo a classical esterification process. The molecular structure of **L4** is shown in Figure 2.2. The carbonyl carbon, C(7), exhibits a distorted trigonal geometry. However the geometry about C(6) is a distorted tetrahedron. The angles vary from 106.2° to 112.49(17)°. The bond distances and angles are similar to those reported by Burzlaff and coworkers (C(4)-N(12), 1.468(3) Å; C(5)-O(5), 1.215(3) Å; O(4)-C(5)-O(5), 125.4(2)°, C(5)-C(4)-N(22), 109.2(2)°) for bis(3,5-ditert-butylpyrazolyl)acetic acid. A molecular packing diagram of **L4** viewed along the *c* axis is shown in Figure 2.3. The pyrazolyl rings are oriented outwards and the acetic acid moieties inwards in the packing diagram; thereby leading to the formation of an oval shaped cage in the centre. The crystallographic data together with selected bond lengths and angles are given in Tables 2.1 and Table 2.2 respectively.

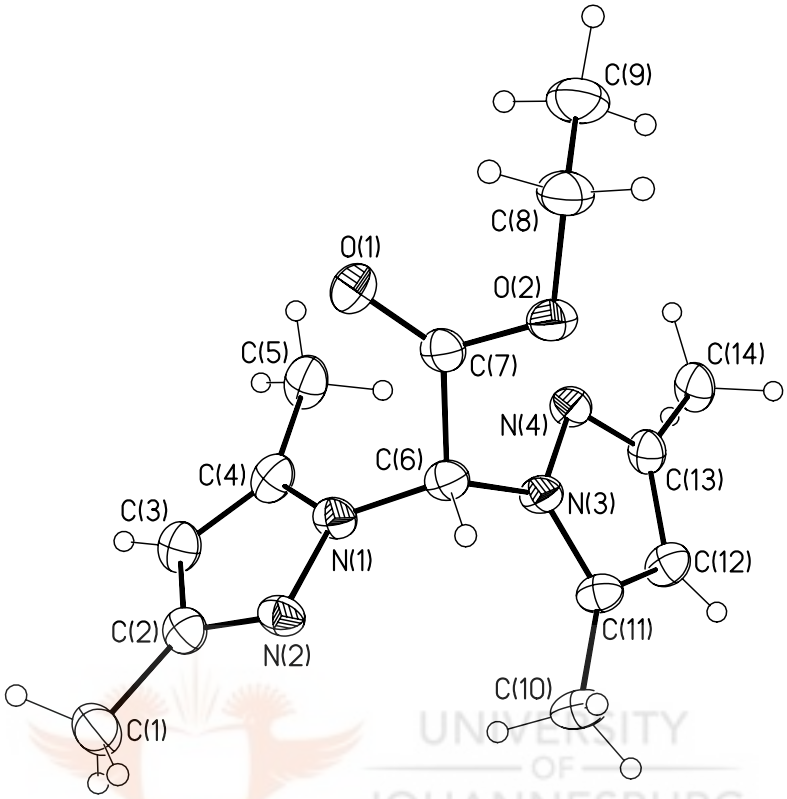

Figure 2.2. A molecular drawing of **L4.**

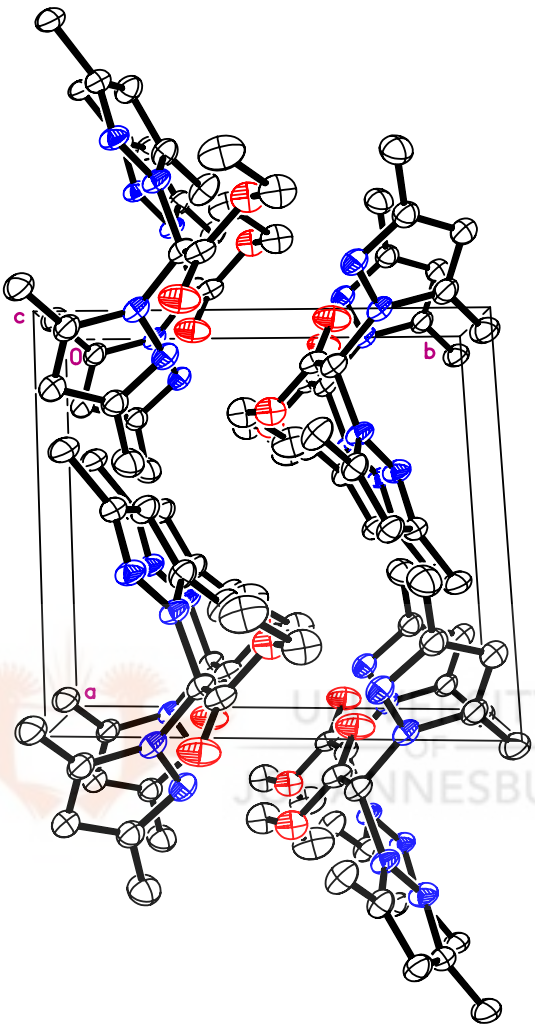

Figure 2.3. A molecular packing diagram of **L4** viewed along the *c* axis**.**

Table 2.1. Crystal data and structure refinement for **L4**

Empirical formula	$C_{14}H_{20}N_4O_2$
Formula weight	276.34
Temperature	100(2) K
Wavelength (Å)	0.71073
Crystal system	Triclinic
Space group	$P\bar{1}$
Unit cell dimensions	a = 8.4121(18) Å
	b = 8.7475(19) Å
	c = 10.809(2) Å
	α = 80.958(3)°
	β = 71.135(3)°
	γ = 84.365(3)°
Volume ($Å^3$)	742.4(3)
Z	2
Density (calculated) (Mg/m^3)	1.236
Absorption coefficient (mm^{-1})	0.085
F(000)	296
Final R indices (R1)	0.0587
Reflections collected	6053
Completeness to theta	98.1 %
Goodness-of-fit on F^2	1.051
Largest diff. peak and hole ($e.Å^{-3}$)	1.337 and -0.218

Table 2.2. Selected bond lengths [Å] and angles [°] for **L4**

L4			
Bond lengths (Å)		*Bond angles (°)*	
C(6)-C(7)	1.534(3)	O(1)-C(7)-O(2)	126.3(2)
O(2)-C(7)	1.328(3)	N(1)-C(6)-C(7)	112.49(17)
O(1)-C(7)	1.198(3)	N(1)-C(6)-N(3)	113.75(17)
N(1)-C(6)	1.447(3)		

2.2.2. Synthesis of metal complexes

The metal complexes **1-6a** (*cis*-[MCl_2(3,5-R_2bpza)] (M = Pd, Pt, R = H, Me) and *cis*-[$AuCl_2$(3,5-R_2bpza)]Cl) (R = H, Me) were prepared by reacting the known ligands bis(pyrazolyl)acetic acid (**L1**) and bis(3,5-dimethylpyrazolyl)acetic acid (**L2**) with equimolar amounts of $K_2[PdCl_4]$, $K_2[PtCl_4]$ or $H[AuCl_4].4H_2O$ (Scheme 2.1 and 2.2). All the complexes were isolated as pale yellow and yellow solids in moderate to good yields. Subsequently complexes **1-6a** were characterised by a combination of IR, NMR spectroscopy, microanalysis and in selected cases mass spectrometry and X-ray crystallography, in the same way it was described for the ligands (cf. section 2.2.1).

The general pattern of ^1H and $^{13}C\{^1H\}$ NMR spectra is similar for all the free ligands, however upon coordination, there was observable splitting of the peaks and they resonated slightly downfield. The two pyrazolyl groups in all the compounds were spectroscopically equivalent and thus showed only one set of signals in the NMR spectra.

For instance, the ^{1}H NMR spectrum of [$PdCl_2$(**L1**)] (**1**) showed three distinct singlets at 8.29 ppm (5H, 5′H; pz), 8.02 ppm (3H, 3′H; pz) and at 8.14 ppm for the CH linker proton (C<u>H</u>COOH) compared to the peaks of **L1** at 7.98 ppm (5H, 5′H; pz), 7.59 ppm (3H, 3′H; pz) and 7.57 (C<u>H</u>COOH) in the spectrum of **L1**. This general downfield shift of peaks of **L1** in complex **1** was attributed to **L1** being de-shielded as a result of its coordination to palladium. Similar ^{1}H NMR spectral patterns was observed for analogues of **1**, that is, [$PtCl_2$(**L1**)] (**3a**) and [$AuCl_2$(**L1**)]Cl (**5a**) complexes. However, there was no significant changes in the $^{13}C\{^{1}H\}$ NMR spectra of complexes **1** and **3a** compared to that of **L1**, with the diagnostic carbonyl carbon (CH<u>C</u>OOH) appearing at *ca*. 166 ppm; but in the $^{13}C\{^{1}H\}$ NMR spectrum of gold complex **5a**, the carbonyl carbon (CH<u>C</u>OOH) resonated much downfield at 174 ppm. This was attributed to the coordination of **L1** to the gold ion. It appears that the strong polarising ability of gold(III) ion facilitates the withdrawal of electrons from the ligand rendering it to be more de-shielded.

In the case of complexes [$PdCl_2$(**L2**)] (**2**), [$PtCl_2$(**L2**)] (**4**) and [$AuCl_2$(**L2**)]Cl (**6a**), their ^{1}H NMR spectra were quite similar to those of complexes **1**, **3a** and **5a** except for the fact that they showed two additional peaks upfield, which were characteristic of the protons of the methyl groups in **L2**. For instance, in the ^{1}H NMR spectrum of complex **4** (Fig. 2.4), there was a distinct separation of the two methyl group protons, thus resonating at 2.07 and 2.17 ppm for CH_3 protons at 3-pz and 5-pz, respectively, as seen in Figure 2.4. This is in contrast to the two methyl groups of **L2** where they overlap at 2.33 ppm, thus giving a clear indication of formation of complex **4**. However, there were no significant shifts in the $^{13}C\{^{1}H\}$ NMR spectra of complexes **2**, **4** and **6a** compared to that of **L2**.

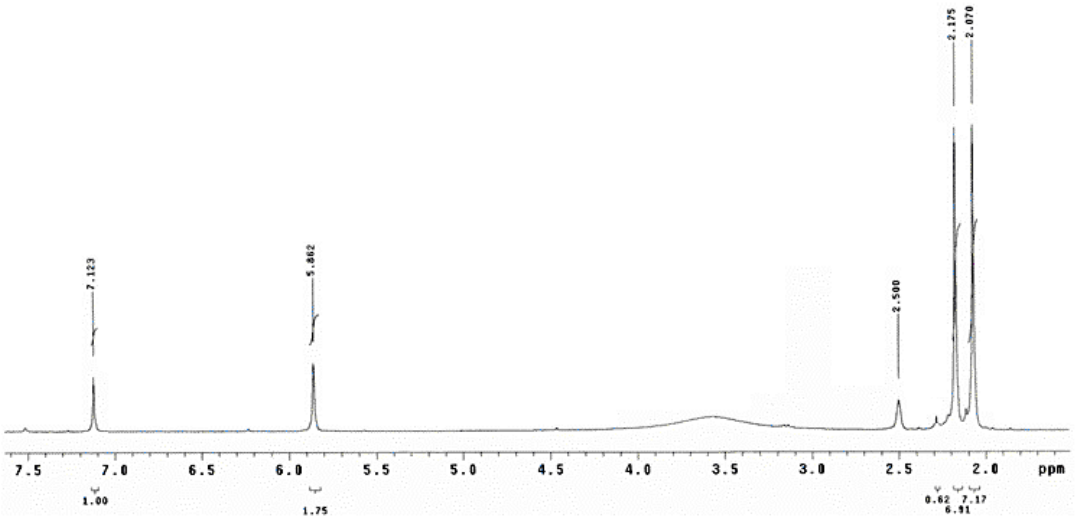

Figure 2.4. ^{1}H NMR spectrum of **4**, [$PtCl_2$(**L2**)] (**L2** = bis(3,5-dimethylpyrazolyl) acetic acid).

From the infrared spectra of complexes **1**-**6a**, it was observed that there was a general shift in the υ(C=O) and υ(O-H) bands of **L1** and **L2** upon complexation. For example in the case of gold complex **6a**, the υ(C=O) and υ(O-H) stretching frequencies were 1765 and 3451 cm^{-1}, respectively, as compared to those of **L2**, which were 1743 and 3402 cm^{-1}. The shift of υ(C=O) and υ(O-H) bands of complexes **1**-**6a** to higher frequencies was attributed to the reduction in the electron density of the ligands (**L1** and **L2**) and by extension reduction in the electron density around the carboxylic moiety. This led to the reduction of the double bond character of C=O as well the O-H moiety thereby appearing at higher frequencies.

As alluded to earlier, mass spectra of selected complexes were acquired. Positive-ion ESI-MS spectra of platinum(II) complexes (**3a** and **4**) and gold complexes (**5a** and **6a**)

recorded in DMSO:H_2O solution, yielded the positive $[M]^+$ ions as the base peaks. In the spectrum of complex **3a**, the molecular ion peak is at m/z 457 (Fig. 2.5). The fragmentation pattern is, however, complicated and could not be interpreted. The positive ESI-MS spectra of complexes **4**, **5a** and **6a**, showed molecular ion peaks present at m/z 514 for $[PtCl_2(\mathbf{L2})]$, 463 for $[AuCl_2(\mathbf{L1})]^+$ and m/z 519 for $[AuCl_2(\mathbf{L2})]^+$, respectively. The molecular ion peak at m/z 542 in the spectra of complex **6a**, is related to $[M+Na]^+$ fragment, with the base peak appearing at m/z 249, which correspond to the ligand (**L2**).

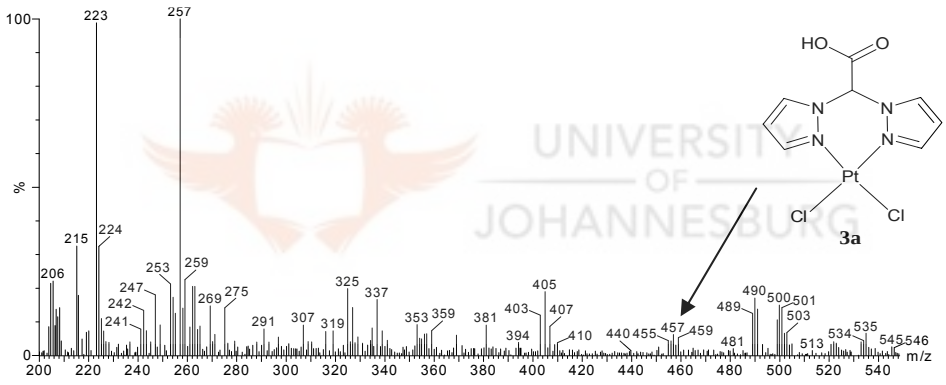

Figure 2.5. ESI-MS spectrum of compound **4a,** $[PtCl_2(\mathbf{L1})]$ (L1 = bis(pyrazolyl) acetic acid).

Complexes **5a** and **6a** (Scheme 2.2) are cationic gold(III) complexes with chloride counterions and are similar to $[AuCl_2(bik)]Cl$ (bik = bis(1-methyl-2-imidazolylketone) and $[AuCl_2(bihm)]Cl$ (bihm = bis(1-methyl-2-imidazolyl)hydroxymethane) complexes recently reported by Bulak *et al*.[9] All the three complexes, **a**, **b** and **c**, were found to be

[9] Bulak E., Sarper O., Dogan A., Lissner F., Schleid T., Kaim W., *Polyhedron*, **2006**, *25*, 2577.

nearly square planar gold(III) with the formation of six-membered chelated rings (Fig. 2.6).

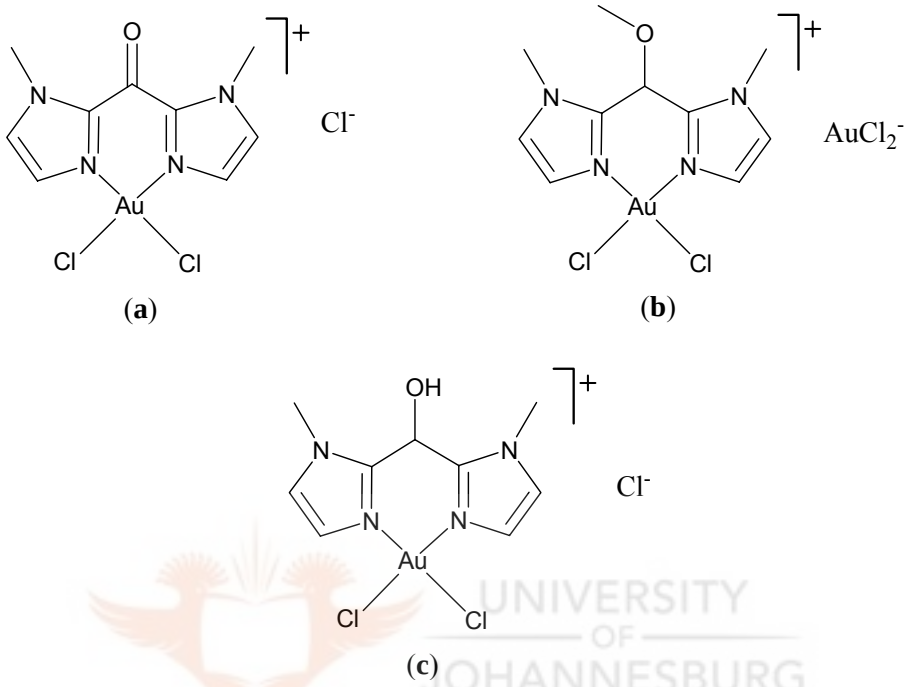

Figure 2.6. Dichlorogold(III) complexes of bis(1-methyl-2-imidazolyl)ketone and related ligands (cf. ref. 9).

Whereas the mechanism of coordination of N^N ligands to MCl_2 (M = Pd, Pt) to form complexes similar to **1-4** has been known for a long time, that of $AuCl_4^-$ has not. For instance, in the case of palladium(II) and platinum(II) complexes **1-4**, the source of MCl_2 is their respective $K_2[MCl_4]$ salts (M = Pd, Pt). The presence of non-bonding electrons and two vacant coordination sites on square planar d^8 complexes, allows them to be occupied by solvent molecules. Thus, many of the reactions of Pt and Pd complexes proceed by an associative mechanism.[10] One might expect that four-coordinate

[10] Cotton F. A., Wilkinson G., *Advanced Inorganic Chemistry*. 3rd Ed., **1972**, pg. 665, 1031.

complexes would be more likely than octahedral ones to react by S_N2 mechanism, where the incoming ligand leads to a formation of a five-coordinate intermediate species followed by a simultaneous loss of the leaving ligand.

The mechanism for the formation of the gold compounds **5a** and **6a** is similar and proceeds as shown in Scheme 2.3. It involves the formation of an intermediate complex **d**. Indirect evidence for the formation of **d** is the pyridine gold(III) compound, $[AuCl_3(Hpcp)]$ (Hpcp = 2-benzoylpyridine), reported by Fuchita *et al*.[11] The availability of only one N-donor atom in Hpcp leads to formation of a tri-chloro gold complex, $[AuCl_3(Hpcp)]$ (see inset in Scheme 2.3). On the contrary, the availability of two N-donor atoms in the pyrazolyl ligands **(L1-L2**), promotes ring closure in intermediate **d** involving the second N atom eliminating the Cl *trans* to the ligand to give **5a** and **6a** (Scheme 2.3).

[11] Fuchita Y., Ieda H., Tsunemune Y., Kinoshita-Nagaoka J., Kawano H., *J. Chem. Soc., Dalton Trans*., **1998**, 791.

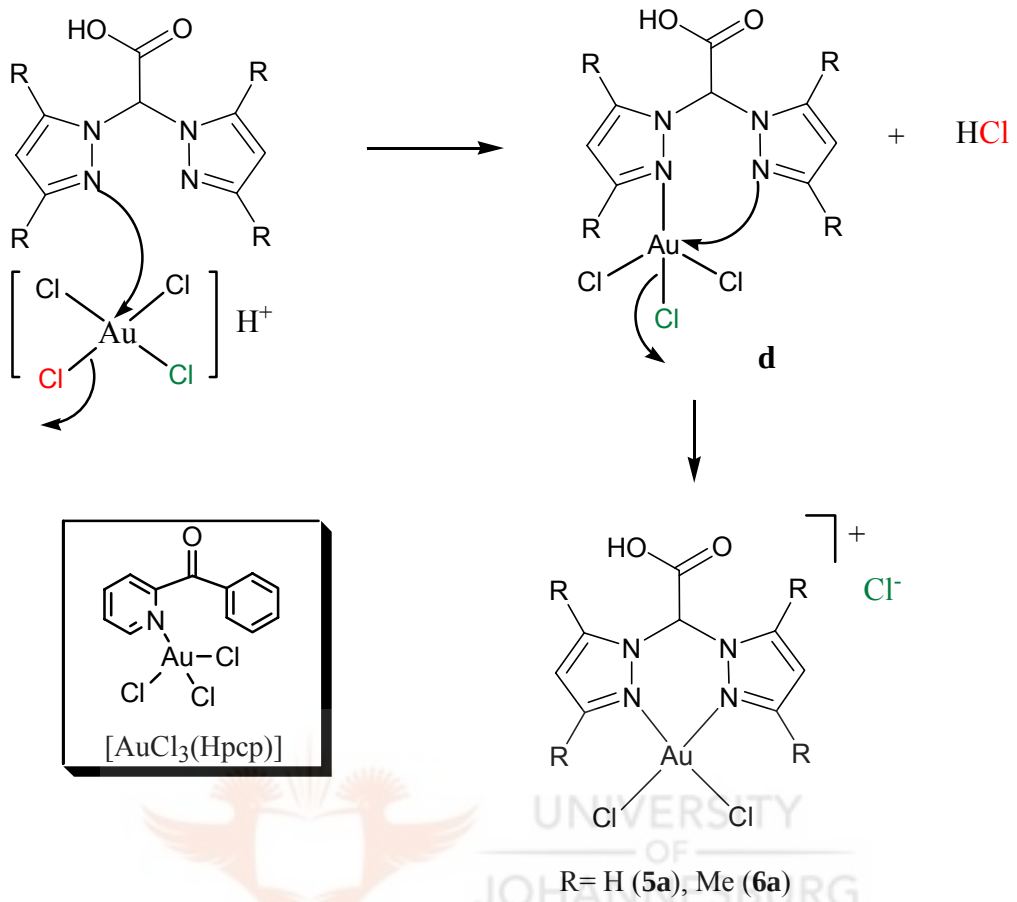

Scheme 2.3. Proposed mechanism of formation of gold(III) compounds **5a** and **6a**.

The ability of the bis(pyrazolyl)ethyl acetate ligands to form complexes was also demonstrated by reacting **L4** and $[PdCl_2(MeCN)_2]$, which gave $[PdCl_2(\mathbf{L4})]$ (**7**). Similarly, the ^{1}H and $^{13}C\{^{1}H\}$ NMR spectra for complex **7** were comparable to those of $[PdCl_2(\mathbf{L2})]$ (**2**) except that for **7** there were additional peaks for the ethyl group (CH_2CH_3) at 1.35 ppm (CH_3) and 4.31 ppm (CH_2) due to the ester ligand. The carbonyl carbon (CHCOOH) peak for complex **7** in the $^{13}C\{^{1}H\}$ NMR spectrum was at 168.5 ppm compared to that of **L4** (166 ppm). The microanalysis data are in agreement with the formulation of **7**.

*2.2.3. Molecular structures of complexes **1**, **2**, **3b** and **5b***

Single crystal X-ray crystallography was used in selected cases to confirm the proposed structures deduced from the NMR and mass spectrometry data. Single crystals of $[PdCl_2(\mathbf{L1})]$ (**1**) were grown by evaporation of an aqueous solution at room temperature while crystals of $[PdCl_2(\mathbf{L2})]$ (**2**) were grown from evaporation of a DMSO solution. The platinum compound, $K_2[Pt_4Cl_8(\mathbf{L1})_2(\text{deprotonated-}\mathbf{L1})_2].2H_2O$ (**3b**), crystallised from aqueous solutions containing $[PtCl_2(\mathbf{L1})]$ (**3a**) when such solutions were left to stand overnight. Tables 2.3 and 2.4 show the crystallographic data, and selected bond lengths and angles respectively. The molecular structure of **1**, **2** and **3b** are shown in Figures 2.7, 2.9 and 2.11 respectively.

In complex **1** the two chlorides are coordinated to palladium in a *cis*-arrangement. The bond angles of N(1)-Pd(1)-N(4), N(4)-Pd(1)-Cl(1), N(1)-Pd(1)-Cl(2), are 88.03(6)°, 90.04(4)° and 90.81(4)°, respectively. The geometry around the palladium metal in **1** is a distorted square planar. It crystallised with one molecule of water in the crystal lattice. The average Pd-Cl bond distances of **1** is 2.2866(5) Å and is similar to the average Pd-Cl distance of 2.301 Å reported to the Cambridge Structural Database (CSD).[12] However, the average Pd-N bond distance (2.0131(15) Å) is shorter than the average Pd-N bond distance of 2.06(9) Å for 607 bonds in 229 relevant complexes reported to the CSD. A molecular packing diagram of **1** viewed along the *b* axis, with one water molecule bridging two units of the complexes is shown in Fig. 2.8.

[12] Allen F. H., *Acta Crystallogr.*, Sect. B, **2002**, *58*, 380.

Compound [$PdCl_2$(**L2**)] (**2**) crystallises with two symmetry independent palladium complex molecules and three molecules of DMSO solvent in the unit cell. The two molecules exhibit similar structural features and reside on a crystallographic inversion centre, with only one half of it being crystallographically independent (Fig. 2.9). Each palladium coordination environment consists of two *cis*-Cl ligands. The bond angles of N(1)-Pd(2)-N(4), N(1)-Pd(2)-Cl(5), Cl(5)-Pd(2)-Cl(3) are 85.8(3)^o, 174.9(2)^o and 89.87(11)^o, respectively. The geometry around the palladium centres is a distorted square planar. The average Pd-Cl bond distances (2.2928(3) Å) and the average Pd-N bond distance (2.0475(8) Å) are similar to those of complex **1** described above. There is intermolecular O-H…O hydrogen bonding observed between two DMSO solvents and two palladium units (Fig. 2.10). However, there are no intramolecular interactions in the crystal unit cell.

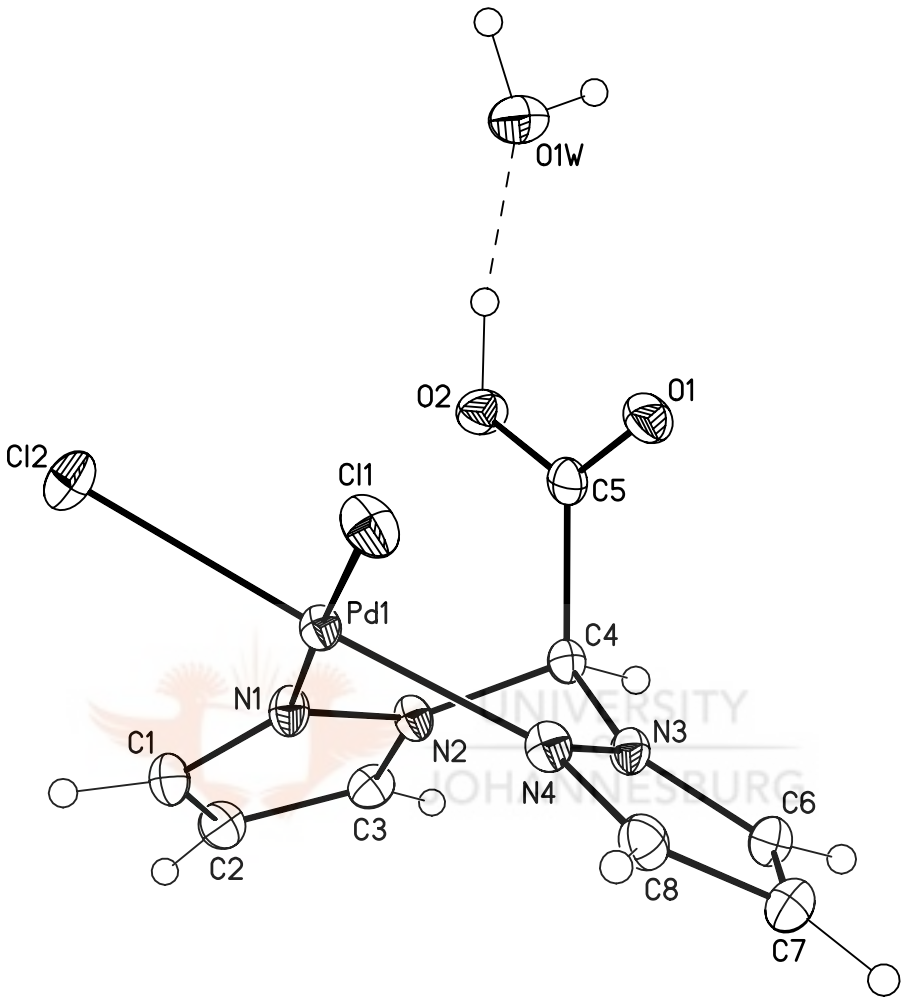

Figure 2.7. A molecular drawing of complex **1**. The hydrogen bonding interaction is shown with a dashed line.

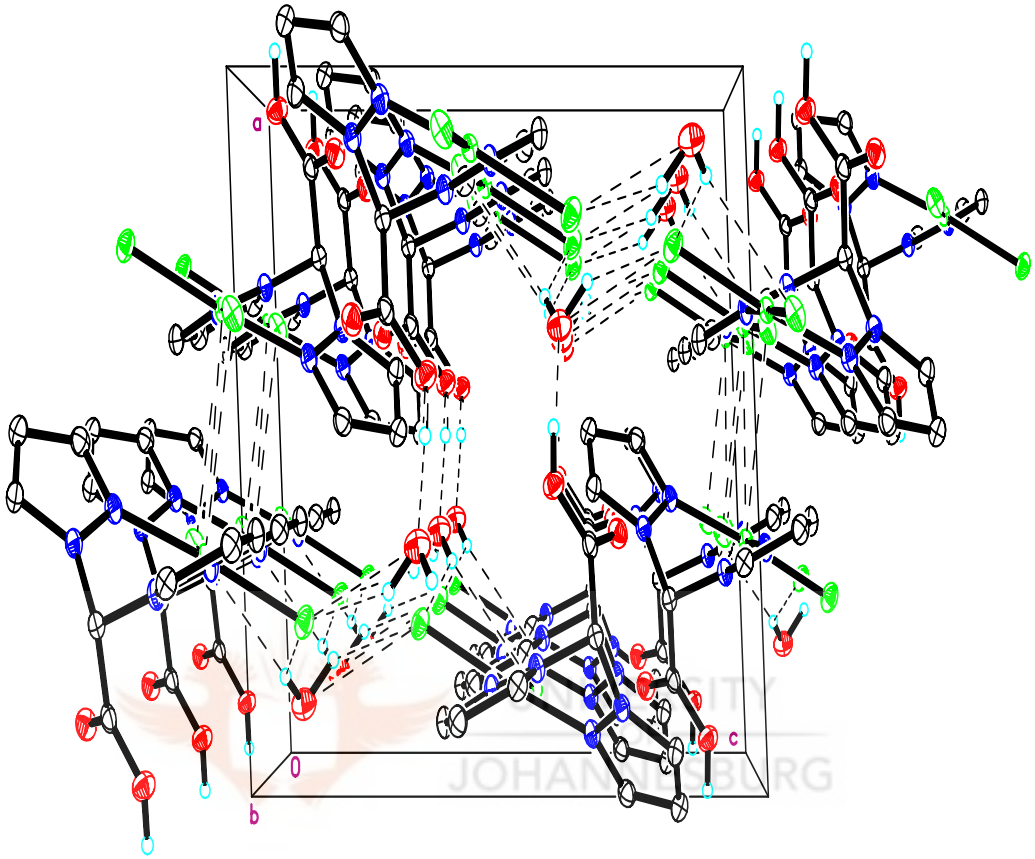

Figure 2.8. A molecular packing diagram of complex **1** viewed along the *b* axis. The hydrogen bonding interactions is shown with the dashed lines, with a water molecule bridging two units of the complexes. Selected H atoms are shown.

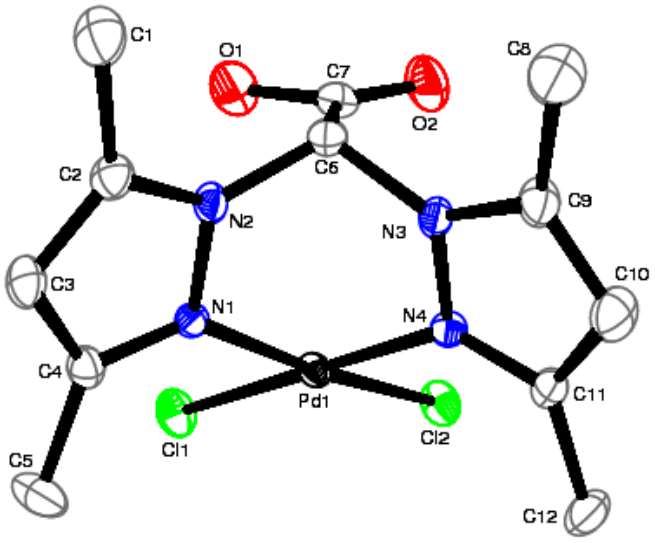

Figure 2.9. A molecular drawing of complex **2**. The hydrogen atoms have been omitted for clarity.

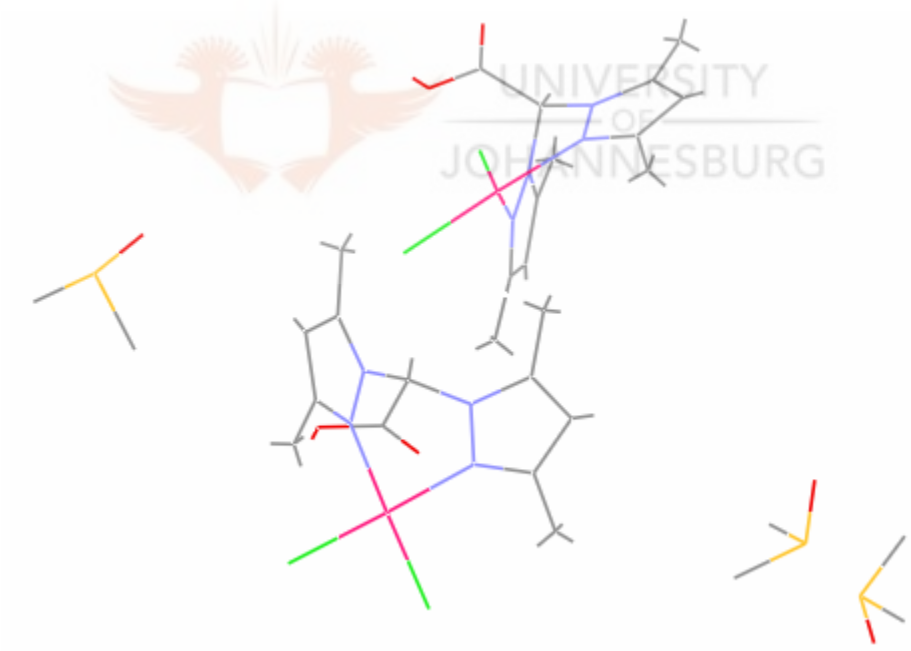

Figure 2.10. A molecular drawing of **2** showing two palladium units and three solvent molecules in the cell unit.

Table 2.3. Crystal data and structure refinement for complexes **1, 2, 3b** and **5b**

Parameter	1	2	3b	5b
Empirical formula	$C_8H_{10}Cl_2N_4O_3Pd$	$C_{30}H_{32}Cl_4N_8O_7S_3Pd$	$C_{32}H_{34}Cl_8K_2N_{16}O_{10}Pt_4$	$C_6H_7AuCl_2N_4$
Formula weight	387.50	1120.64	1944.91	403.02
Temperature (K)	105(2)	298(2)	100(2)	100(2)
Wavelength (Å)	0.71073	0.71073	0.71073	0.71073
Crystal system	Monoclinic	Triclinic	Monoclinic	Monoclinic
Space group	$P2_1/n$	P2n	$P2_1/n$	C2/c
Unit cell dimensions				
a(Å)	10.9934(10)	8.7960(14)	10.7762(8)	9.1848(6)
b(Å)	9.7436(9)	16.238(2)	14.4036(11)	14.8376(10)
c(Å)	11.9243(11)	16.430(2)	16.6971(13)	14.9738(10)
α	90°	78.038(10)°	90°	90°
β	93.0620(10)°	77.817(11)°	104.494(2)°	100.9060(10)°
γ	90°	89.970(10)°	90°	90°
Volume ($Å^3$)	1275.5(2)	2241.7(6)	2509.2(3)	2003.8(2)
Z	4	4	2	8
Density (Calculated) (Mg/m^3)	2.021	1.608	2.574	2.672
Absorption coefficient (mm^{-1})	1.882	1.230	11.777	15.174
F(000)	760	1100	1808	1472
Final R indices (R1)	0.0180	0.1087	0.0205	0.0172
Reflections collected	20998	21122	20392	13947
Completeness to theta	100 %	99.3 %	99.7 %	98.4 %
Goodness of fit on F^2	1.057	1.172	1.023	1.075
Largest diff. peak and hole ($e.Å^{-3}$)	0.523 and -0.370	4.347 and -2.208	1.234 and -0.792	1.401 and -02.024

Table 2.4. Selected bond lengths [Å] and angles [°] for complexes **1, 2, 3b** and **5b**

	1	**2**	**3b**	**5b**
		Bond lengths (Å)		
M(1)-N(1)	2.007(4)	2.036(8)	2.005(3)	1.998(2)
M(1)-N(3)	2.031(4)	2.047(8)	2.016(3)	2.002(2)
M(1)-Cl(1)	2.2803(13)	2.298(3)	2.2909(10)	2.3033(6)
N(1) –N(2)	1.366(6)	1.382(10)	1.359(4)	1.353(3)
O(1)-C(5)	1.204(2)	1.314(14)	-	-
O(2)-C(8)	-	-	1.215(5)	-
O(3)-C(16)	-	-	1.224(5)	--
K(1)-Cl(2)	-		3.1822(13)	-
Pt(1)-K(1)			3.8397(9)	
		Bond angles (°)		
N(1)-M(1)-N(3)	87.39(17)	85.8(3)	90.11(13)	86.77(9)
N(1)-M(1)-Cl(2)	177.63(12)	174.9(2)	177.87(9)	176.63(7)
N(1)-M(1)-Cl(1)	91.07(12)	89.87(11)	89.11(9)	92.59(7)

The structure of complex **3b** ($K_2[Pt_4Cl_8(\mathbf{L1})_2$(deprotonated $\mathbf{L1})_2].2H_2O$) (Fig. 2.11) is a centrosymmetric complex, with two potassium ions and four platinum ions. It consists of four independent platinum complexes each with a platinum centre that has a slightly distorted square-planar geometry. Only one half of it is crystallographically independent. Each platinum coordination environment consists of two *cis*-Cl ligands and one κ^2-$N\hat{}N_{(\mathbf{L1})}$ unit (**L1** = bis(pyrazolyl)acetic acid). Two of the platinum moieties in **3b** have deprotonated carboxylic acid units and two K^+ counter ions. Interestingly, the pyrazolyl rings in the bpza and deprotonated bpza units are not coplanar with the platinum coordination sphere and the six-membered heterocycle Pt-N-N-C-N-N adopt a boat conformation which in this structure resembles a butterfly; the dihedral folding angle along the Pt…C(N,N) line averages 48.7(2)º for the two crystallographically independent complexes. In the centre of **3b** is a K_2Cl_4 fragment that has a shape of a trigonal antiprism. Each potassium atom is seven-coordinate forming bonds to five Cl atoms from three platinum complexes, one oxygen atom belonging to a carboxylic acid unit, and a solvent water molecule. The coordination environment about K1 is a distorted capped trigonal prism (the trigonal prism is formed by facets C(l3)-C(l4)-O(5) and C(l2)-C(l3A)-C(l4A) and capped with O(2). Atom K1 forms ionic distal interactions of various lengths with the Cl and O atoms, which is typical for potassium cations. Each potassium atom is also part of two K-Cl-K-Cl four-membered rings, two K-Cl-Pt-Cl four-membered rings, and two 8-membered K-Cl-Pt-N-N-C-C-O rings. While there are several intramolecular O-H…O hydrogen bonding interactions within **3b**, there are no intermolecular interactions in its lattice. The crystal formation is represented in equation 2.2 below.

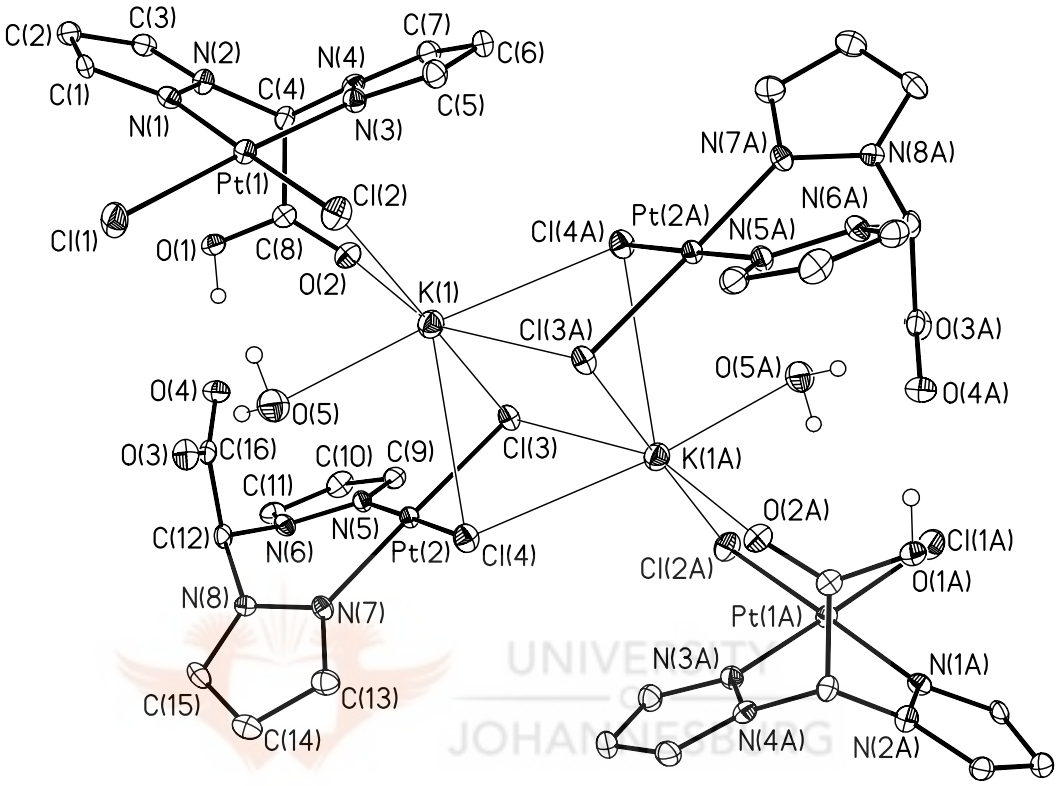

Figure 2.11. The solid state structure of **3b** with four platinum atoms and two potassium atoms. Selected H atoms are shown.

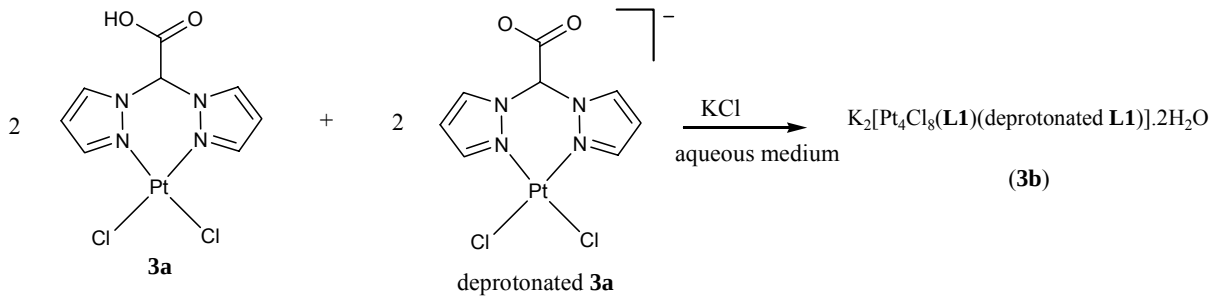

(**2.2**)

Attempts to crystallise [$AuCl_2$(**L1**)]Cl (**5a**) led to the formation of a hydrolysed product, [$AuCl_2$(pz)(pzH)] (**5b**), as confirmed by X-ray crystallography. The ^{1}H NMR spectrum (Fig. 2.12a) of powder solids of **5a,** has peaks around 7.56 ppm that are due to the 3H, 3′H and the CH linker proton (6H) of the acetic acid moiety. However, the ^{1}H NMR spectrum of crystals of **5b** showed only one broad peak at 7.15 ppm (Fig. 2.12b), which is due to 3H and 3′H. From this spectrum (Fig. 2.12b), the peak due to the CH linker proton (6H) is missing, signifying emergence of the hydrolysed product **5b**.

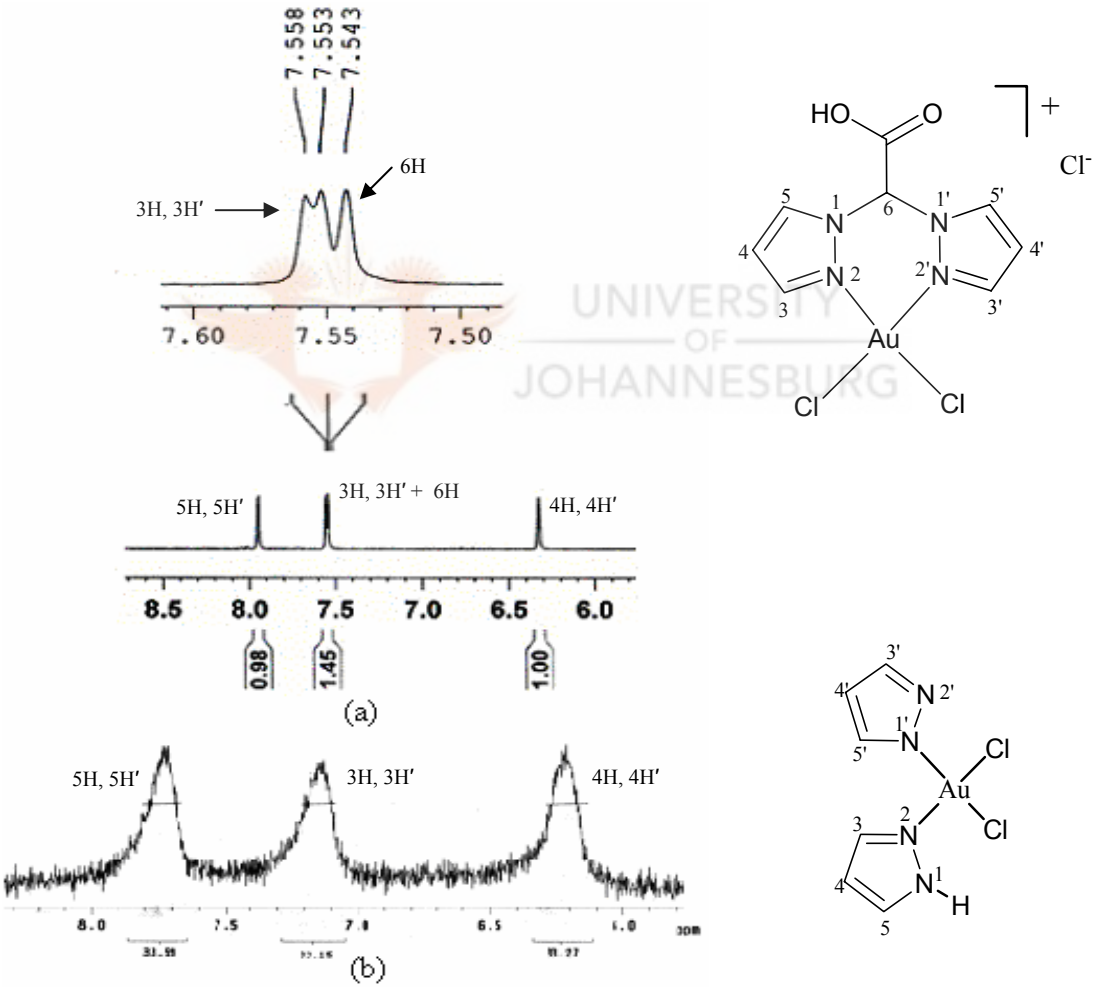

Figure 2.12. ^{1}H NMR spectrum of **5a** and **5b** at 300 MHz and 200 MHz, respectively (DMSO-d_6).

Notably, the peak due to N-H proton at *ca*. 9 ppm in the ^{1}H NMR spectrum of **5b** was missing. This is possibly due to the proton-deuterium exchange in solution. The broadness observed in the ^{1}H NMR spectrum of **5b**, was attributed to difficulties encountered in shimming during acquisition of this spectrum. The spectroscopic data as well as the solid state structure of complex **5b** (Fig. 2.15) indicate that complex **5a** hydrolysed in solution to produce **5b** (eq. 2.3). Recently Cao *et al*. [13] reported the amine-amide hydrolysis of a gold(III) compound that was attributed to the high polarising nature of the gold(III) centre in this compound. Several reports on the polarising effect of gold(III) have appeared in the literature.[14,15] A similar polarising effect of gold(III) in complex **5a** could explain the hydrolysis observed.

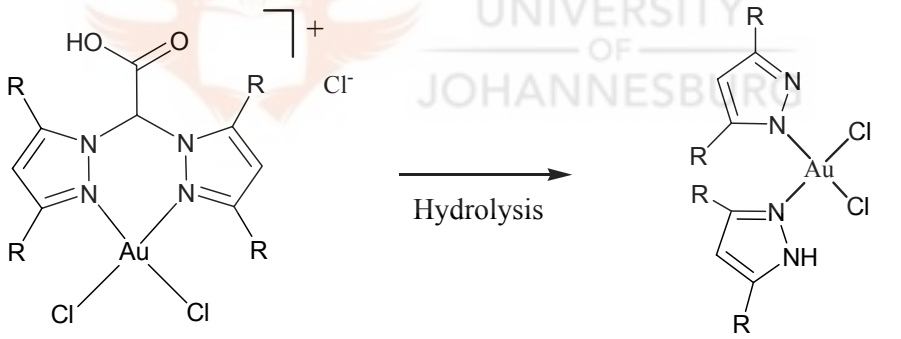

R = H (**5a**), Me (**6a**) R = H (**5b**), Me (**6b**)

(**2.3**)

[13] Cao L., Jennings M. C., Puddephat R. J., *Inorg. Chem*., **2007**, *46*, 1361.

[14] Vicente J., Bermudez M. D., Chicote M. T., Sanchez-Santano M. J., *J. Chem. Soc., Dalton Trans*., **1990**, 1945.

[15] Fan D., Yang C. T., Ranford J. D., Vittal J. J., *Dalton Trans*., **2003**, 4749.

Owing to the isolation of **5b**, further attempts to investigate the hydrolysis process observed in the gold(III) complex **5a** were made by using $[AuCl_2(\mathbf{L2})]Cl$ (**6a**). The process was monitored by ^1H NMR spectroscopy where the spectra were acquired at different intervals spanning 30 days. Figure 2.13 shows a profile of the hydrolysis process. The methyl region (2-3 ppm) has been excluded as the methyl peaks overlap and hence could not be clearly distinguished. For this reason, the 4-10 ppm region was monitored. At 0 days, there were two peaks (5.88 and 6.87 ppm) corresponding to **6a** (Fig. 2.13). After 3 days an emergence of a sharp peak at 6.04 ppm was observed signifying the formation of a new product. After 8 days, the peak at 6.04 ppm was more pronounced and consequently the emergence of a broad peak at 9.58 ppm was also observed. The peak at 6.04 ppm is representative of proton at the 4th position of the pyrazole in the new hydrolysed product, whilst that at 9.58 ppm is characteristic of an N-H proton.

There was an increase in the intensity of the broad peak (9.58 ppm) after 12 h and onwards. Even though the hydrolysis process was not followed to completion, the ^1H NMR data acquired for 20 days (Fig. 2.13) provided enough evidence for the formation of hydrolysed product $[AuCl_2(3,5\text{-}Me_2pz)(3,5\text{-}Me_2pzH)]$ (**6b**) (eq. 2.3). This was similar to observations made for **5a**, which led to formation of $[AuCl_2(pz)(pzH)]$ (**5b**) (Fig. 2.15). The $^{13}C\{^1H\}$ NMR spectrum of the hydrolysed products of **6a** showed a mixture of $[AuCl_2(3,5\text{-}Me_2bpza)]Cl$ (**6a**) and $[AuCl_2(3,5\text{-}Me_2pz)(3,5\text{-}Me_2pzH)]$ (Fig. 2.14). However, the pathway to formation of **5b** and **6b** has not been established fully.

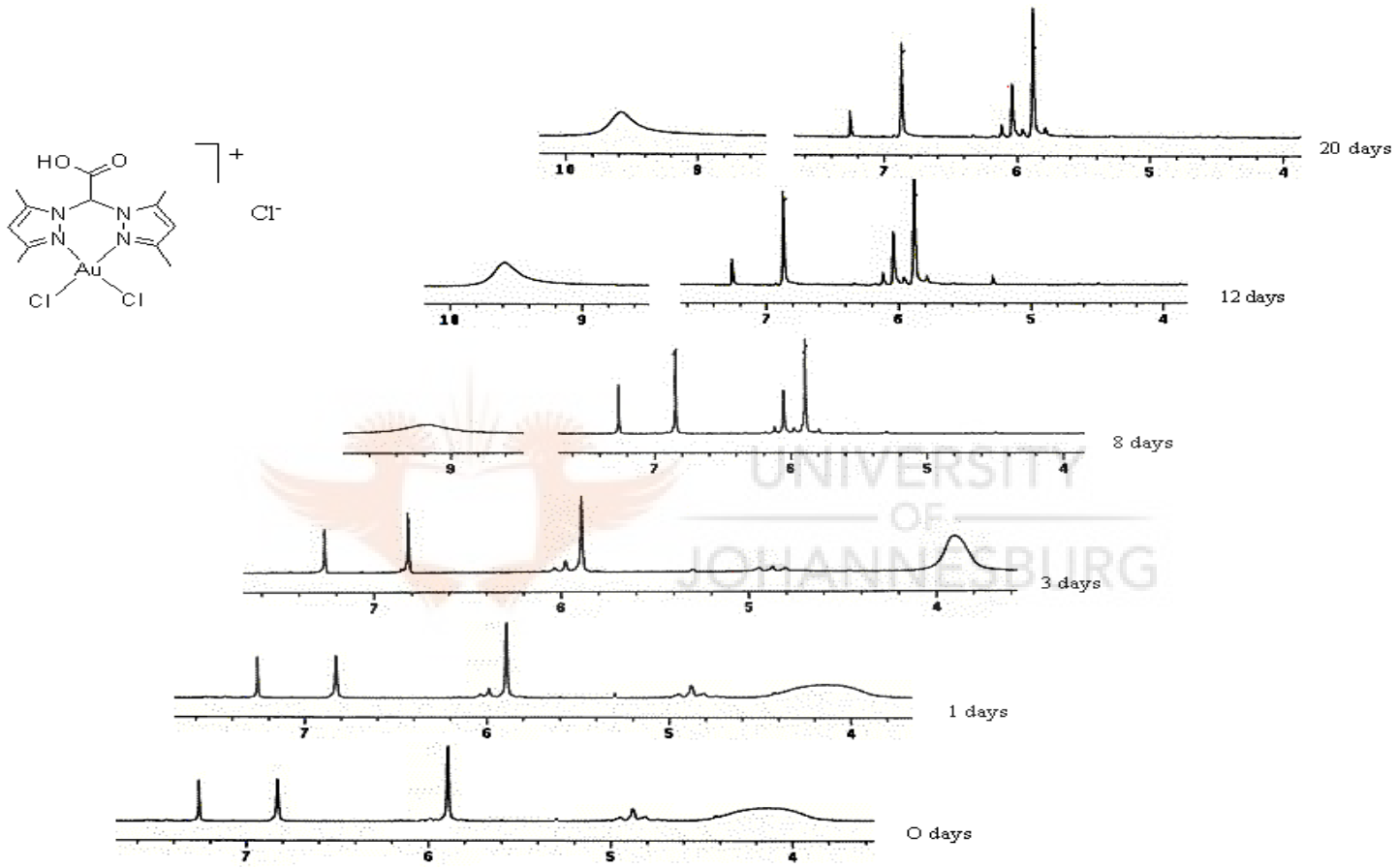

Figure 2.13. ^{1}H NMR spectra monitoring of hydrolysis process (in solution) observed during attempts to crystallize **6a.** (Similar to observations made for **5a**). Solvent = DMSO-d_6.

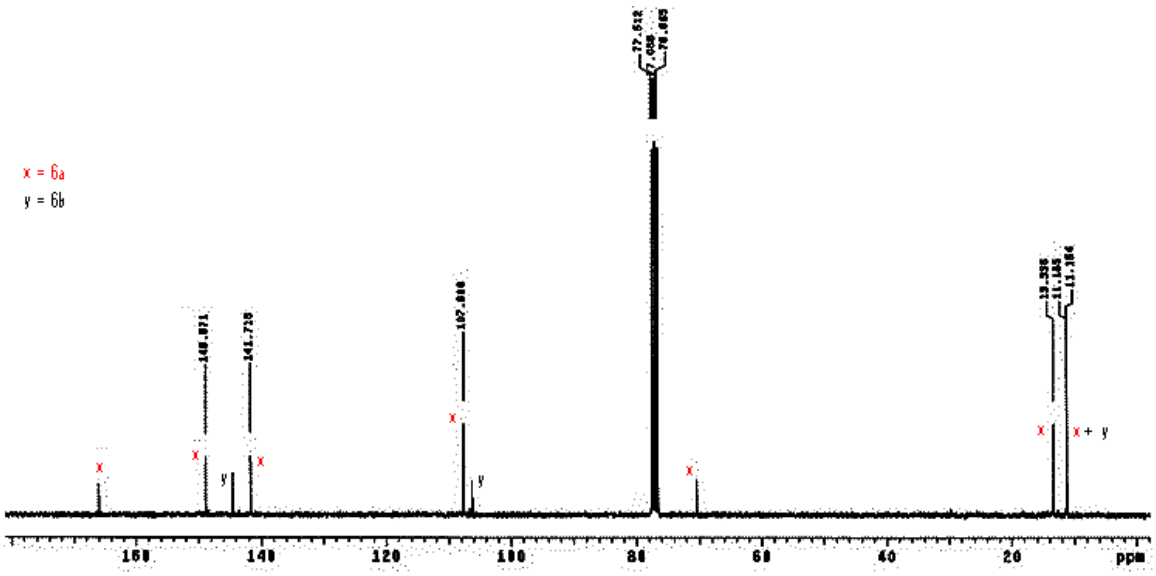

Figure 2.14. $^{13}C\{^{1}H\}$ NMR spectrum showing a mixture of **6a** and **6b** products

The molecular structure of **5b** is shown in Figure 2.15. The bond distances, Au(1)- N(1) (1.998(2) Å), Au(1)- N(3) (2.002(2) Å), Au(1)-Cl(1) (2.3033(6) Å) and Au(1)-Cl(2) (2.2933(7) Å) are statistically longer compared to those reported for dichloro-picolinaminatogold(III) complex (Au(1)-N(2); (1.969(5) Å and Au(1)-Cl(1); (2.2971(14) Å) by Fan *et al*. The Au-N mean distance is also considerably shorter than Au-N distances in $[Au(dmtc)(damp)]BPh_4$ (dmtc = $(CH_3)_2NCS_2$, damp = *o*-$C_6H_4CH_2$-$N(CH_3)_2$) complex. This is as a result of delocalisation of the π-electrons in the pyrazolyl ring. In addition to the two N atoms of the ligand, Au atom is coordinated to two chlorine atoms. The bond angles, N(1)-Au(1)-N(3) (86.77(9)°); Cl(2)-Au(1)-Cl(1) (90.73(2)°); N(3)-Au(1)-Cl(2) (89.89(7)°) and N(1)-Au(1)-Cl(1) (92.59(7)°) indicate a distorted square-planar geometry with a AuN_2Cl_2 coordination sphere. Coordination around the metal is close to linearity along N(1)-Au(1)-Cl(2) (176.64°) and N(3)-Au(1)-Cl(1) (177.99°). It was also observed that in **5b**, one hydrogen is equally disordered between the N(2) and

N(4) of the pyrazole rings and that Figure 2.15 depicts the structure with hydrogen atom on the N(2) atom. Figure 2.16 shows the molecular packing diagram of **5b** viewed along the *c* axis. At the peripheries of the unit cell, formation of pseudo-square cubanes, defined by N-Au-Cl repetitive units of the neighbouring monomeric complexes, is evident. Moreover, the π- π interactions of the pyrazole rings at the centre of the unit cell leads to formation of a figure-eight shape.

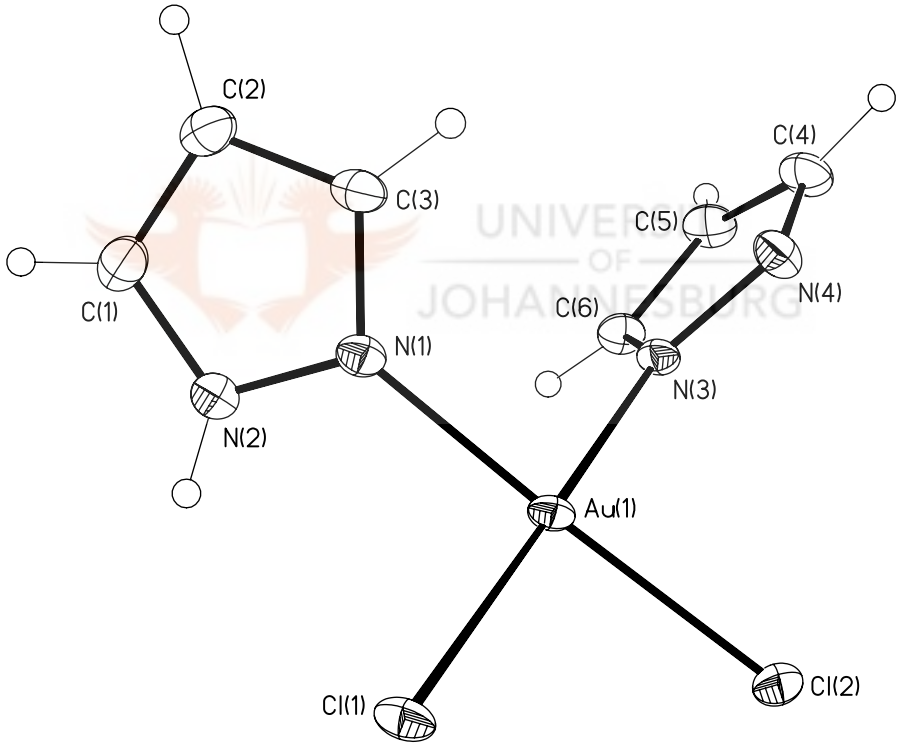

Figure 2.15. A molecular drawing of **5b**; only one position of the hydrogen equally disordered between N(2) and N(4) is shown.

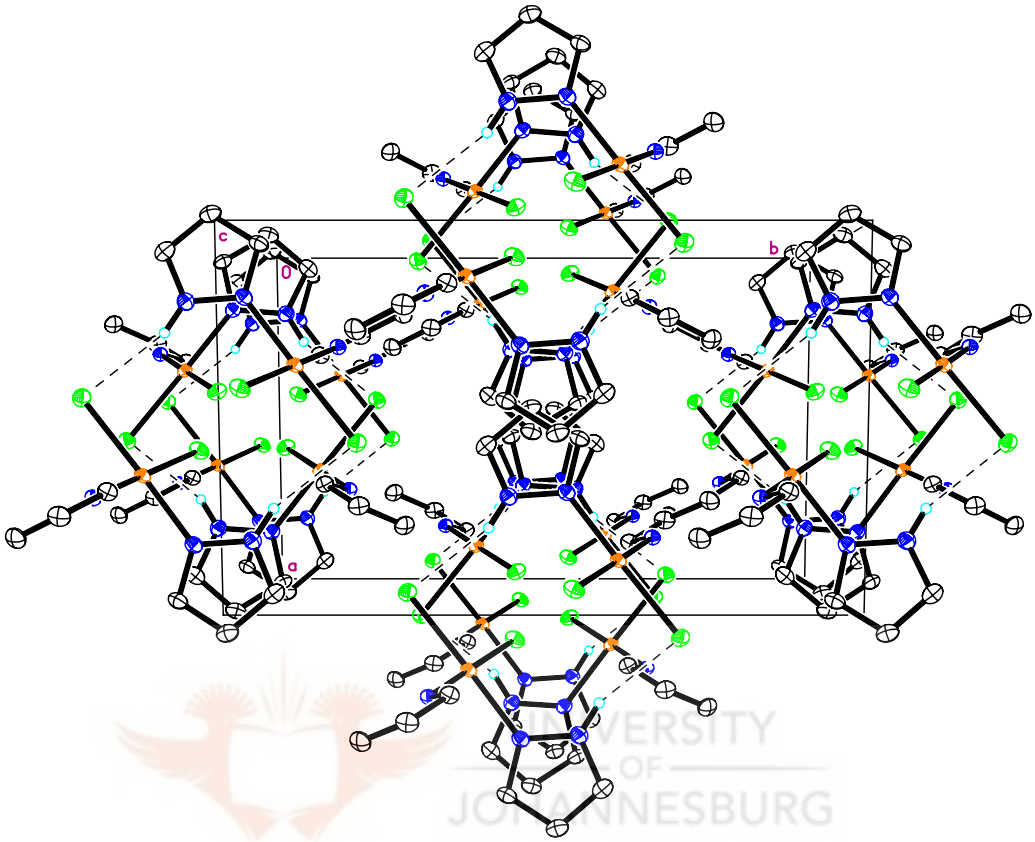

Figure 2.16. A molecular packing diagram of **5b** along *c* axis. It shows formation of cubes by the pyrazolyl rings in the centre, with the dotted line showing H···Cl interactions.

2.3. Conclusions

New bis(pyrazolyl)ethyl acetate ligands **L3** and **L4** were prepared by reacting bis(pyrazolyl)acetic acid ligands (R_2bpza) (**L1** and **L2**) with excess ethanol under acidic conditions. The isolation of **L4** showed that the R_2bpza undergo a classical esterification process. In the solid state structure of **L4**, the carbonyl carbon, C(7), exhibits a distorted trigonal geometry. Isolation of [$PdCl_2$(**L4**)] (**7**) demonstrates the ability of bis(pyrazolyl)ethyl acetate ligands to form such complexes.

Structural investigations of the new pyrazolyl palladium(II), platinum(II) and gold(III) compounds indicates that R_2bpza ligands coordinate to these metals in a bidentate fashion This is evident in the solid state structures of [$PdCl_2$(**L1**)] (**1**), [$PdCl_2$(**L2**)] (**2**) and $K_2[Pt_4Cl_8$(**L1**)$_2$(deprotonated **L1**)$_2$].$2H_2O$ (**3b**). Generally, the geometry around the metals is a distorted square planar. Each palladium coordination environment consists of two *cis*-Cl ligands. Owing the acidic nature of R_2bpza ligands, its deprotonation leads to a reproducible formation of platinum(II) complex **3b**. Two of the platinum moieties in **3b** have deprotonated carboxylic acid units and two K^+ counter ions. Each platinum coordination environment consists of two *cis*-Cl ligands and one κ^2-N^N$_{(L1)}$ unit (**L1** = bis(pyrazolyl)acetic acid). Complex **3b** is quite soluble in water and judging from its size, molecular packing would produce interesting supramolecular compounds that can be explored for various applications e.g. as pockets for gaseous materials.

For the gold(III) complexes [$AuCl_2$(**L1**)]Cl (**5a**) and [$AuCl_2$(**L2**)]Cl (**6a**), spectroscopic, mass spectral and microanalysis data were a confirmation of their existence. The observed hydrolysis of these complexes seems to be due to; (i) the strong polarising ability of the gold(III) and (ii) the fact that pyrazoles are moderate π-donors; which means that excessive withdrawal of electron from the pyrazolyl ligands could possibly lead to their disintegration. Isolation and structural characterisation of **5b** points to these two possibilities being the possible causative reasons for the hydrolysis observed. Overall the project was a success as it led to isolation of the target complexes.

The major finding is:

- That the flexible coordination and water solubility of bis(pyrazolyl) acetic acid ligands (R_2bpza) (**L1**-**L2**) offer the possibility of water soluble complexes. For instance the platinum(II) and gold(III) complexes obtained by utilising R_2bpza ligands were slightly soluble in water and readily soluble in DMSO. Furthermore, the σ-donor ability of R_2bpza ligands stabilises unstable gold(III) compounds. This finding confirms that N-donor ligands are best suited to stabilise gold(III) compounds.

CHAPTER 3

EVALUATION OF ANTI-TUMOUR ACTIVITY OF PALLADIUM(II), PLATINUM(II) AND GOLD(III) PYRAZOLYL COMPLEXES AGAINST CHO-22 CELLS AND KINETIC STUDIES

Screening of the complexes for their in vitro anticancer activities were performed by Mr Kanyanda of University of the Western Cape (SA), but the interpretation and discussion of results is by the candidate.

3.0. Introduction

Platinum group metals compounds are of interest because of their development as metallodrugs. This includes efforts to improve the effectiveness of existing platinum and gold compounds as drugs.[1] Currently there is also considerable interest in the coordination chemistry of gold because of biological activities exhibited by these compounds. Similarly, palladium compounds have also shown activity against cancer cells. Although the anticancer activity of *cis*-$[PtCl_2(NH_3)_2]$ (cisplatin) and other related compounds is by interacting with DNA,[2] reactions with other biomolecules like glutathione, cysteine and metallothionein, in biological *milieu* are likely to affect the efficacy of these compounds.[3] Palladium and gold compounds react with these biomolecules too. As a result, the widespread use of cisplatin and related complexes as

[1] Hartinger C. G., *Platinum Metals Rev*., **2008**, *52*, 96.
[2] Takahara P. M., Rosenzweig A. C., Frederick C. A., Lippard S. J., *Nature*, **1995**, *377*, 649.
[3] El-Khateeb M., Appleton T. G., Gahan L. R., Charles B. G., Berners-Price S. J., Bolton A., *J. Inorg. Biochem*., **1999**, *77*, 13.

therapeutic agents has engendered great interest in the aqueous solution chemistry of dichloro-platinum compounds.[4]

As mentioned before, it has been accepted that the efficiency of cisplatin is based on its strong binding to DNA nucleobases resulting in a locally unwound and kinked helix. The binding of cisplatin towards DNA has been shown to be kinetically and not thermodynamically controlled.[5] Experiments involving inosine, a is purine nucleoside, indicate that platinum(II) complexes binds DNA *via* a solvent-assisted mechanism.[6] These experiments suggest that the first step of reaction of cisplatin with DNA involves replacement of one chloride with a water molecule to give monofunctional adduct, *cis*-$[PtCl(NH_3)_2(H_2O)]^+$. This process has been shown by *in vitro* experiments to be of the first order, with the rate constant of hydrolysis of *cis*-$[PtCl_2(NH_3)_2]$ to *cis*-$[PtCl(NH_3)_2(H_2O)]^+$ to be *ca*. 10.2 x 10^{-5} s^{-1}.[7,8]

The mechanism for cisplatin-DNA interactions is presented in Scheme 3.1. The formation of platinum-DNA monofunctional adducts and the successive formation platinum-DNA bifunctional adducts display sequence-dependent kinetics (Scheme 3.1).[9] Firstly one chloride in cisplatin is replaced by a water molecule. Subsequently, the first platinum-N7 bond is formed preferentially on guanines involved in G_n tracts ($n \geq 2$) by displacing the water molecule to give monofunctional adducts.[8,9] This step is followed by

[4] Erickson E. L., Schneider Y., Takara T. J., Wezeman A. S., *Inorg. Chim. Acta*., **2007**, *360*, 3560.
[5] Mansy S., Chu G. Y. H., Duncan R. E., Tobias R. S., *J. Am. Chem. Soc*., **1978**, *100*, 607
[6] Arpalahti J., Mikola M., Mauristo S., *Inorg. Chem*., **1993**, *32*, 3327.
[7] Bancroft D. P., Lepre C. A., Lippard S. J., *J. Am. Chem. Soc*., **1990**, *112*, 6860.
[8] Bruhn S. L., Toney J. H., Lippard S. J., *Progress in Inorganic Chemistry: Bioinorganic Chemistry*, Vol. 38, Edited by Lippard, **1990**, 447.

replacement of the second chloride with a water molecule. Subsequent closure of monofunctional adducts to form bifunctional adducts, by loosing the second water molecule, completes the process of formation of platinum-DNA adduct as shown in Scheme 3.1. Even though the most favoured binding site is N7 position of guanine to give a GG adduct, other binding sites appear to be guanine-adenine which gives AG adduct. This selectivity of the initial binding step determines the final distribution of the bifunctional adducts. Previous work has shown that the main adducts are GG (60 - 65%) and AG (~ 20%) intrastrand chelates.[9,10]

The substitution of the Cl^- in Pt-DNA monofunctional adducts follows first order kinetics (4-10 $\times 10^{-5}$ s^{-1}) at 37 ^oC.[7,8,9] The rates of hydrolysis of the second chloride ligand in cisplatin suggests that conversion of the chloro-monofunctional adducts to bifunctional adducts is the rate-limiting step.[8,9] However, it is worth mentioning that cisplatin could also undergo hydrolysis of both chloro ligands before reacting with nuclear DNA. Jestin *et al*.[11] have suggested that the second aquation step could occur within the outersphere complex formed between *cis*-$[PtCl(NH_3)_2(H_2O)]^+$ and DNA.

[9] Kozelka J., Legendre F., Reeder F., Chottard J., *Coord. Chem. Rev*., **1999**, *190*, 61.
[10] Saris C. P., van de Vaart P. J. M., Rietbroek R. C., Blommaert F. A., *Carcinogenesis*, **1996**, *17*, 2763.
[11] Jestin J. L., Lambert B., Chottard J. C., *JBIC*, **1998**, *3*, 515.

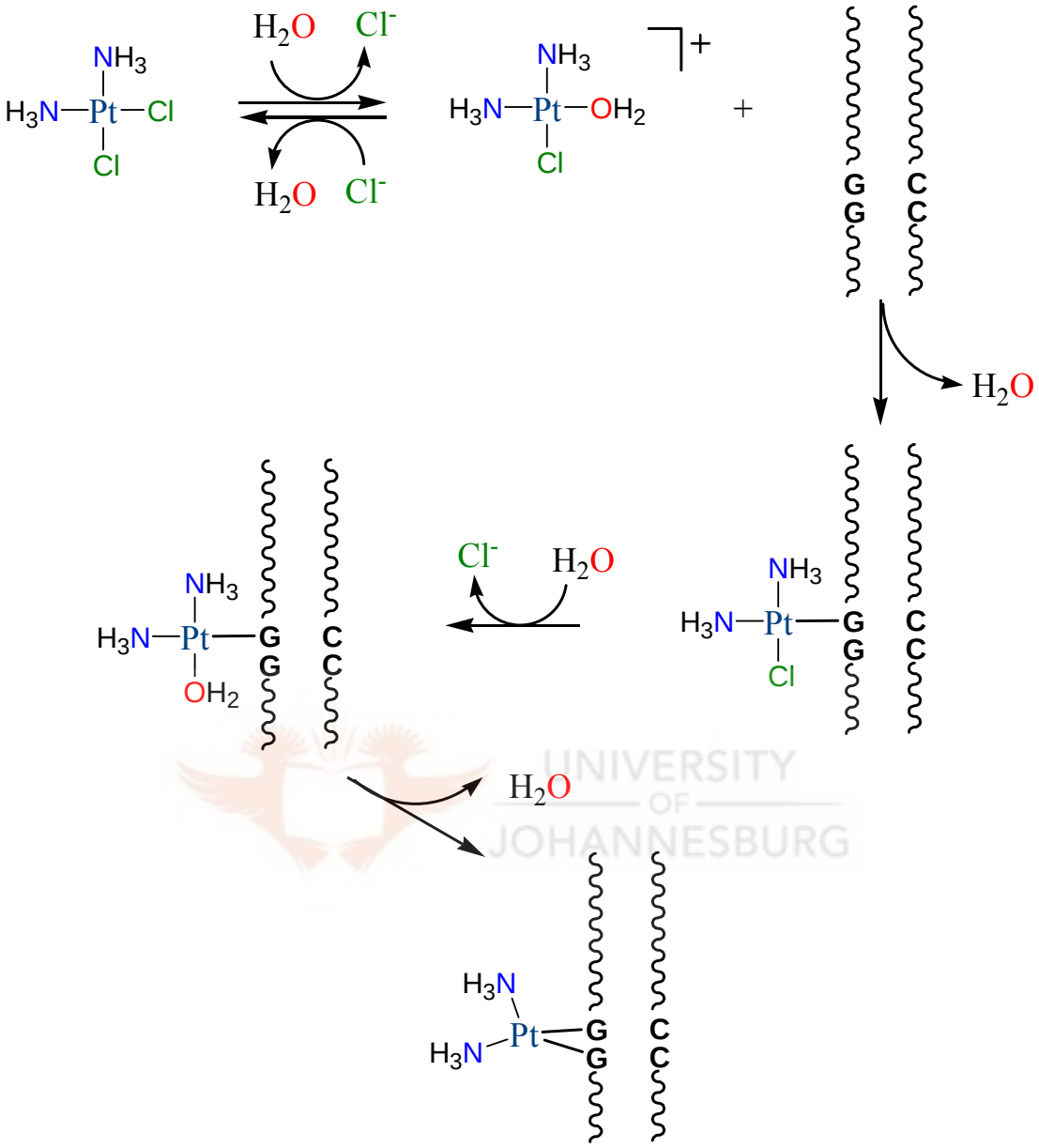

Scheme 3.1. General mechanism for cisplatin-DNA interactions (taken from *Coord. Chem. Rev.*, **1999**, 190, 61 (cf. ref. 9))

Reactions of biomolecules present in blood and cells, e.g., glutathione, L-methionine, metallothionein and L-cysteine, with cisplatin and other metallodrugs is much dependent on the structures and chemical reactivity of the biomolecules.[12,13] These biomolecules together with other proteins and enzymes have the potential to react with platinum complexes before they reach the DNA, thereby reducing their activities. Thus, understanding the dynamics of substitution reactions of potential anticancer compounds with biological nucleophiles is of relevant and great importance in the current drug research.

Substitution reactions of d^8 transition metals are of importance in cancer chemotherapy.[14] This is because it does not just allow for the establishment of reactions rates of various metal complexes, but also facilitate investigations into whether there is any relationship with their observed biological activities. Normally guanosine-5′-monophosphate is used as a model for DNA binding of platinum complexes, and L-cysteine (Cys) as a model for interaction of metal compounds with proteins that contain Cys residues. In addition, L-cysteine just like thiourea, is a very convenient substitute and is often employed as a nucleophile to study ligand substitution reactions. Although available data suggest that mechanism for substitution reactions for platinum(II) may apply to other square-planar complexes, there is scant information on the substitution reactions of palladium(II)[15] and gold(III) complexes due to their kinetic instability. For instance, gold(III) compounds are

[12] Hall M. D., Hambley T. W., *Coord. Chem. Rev*., **2002**, *232*, 49.
[13] Summa N., Schiess W., Puchta R., Hommes N. E., Van Eldik R., *Inorg. Chem*., **2006**, *45*, 2948.
[14] Fekl M., van Eldik R.., *Eur. J. Inorg. Chem*., **1998**, 389.
[15] Cotton F. A., Wilkinson G., Advanced Inorganic Chemistry, 6th Ed, John Wiley and Sons, New York, **1999**, 1064.

relatively unstable, light sensitive in solution, and easily reduced to metallic gold under physiological conditions due to their rapid kinetics and high redox potential than platinum(II).[16] In addition, gold(III) complexes react *ca*. 10^3 times faster compared to platinum(II) analogues, while palladium(II) complexes react 10^5-10^6 times faster[17,18] and is not always easy to follow their reactivities. This chapter reports on the investigation of the possible antitumour activities of dichloro-(bis(pyrazol-1-yl)aceticacid)palladium(II) ([$PdCl_2$(**L1**)], **1**), dichloro-(bis(3,5-dimethylpyrazol-1-yl)acetic acid)palladium(II) ([$PdCl_2$(**L2**)], **2**), dichloro-(bis(pyrazol-1-yl)aceticacid)platinum(II) ([$PtCl_2$(**L1**)], **3a**), dichloro-(bis(3,5-dimethylpyrazol-1-yl)acetic acid)platinum(II) ([$PtCl_2$(**L2**)], **4**), dichloro-(bis(pyrazol-1-yl)aceticacid)gold(III)chloride ([$AuCl_2$(**L1**)]Cl, **5a**) and dichloro-(bis(3,5-dimethylpyrazol-1-yl)aceticacid)gold(III) chloride ([$AuCl_2$(**L2**)]Cl, **6a**) against mammalian CHO-22 cells. The substitution behaviour, mechanism and associated kinetics of these complexes with L-cysteine have been performed as part of a study to establish whether there is any relationship between the observed antitumour activities against the CHO-22 cells and the kinetic labilities of the complexes.

[16] Fan D., Yang C. T., Ranford J. D., Lee P. F., Vittal J. J., *J. Chem. Soc., Dalton Trans*., **2003**, 2680.
[17] Schmulling M., Ryabov A. D., Van Eldik R., *Dalton Trans*., **1994**, 1257.
[18] Elmroth S., Bugarcic Z., Elding L. I., *Inorg. Chem*., **1992**, *31*, 3551.

3.1. Experimental

3.1.1 Biological reagents and instrumentation

All commercial chemicals and other reagents, other than those described below, were used as received. All cell culture reagents were supplied by Invitrogen Ltd. Cisplatin and neutral red (NR) dye was purchased from Sigma Aldrich. NR dye is a supravital dye used in histological staining.[19] The Hams F-12 medium containing 10% foetal calf serum and 0.2% pn-streptomycin was prepared from the stock Hams F-12 medium. The NR dye was prepared at 100μg/mL using an elution buffer prepared from an acetic acid:ethanol:water (50%:1%:49%) solution. Solutions of the six palladium(II), platinum(II) and gold(III) complexes (**1**-**6a**) screened, were prepared as 10 mM stock solutions using 0.2% DMSO solution. CHO-22 cells were obtained from the Department of Biochemistry, University of the Western Cape. The absorbance readings of the stained cells were measured spectrophotometrically at 492 nm.

3.2 Biological testing

3.2.1. Cell culture and drug treatment

CHO cells were cultured in 96 well plates at a population of 2 x 10^4 cells per well using Hams F-12 medium. The cells were incubated for 24 h at 37^{o}C in a 5% CO_2 atmosphere. At 80% cell confluence, the Ham F-12 medium was removed, cells washed with phosphate buffered saline (PBS) and 100 μL of fresh Ham F-12 medium containing the

[19] Babich H., Borenfreund E., *Appl. Environ. Microbiol.*, **1991**, *57*, 2101.

test compounds added. After 24 h of incubation at 37 °C in a 5% CO_2 atmosphere, the cells were then washed twice with PBS and 100 μL of serum free Ham F-12 medium containing NR dye (100 μg/mL) added to each well and further incubated for 3h. Finally the cells were washed twice with PBS. Thereafter, 50 μL of the elution buffer was used to lyse the cells and the concentration of accumulated NR dye, which is a marker for cell viability, measured spectrophotometrically at 492 nm. The percentage (%) cellular viability values were calculated from the absorbance (Abs) readings using the formula below; and the IC_{50} values obtained by extrapolation from the plots of % cellular viability versus concentrations.

$$\% \text{ inhibition} = 100 - \frac{\text{Abs of test reagent}}{\text{Abs of untreated control}} \times 100 \qquad \textbf{(3.1)}$$

3.2.2 Complexes and L-cysteine solutions

Dichloro-(bis(pyrazol-1-yl)acetic acid)palladium(II), (**1**) and dichloro-(bis(3,5-dimethyl-pyrazol-1-yl)acetic acid)palladium(II) (**2**), dichloro-(bis(pyrazol-1-yl)-acetic acid)platinum(II) (**3a**), dichloro-(bis(3,5-dimethyl-pyrazol-1-yl)acetic acid)platinum(II) (**4**), dichloro-(bis(pyrazol-1-yl)acetic acid)gold(III)chloride (**5a**), dichloro-(bis(3,5-dimethylpyrazol-1-yl)acetic acid)gold(III)chloride (**6a**), (Scheme 3.2) used in this study were synthesised as reported in chapter 2. L-cysteine was purchased from Sigma-Aldrich and used with no further purification. Diaqua complexes, **8-11**, were prepared *in situ* by addition of 1.99 molar equivalents of $AgClO_4$ to a 0.2% DMSO

solution of known amounts of the palladium(II) and platinum(II) chloro complexes (**1**, **2** and **3a**) and 2.99 molar equivalents of $AgClO_4$ to gold(III) complex, **5a**, in 0.1 M $HClO_4$. The resulting solution was filtered using a 0.5μm Miller-LCR filter and the solution made up to 50 mL to obtain the desired concentration of the stock solution. The water used was double-distilled passed through quartz. A 7.5 x 10^{-3} M (pH = 2.13) L-cysteine stock solution was prepared by dissolving 0.091 g of L-cysteine in 100 mL of double distilled water. Subsequently, L-cysteine solutions of concentrations, 1 x 10^{-3}, 2 x 10^{-3}, 3 x 10^{-3}, 4 x 10^{-3} and 5 x 10^{-3} M were prepared from the stock solution.

Caution: Perchlorate salts of metal complexes with organic ligands are potential explosives.

3.2.3 Kinetic measurements

Kinetic studies were performed using a Shimadzu UV-2501PC UV-Vis spectrophotometer for the slow reactions and a Hi-Tech SF-61 DX2 stopped-flow spectrophotometer for the fast reactions. The cell compartments for both instruments were well thermostatted for constant temperature measurements using a Shimadzu thermoelectric temperature controller, TCC-240A, with the UV-2501PC UV-Vis spectrophotometer, while water of regulated temperature was circulated from a Neslab RTE 7 thermocirculator to the cell compartment of the stopped-flow equipment. Temperatures were maintained to an accuracy of ±0.1^{o}C, while the ionic strength was maintained at 0.10M $HClO_4/LiClO_4$ in all the reactions monitored. Kinetic data were collected by measuring absorbance at fixed λ_{max} 315 nm for the palladium(II) complex,

285 nm for the platinum(II) complex and 239 nm for the gold(III) complex. Preliminary investigations showed that the reactions were inversely dependent on pH. Thus all reactions were studied under pseudo-first-order conditions in the pH range of 2.92 to 3.72, which guaranteed the presence of the diaqua form of the complexes. Van Eldik and co-workers showed in a similar study involving $[Pt(diaminocyclohexane)(H_2O)_2]^{2+}$ and $[Pt(ethylenediamine)(H_2O)_2]^{2+}$ among other platinum complexes, that the diaqua species are maintained in a low pH range (1-4). Presumably in this pH range, the pKa values of complexes **8-11** are comparable to those of compounds reported by Van Eldik and co-workers.[13] A large excess of L-cysteine was used in the reactions with a 10:1 ratio of [Cys]:[complex]. All kinetic studies were followed for at least 4 half-lives. For slow processes, pseudo first-order rate constants, k_{obs}, were obtained by importing absorbance changes data measured on a UV-Vis spectrophotometer into the single exponential fitting of the KinetAsyst^{TM}3 software program. The k_{obs} values for fast processes were obtained directly from the stopped-flow equipment software program using KinetAsyst^{TM}3 by fitting the curves to a single exponential analysis.

3.3. Results and discussion

3.3.1. Biological results

Six complexes, **1-6a**, shown in Scheme 3.2 were investigated for their anti-proliferative activities against chinese hamster ovary (CHO-22) cells. The cells were treated with various concentrations, 0.025, 0.05, 0.1, 0.2, 1, 2, 4 and 8 mM, of the complexes and cisplatin. The cells were incubated for 24 h. All data were acquired in triplicate. A summary of the IC_{50} values are given in Table 3.1.

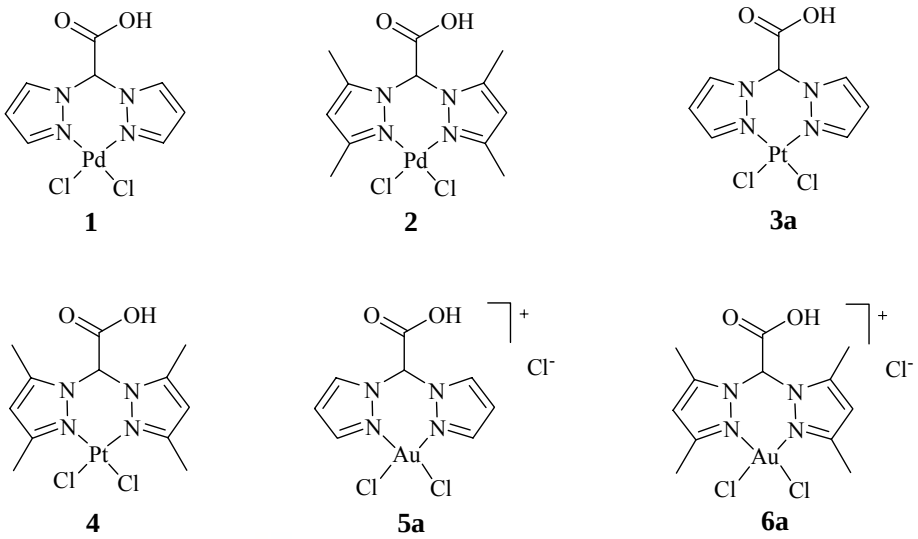

Scheme 3.2. Complexes tested for anti-tumour their anti-tumour against CHO-22 cells.

Table 3.1. Growth inhibition values of compounds **1**–**6a** tested against CHO-22 cells.

Agent	IC_{50} (mM)	Agent	IC_{50} (mM)
1	1.5 ± 0.2	**4**	4.0 ± 1.2
2	1.3 ± 0.2	**5a**	1.5 ± 0.1
3a	1.5 ± 0.1	**6a**	5.4 ± 0.1
Cisplatin	0.07 ± 0.01		

IC_{50} is the concentration of compounds required to inhibit cell growth by 50 %.

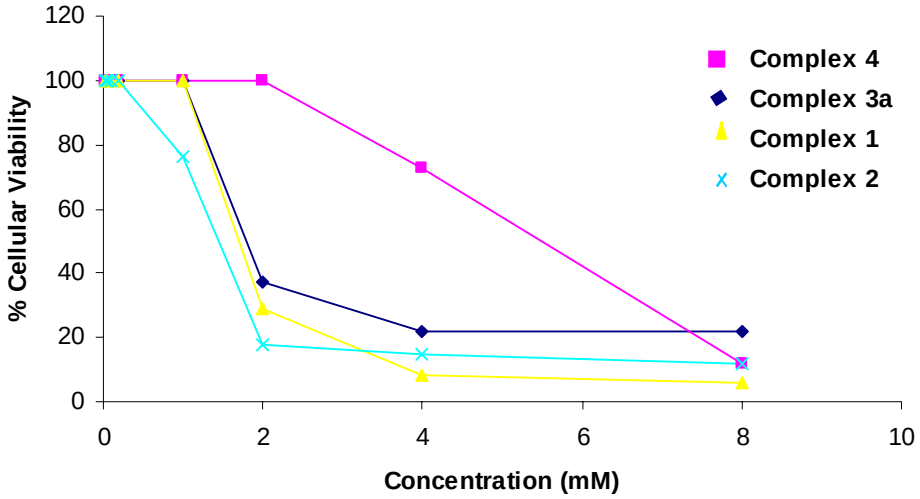

Figure 3.1. Cellular viability results showing growth inhibition in CHO-22 cells by compounds **1**, **2**, **3a** and **4**.

Palladium(II) and platinum(II) compounds **1-4** showed no inhibition at concentrations less than 1.0 mM (Fig. 3.1). This is not surprising as palladium compounds tend to undergo translabilisation easily. Thus, it is possible that these palladium(II) complexes reacted with thiol containing molecules in the culture medium hence undergoing thiol deactivation. This could therefore explain the low activities observed against CHO-22 cells. Nevertheless, at higher concentrations (2.0 mM) the palladium(II) compounds showed growth inhibition of 72 and 82% for [$PdCl_2$(**L1**)] (**1**) and [$PdCl_2$(**L2**)] (**2**), respectively, compared to their platinum(II) analogue, [$PtCl_2$(**L1**)] (**3a**), with 64% growth inhibition at the same concentration (Fig. 3.1). The complex [$PtCl_2$(**L2**)] (**4**), however, showed no growth inhibition at the same concentration. Notably, the antitumour activities of platinum drugs are to a greater extent attributed to the kinetics of ligand displacement

reactions.[20,21] As a result, it is possible that the low activity of **4** is due to its kinetic stability, which would slow down the process of formation of the active species ($[PtCl(\mathbf{L2})(OH_2)]^+$). Another inference drawn from the activities of the platinum(II) complexes, is that the less bulky complex, **3a**, was more active than the more bulky **4**. While it could be true that sterically hindered platinum compounds exert better activities than the less sterically hindered ones, this was not true for complex **4**. It is possible that a greater steric hindrance provided by bis(3,5-dimethylpyrazolyl)acetic acid ligand could have exceeded the optimum bulkiness for its activity. However, it should also be noted that this is always not the case and more work is needed to support this argument for the series of complexes in this thesis.

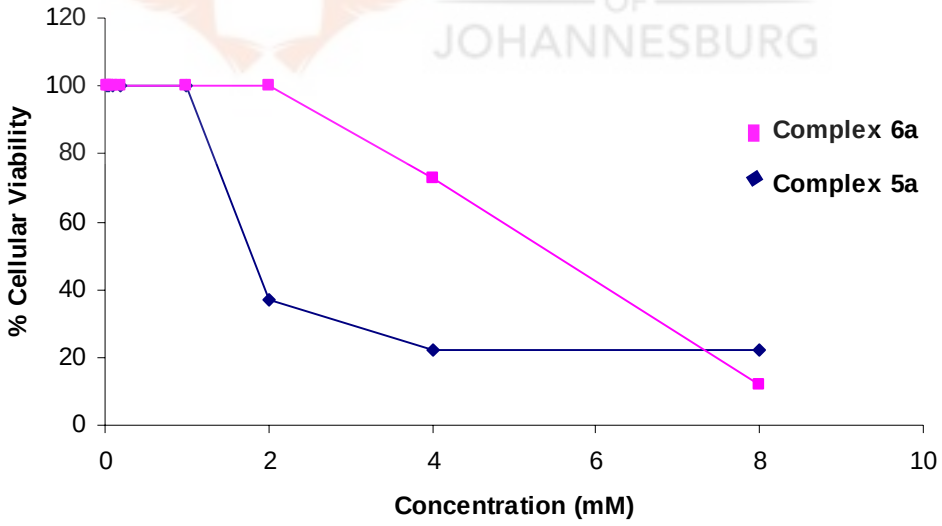

Figure 3.2. Cellular viability results showing growth inhibition in CHO-22 cells by complexes **5a** and **6**.

[20] Berners-Price S. J., Appleton T. G., *Platinum-Based Drugs in Cancer Therapy*, Humana Press, Totowa, NJ, USA, **2000**, 3.
[21] Huq F., Tayyem H., Beale P., Yu J. Q., *J. Inorg. Biochem.*, **2007**, *101*, 30.

A similar trend was observed for the gold(III) complexes, which showed no appreciable growth inhibition of HeLa cells at concentrations less than 1.0 mM (Fig. 3.2). However, at 2.0 mM compound $[AuCl_2(\mathbf{L1})]Cl$ (**5a**) showed 75% growth inhibition whereas its dimethyl analogue, $[AuCl_2(\mathbf{L2})]Cl$ (**6a**), had no inhibition at the same concentration in spite of their structural similarity (Fig. 3.2). The IC_{50} of compounds **5a** and **6a** were found to be 1.6 and 5.4 mM respectively. One of the main problems associated with gold(III) complexes in comparison with platinum(II), is the observed low stability in solution under physiological conditions. It has been reported that they undergo a faster hydrolysis and/or reduction to gold(I) accompanied by the formation of colloidal gold in some cases, meaning that the compounds are of low clinical usefulness.[22] The low activities of gold(III) complexes **5a** and **6a** were attributed to their fast hydrolysis rates as well as their possible low stabilities in physiological conditions. However, there was no physical evidence of the formation of colloidal gold in the cases of **5a** and **6a**, as reported in the literature.

It is clear that the IC_{50} values of complexes **1**-**6a** (Table 3.1) are higher than that of cisplatin (0.07 mM), thus ruling them out as potential anticancer drugs. Nevertheless, the kinetic labilities of these complexes were investigated in order to find out if there was any relationship between their ligand substitution reaction rates and the observed low biological activities. The next section deals with the kinetic studies.

[22] [a]Criado J. J., Manzano J. L., Rodriguez-Fernandez E., *J. Inorg. Biochem*., **2003**, *96*, 311; bCalamai P., Carotti S., Guerri A., Mazzei T., Messori L., Mini E., Orioli P., Speroni G. P., *J. Inorg. Biochem*., *1997*, *66*, 103.

3.3.2 Kinetics of reaction of L-cysteine with palladium(II), platinum(II) and gold(III) complexes

Reactions of L-cysteine with four selected complexes, **1**, **2**, **3a** and **5a** (Scheme 3.2)**,** was studied by UV-Vis and stopped-flow spectrophotometry. This was achieved by measuring the absorbance changes with time. Initial investigations showed that the kinetics of the chloro complexes **1**, **2**, **3a** and **5a** were very slow, hence they were converted to the diaqua forms, $[Pd(\mathbf{L1})(OH_2)_2]^{2+}$ (**8**), $[Pd(\mathbf{L2})(OH_2)_2]^{2+}$ (**9**), $[Pt(\mathbf{L1})(OH_2)_2]^{2+}$ (**10**) and $[Au(\mathbf{L1})(OH_2)_2]^{3+}$ (**11**) (Scheme 3.3).

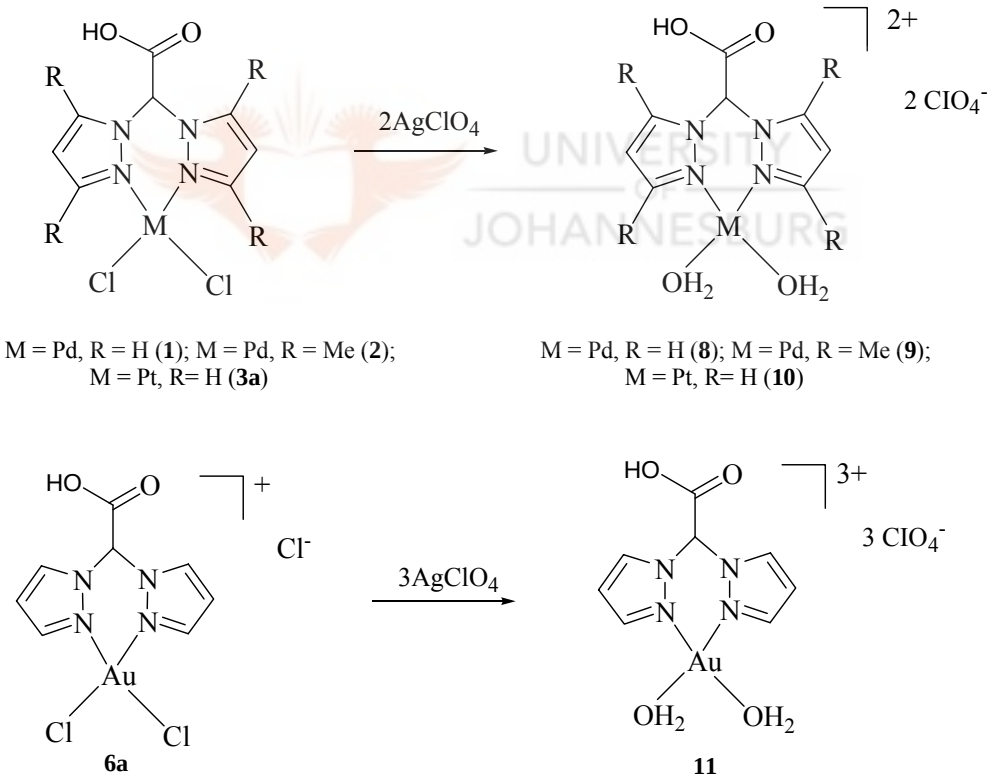

Scheme 3.3. The preparation of the diaqua complexes **8-10**

The reactions of L-cysteine with the palladium(II) and platinum(II) complexes (**8-10**) were similar and established to be simple substitution processes. The difference is in the reaction rates, with palladium(II) complexes (**8** and **9**) displaying fast kinetic reactions compared to the analogous platinum(II) complex (**10**). This was deduced from the pseudo-first-order rate constants (k_{obs}) values (Tables 3.2-3.4) obtained from plotting the absorbance values versus time according to equation 3.2 below:

$$\ln(A_\infty - A_t) = -k_{obs}t \qquad (\mathbf{3.2})$$

The substitution of the aqua ligands in complexes **8**, **9** and **10** with L-cysteine, to give bis(cysteine) complexes, can be represented as shown in Scheme 3.4. Figure 3.3 illustrate typical kinetic trace for the substitution reaction of complex **10** with L-cysteine.

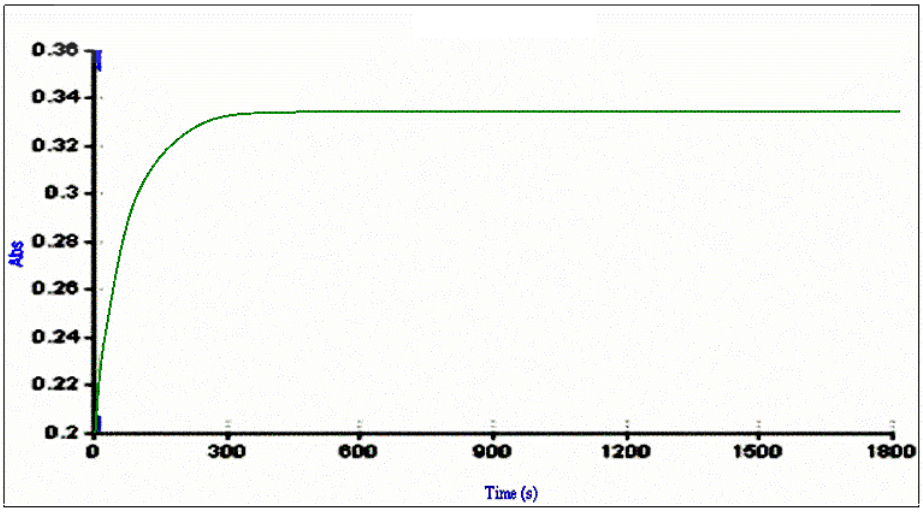

Figure 3.3. Kinetic trace for the reaction of complex **10** (5×10^{-5} M) with L-Cysteine (10×10^{-4}M) at 285 nm, **T** = 298 K.

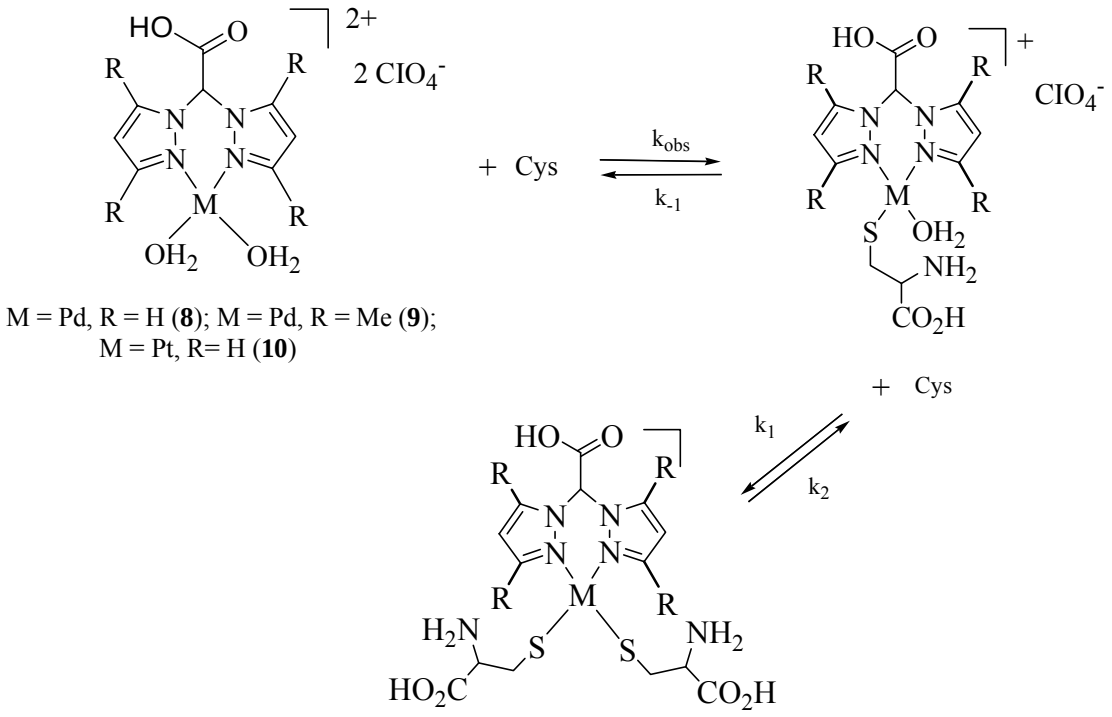

M = Pd, R = H (**8**); M = Pd, R = Me (**9**);
M = Pt, R= H (**10**)

M = Pd, R = H (**12a**); M = Pd, R = Me (**12b**);
M = Pt, R = H (**12c**)

Scheme 3.4. The reaction of the palladium(II) and platinum(II) diaqua complexes (**8-10**) with L-cysteine.

Subsequently, plots of the pseudo-first-order rate constants k_{obs} versus L-cysteine concentration ([Cys]) were linear according to the two-term rate law:

$$k_{obs} = k_{-1} + k_1[Cys] \qquad (\mathbf{3.3})$$

This is typical of two-term rate equations for nucleophilic substitution in d^8 square planar complexes, where k_1 denotes a second-order rate constant for the direct substitution of water molecules, and k_{-1} represents first-order rate constant for the reverse reaction where a water molecule replaces the coordinated nucleophile.[23] Plots of k_{obs} versus L-cysteine

[23] Shoukry A., Brindell M., Van Eldik R., *Dalton Trans*., **2007**, 4169.

concentration obtained for palladium(II) complexes **8** and **9** were linear with non-zero intercepts, that is, k_{-1} = 2.0 x 10^{-1} s^{-1} and 1.8 s^{-1}, respectively, signifying reversibility of this step (Fig. 3.4). Similar patterns of reverse aquation processes were reported by Schmülling *et al*. in their study of substitution reactions of $[Pt\{C_6H_3X(CH_2NMe_2)\}(NC_5H_4SO_3)(H_2O)]$ complexes (X = H, 3-OMe) with thiourea. However, for platinum(II) complex **10** no reversibility of this first step was observed, as indicated by the insignificant intercept (k_{-1} = 6.4 x 10^{-4} s^{-1}) (Fig. 3.5).

Table 3.2. Rate constants for the reaction of L-cysteine with complex **8**.

[Cyst] x 10^{-4} M	**k_{obs} x 10^{-3} (s^{-1})**				
	293 K	**298 K**	**303 K**	**308 K**	**313 K**
3	153.8	347.5	451.2	595.3	788.8
6	260.1	525.1	667.3	912.6	1361
9	366.4	671.4	940.1	1251.0	1846.6
12	472.6	862.7	1172.2	1690.0	2452.4
15	578.6	1076.1	1409.0	2036.3	3007.5
k_1 ($M^{-1}s^{-1}$)	**354.2**	**598.2**	**806.8**	**1220**	**1842**

[Pd(II)] = 3 x 10^{-5}M, ***I*** = 0.1 M

Table 3.3. Rate constants for the reaction of L-cysteine with complexe **9**.

[Cyst] x 10^{-4} M	k_{obs} x 10^{-3} (s^{-1})				
	293 K	**298 K**	**303 K**	**308 K**	**313 K**
3	740.4	1479.0	2484.7	3653.6	5791.4
6	1030.3	1881.0	3092.0	4782.7	7044.6
9	1318.6	2402.4	3761.5	5791.0	8689.2
12	1610.5	2810.8	4436.7	6905.4	10410.1
15	1875.0	3226.6	5082.2	8006.5	11710.2
k_1 ($M^{-1}s^{-1}$)	**451.9**	**701.3**	**1038**	**1718**	**2414**

[Pd(II)] = 3.8 x 10^{-5}M, ***I*** = 0.1 M

Table 3.4. Rate constants for the reaction of L-cysteine with complex **10**.

[Cyst] x 10^{-4} M	k_{obs} x 10^{-3} (s^{-1})				
	293 K	**298 K**	**303 K**	**308 K**	**313 K**
10	1.4	1.9	2.6	3.3	4.2
20	2.0	3.0	4.5	5.6	7.2
30	2.8	4.0	5.8	7.8	10.0
40	3.6	4.9	7.5	9.5	12.7
50	4.2	6.0	8.7	11.9	14.7
k_1 ($M^{-1}s^{-1}$)	**0.7**	**1.02**	**1.5**	**2.1**	**2.6**

[Pt(II)] = 5 x 10^{-5}M, ***I*** = 0.1 M

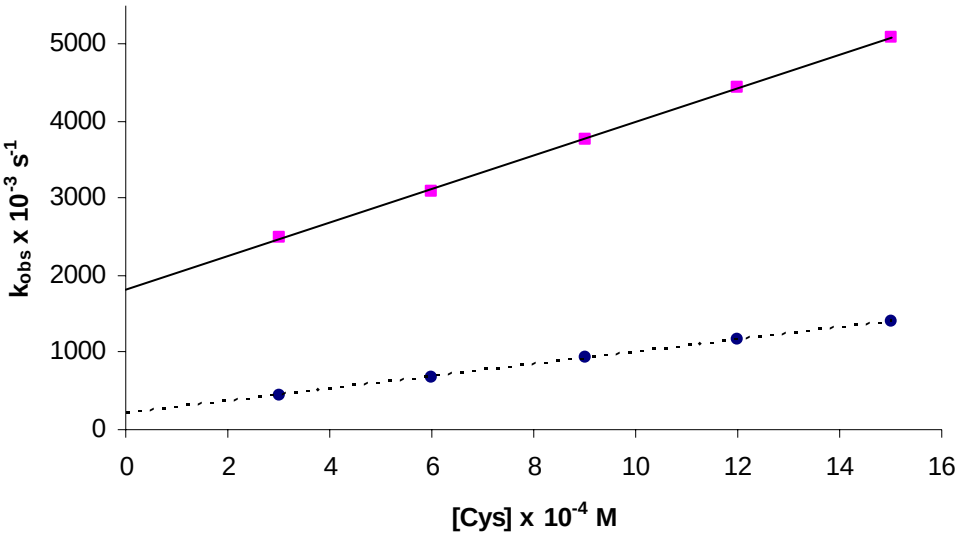

Figure 3.4. Plots of k_{obs} vs. [Cys] for palladium complexes **8** (3.0 x 10^{-5} M) (---) and **9** (3.8 x10^{-5} M) (—) at 303 K, ***I*** = 0.1 M.

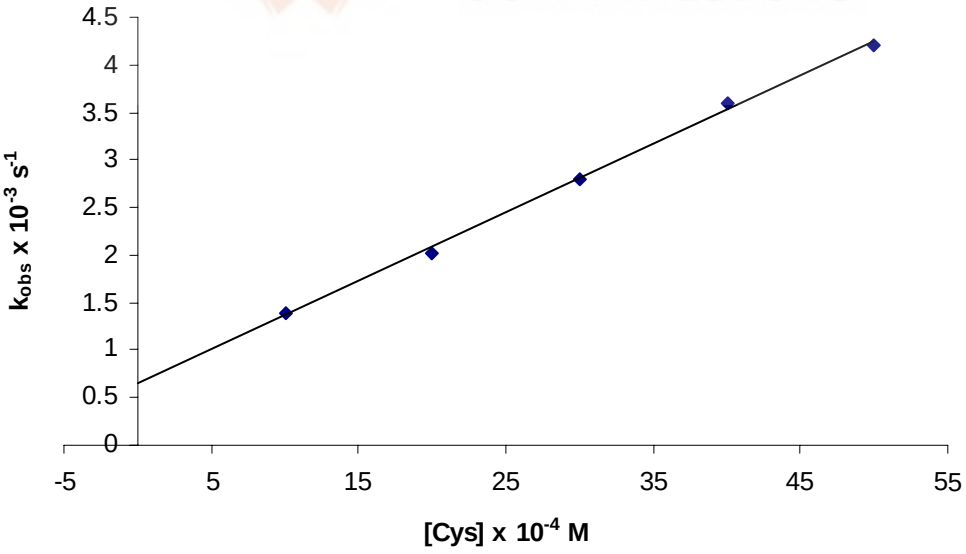

Figure 3.5. Plots of k_{obs} vs. [Cys] for complex **10** (5.0 x 10^{-5} M) at 293 K, ***I*** = 0.1 M.

Contrary to the substitutions reactions of **8-10** with L-cysteine, reactions of L-cysteine with the gold(III) complex (**11**) exhibited an initial fast substitution step (Table 3.5, Fig. 3.6) followed by a much slower process. It is possible that this slow process is due to the reduction of **11** to gold(I) species (Table 3.6, inset in Fig 3.6). The pseudo-first-order rate constants k_{obs} for the fast substitution process in **11** were obtained in the same way as for **8** and **9**, using equation 3.2. Subsequently, the second rate constants for the substitution reactions were obtained from plotting k_{obs} versus L-cysteine concentration. The plots were linear according to the two-term rate law given in equation 3.3. The non-zero intercepts in the plots of k_{obs} vs [Cys] for **11** ($k_{-1} \approx 5.0 \times 10^{-1}$ s^{-1}) signifies the reversibility of the substitution process, where a coordinated L-cysteine is replaced by a water molecule. The substitution rates of **11** are three times faster than for platinum complex **10**. For example, the substitution in **11** was fast with a second order rate constant of 321.8 M^{-1} s^{-1} at 298 K compared to that of **10** (1.0 M^{-1} s^{-1}) at the same conditions.

The consequent presumptive reduction process of **11** to gold(I) was quite slow and was captured on the conventional UV-Vis spectrophotometer. The pseudo-first-order rate constants k_{obs} for this process were obtained by plotting the absorbance values versus time according to equation 3.2, whilst the second order rate constants (k_3) for this process were obtained from plots of k_{obs} versus [Cys] according to equation 3.4 below. The plots (Fig. 3.7) were linear with insignificant intercepts ($k_{-1} \approx 1.0 \times 10^{-4}$ s^{-1}), thus indicating the irreversible nature of the reduction process in **11**.

$$k_{obs} = k_{-1} + k_3[Cys] \approx k_3[Cys] \quad (\mathbf{3.4})$$

The parameter k_3 represents second rate constants for the reduction process, which follows the substitution reactions of complex **11** with L-cysteine (Scheme 3.5). The k_{obs} and k_3 values for the reduction process in **11** were much smaller than its corresponding values for the substitution process (Tables 3.5 and 3.6). For example, the second order rate for the reduction process was found to be 1.0 M^{-1} s^{-1} at 298 K (Table 3.6). It is three times slower than that of the preceding substitution process (321.8 M^{-1} s^{-1}). From the results obtained (k_{obs}), this reduction process is linearly dependent on the L-cysteine concentration.

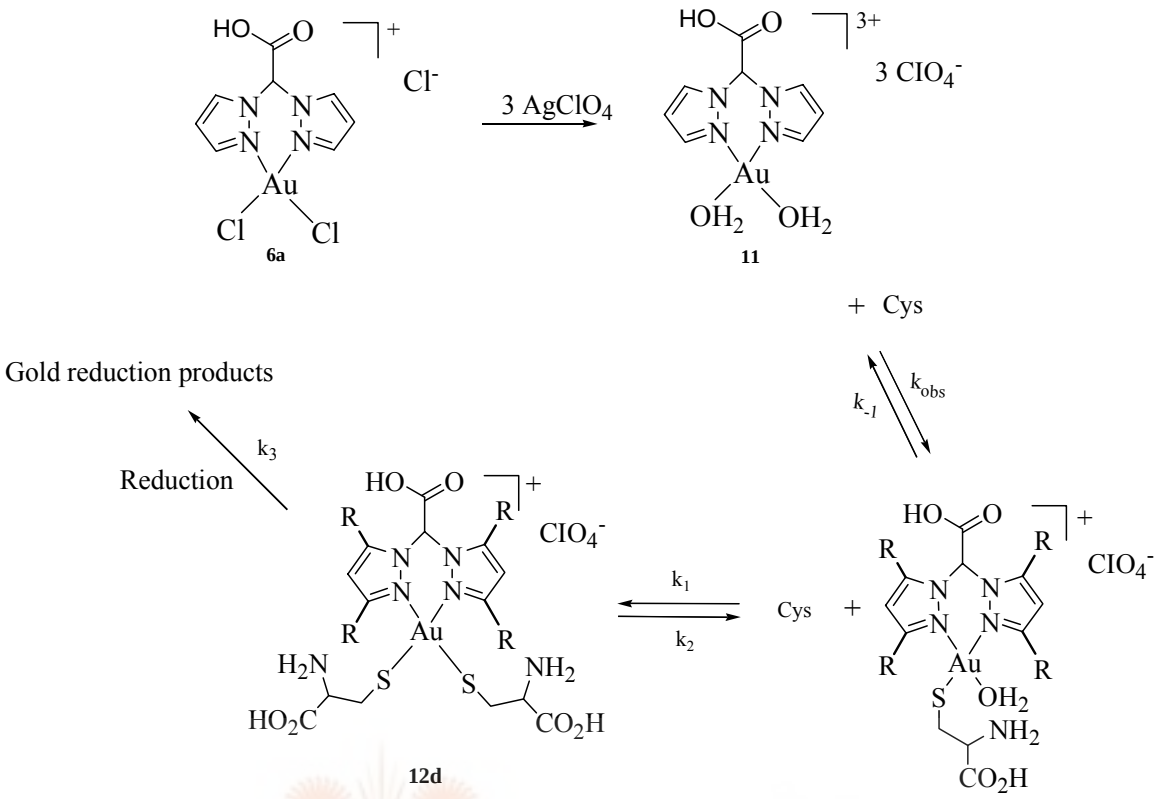

Scheme 3.5. The reaction of the gold diaqua complex **11** with L-cysteine.

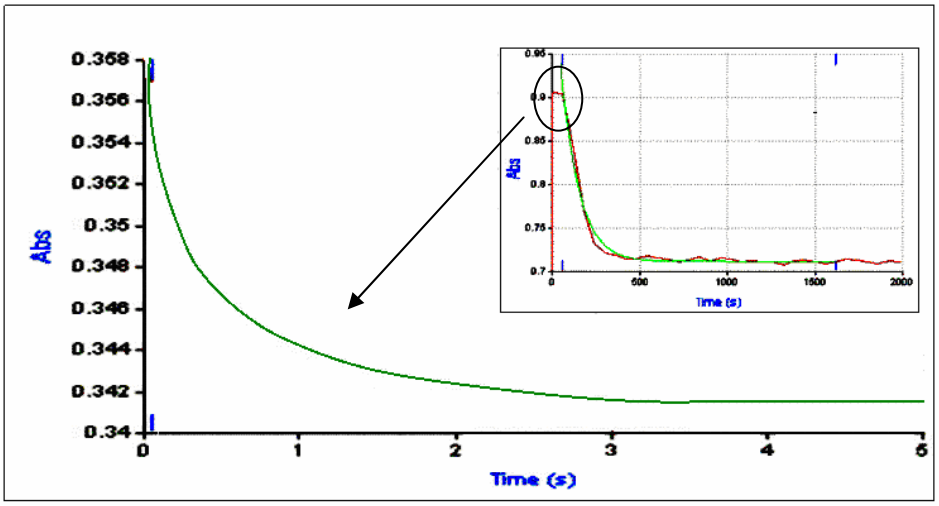

Figure 3.6. Kinetic trace for the reaction of complex **11** (5 x 10^{-5} M) with L-Cysteine (10 x 10^{-4}M) at 239 nm, **T** = 298 K. The slow reduction process is shown in the inset.

Table 3.5. Rate constants for the reaction of L-cysteine with **11**.

	k_{obs} x 10^{-3} (s^{-1})				
[Cyst] x 10^{-4} M	**293 K**	**298 K**	**303 K**	**308 K**	**313 K**
5	472.7	591.2	917.6	1053.1	1201.3
10	619.2	856.4	1061.3	1251.0	1366.0
20	880.1	1170.2	1405.4	1675.0	1739.2
30	1251.5	1446.0	1766.0	1899.2	2201.4
40	1492.0	1756.0	2062.2	2356.4	2589.7
50	1829.2	2101.4	2462.0	2658.2	2892.5
k_1 ($M^{-1}s^{-1}$)	**300.8**	**321.8**	**341.6**	**357.4**	**387.4**

[Au(III)] = 5 x 10^{-5} M; ***I*** = 0.1 M

Table 3.6. Rate constants of the reduction of **11** to gold(I).

[Cyst] x 10^{-4} M	k_{obs} x 10^{-3} (s^{-1})				
	293 K	**298 K**	**303 K**	**308 K**	**313 K**
10	1.1	2.1	3.4	4.3	5.0
20	2.0	2.9	4.4	5.5	6.3
30	2.6	3.9	5.3	6.6	7.6
40	3.5	4.9	6.5	8.0	9.7
50	4.4	5.9	7.9	9.7	10.9
k_3 (M^{-1} s^{-1})	**0.8**	**1.0**	**1.1**	**1.3**	**1.5**

[Au(III)] = 5 x 10^{-5}M, ***I*** = 0.1 M.

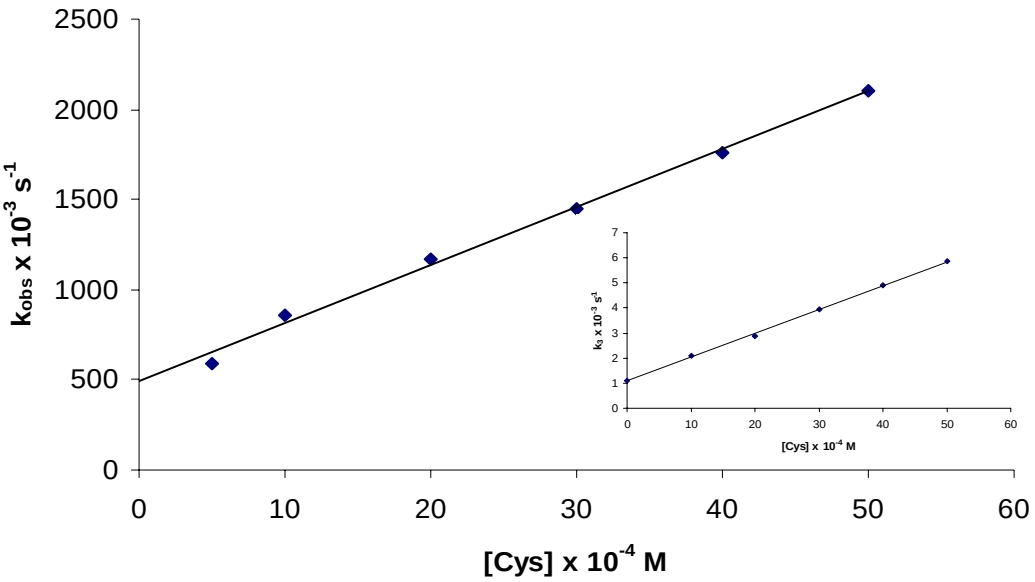

Figure 3.7. Plots of k_{obs} vs. [Cys] for **11** (5.0×10^{-5} M) at 298 K, ***I*** = 0.1 M. Inset depicts plots of k_1 vs. [Cys] for the reduction process of **11**.

In general, the rates of substitution reactions of complexes **8-11** with L-cysteine were found to be pseudo-first-order. The first step is the substitution of the first aqua ligand, followed by a second substitution step, which was slower and is attributed to the substitution of the second aqua ligand. Similar substitution reactions patterns with different nucleophiles have been observed for many platinum(II) compounds and a few palladium(II) compounds. For example $[Pt(bpy)(H_2O)_2]^{2+}$ (bpy = N,N'-bipyridine), $[Pt(en)(H_2O)_2]^{2+}$ (en = ethylenediamine) and [Pd(en)(cbdca)] (en = ethylenediamine, cbdca = cyclobutane-1,1-dicarboxylate)[24] react with thiourea in a similar way as observed for compounds **8-11** herein (*vide supra*). However, gold(III) complex **11** undergo a further reduction process presumably to gold(I) species. No efforts were made

[24] Shoukry A., Rau T., Shoukry M., Van Eldik R., *J. Chem. Soc., Dalton Trans*., **1998**, 3105.

to characterise the reduction products. The rate constants for the substitution reactions of L-cysteine in palladium(II) complexes **8** and **9** are faster than in platinum(II) (**10**) and gold(III) (**11**) complexes (Tables 3.2-3.5); and in agreement with literature reports that substitution reactions of square planar palladium(II) complexes are faster than for square planar gold(III) and platinum(II) complexes respectively.[15,17]

The rate of substitution in **10** (prepared from **3a**) is slower than in complexes **8**, **9** and **11** (prepared from **1, 2** and **5a**, respectively) (Schemes 3.4 and 3.5). Although these slow rates suggest that platinum(II) complex **3a** would have better chance of reaching the target in cells compared to palladium(II) complexes (**1** and **2**) and gold(III) complex **5a**, the IC_{50} values (Table 3.1) are similar for all the four compounds; suggesting that there is no relationship between the observed anticancer activities of these complexes with their kinetic labilities. Nevertheless, the L-cysteine substitution reactions have some interesting observations.

There are a number of thermodynamic parameters that could be derived from the kinetic data to shed more light on the mechanism of the L-cysteine substitution reactions. For all the reactions studied, the rate constants increased with increasing temperature; and from the second order rate constants at different temperatures, activation parameters $\Delta H^{\ddagger}$ and $\Delta S^{\ddagger}$ were obtained (Table 3.7).

Table 3.7. Activation parameters determined from the temperature dependence of the rate constants for the substitution of Pd(II), Pt(II) and Au(III) complexes, and reduction of Au(III).

Activation parameter	**8**	**9**	**10**	**11**	Reduction of **11** to gold(I)
$\Delta H^{\ddagger}$ (kJ mol^{-1})	42.6	62.2	48.3	6.8	18.4
$\Delta S^{\ddagger}$ (kJ mol^{-1})	-47.8	+18.4	-82.6	-174	-183

The activation entropy ($\Delta S^{\ddagger}$) changes for all the substitutions, except for palladium(II) complex **9**, are largely negative and in agreement with the fact that substitution reactions involving square planar complexes are invariably accompanied by large negative entropy changes.[25] The entropy change for **9** is positive ($\Delta S^{\ddagger}$ = +18.4 J K^{-1} mol^{-1}), but is relatively low to fit an associative mechanism of substitution. Unlike **8**, **10** and **11**, compound **9** has a more bulky ligand, bis(3,5-dimethylpyrazolyl)acetic acid. It is possible that the steric bulkiness hinders the entrance of L-cysteine; thereby leading to less ordered transition state. Moreover, such low values (+18.4 J K^{-1} mol^{-1}) are always regarded as close to zero and are attributed to associative interchange mechanisms.[24,26,27] Generally, the data obtained show that the substitution of aqua ligands in complexes **8**-**11** is *via* an associative mechanism. The data also show that the slower reactions have higher $\Delta H^{\ddagger}$ values, consistent with literature findings that substitution reactions of platinum(II)

[25] Wilkins G. R., The Study of Kinetics and Mechanism of Reactions of Transition Metal Complexes, Allyn and Bacon, Inc. Boston, **1974**, 227.
[26] Rau T., Shoukry M., van Eldik R., *Inorg. Chem.*, **1997**, *36*, 1454.
[27] Hohmann H., Hellquist B., van Eldik R., *Inorg. Chem.*, **1992**, *31*, 1090.

complexes are largely $\Delta H^{\ddagger}$-controlled.[28] Tables 3.8 and 3.9 show data for calculation of the energy parameters, whilst Figure 3.8 show the corresponding Eyring plots.

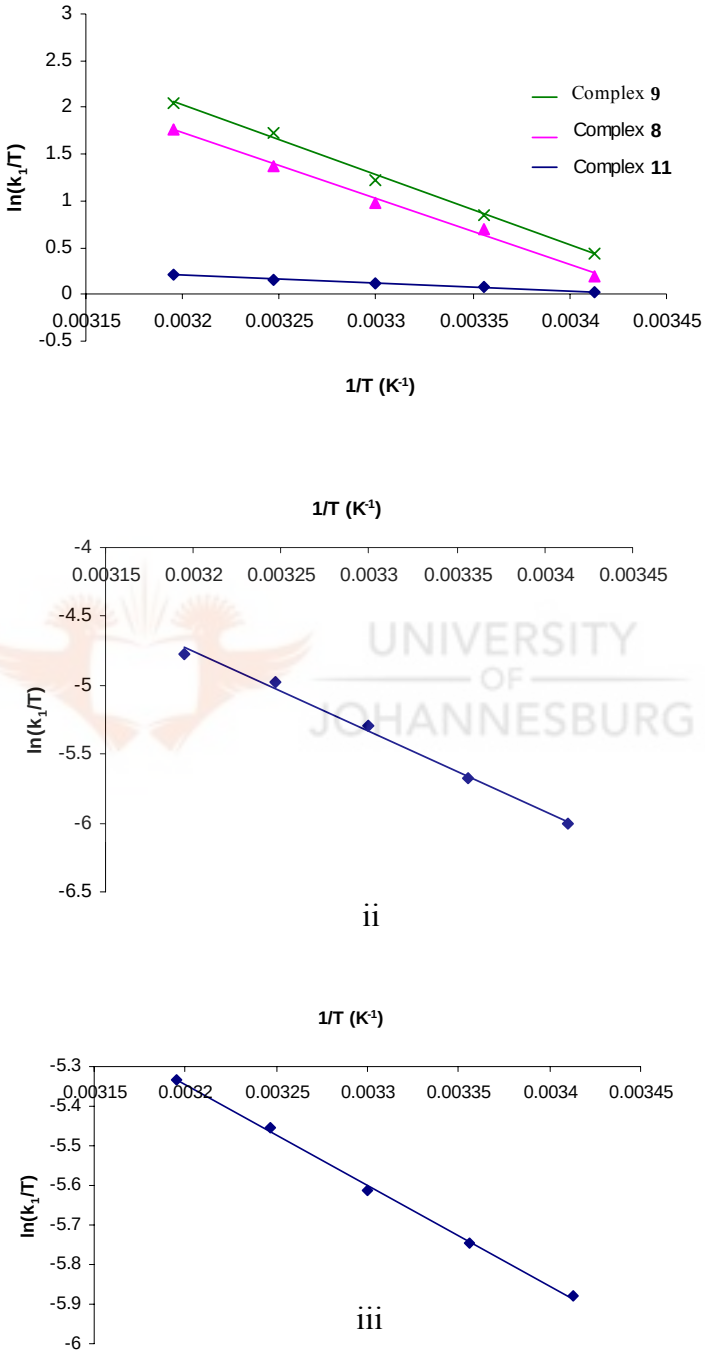

Figure 3.8. Temperature dependence plots for the reaction of complexes with L-cysteine. (i) **8**, **9** and **11**, (ii) **10**, (iii) reduction of **11.**

[28] Bajaj H. C., van Eldik R., *Inorg. Chem.*, **1988**, *27*, 4052.

Table 3.8. Calculation of energy parameters.

	8	**9**	**10**	**11**	Reduction of **11**
Slope	-7054.8	-7489	-5814.2	-817.5	-2543.5
Intercept	24.299	25.987	13.852	2.8166	2.7943

Slope = $- \Delta H^{\ddagger}/R$, Intercept = $\ln(k/h) + \Delta S^{\ddagger}/R$

Table 3.9. Variation of k_1 and k_3 rate constants with temperature for complexes **8**, **9**, **10** and **11**.

T(K)	1/T (K^{-1})	**8**		**9**		**10**		**11**		Reduction of **11**	
		k_1 ($M^{-1}s^{-1}$)	In(k_2/T)	k_1 ($M^{-1}s^{-1}$)	In(k_2/T)	k_1 ($M^{-1}s^{-1}$)	In(k_2/T)	k_1 ($M^{-1}s^{-1}$)	In(k_2/T)	k_3 ($M^{-1}s^{-1}$)	In(k_2/T)
293	0.003413	354.2	0.19	451.9	0.43	0.7186	-6.01	300.8	0.03	0.8190	-5.88
298	0.003356	598.2	0.70	701.3	0.86	1.021	-5.67	321.8	0.08	0.9524	-5.75
303	0.003300	806.8	0.98	1038	1.23	1.521	-5.29	341.6	0.12	1.106	-5.61
308	0.003247	1220	1.38	1718	1.72	2.114	-5.98	357.4	0.15	1.319	-5.45
313	0.003195	1842	1.77	2414	2.04	2.639	-4.78	387.4	0.21	1.512	-5.33

Product formation in the substitution reactions involving complexes **1**, **2**, **3a** and **5a** with L-cysteine could be followed by ^{1}H NMR spectroscopy. In a typical experiment, a direct reaction of **1** with L-cysteine gave [Pd(**L1**)(Cys)$_2$] (**12a**). An attempt was made to follow the formation of compound **12a** by ^{1}H NMR spectroscopy in DMSO-d_6. However, the stepwise formation of **12a** could not be captured clearly, probably due to the fast nature of the substitution process. Nevertheless, the spectrum of solution containing L-cysteine and **1** shows peaks due to **1** and L-cysteine.

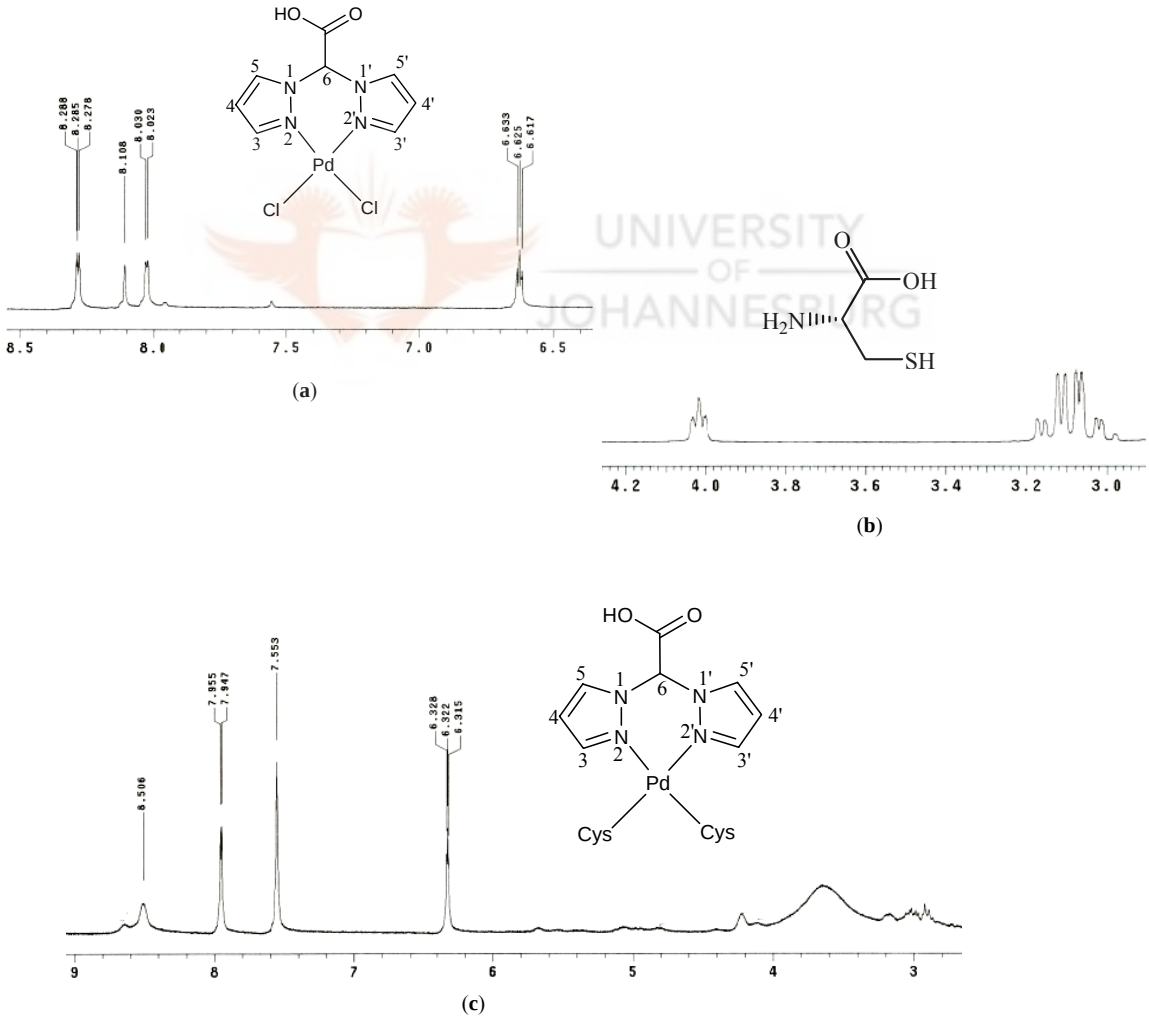

Figure 3.9. ^{1}H NMR spectra of (**a**) [PdCl$_2$(**L1**)] (**1**), (**b**) L-cysteine and (**c**) [Pd(**L1**)(Cys)$_2$] (**12a**) acquired after 5 min (solvent, DMSO-d_6)

The spectrum (Fig. 3.9**c**) acquired after 5 min shows major upfield shifts of the proton peaks of the bis(pyrazolyl)acetic acid ligand (bpza) at 7.95 ppm (5H, 5H′), 7.55 ppm (3H, 3H′ + CH linker proton) and 6.32 ppm (4H, 4H′) (Fig. 3.9**c**) in comparison with that of **1** (Fig. 3.9**a**), which has the four peaks at 8.29 ppm (5H, 5H′), 8.11 ppm (CH linker proton), 8.03 ppm (3H, 3H′) and at 6.63 ppm (4H, 4H′). The spectrum in Figure 3.9**c** also displays five faint humps at 4.18 ppm, 4.81, 5.09, 5.72 ppm and at 8.65 ppm, possibly due to the intermediate monodentate species. The humps disappeared 30 min thereafter, pointing to the diminishment of the intermediate species. The spectrum acquired after 48 h display peaks at 7.96, 7.56 and 6.32 ppm corresponding to the bpza ligand (*vide supra*); and at 8.52 ppm (COOH), 4.22 ppm (CH), 3.31 ppm (CH_2) and 2.92 ppm (NH_2), which correspond to L-cysteine (Fig. 3.9**c**).

Further efforts to confirm the final products of the substitution reactions were pursued by setting an experiment on a preparative scale. Compound $[Pd(\mathbf{L2})(OH_2)_2]^{2+}$ (**9**) was generated from $[PdCl_2(\mathbf{L2})]$ (**2**) as described in Scheme 3.2 and reacted with L-cysteine to form $[Pd(\mathbf{L2})(Cys)_2]$ (**12b**). The ESI-MS of compound **12b** (Fig. 3.10) showed a molecular ion peak at m/z = 601, which corresponds to formation of **12b**. Substitution reactions in diaqua metal complexes leading to formation of bis(L-cysteine)metal complexes are known.[29] Based on the kinetics, spectroscopic and mass spectrometry data, it was proposed that the substitution of aqua ligands in complexes **8-11** proceed by the sequence of reactions in Scheme 3.4 and 3.5.

---

[29] Bose R. N., Ghosh S. K., Moghaddas S., *J. Inorg. Biochem.*, **1997**, *65*, 199.

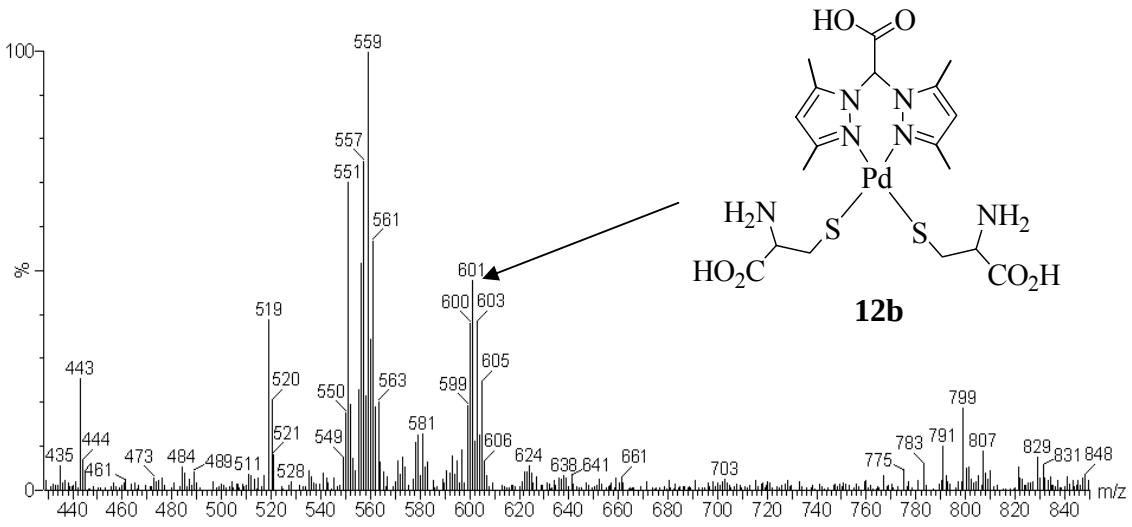

Figure 3.10. ESI-MS spectrum of compound **12b**.

3.4. Conclusions

As mentioned in chapter 2, the coordination of bis(pyrazolyl)acetic acid ligands to gold(III), platinum(II) and palladium(II) form complexes that a relatively stable and closely related to cisplatin. In spite of this advantage, complexes **1**-**6a** had no appreciable biological activities against CHO-22 cells.

Overall, the kinetics results evidently showed that there was no relationship between the observed anticancer activities of complexes **1**-**6a** and their reaction rates. Nevertheless, kinetics study was carried out to establish the probable mechanisms and products formed from reactions of these complexes and L-cysteine. The substitution reactions of $[Pt(\mathbf{L1})(OH_2)_2]^{+}$ (**10**) with L-cysteine was found to be slow compared to those of $[Pd(\mathbf{L1})(OH_2)_2]^{2+}$ (**8**), $[Pd(\mathbf{L2})(OH_2)_2]^{2+}$ (**9**) and $[Au(\mathbf{L1})(OH_2)_2]^{3+}$ (**11**). Furthermore, the substitution reaction involving gold(III) complex **11** showed a two-step reaction

involving the substitution of aqua ligands and a subsequent slow process, possibly due to reduction of **11** to gold(I). The substitution reactions of L-cysteine with the diaqua metal complexes **8**-**11** were found to be temperature dependent and occurred *via* an associative mechanism. The largely negative entropy values registered are supportive of an associative mechanism of substitution. The mass spectrum data points to formation bis(cysteine)metal complexes, but for gold complex **11**, the second slow process observed suggests that the final products are not necessarily bis(cysteine) complexes.

CHAPTER 4

PLATINUM(II) AND GOLD(I) DITHIOCARBAMATE COMPLEXES

*X-ray structures **15**, **17b**, **25** and **L10** were solved by Dr. Guzei and Mrs. Spencer both of Wisconsin University (USA), whilst X-ray structure of **L9** was solved by the candidate and Dr. Omondi (University of Johannesburg). All the crystal structure discussions are the work of the candidate except for **17b**, where Dr. Guzei helped with the discussion.*

4.0. Introduction

There has been increasing interest in the synthesis and reactivity of mononuclear metal complexes with sulfur-containing ligands because of their relevance as models of biologically redox-active metalloproteins.[1,2,3] For this reason, the dithiocarbamate ligand (dtc), first identified during the early days of organosulfur chemistry, has been studied and applied widely.[4] Free dithiocarbamic acids (R_2NCS_2H) are highly unstable and are normally isolated as their alkali metal salts. Most studied dtcs prepared from secondary amines, because they are stable and possess interesting electrochemical and optical properties.[4,5] Dithiocarbamates are synthesised by reacting amines with carbon disulfide under basic conditions as illustrated in Scheme 4.1.

[1] Power P. P., Shoner S. C., *Angew. Chem., Int. Ed. Engl*., **1991**, *30*, 330.
[2] Ruiz J., Giner J., Rodríguez V., López G., Casabó J., Molins E., Miravitlles C., *Polyhedron,*, **2000**, *19*, 1627.
[3] Holm R. H., Kennepohl P., Solomon E. I., *Chem. Rev*., **1996**, *96*, 2239.
[4] Cookson J., Beer P. D., *Dalton Trans*., **2007**, 1459.
[5] Bond A. M., Martin R. L., *Coord. Chem. Rev*., **1984**, *54*, 23.

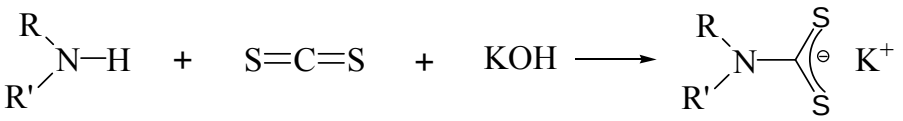

R = H, Alkyl, Aryl; R' = Alkyl, Aryl

Scheme 4.1. Preparation of dithiocarbamate ligands (taken from ref. 4)

The coordination chemistry of the dithiocarbamate ligands have been extensively studied[6] and are known to display both mono and bidentate coordination to transition metal centres. Dithiocarbamato ligands mostly act as uninegative bidentate ligands,[7] coordinating through one or both sulfur atoms with many transition metals. Transition metal complexes of dithiocarbamates present a wide range of applications, such as, in agriculture (as pesticides),[8] industry[9] and in medicine.[10] Palladium(II)[11a] and copper(II)[11b] dithiocarbamato complexes have attracted significant attention due to their potential biological applications. More central to this study is that dithiocarbamate complexes of platinum(II)[10a] and thiolate gold(I)[10b] complexes are known to exhibit antitumour properties and cytotoxic properties.

Part of the study reported in this thesis was aimed at developing anticancer agents by utilising dithiocarbamates as ligands. It is worth noting that while pursuing this goal, the possibility of gold compounds to luminescence also became of interest. Owing to the popularity of cisplatin as an anticancer agent, other platinum(II) and analogous palladium(II)

---

[6] Hogarth G., *Prog. Inorg. Chem*., **2005**, *53*, 71.
[7] [a]Gimeno M. C., Jambura E., Laguna A., Laguna M., Murray H. H., Terroba R., *Inorg. Chim. Acta*, 1996, *249*, 69. [b]Victoriano L. I., *Coord. Chem. Rev*., **2000**, *196*, 383.
[8] Fitsanakis V. A., Amarnath V., Moore J. T., Montine K. S., Zhang J., Montine T. J., *Free Radical Biol. Med.*, **2002**, *33*, 1714.
[9] Birri A., Harvey B., Hogarth G., Subasi E., Ugur F., *J. Organomet. Chem*., **2007**, *692*, 2448.
[10] [a]Alverdi V., Giovagnini L., Marzano C., Seraglia R., Bettio F., Sitran S., Graziani R., Fregona D., *J. Inorg. Biochem*., **2004**, *98*, 1117; [b]Ahmad S., Isab A. A., Ali S., Al-Arfaj A. R., *Polyhedron*, **2006**, *25*, 1633.
[11] [a]Shaheen F., Badshah A., Gielen M., Gieck C., de Vos D., *Appl. Organomet. Chem.*, **2007**, *21*, 633;

complexes have since been pursued vigorously as potential anticancer agents. In this work, palladium(II) and platinum(II) dithiocarbamate complexes were also prepared and probed for their anticancer activities. The following sections highlight a few examples of palladium(II), platinum(II) and gold(I) metal complexes utilising various dithiocarbamates and related thiolates as ligands.

4.1. Palladium and platinum thiolate based complexes

Efforts to prepare antitumour compounds that have reduced toxicity compared to cisplatin and its analogues, have led to the development of palladium(II) and platinum(II) complexes containing N and S donor atoms.[12] Interest in palladium and platinum complexes with dithiocarbamates and related thiolates emanates from the demonstration that sulfur ligands act as detoxicant agents against metal containing drugs.[13] For instance, dithiocarbamates have been evaluated for their efficacy as inhibitors of cisplatin induced nephrotoxicity.[12,13] Thus, it is envisaged that preparing palladium and platinum thiolate based complexes could possibly offer compounds that impart anticancer activity with reduced toxicity. Even though platinum has always been the obvious choice for preparing metal based anticancer compounds - owing to the discovery of cisplatin - palladium dithiocarbamate complexes are also starting to gain popularity due to their biological activities. Examples include the dithiocarbamate based complexes, $[M(S_2CNEt_2)(L)]NO_3$ (M = Pd; L = 2,2′-bipyridyl or 1,10-

---

[b]Haiyuan Z., Jiu-sheng W., Fangyu P., *Anti-Cancer Drugs*., **1996**, *19*, 125.

[12] Faraglia G., Fregona D., Sitranb S., Giovagninia L., Marzanoc C., Baccichetti F., Casellato U., Graziani R., *J. Inorg. Biochem*., **2001**, *83*, 31.

[13] Fregona D., Giovagnini L., Ronconi L., Marzano C., Trevisan A., Sitran S., Biondi B., Bordin F., *J. Inorg. Biochem*., **2003**, *93*, 181.

phenanthroline) (Fig. 4.1), which have shown antitumour activities against leukemia cells.[14] The anticancer effect of $[M(S_2CNEt_2)(L)]NO_3$ complexes is attributed to these complexes associating to double-stranded DNAs by means of intercalation.[14,15]

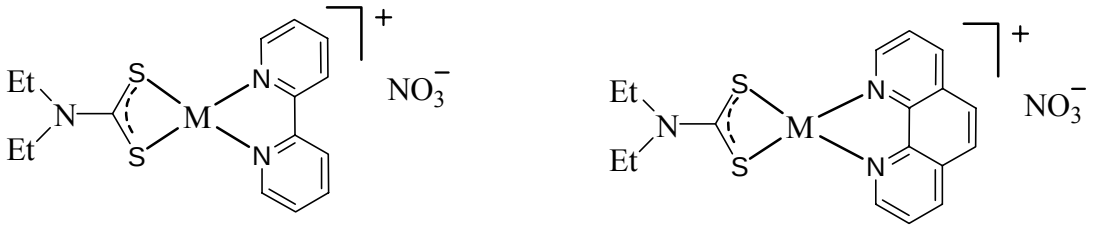

M = Pd, Pt

Figure 4.1. Structures of dithiocarbamate based complexes, $[M(S_2CNEt_2)(L)]NO_3$.

As an extension to $[M(S_2CNEt_2)(L)]NO_3$ complexes (Fig. 4.1), Faraglia and co-workers[12] prepared palladium(II) and platinum(II) complexes with the dithioesters ligands ESDTM ($EtO_2CCH_2(CH_3)NCS_2Me$) (ESDT = methylamino-acetic acid ethyl ester-dithiocarboxylate) and ESDTE ($EtO_2CCH_2(CH_3)NCS_2Et$) (Fig. 4.2). However, the anticancer activities of these complexes against HeLa cells were lower than that of cisplatin (IC_{50} = 6.33 μM).[12,16] Other closely related examples include [M(DMDT)(Mol)]Cl (M = Pd, Pt; DMDT = $Me_2NCS_2^-$; Mol = L-methioninol).[17] In all the examples mentioned above, the dithiocarbamate binds to the metal in an κ^2-S^S′ chelate fashion.

[14] Mital R., Jain N., Srivastava T. S., *Inorg. Chim. Acta,* **1993**, *166*, 135.
[15] Howe-Grant M., Wu K. C., Bauer W. R., Lippard S. J., *Biochemistry*, **1976**, *15*, 4339.
[16] Marzano C., Trevisan A., Giovagnini L., Fregona D., *Toxicol. In Vitro*, **2002**, *16*, 413.
[17] Faraglia G., Fedrigo M. A, Sitran S., *Transition Met. Chem*., **2002**, *27*, 200.

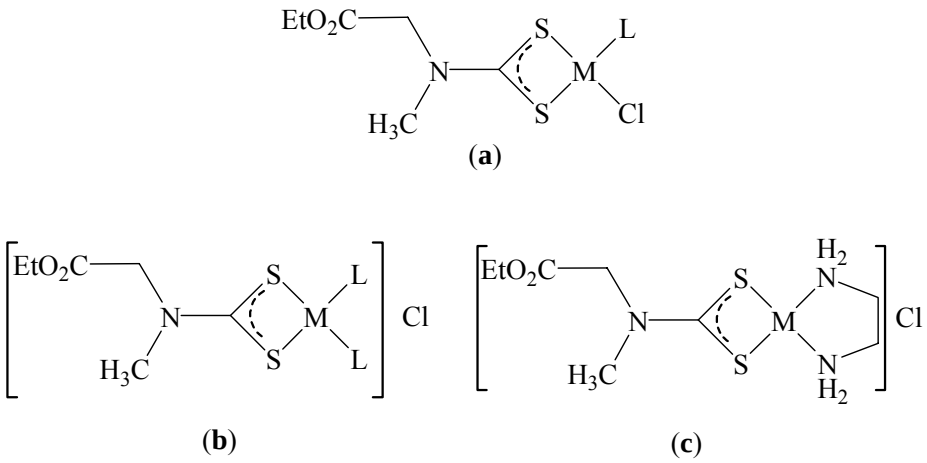

Figure 4.2. Structures of (**a**) [M(ESDT)(L)Cl], (**b**) [M(ESDT(L)$_2$]Cl, (**c**) [M(ESDT)(en)]Cl. M = Pd(II), Pt(II), L = n-propylamine, cyclobutylamine, pyridine.

Other examples of palladium-dithiocarabamato complexes include bis(piperidine-1-dithiocarbamato)Pd(II), bis(4-methylpiperidine-1-S^S′-dithiocarbamato)Pd(II) and chloro[(4-methylpiperidine-1-S^S′-dithiocarbamato)(PPh_3)]Pd(II) recently reported by Shaheen and co-workers,[18] as well as six palladium(II) aminedithiocarbamates of general formula [Pd(AmDTC)$_2$], where H(AmDTC) = aminedithiocarbamic acid.[19] These [Pd(AmDTC)$_2$] compounds were found to exhibit antibacterial and cytotoxic activities. From the structural studies performed, the ligands bind to the metal symmetrically in a bidentate fashion.

Additional derivatives of [Pd(AmDTC)$_2$] complexes include the stable 1,2-enedithiolates palladium(II) and platinum(II) complexes, [(dppe)M(S_2C_2-(R)(R′)] (M = Pd, Pt; dppe = 1,2-bis(diphenyldiphosphino)ethane; R (R′) = 2-, 3-, and 4-pyridine, 2-pyrazine and 2-

[18] [a]Shaheen F., Badshah A., Anjum S., Ali S., *Acta. Crystallgr*., Sect. E, **2006**, 62, m329; [b]Shahzadi S., Ali S., Badshah A., Shaheen F., Ahmad F., Fettouhi M., *J. Chem. Crystallogr*., **2006**, 36, 567; [c]Shaheen F., Hag M. N., Badshah A., Wurst K., Ali S., *Acta Crystallogr*., Sect. E, **2006**, 62, m138.

[19] Shaheen F., Badshah A., Gielen M., Dusek M., Fejfarova K., de Vos D., Mirza B., *J. Organomet. Chem*., **2007**, 692, 3019.

quinoxaline.[20] The [(dppe)M(S_2C_2-(R)(R′)] compounds are further stabilised by the dppe ligand in addition to the chelating 1,2-enedithiolates. However, interest in [(dppe)M(S_2C_2-(R)(R′)] complexes concerned physical properties and not biological activities. Other classes of palladium and platinum thiolate complexes are the salts of $[M(II)(mnt)_2]^-$ (M = Pd, Pt; mnt = maleonitriledithiolato) anions (Fig. 4.3).[21] The molecular structures of $[M(II)(mnt)_2]^-$ exhibit the expected square planar geometry, with the metal bound to four sulfur atoms. Compounds $[M(II)(mnt)_2]^-$ were reported to show antiferromagnetic properties.[21] In general, palladium and platinum dithiocarbamate complexes are a promising class of potential anticancer agents.[22]

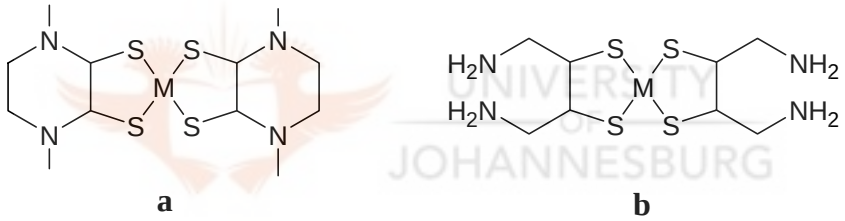

a **b**

M = Pd, Pt

Figure 4.3. The structures of planar $[M(II)(mnt)_2]^-$ complexes.

Similar to palladium(II) and platinum(II) thiolate complexes, gold(I) thiolate based complexes have also been of interest as potential anticancer agents since it was shown that the well known antiarthritic agent, auranofin (Fig. 4.4),[23,24] and other gold compounds such

[20] Kaiwar S. P., Hsu J. K., Liable-Sands L. M., Rheingold A. L., Pilato R. S., *Inorg. Chem*., **1997**, 36, 4234.
[21] Bigoli F., Deplano P., Mercuri M. L., Marchio L., Pilia L., Serpe A., Concas G., Congiu F., Sanna S., *Chem. Phys. Lett*., **2006**, 421, 361.
[22] Giovagnini L., Marzano C., Bettio F., Fregona D., *J. Inorg. Biochem*., **2005**, *99*, 2139.
[23] [a]Simon T. M., Kunishima D. H., Vibert G. J., Lorber A., *Cancer*, **1979**, *44*, 1965; [b]Simon T. M., Kunishima D. H., Vibert G. J., Lorber A., *Cancer Res.*, **1981**, *41*, 94.
[24] Mirabelli C. K., Johnson R. K., Sung C., Faucette L. F., Muirhead K., Crooke S. T., *Cancer Res*., **1985**, *45*, 32.

as Ph_3PAuCl,[25] exert antitumour activity. The improved activity of auranofin is possibly due to its P-Au-S moiety. Work reported by Mirabelli *et al*. involving various gold compounds of general formula R_3P-Au-X (X = Cl, thiosugar), in which the chloride is replaced with a thiosugar, provides structural basis of selectivity for antitumour activity. Notably, the phosphine gold(I) thiolate compounds were found to be more active than non-phosphine gold(I) thiolates; suggesting the importance of the phosphine ligands as they seem to increase the liphophilicity of the resultant phosphine gold(I) complexes. Thus, it appears that phosphine gold(I) thiolate compounds with P-Au-S moiety show good anticancer activities. Hence, several phosphine gold(I) thiolate complexes have since been prepared and investigated for their antitumour activities; and the following section highlights a few examples of these phosphine gold(I) thiolate complexes.

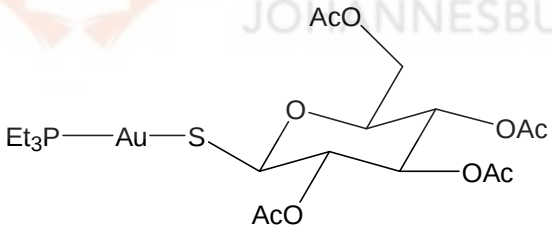

Figure 4.4. The structure of auranofin.

4.2. Phosphine gold(I) thiolate complexes

Gold-based drugs have been successfully used for treatment of rheumatoid arthritis over many years.[26] Research have shown that gold(I) compounds also display some antitumour

[25] Mirabelli C. K., Johnson R. K., Hill D. T., Faucette L. F., Girard G. R., Kuo G. Y., Sung C., Crooke S. T., *J. Med. Chem*., **1986**, 29, 218.
[26] Ahmad S., Isab A. A., *J. Inorg. Biochem*., **2002**, 88, 44.

activity.[27,28,29] Currently there is great interest in isolating new gold(I) complexes with potential anticancer activities and to understand the mechanism through which the gold(I) compounds exert antitumour activity. There is an array of gold(I) thiolate complexes reported in the literature and for the purposes of this thesis few examples are cited, i.e., phosphines gold(I) thiolate complexes, since all the new gold(I) complexes reported in this thesis are phosphine based gold(I) complexes.

4.2.1. Monophosphine gold(I) thiolate complexes

The starting point was the examination of the antitumour activity of auranofin (Fig. 4.4). It was found to be an effective agent against P388 lymphocytic leukemia. Literature reports indicate that auranofin exert its activity by affecting mitochondrial function.[24,25,30] Recent work by Bindoli and co-workers evidently substantiate that auranofin and other gold(I) compounds exert its activity by affecting the mitochondria.[31] They demonstrated that auranofin inhibits thioredoxin reductase in its mitochondrial environment. Human thioredoxin reductase is an homodimeric flavoenzyme closely related to glutathione.[32] It differs from glutathione due to the Cy-SeCys (selenocysteine) sequence fragment, which makes it a selenoenzyme. It is hugely expressed around tumours and thus makes it a target for the new potential gold(I) compounds.[33] It is believed that the binding of Au(I) to the C-

[27] Tiekink E. R. T., *Crit. Rev. Oncol. Hematol*., **2002**, *42*, 225.
[28] Pillarsetty N., Katti K. K., Hoffman T. J., Volkert W. A., Katti K. V., Kamei H., Koide T., *J. Med. Chem*., **2003**, 46, 1130.
[29a]Shaw III C. F., Chem. Rev., **1999**, 99, 2589; [b]*Gold Progress in Chemistry, Biochemistry and Technology*. Shaw III C. F., Ed. Schmidbaur H., John Wiley & Sons, Chichester, England, **1999**, 260.
[30] McKeage M. J., Maharaj L., Berners-Price S. J., *Coord. Chem. Rev*., **2002**, *232*, 127.
[31] Rigobello M. P., Scutari G., Boscolo R., Bindoli A., *Br. J. Pharmacol*., **2002**, *136*, 1162. [b]Rigobello M. P., Scutari G., Folda A., Bindoli A., *Biochem. Pharmacol*., **2004**, *67*, 689.
[32] Gromer S., Arscott L. D., Williams Jr. C. H., Schirmer R. H., Becker K., *J. Biol. Chem*., **1998**, *273*, 20096.
[33] Barnard P. J., Berners-Price S. J., *Coord. Chem. Rev*., **2007**, *251*, 1889

terminal of the redox active selenocysteine leads to cytotoxic effects.[33,34,35] Some phosphine gold(I) thiolate complexes that have been prepared and investigated for their antitumour activities include, [Au(2-mba)(PR_3)] (R = Et, Ph, Cy; 2-mba = 2-mercaptobenzoic acid) (Fig. 4.5).[36] Structural studies on complex [Au(2-mba)(Ph_3)] show that the geometry around the gold is linear and is defined by PPh_3 and 2-mba anion (Fig. 4.5).

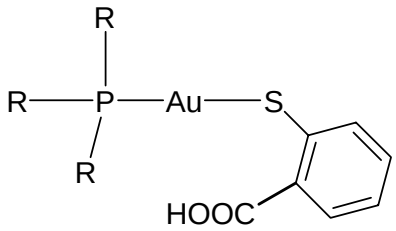

Figure 4.5. Structures of complexes [Au(2-mba)(PR_3)] (R = Et, Ph, Cy; 2-mba = 2-mercaptobenzoic acid).

Casas and co-workers[37] have recently explored a biologically active thiol, pyridoxalrhodanine, to prepare a novel gold(I) 7-azacoumarin complex. However, a mixture of pyridoxalrhodanine, triethylphosphinegold(I) chloride and sodium methoxide in methanol unexpectedly gave [Au(TS)(PEt_3)] (TS = 5-(hydroxymethyl)-8-methyl-3-thiol-7-azacoumarin) (Fig. 4.6). Nevertheless, compound [Au(TS)(PEt_3)] exhibits linear geometry and showed *in vitro* anticancer activity against the cisplatin-resistant line A2780cis with the IC_{50} value of 0.59 μM compared to cisplatin (IC_{50} = 4.2 μM).

[34] Urig S., Fritz-Wolf K., Réau R., Herold-Monde C., Tóth K., Davioud-Charvet E., Becker K., *Angew. Chem. Int. Ed*., **2006**, *45*, 1881.
[35] Hill K. E., McCollum G. W., Boeglin M. E., Burk R. F., *Biochem. Biophys. Res. Commun*., **1997**, *234*, 293.
[36] de Vos D., Clements P., Pyke S. M., Smyth D. R., Tiekink E. R. T, *Metal-Based Drugs*, **1999**, 6, 31.
[37] Casas J. S., Castellano E. E., Couce M. D., Crespo O., Ellena J., Laguna A., Sanchez A., Sordo J., Taboada C., *Inorg. Chem*., **2007**, *46*, 6236.

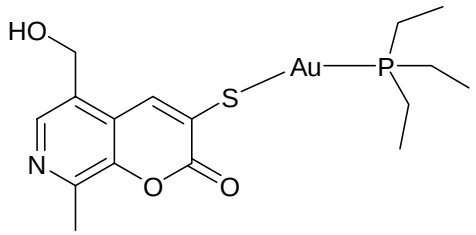

Figure 4.6. A structure of gold(I) 7-azacoumarin complex, [Au(TS)(PEt_3)].

Further efforts to search for more phosphine gold(I) thiolate compounds has been pursued by preparing phosphine gold(I) complexes of sulfur containing biomolecules. For instance, the vitamin K_3 (menadione) derivative {NaK_3TSC (NaK_3TSC = menadione sodium bisulfite thiosemicarbazone)} has been used as a ligand to the prepare gold(I) complex [$AuPEt_3(K_3TSC)$] (Fig. 4.7).[38] Compound [$AuPEt_3(K_3TSC)$] has the gold(I) atom coordinated almost linearly to the K_3TSC^- sulfur and the phosphine P atom.[38] *In vitro* screening showed significant anticancer activity (IC_{50} = 0.4 μM) against the cisplatin-resistant cells, A27780cis. The activity of the ligand, NaK_3TSC, was quite insignificant (IC_{50} = 3732 μM), reiterating the fact that phopshine ligands are necessary for cytotoxic activities.

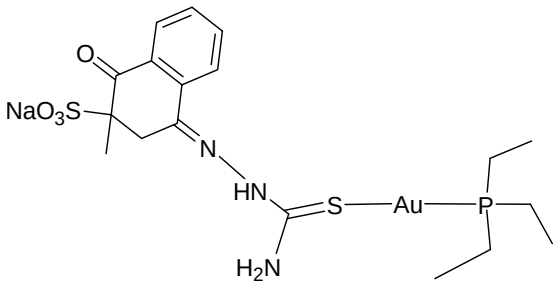

Figure 4.7. The structure of [$Au(K_3TSC)PEt_3$].

[38] Casas J. S., Castellano E. E., Couce M. D., Ellena J., Sanchez A., Sordo J., Taboada C., *J. Inorg. Biochem*., **2006**, *100*, 1858.

4.2.2. Diphosphine gold(I) thiolate complexes.

The chemistry of phosphine gold(I) mononuclear complexes discussed above, has been extended to gold(I) dinuclear complexes, e.g. complex $[(AuSTg)_2(dppe)]$ (STg^- = β-1-D-thioglucose salt, dppe = bis(diphenylphosphino)ethane) (Fig. 4.8**a**) reported by Mirabelli *et al*.[39] Experiments involving $[(AuSTg)_2(dppe)]$ showed that it was more active (IC_{50} = 4 μM) than the analogous $[(AuCl)_2(dppe)]$ (IC_{50} = 8 μM) against B16 melanoma cells *in vitro*.

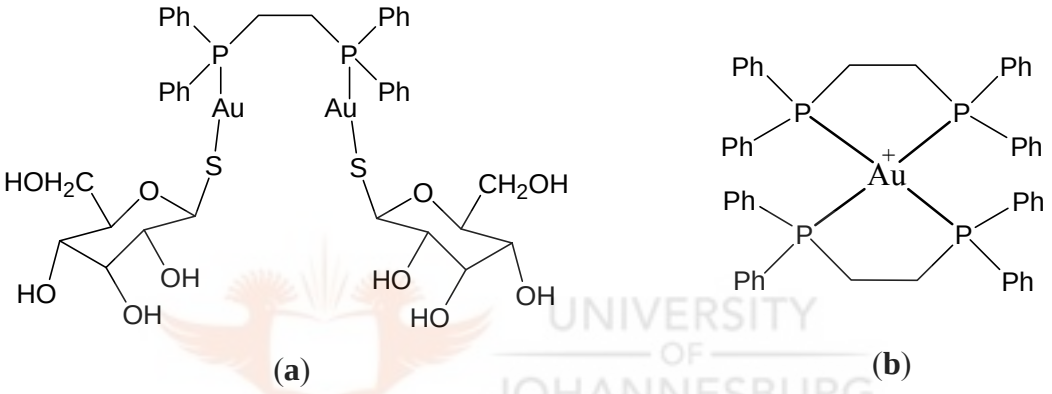

Figure 4.8. The structure of $[(AuSTg)_2(dppe)]$ and (**b**) $[Au(dppe)_2]^+$.

The activity of $[(AuSTg)_2(dppe)]$ may be due to its *in vivo* conversion to active bis-chelated $[Au(dppe)_2]^+$. The formation of the active species, $[Au(dppe)_2]^+$ (Fig. 4.8**b**),[40] was demonstrated by Berners-Price and co-workers in the experiments involving $[(AuCl)_2(dppe)]$ and $[(AuSTg)_2(dppe)]$.[41] The interaction of $[(AuCl)_2(dppe)]$ with thiols in the biological *milieu* leads to formation of the intermediate, $[(AuSR)_2(dppe)]$, that leads to the formation of

[39] Mirabelli C. K., Jensen B. D., Mattern M. R., Sung C. M., Mong S. M., Hill D. T., Dean S. W., Schein P. S., Johnson R. K., Crooke S. T., *Anti-Cancer Drug Des*., **1986**, *1*, 223.
[40] Berners-Price S. J., Girard G. R., Hill D. T., Sutton B. M., Jarrett P. S., Faucette L. F., Johnson R. K., Mirabelli C. K., Sadler P. J., *J. Med. Chem*., **1990**, *33*, 1386.
[41] Berners-Price S. J., Jarrett P. S., Sadler P. J., *Inorg. Chem*., **1987**, *26*, 3074.

the active gold(I) metabolite, $[Au(dppe)_2]^+$.[41,42] Thus, it appears that the formation of the active species $[Au(P\text{-}P)_2]^+$ from bis(diphenylphosphino)ethane gold(I) thiolate compounds would be expedited in comparison to their analogous phosphine chloro gold(I) complexes; hence better efficacies.

Other related diphosphine gold(I) thiolate examples include a series of complexes $[(AuOmS)_2(R_2P(CH_2)_nPR_2)]$ (where OmS = octahydro-quinolizin-1-yl)methane thiolate; R = Me, Ph; and n = 2, 3;) (Fig. 4.9), which were isolated as hydrochloride salts.[43] They were shown to have profound antitumour activities against ovarian carcinoma. Based on the studies involving $[(AuSTg)_2(dppe)]$ discussed above, the $[(AuOmS)_2(dppe)]$ would also be converted *in vivo* to the active bis-chelated $[Au(dppe)_2]^+$.

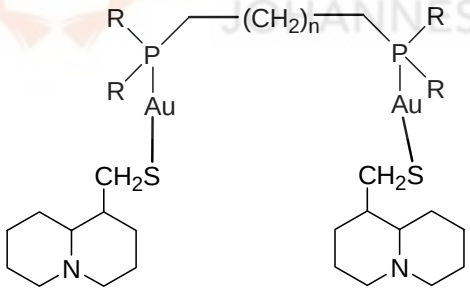

R = Me, n = 2 (a); R = Ph, n = 3 (b);
R = Ph, n = 3 (c)

Figure 4.9. Structure of phosphine gold(I) complexes, $[(AuOmS)_2(R_2P(CH_2)_nPR_2)]$.

[42] Berners-Price S. J., Mirabelli C. K., Johnson R. K., Mattern M. R., McCabe F. L., Faucette L. F., Sung C. M., Mong S. M., Sadler P. J., Crooke S. T., *Cancer Res*., **1986**, *46*, 5486.
[43] Cagnoli M., Alama A., Barbieri F., Novelli F., Bruzzo C., Speratore F., *Anti-Cancer Drugs*, **1998**, *9*, 603.

Other examples of diphosphine gold(I) complexes include $[Au_2(\mathbf{L})_2(dppe)]$ (**L** = $R_1R_2NC(=S)NR_3$, R_1R_2 = $(CH_2CH_2)_2O$, HMe; R_3 = Ph; dppe = bis(diphenylphosphino)ethane) (Fig. 4.10), which showed activity against P388 leukemia cancer cells.[44] The most active complex was $[Au_2\{(SC(=NPh_3)N(CH_2CH_2)_2O)\}_2(dppe)]$ (Fig. 4.11**a**) (IC_{50} = 10 μM). Several other examples, such as, $[Au_2(SC_6H_5)_2(dppf)$,[45] $[Au_2(1,2\text{-}S_2C_6H_4)(dppf)]$ and $[Au_2\{(SC(=NPh_3)N(CH_2CH_2)_2O)\}_2(dppf)]$ (dppf = bis-(diphenylphosphino)ferrocene) are known. All the diphosphine gold(I) compounds mentioned above are structurally similar, with almost linear P-Au-S motifs.

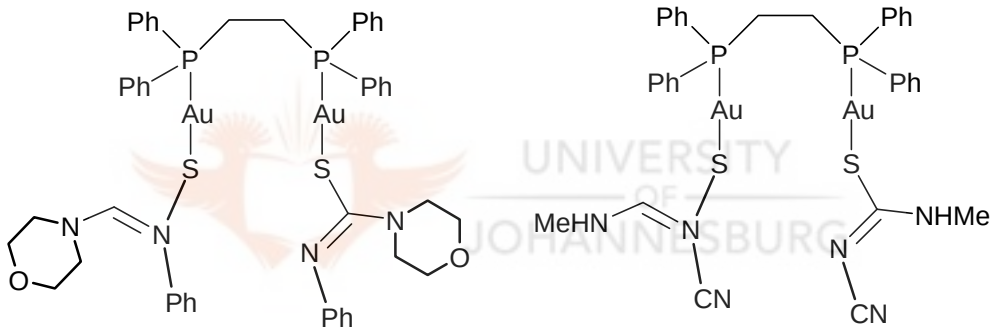

a **b**

Figure 4.10. Phosphinegold(I) thiourea complexes.

In summary, interest in the coordination chemistry of gold(I) complexes arises in part from the use and potential use of such complexes in medicine. Water-soluble, polymeric gold(I) thiolates such as gold sodium thiomalate (mycochrysin), gold sodium thiosulfate (sanochrysin) and auranofin are used in the treatment of rheumatoid arthritis.[46] In addition, research findings indicate that gold(I) compounds have also shown good anticancer activities

[44] Henderson W., Nicholson B. K., Tiekink E. R. T., *Inorg.Chim. Acta*, **2006**, *359*, 204.
[45] Viotte M., Gautheron B., Nifant'ev I., Kuz'mina L. G., *Inorg. Chim. Acta,* **1996**, *253*, 71.

against numerous cell lines.[47] Certain thiosemicarbazones and gold-thiosemicarbazone complexes have also shown considerable antitumour activity.[48]

Apart from the fact that phosphine and sulfur containing ligands stabilises gold(I) compounds, the phosphine ligands in particular, also increase the biological properties of the resultant gold(I) complex. This is supported by literature reports on various phosphine gold(I) thiolate compounds described in section 4.2. It is for this reason that this study embarked on the design of new phosphine gold(I) thiolate complexes possessing P-Au-S motifs by using triphenylphosphine (PPh_3), 1,2-bis(diphenylphosphine)ethane (dppe), 1,2-bis(diphenylphosphine)propane (dppp), 1,2-bis(diphenylphosphine)hexane (dpph) and the unexploited pyrazol-1-yl-, indazol-1-yl- and imidazol-1-yl-based dithiocarbamate ligands (dtcs). Platinum(II) dithiocarbamate compounds were also prepared and their anticancer activities determined. Details of the syntheses, characterisation and molecular structures are discussed in this chapter. The compounds discussed in this chapter are given in schemes 4.2 and 4.3 below.

---

[46] Parish R. V., Cotrill S. M., *Gold Bull*., **1987**, *20*, 3.
[47] [a]Zhang C. X., Lippard S. J., *Curr. Opin. Chem. Biol*., **2003**, *7*, 481; [b]McKeage M. J., Papathanasiou P., Salem G., Sjaarda A., Swiegers G. F., Warning P., Wild S. B., *Met-Based Drugs*, **1999**, 217.
[48] Beraldo H., Gambino D., *Mini Rev. Med. Chem*., **2004**, *4*, 159.

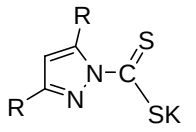

R = H (**L5**), Me (**L6**)

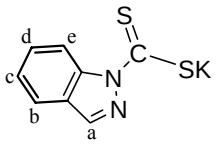

L7

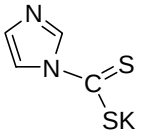

L8

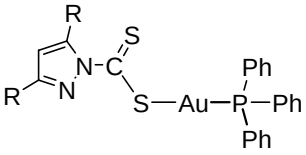

R = H (**13**), Me (**14**)

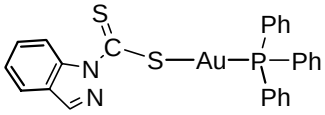

15

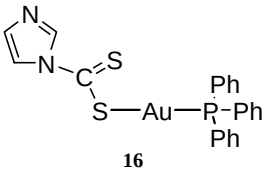

16

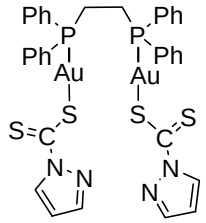

17a

$[Au_{18}S_8(dppe)_6]^{2+}$

17b

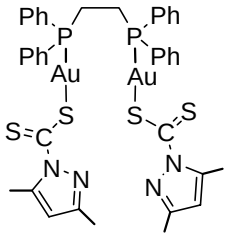

18

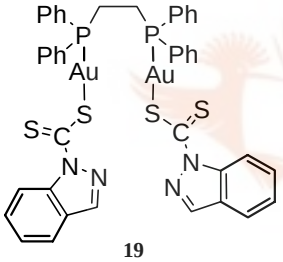

19

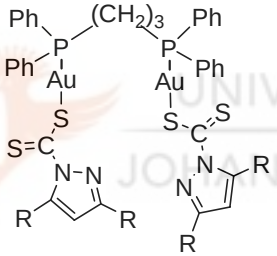

R = H (**20**), Me (**21**)

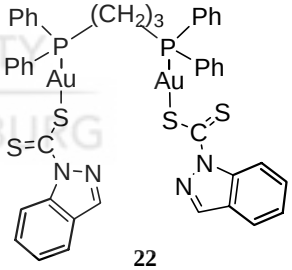

22

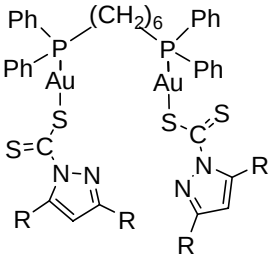

R = H (**23**), Me (**24**)

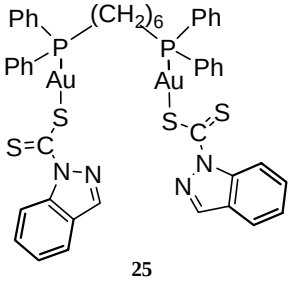

25

Scheme 4.2. Ligands and gold complexes.

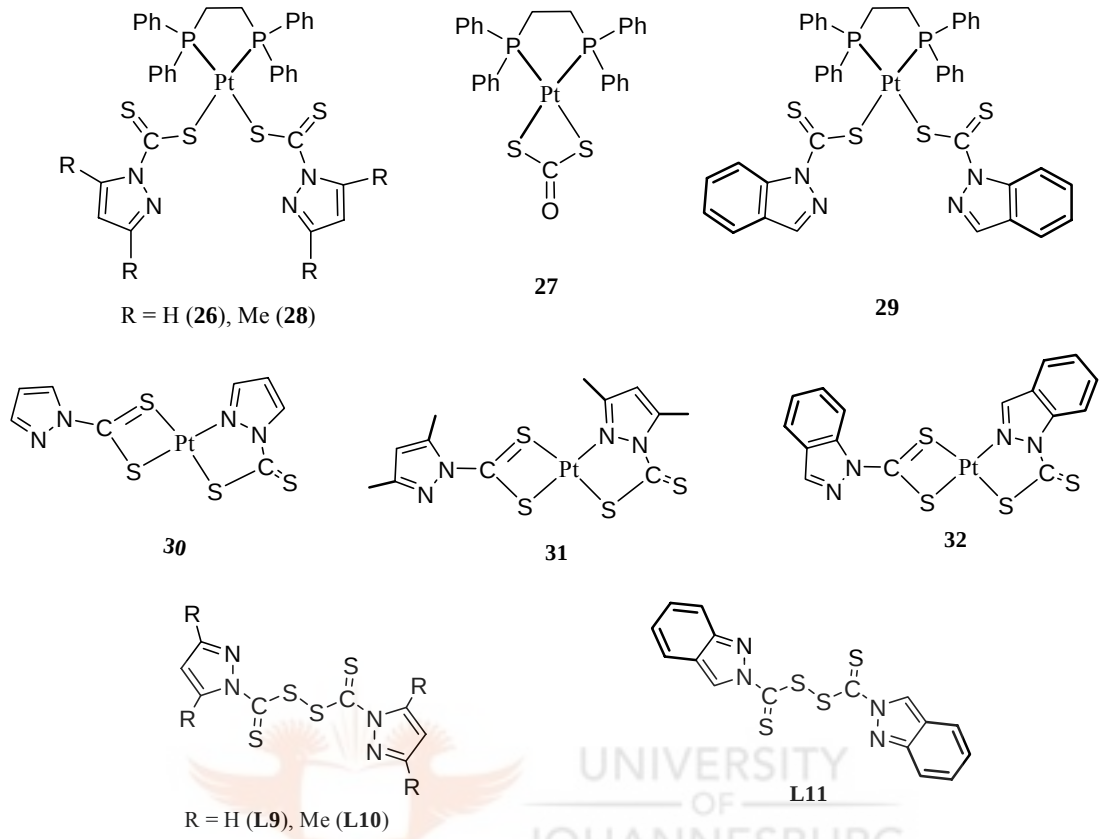

Scheme 4.3. Platinum complexes and bis(dithiocarbamato)disulfide ligands.

4.3. Experimental

4.3.1. Reagents, starting materials and instrumentation

All commercial chemicals were used as received. $K_2[PtCl_4]$, pyrazole, 3,5-dimethylpyrazole, indazole, imidazole, KOH, CS_2 and $MgSO_4$ were purchased from Sigma-Aldrich and used without further purification. Pyrazol-1-yldithiocarbamate (**L5**) and 3,5-dimethylpyrazol-1-yldithiocarbamate (**L6**) were synthesised according to the literature procedures with minor modifications.[49] Gold starting materials, $[HAuCl_4].4H_2O$,[50] $[AuCl(PPh_3)]$,[51] $[Au_2Cl_2(dppe)]$,

[49] Trofimenko S. J., *Org. Chem*., **1968**, *33*, 890.
[50] Block B. P., *Inorg. Synth*., **1953**, *4*, 14.
[51] Bruce I., Nicholson B. K., Bin Shawkataly O., *Inorg. Synth*., **1989**, pp. 324.

$[Au_2Cl_2(dppp)]$, and $[Au_2Cl_2(dpph)]$[51] (dppe = 1,2-bis(diphenylphosphine)ethane; dppp = 1,2-bis(diphenylphosphine)propane; dpph = 1,2-bis(diphenylphosphine)hexane) were synthesised according to the literature procedures. All the solvents were also purchased from Sigma-Aldrich and dried using conventional methods. Tetrahydrofuran (THF) was dried over sodium with sodium benzoate as an indicator, while dichloromethane (CH_2Cl_2) was dried over phosphorous pentoxide with sodium benzoate as an indicator. The water used was double distilled. All manipulations of air-and/or moisture sensitive compounds were performed under dry, deoxygenated nitrogen atmosphere using Schlenk techniques.

IR spectra were recorded as nujol mulls using NaCl cells, KBr cells and some as KBr pellets on a on a Bruker Tensor27 spectrophotometer. In other cases IR spectra were recorded as pure solids on a Bruker Tensor27 fitted with an ATR-IR probe. ^{1}H and $^{13}C\{^{1}H\}$ NMR spectra were recorded on a Bruker Avance DPX 300 spectrometer (^{1}H, 300 MHz, ^{13}C, 75.4 MHz and ^{31}P, 121.5 MHz) in $CDCl_3$ and D_2O at room temperature. ^{1}H and ^{13}C chemical shifts of the compounds were referenced to the signals of the residual proton and carbon peaks of the NMR solvents and are quoted in ppm as follows; (i) $CDCl_3$ at 7.26 and 77.0 ppm for ^{1}H and ^{13}C signals, respectively and (ii) for D_2O at 4.82 ppm for the $^{1}H_2O$ signal. Splitting patterns are represented as; s, singlet; bs, broad singlet; d, doublet; m, double of doublets; qt, quasi triplet. Elemental analyses were performed on a Fisons elemental analyser at the University of Cape Town, South Africa. ESI-MS spectra were recorded on a Waters API Quattro Micro spectrotometer at the University of Stellenbosch, South Africa. The spectra were collected using 3.0 s cyclical scans and applying the sample cone voltage of 15 V at the source block temperature of 100 ^{o}C. Desolvation temperature was 350 ^{o}C and

desolvation cone gas flow rate 350L/h. UV-Vis spectra were recorded on a Varian Cary 100 Conc UV-Vis spectrophotometer.

4.3.2. Synthesis and complexation

*4.3.2.1. Synthesis of potassium-pyrazol-1-yldithiocarbamate (**L5**)*

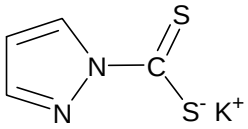

To a solution of pyrazole (1.0 g, 14.7 mmol) in THF (20 mL) was added finely powdered KOH (0.84 g, 14.7 mmol). The mixture was left to stir for 2 min and CS_2 (1.12 g, 14.7 mmol, 0.89 mL) added dropwise while stirring the solution. The solution turned from a yellow to orange and a copious amount of precipitate formed. After 20 min, the product was isolated as a yellow precipitate by filtration using a G4 frit, washed with diethylether and dried *in vacuo*. Yield = 1.98 g (74%). ^{1}H NMR (D_2O): δ 8.95 (d, 1H, $^{3}J_{HH}$ = 2.1 Hz, 5-pz); 7.81 (s, 1H, 3-pz); 6.53 (t, 1H, $^{3}J_{HH}$ = 1.8 Hz, 4-pz). $^{13}C\{^{1}H\}$ NMR (D_2O): δ 218.6 (C(C=S)); 144.3 (C(5-pz); 130.5 (C(3-pz)); 108.9 (C(4-pz)). IR (ATR, cm^{-1}): $\upsilon_{C=N}$ = 1528, υ_{C-S} = 1198, $\upsilon_{C=S}$ = 843.

Synthesis of compounds **L6-L8** were prepared using the procedure described for **L5** above, but using the reagents indicated for each compound.

*4.3.2.2. Synthesis of potassium-3,5-dimethylpyrazol-1-yldithiocarbamate (**L6**)*

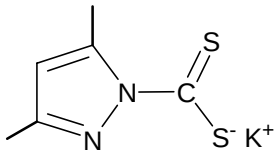

KOH (0.58 g, 10.3 mmol); 3,5-dimethylpyrazole (0.97 g, 10.0 mmol); CS_2 (0.99 g, 13.0 mmol, 0.78 mL). Yield = 1.58 g (75%). ^{1}H NMR (D_2O): δ 5.92 (s, 1H, 4-pz); 2.38 (s, 3H, 5-pz); 1.99 (s, 3H, 3-pz). $^{13}C\{^1H\}$ NMR (D_2O): δ 222.2 (C(C=S)); 149.7 (C(5-pz); 142.0 (C(3-pz)); 109.8 (C(5-pz)); 14.7 (C($\underline{C}H_3$, 5-pz); 10.8 (C($\underline{C}H_3$, 3-pz). IR (ATR, cm^{-1}): $\upsilon_{C=N}$ = 1578, υ_{C-S} = 1224, $\upsilon_{C=S}$ = 873.

*4.3.2.3. Synthesis of potassium-indazol-1-yldithiocarbamate (**L7**)*

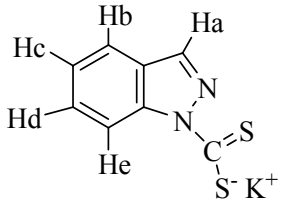

KOH (0.48 g, 8.46 mmol); indazole (1.0 g, 8.46 mmol); CS_2 (0.46 g, 8.46 mmol, 0.36 mL). Yield = 1.54 g (79%). ^{1}H NMR (D_2O): δ 8.75 (d, 1H, $^4J_{HH}$ = 8.7 Hz, (He)); 7.89 (s, 1H, Ha); 7.49 (d, 1H, $^3J_{HH}$ = 8.7 Hz, Hb); 7.24 (t, 1H, $^4J_{HH}$ = 15.0 Hz, Hd); 7.01 (t, 1H, $^4J_{HH}$ = 15 Hz, Hc). $^{13}C\{^1H\}$ NMR (D_2O): δ 219.2 (C(C=S)); 138.6 (C(5C-pz); 129.0 (C(3C-pz)); 126.9 (C(7C-Ph)); 123.6 (C(4C-Ph); 121.4 (C(8C, 9C-Ph)); 117.2 (C(6C-Ph)). IR (ATR, cm^{-1}): $\upsilon_{C=N}$ = 1608, υ_{C-S} = 1297, $\upsilon_{C=S}$ = 852.

*4.3.2.4. Synthesis of potassium-imidazol-1-yldithiocarbamate (**L8**)*

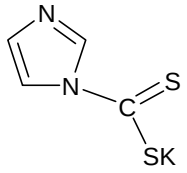

Imidazole (1.0 g, 14.7 mmol); KOH (0.84 g, 14.7 mmol); CS_2 (1.12 g, 14.7 mmol, 0.89 mL). Yield = 1.89 g (71%). ^{1}H NMR: (D_2O): δ 8.79 (s, 1H, 5-Im); 8.12 (s, 1H, 3-Im); 6.99 (s, 1H, 4-Im). $^{13}C\{^1H\}$ NMR: (D_2O): δ 218.5 (C(C=S)); 136.8 (C(5-Im); 128.5 (C(3-Im)); 119.5 (C(4-Im)). IR (KBr, cm^{-1}): $\upsilon_{C=N}$ = 1526, υ_{C-S} = 1099, $\upsilon_{C=S}$ = 837.

*4.3.2.5. Synthesis of bis(pyrazol-1-yldithiocarbamato)disulfide (**L9**)*

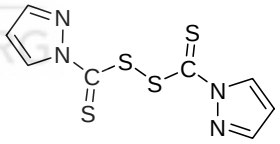

To a solution of **L5** (0.31 g, 1.45 mmol) in methanol (20 mL), was added iodine pellets (0.18 g, 0.72 mmol). The resultant solution was stirred at room temperature during which a yellow precipitate was formed. The reaction was left for 15 min and the product isolated as a yellow solid by filtration. Yield = 0.15 g (75%). ^{1}H NMR ($CDCl_3$): δ 8.54 (s, 2H, $^3J_{HH}$ = 3.6 Hz, 5-pz); 7.91 (s, 2H, $^3J_{HH}$ = 3.3 Hz, 3-pz); 6.56 (s, 2H, $^3J_{HH}$ = 3.9 Hz, 4-pz). $^{13}C\{^1H\}$ NMR ($CDCl_3$): δ 192.3 (C(C=S); 145.6 (C(5, 5′-pz)); 131.5 (C(3, 3′-pz)); 111.6 (C(4, 4′-pz)). IR (ATR, cm^{-1}): $\upsilon_{C=N}$ = 1533, υ_{C-S} = 1254, $\upsilon_{C=S}$ = 869. Anal. Calc. for $C_8H_6N_4S_4$: C, 33.55; H, 2.11; N, 19.56; S, 44.78%. Found: C, 33.73; H, 2.64; N, 18.95; S, 44.32%.

Synthesis of compounds **L10** and **L11** were prepared using the procedure described for **L11** above, but using the reagents indicated for each compound.

*4.3.2.6. Synthesis of bis(3,5-dimethylpyrazol-1-yldithiocarbamato)disulfide (**L10**)*

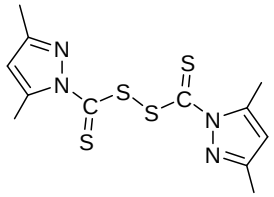

L6 (0.2 g, 0.95 mmol); iodine (0.12 g, 0.48 mmol). Yield = 0.12 g (73%). ^{1}H NMR ($CDCl_3$): δ 6.23, 6.16 (s, 2H, 4-pz); 2.83, 2.70 (s, 6H, 5-pz); 2.40, 2.33 (s, 6H, 3-pz). $^{13}C\{^{1}H\}$ NMR ($CDCl_3$): δ 193.2 (C(C=S)); 152.8 (C(5-pz)); 146.6 (C(3-pz); 113.8 (C(4-pz)); 17.1 (C($\underline{C}H_3$, 5-pz); 13.8 (C($\underline{C}H_3$, 3-pz). IR (ATR, cm^{-1}): $\upsilon_{C=N}$ = 1533, υ_{C-S} = 1261, $\upsilon_{C=S}$ = 879.

*4.3.2.7. Synthesis of bis(indazol-1-yldithiocarbamato)disulfide (**L11**)*

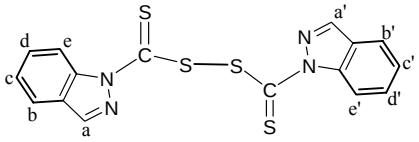

L7 (0.3 g, 1.29 mmol); iodine (0.16 g, 0.65 mmol). Yield = 0.14 g (56%). ^{1}H NMR ($CDCl_3$):δ 9.06 (d, 2H, $^{4}J_{HH}$ = 9.0 Hz, He); 8.35 (s, 1H, Ha); 7.85 (d, 1H, $^{3}J_{HH}$ = 8.4 Hz, Hb); 7.64 (1H, $^{3}J_{HH}$ = 15.0 Hz , Hd); 7.47 (t, 1H, $^{4}J_{HH}$ = 15 Hz, Hc). $^{13}C\{^{1}H\}$ NMR ($CDCl_3$): δ 191.8 (C(C=S)); 141.1 (C(5C-pz); 130.9 (C(3C-pz)); 131.2 (C(7C-Ph)); 126.2 (C(4C-Ph); 121.8 (C(8C, 9C-Ph)); 116.8 (C(6C-Ph)). IR (ATR, cm^{-1}): $\upsilon_{C=N}$ = 1605, υ_{C-S} = 1334, $\upsilon_{C=S}$ = 901. Anal. Calc. for $C_{16}H_{10}N_4S_4$: C 49.72; H 2.61; N 14.49; 33.18%. Found: C, 48.82; H, 2.46; N, 13.83; S, 33.18%.

*4.3.2.8. Synthesis of pyrazolyl-1-dithiocarbamato-triphenylphosphinegold(I) (**13**)*

L5 (0.05 g, 0.3 mmol) was dissolved in deionised water (10 mL) and stirred for 2 min. To the resultant solution was added [AuCl(PPh_3)] (0.15 g, 0.3 mmol) in dichloromethane (10 mL) and the bi-phasic mixture stirred vigorously at room temperature. A colour change in the organic layer from colourless to red was observed, and after 30 min the two layers were separated. The dichloromethane solution was dried over anhydrous $MgSO_4$. The solvent was then removed *in vacuo* to afford an orange-yellow solid. Yield = 0.17 g (93%). ^{1}H NMR ($CDCl_3$): δ 7.63 (s, 1H, 5-pz); 7.57 (s, 1H, 3-pz); 7.49 (m, 9H, P<u>Ph</u>$_3$); 7.35 (m, 6H, P<u>Ph</u>$_3$); 6.27 (s, 1H, 4-pz). ^{13}C{^{1}H} NMR ($CDCl_3$): δ 213.4 (C(C=S)); 144.0 (C(5-pz); 134.2-129.1 (Phenyl region); 140.8 (C(3-pz)); 106.1 (C(4-pz)). IR (KBr, cm^{-1}): $\upsilon_{C=N}$ = 1620, υ_{C-S} = 1121, $\upsilon_{C=S}$ = 884. ^{31}P{^{1}H} NMR ($CDCl_3$): δ 35.2 (P(PPh_3)). Anal. Calc. for $C_{24}H_{22}AuN_2PS_2$: C 43.86, H 3.01, N 4.65. Found: C 43.53, H 3.05, N 4.62%.

Synthesis of compounds **14-16** were prepared using the procedure described for **13** above, but using the reagents indicated for each compound.

*4.3.2.9. Synthesis of 3,5-dimethylpyrazolyl-1-dithiocarbamato-triphenylphosphinegold(I) (**14**)*

L6 (0.1g, 0.47 mmol), [AuCl(PPh_3)] (0.24 g, 0.47 mmol). Yield = 0.17 g (57%). ^{1}H NMR ($CDCl_3$): δ 7.44, 7.29 (m, 15H, P<u>Ph</u>$_3$); 6.12, 5.82 (s, 1H, 4-pz); 2.29 (m, 6H, 3-pz, 5-pz). ^{13}C{^{1}H} NMR ($CDCl_3$): δ 215.5 (C(C=S)); 149.7 (C(5-pz); 134.1-128.7 (Phenyl region);

142.1 (C(3-pz)); 112.4, 104.1 (C(5-pz)); 13.9 (C($\underline{C}H_3$, 5-pz); 12.3 (C($\underline{C}H_3$, 3-pz). IR (KBr, cm^{-1}): $\upsilon_{C=N}$ = 1580, υ_{C-S} = 1154, $\upsilon_{C=S}$ = 854. $^{31}P\{^1H\}$ NMR ($CDCl_3$): δ 33.8 ($P(PPh_3)$). Anal. Calc. for $C_{24}H_{22}AuN_2PS_2$: C 45.72, H 3.52, N 4.44. Found: C 45.89, H 3.89, N 3.29%.

4.3.2.10. Synthesis of indazolyl-1-dithiocarbamato-triphenylphosphinegold(I) ***(15)***

L7 (0.1 g, 0.4 mmol), [$AuCl(PPh_3)$] (0.2 g, 0.4 mmol). Yield = 0.15 g (58%). ^1H NMR ($CDCl_3$): δ 9.21 (d, 1H, $^4J_{HH}$ = 9.0 Hz, Ha); 8.17 (s, 1H, Hb); 7.73 (d, 1H, $^3J_{HH}$ = 8.4 Hz, He); 7.61, 7.50 (m, 15H, P$\underline{Ph}_3$); (7.58 (1H, Hd); 7.35 (t, 1H, $^4J_{HH}$ = 15 Hz, Hc). $^{13}C\{^1H\}$ NMR ($CDCl_3$): δ 214.2 (C(C=S)); 139.5 (C(5C-pz); 134.7-129.5 (Phenyl region); 129.5 (C(3C-pz)); 126.9 (C(7C-Ph)); 124.6 (C(4C-Ph); 121.4 (C(8C, 9C-Ph)); 118.7 (C(6C-Ph)). IR (KBr, cm^{-1}): $\upsilon_{C=N}$ = 1601, υ_{C-S} = 1148, $\upsilon_{C=S}$ = 905. $^{31}P\{^1H\}$ NMR ($CDCl_3$): δ 36.8 ($P(PPh_3)$). Anal. Calc. for $C_{26}H_{20}AuN_2PS_2$: C 47.86, H 3.09, N 4.29. Found: C 47.41, H 3.04, N 3.85%.

4.3.2.11. Synthesis of imidazolyl-1-dithiocarbamato triphenylphosphinogold(I) ***(16)***

L8 (0.1 g, 0.4 mmol), [$AuCl(PPh_3)$] (0.2 g, 0.4 mmol). Yield = 0.15 g (65%). ^1H NMR ($CDCl_3$): δ 7.82 (s, 1H, 5-Im); 7.52 (s, 1H, 3-Im); 7.49 (m, 9H, P$\underline{Ph}_3$); 7.35 (m, 6H, P$\underline{Ph}_3$); 6.71 (s, 1H, 4-Im).$^{13}C\{^1H\}$ NMR ($CDCl_3$): δ 219.4 (C(C=S)); 137.2 (C(2-Im); 133.7-129.4 (Phenyl region); 128.8 (C(5-Im)); 120.1 (C(4(C-Im)). IR (KBr, cm^{-1}): $\upsilon_{C=N}$ = 1592, υ_{C-S} = 1102, $\upsilon_{C=S}$ = 814. $^1P\{^1H\}$ NMR ($CDCl_3$): δ 36.3 ($P(PPh_3)$). Anal. Calc. for $C_{26}H_{20}AuN_2PS_2$: C 47.86, H 3.09, N 4.29. Found: C 47.41, H 3.04, N 3.85%.

*4.3.2.12. Synthesis of bis-(pyrazolyl-1-dithiocarbamato)-bis-(diphenylphosphino)-ethanegold(I) (**17a**) and [$Au_{18}S_8(dppe)_6$]2Cl (**17b**)*

To a solution of [Au_2Cl_2(dppe)] (0.08 g, 0.09 mmol) in CH_2Cl_2 (10 mL), was added **L5** (0.03 g, 0.19 mmol) previously dissolved in water (10 mL). The resultant mixture was stirred at room temperature for 20 min during which time the CH_2Cl_2 layer changed colour from a white suspension to a clear orange solution, whilst the water layer became clear. The mixture was separated and the organic layer dried over anhydrous $MgSO_4$. The yellow solids were isolated as products upon *in vacuo* evaporation of the solvent. Yield = 0.07 g (73%). ^{1}H NMR ($CDCl_3$): δ 8.78 (d, 2H, $^3J_{HH}$ = 2.7 Hz, 5-pz); 7.80 (s, 2H, 3-pz); 7.78 (m, 8H, ($\underline{Ph}$)$_2$P(CH_2)$_2$P($\underline{Ph}$)$_2$); 7.49 (m, 12H, ($\underline{Ph}$)$_2$P(CH_2)$_2$P($\underline{Ph}$)$_2$); 6.43 (s, 2H, 4-pz); 2.87 (bs, 4H, CH_2, (Ph)$_2$P(C$\underline{H_2}$)$_2$P(Ph)$_2$). ^{13}C{^{1}H} NMR ($CDCl_3$): δ 214.2 (C(C=S)); 149.7 (C(5-pz); 142.0 (C(3-pz)); 134.1-128.7 (Phenyl region); 111.4 (C(4-pz)); 24.6 (C(Ph_2P($\underline{C}H_2$)$_2$PPh_2). IR (KBr, cm^{-1}): $\upsilon_{C=N}$ = 1590, υ_{C-S} = 1190, $\upsilon_{C=S}$ = 889. ^{31}P{^{1}H} NMR: ($CDCl_3$): δ 36.1 ($Ph_2\underline{P}(CH_2)_2\underline{P}Ph_2$). Anal. Calc. for $C_{34}H_{30}Au_2N_4P_2S_4$: C 37.85, H 2.80, N 5.14, S 11.89. Found: C 38.18, H 3.01, N 4.57, S 11.73%.

Efforts to crystallise **17a** in dichloromethane/ether solution led to the formation of a gold(I) cluster, [$Au_{18}S_8(dppe)_6$]2Cl (**17b**), Anal. Calc. for $C_{26}H_{20}AuCl_2N_2PS_2$: C 29.71, H 2.32, N 4.10. Found: C 28.90, H 2.00, N 3.80%.

Synthesis of compounds **18-25** were prepared using the procedure described for **17a** above, but using the reagents indicated for each compound.

*4.3.2.13. Synthesis of bis-(3,5-dimethylpyrazolyl-1-dithiocarbamato)-bis-(diphenylphosphino)ethanegold(I) (**18**)*

L6 (0.04 g, 0.19 mmol), $[Au_2Cl_2(dppe)]$ (0.1 g, 0.09 mmol). Yield = 0.09 g (88%). ^1H NMR ($CDCl_3$): δ 7.64 (m, 8H, $\underline{Ph}_2P(CH_2)_2P\underline{Ph}_2$); 7.35 (m, 12H, $\underline{Ph}_2P(CH_2)_2P\underline{Ph}_2$); 6.09 (s, 2H, 4-pz); 2.69 (bs, 4H, $Ph_2P(C\underline{H}_2)_2PPh_2$); 2.26 (d, 12H, $C\underline{H}_3$, 3,5-pz). $^{13}C\{^1H\}$ NMR ($CDCl_3$): δ 216.5 (C(C=S)); 152.7 (C(5-pz); 143.1 (C(3-pz)); 135.1-128.6 (Phenyl region); 112.6 (C(4-pz)); 14.0 (C(5-pPz); 12.4 (C(3-pz)); 25.7 ($C(Ph_2P(\underline{C}H_2)_2PPh_2$). IR (KBr, cm^{-1}): $\upsilon_{C=N}$ = 1603, υ_{C-S} = 1263, $\upsilon_{C=S}$ = 989. $^{31}P\{^1H\}$ NMR: ($CDCl_3$): δ 35.7 ($Ph_2\underline{P}(CH_2)_2\underline{P}Ph_2$). Anal. Calc. for $C_{38}H_{38}Au_2N_4P_2S_4$: C 40.22, H 3.37, N 4.94, S 11.30. Found: C 39.89, H 3.59, N 4.67, S 11.15%.

*4.3.2.14. Synthesis of bis-(indazolyl-1-dithiocarbamato)-bis-(diphenylphosphino)ethanegold(I) (**19**)*

L7 (0.04 g, 0.19 mmol), $[Au_2Cl_2(dppe)]$ (0.08 g, 0.09 mmol). Yield 0.07 g (63%). ^1H NMR ($CDCl_3$): δ 9.16 (s, 1H, Ha); 8.06 (s, 1H, Hb); 7.78 (m, 8H, $(\underline{Ph})_2P(CH_2)_2P(\underline{Ph})_2$); 7.49 (m, 12H, $(\underline{Ph})_2P(CH_2)_2P(\underline{Ph})_2$); 7.67 (d, 1H, $^3J_{HH}$ = 8.4 Hz, He); 7.71 (1H, Hd); 7.43 (t, 1H, $^4J_{HH}$ = 15 Hz, Hc); 2.87 (bs, 4H, CH_2, $(Ph)_2P(C\underline{H}_2)_2P(Ph)_2$). $^{13}C\{^1H\}$ NMR ($CDCl_3$): δ 213.9 (C(C=S)); 142.1 (C(5-Pz); 139.0 (C(3-Pz)); 134.1-129.7 (Phenyl region); 126.1 (C(7C-Ph)); 123.1 (C(4C-Ph)); 122.2 (C(8C-Ph, 9C-Ph)); 117.5 (C(6C-Ph) 25.2 ($C(Ph_2P(\underline{C}H_2)_2PPh_2$). $^{31}P\{^1H\}$ NMR: ($CDCl_3$): δ 34.9 ($Ph_2\underline{P}(CH_2)_2\underline{P}Ph_2$). Anal. Calc. for $C_{42}H_{34}Au_2N_4P_2S_4$: C 42.79, H 2.91, N 4.75, S 10.88. Found: C 43.24, H 2.82, N 4.65, S 9.97%.

*4.3.2.15. Synthesis of binuclear bis(pyrazol-1-yldithiocarbamato)-bis-(diphenylphosphino)propane gold(I) (**20**)*

L5 (0.08 g, 0.46 mmol), $[Au_2Cl_2(dppp)]$ (0.2 g, 0.23 mmol). Yield = 0.15 g (59%). ^1H NMR ($CDCl_3$): δ 8.73 (s, 2H, $^3J_{HH}$ = 2.7 Hz, 5-pz); 7.73 (m, 8H, $\underline{Ph_2}P(CH_2)_3P\underline{Ph_2}$); 7.51 (s, 4H, $^3J_{HH}$ = 1.8 Hz, 3-pz); 7.41 (m, 12H, $\underline{Ph_2}P(CH_2)_3P\underline{Ph_2}$); 6.41 (s, 2H, $^3J_{HH}$ = 2.7 Hz, 4-pz); 2.93 (m, 2H, $Ph_2PCH_2C\underline{H_2}CH_2PPh_2$); 1.99 (m, 4H, $Ph_2PC\underline{H_2}CH_2C\underline{H_2}PPh_2$). $^{13}C\{^1H\}$ NMR ($CDCl_3$): δ 218.9 (C(C=S)); 147.5 (C(5-pz); 140.8 (C(3-pz)); 133.2-129.2 (Phenyl region); 106.2 (C(4-pz)); 28.5 (2C, $^1J_{C-P}$ = 62.7 Hz, P-CH_2, $Ph_2P\underline{C}H_2CH_2\underline{C}H_2PPh_2$); 21.4 (C, $Ph_2PCH_2\underline{C}H_2CH_2PPh_2$). IR (KBr, cm^{-1}): $\upsilon_{C=N}$ = 1628, υ_{C-S} = 1088, $\upsilon_{C=S}$ = 891. $^{31}P\{^1H\}$ NMR ($CDCl_3$): δ 32.8. Anal. Calc. for $C_{35}H_{32}Au_2N_4P_2S_4$: C 38.47, H 2.95, N 5.13, S 11.74. Found: C 38.99, H 3.08, N 4.09, S 11.45%.

*4.3.2.16. Synthesis of binuclear bis(3,5-dimethylpyrazol-1-yldithiocarbamato)-bis-(diphenylphosphino)propanegold(I) (**21**)*

L6 (0.1 g, 0.46 mmol), $[Au_2Cl_2(dppp)]$ (0.2 g, 0.23 mmol). Yield = 0.13 g (50%). ^1H NMR ($CDCl_3$): δ= 7.66 (m, 8H, $\underline{Ph_2}P(CH_2)_3P\underline{Ph_2}$); 7.34 (m, 12H, $\underline{Ph_2}P(CH_2)_3P\underline{Ph_2}$); 5.85 (s, 2H, 4-pz); 2.91 (m, 2H, $Ph_2PCH_2C\underline{H_2}CH_2PPh_2$); 1.88 (m, 4H, $Ph_2PC\underline{H_2}CH_2C\underline{H_2}PPh_2$); 2.24, 2.26 (d, 12H, $C\underline{H_3}$, 3,5-pz). $^{13}C\{^1H\}$ NMR ($CDCl_3$): δ 215.9 (C(C=S)); 153.3 (C(5-pz); 144.2 (C(3-pz)); 133.4-129.2 (Phenyl region); 112.5 (C(4-pz)); 27.9 (2C, $^1J_{C-P}$ = 58.4 Hz, P-CH_2, $Ph_2P\underline{C}H_2CH_2\underline{C}H_2PPh_2$); 20.2 (C, $Ph_2PCH_2\underline{C}H_2CH_2PPh_2$); 13.8 (C($\underline{C}H_3$, 5-pz); 13.2 (C($\underline{C}H_3$, 3-pz). IR (KBr, cm^{-1}): $\upsilon_{C=N}$ = 1653, υ_{C-S} = 1099, $\upsilon_{C=S}$ = 957. $^{31}P\{^1H\}$ NMR ($CDCl_3$): δ 29.2.

Anal. Calc. for $C_{39}H_{40}Au_2N_4P_2S_4$: C 40.77, H 3.51, N 4.88, S 11.16. Found: C 40.99, H 3.74, N 4.79, S 11.16%.

*4.3.2.17. Synthesis of binuclear bis(indazol-1-yldithiocarbamato)-bis-(diphenylphosphino)propane gold(I) (**22**)*

L7 (0.04 g, 0.22 mmol), $[Au_2Cl_2(dppp)]$ (0.1 g, 0.11 mmol). Yield = 0.07 g (54%). ^{1}H NMR ($CDCl_3$): δ 9.13 (s, 1H, Ha); 8.16 (s, 1H, Hb); 7.73 (1H, Hd); 7.69 (d, 1H, $^3J_{HH}$ = 8.0 Hz, He); 7.66 (m, 8H, $\underline{Ph_2}P(CH_2)_3P\underline{Ph_2}$); 7.45 (t, 1H, $^4J_{HH}$ = 16.8 Hz, Hc); 7.42 (m, 12H, $\underline{Ph_2}P(CH_2)_3P\underline{Ph_2}$); 2.89(m, 2H, $Ph_2PCH_2C\underline{H_2}CH_2PPh_2$); 1.92 (m, 4H, $Ph_2PC\underline{H_2}CH_2C\underline{H_2}PPh_2$). $^{13}C\{^1H\}$ NMR ($CDCl_3$): δ 213.8 (C(C=S)); 140.3 (C(5C-pz); 139.1 (C(3C-pz)); 133.5-129.2 (Phenyl region); 127.9 (C(7C-Ph)); 124.2 (C(4C-Ph)); 121.1 (C(8C-Ph, 9C-Ph)); 118.3 (C(6C-Ph)); 28.6 (2C, $^1J_{C-P}$ = 64.2 Hz, P-CH_2, $Ph_2P\underline{C}H_2CH_2\underline{C}H_2PPh_2$); 19.8 ($Ph_2PCH_2\underline{C}H_2CH_2PPh_2$). IR (KBr, cm^{-1}): $\upsilon_{C=N}$ = 1606, υ_{C-S} = 1150, $\upsilon_{C=S}$ = 993. $^{31}P\{^1H\}$ NMR ($CDCl_3$): δ 29.2. ESI-MS: m/z 1190.9 $[Au_2(\mathbf{L7})_2(dppp)]^+$ (5%). Anal. Calc. for $C_{43}H_{36}Au_2N_4P_2S_4$: C 43.29, H 3.04, N 4.70, S 10.75. Found: C 43.23, H 3.05, N 4.62, S 10.36%.

*4.3.2.18. Synthesis of binuclear bis(pyrazol-1-yldithiocarbamato)-bis-(diphenylphosphino)hexane gold(I) (**23**)*

L5 (0.02 g, 0.11 mmol), $[Au_2Cl_2(dpph)]$ (0.05 g, 0.05 mmol). Yield = 0.04 g (70%). ^{1}H NMR ($CDCl_3$): δ 8.78 (d, 2H, $^3J_{HH}$ = 2.7 Hz, 5-pz); 7.80 (s, 2H, 3-pz); 7.78 (m, 8H,

($\underline{Ph}$)$_2$P(CH$_2$)$_6$P($\underline{Ph}$)$_2$); 7.49 (m, 12H, ($\underline{Ph}$)$_2$P(CH$_2$)$_6$P($\underline{Ph}$)$_2$); 6.43 (s, 2H, 4-pz); 2.87 (bs, 4H, Ph$_2$P(CH$_2$)$_2$(C$\underline{H}_2$)$_2$(CH$_2$)$_2$PPh$_2$); 1.49 (bs, 8H, Ph$_2$P(C$\underline{H}_2$)$_2$(CH$_2$)$_2$(C$\underline{H}_2$)$_2$PPh$_2$).. ^{13}C{^{1}H} NMR ($CDCl_3$): δ 213.8 (C(C=S)); 140.3 (C(5C-pz); 139.1 (C(3C-pz)); 133.5-129.2 (Phenyl region); 127.9 (C(7C-Ph)); 124.2 (C(4C-Ph)); 121.1 (C(8C-Ph, 9C-Ph)); 118.3 (C(6C-Ph)); 30.1 (4C, PPh$_2$($\underline{C}$H$_2$)$_2$(CH$_2$)$_2$($\underline{C}$H$_2$)$_2$PPh$_2$); 25.9 (2C, Ph$_2$P(CH$_2$)$_2$($\underline{C}$H$_2$)$_2$(CH$_2$)$_2$PPh$_2$). IR (KBr, cm^{-1}): $\upsilon_{C=N}$ = 1620, υ_{C-S} = 1108, $\upsilon_{C=S}$ = 960. ^{31}P{^{1}H} NMR ($CDCl_3$): δ 32.3. Anal. Calc. for $C_{38}H_{38}Au_2N_4P_2S_4$: C 40.22, H 3.37, N 4.94, S 11.30. Found: C 40.17, H 3.45, N 4.36, S 10.28%.

*4.3.2.19. Synthesis of binuclear bis(3,5-dimethylpyrazol-1-yldithiocarbamato)-bis-(diphenylphosphino)hexane gold(I) (**24**)*

L6 (0.09 g, 0.42 mmol), [Au$_2$Cl$_2$(dpph)] (0.2 g, 0.2 mmol). Yield = 0.12 g (50%). ^{1}H NMR ($CDCl_3$): δ 7.67 (m, 8H, $\underline{Ph_2}$P(CH$_2$)$_6$P$\underline{Ph_2}$); 7.40 (m, 12H, $\underline{Ph_2}$P(CH$_2$)$_6$P$\underline{Ph_2}$); 6.00 (s, 2H, 4-pz); 2.76 (bs, 4H, Ph$_2$P(CH$_2$)$_2$(C$\underline{H}_2$)$_2$(CH$_2$)$_2$PPh$_2$); 2.18, 2.27 (d, 12H, C$\underline{H}_3$, 3,5-pz). 1.60, 1.52 (bs, 8H, Ph$_2$P(C$\underline{H}_2$)$_2$(CH$_2$)$_2$(C$\underline{H}_2$)$_2$PPh$_2$). ^{13}C{^{1}H} NMR ($CDCl_3$): δ 215.9 (C(C=S)); 153.3 (C(5-pz); 144.2 (C(3-pz)); 133.4-129.2 (Phenyl region); 112.5 (C(4-pz)); 31.2 (4C, PPh$_2$($\underline{C}$H$_2$)$_2$(CH$_2$)$_2$($\underline{C}$H$_2$)$_2$PPh$_2$); 26.7 (2C, Ph$_2$P(CH$_2$)$_2$(C$\underline{H}_2$)$_2$(CH$_2$)$_2$PPh$_2$); 13.8 (C(5-pz); 13.2 (C(3-pz). IR (KBr, cm^{-1}): $\upsilon_{C=N}$ = 1653, υ_{C-S} = 1099, $\upsilon_{C=S}$ = 957. IR (KBr, cm^{-1}): $\upsilon_{C=N}$ = 1657, υ_{C-S} = 1099, $\upsilon_{C=S}$ = 994. ^{31}P{^{1}H} NMR ($CDCl_3$): δ 32.7. Anal. Calc. for $C_{42}H_{46}Au_2N_4P_2S_4$: C 42.36, H 3.89, N 4.70, S 10.77. Found: C 41.82, H 3.84, N 4.62, S 10.56%.

*4.3.2.20. Synthesis of binuclear bis(indazol-1-yldithiocarbamato)-bis-(diphenylphosphino)hexane gold(I) (**25**)*

L7 (0.1 g, 0.44 mmol), $[Au_2Cl_2(dpph)]$ (0.2 g, 0.22 mmol). Yield = 0.14 g (52%). ^{1}H NMR ($CDCl_3$): δ 9.18 (d, 1H, $^4J_{HH}$ = 8.4 Hz, (Ha)); 8.10 (s, 1H, Hb); 7.49 (d, 1H, $^3J_{HH}$ = 8.7 Hz, He); 7.24 (t, 1H, $^4J_{HH}$ = 15.0 Hz, Hd); 7.32 (t, 1H, $^4J_{HH}$ = 15.0 Hz, Hc); 7.66 (m, 8H, $\underline{Ph_2}P(CH_2)_6P\underline{Ph_2}$); 7.42 (m, 12H, $\underline{Ph_2}P(CH_2)_6P\underline{Ph_2}$); 2.39 (m, 4H, $Ph_2P(CH_2)_2(C\underline{H_2})_2(CH_2)_2PPh2$); 1.57 (m, 8H, $Ph_2P(C\underline{H_2})_2(CH_2)_2(C\underline{H_2})_2PPh_2$). $^{13}C\{^1H\}$ NMR ($CDCl_3$): δ 213.8 (C(C=S)); 140.3 (C(5C-pz); 139.1 (C(3C-pz)); 133.5-129.2 (Phenyl region); 127.9 (C(7C-Ph)); 124.2 (C(4C-Ph)); 121.1 (C(8C-Ph, 9C-Ph)); 118.3 (C(6C-Ph)); 28.9 (4C, $\underline{C}H_2)_2(CH_2)_2(\underline{C}H_2)_2PPh_2$); 25.6 (2C, $Ph_2P(CH_2)_2(\underline{C}H_2)_2(CH_2)_2PPh_2$). IR (KBr, cm^{-1}): $\upsilon_{C=N}$ = 1657, υ_{C-S} = 1099, $\upsilon_{C=S}$ = 994. $^{31}P\{^1H\}$ NMR $CDCl_3$): δ 31.8. Anal. Calc. for $C_{46}H_{42}Au_2N_4P_2S_4$: C 44.74, H 3.43, N 4.54, S 10.39. Found: C 44.37, H 3.46, N 4.50, S 10.32%.

*4.3.2.21. Synthesis of bis-(pyrazol-1-yl-dithiocarbamato)-bis(diphenylphosphino)ethane platinum(II) (**26**)*

To a solution of **L5** (0.06 g, 0.3 mmol) in deionised water (5 mL) was added $[PtCl_2(dppe)]$ (0.1 g, 0.16 mmol) in dichloromethane (10 mL) and the bi-phasic mixture stirred vigorously at room temperature. A colour change in the organic layer from colourless to yellow was observed, and after 30 min the two layers were separated. The dichloromethane solution was dried over anhydrous $MgSO_4$. The solvent was then removed *in vacuo* to afford a yellow solid. Efforts to grow crystals of **26**, by re-dissolving **26** in dichloromethane and layering it

with hexane or diethyl ether, led to formation of green single crystals **27** suitable for X-ray analysis. Yield **26** = 0.13 g (93%). ^{1}H NMR ($CDCl_3$): δ 8.49 (s, 2H, 5-pz); 7.76 (m, 8H, $\underline{Ph_2}P(CH_2)_2P\underline{Ph_2}$); 7.74 (s, 2H, 3-pz); 7.48 (m, 12H, $\underline{Ph_2}P(CH_2)_2P\underline{Ph_2}$); 6.22 (s, 2H, 4-pz); 3.19 (qt, 4H, $^{2}J_{P\text{-}H} + {}^{3}J_{P\text{-}H}$ = 18.0 Hz, $Ph_2P(C\underline{H_2})_2PPh_2$). $^{31}P\{^{1}H\}$ NMR ($CDCl_3$): δ 39.3 (2P, $J_{Pt\text{-}P}$ = 3678 Hz, $Ph_2\underline{P}(CH_2)_2\underline{P}Ph_2$). IR (KBr, cm^{-1}): $\upsilon_{C=N}$ = 1609, $\upsilon_{C\text{-}S}$ = 1099, $\upsilon_{C=S}$ = 821. Anal. Calc. for $C_{34}H_{30}N_4P_2PtS_4$: C 46.41, H 3.44, N 6.37, S 14.58. Found: C 46.51, H 2.98, N 5.81, S 14.01%.

Synthesis of compounds **28**-**30** were prepared using the procedure described for **26** above, but using the reagents indicated for each compound.

*4.3.2.22. Synthesis of bis-(3,5-dimethylpyrazol-1-yldithiocarbamato)-bis-(diphenylphosphino)ethaneplatinum(II) (**28**)*

L6 (0.06 g, 0.3 mmol); $[PtCl_2(dppe)]$ (0.1 g, 0.15 mmol). Yield = 0.12 g (86%). ^{1}HNMR ($CDCl_3$): δ 7.76 (m, 8H, $\underline{Ph_2}P(CH_2)_2P\underline{Ph_2}$); 7.54 (m, 12H, $\underline{Ph_2}P(CH_2)_2P\underline{Ph_2}$); 5.91 (s, 2H, 4-pz); 3.11 (qt, 4H, $^{2}J_{P\text{-}H} + {}^{3}J_{P\text{-}H}$ = 18.9 Hz, $Ph_2P(C\underline{H_2})_2PPh_2$); 2.72 (s, 6H, 5-pz); 2.32 (s, 6H, 3-pz). $^{31}P\{^{1}H\}$ NMR ($CDCl_3$): δ 44.2 (2P, $J_{Pt\text{-}P}$ = 3897 Hz, $Ph_2\underline{P}(CH_2)_2\underline{P}Ph_2$). IR (KBr, cm^{-1}): $\upsilon_{C=N}$ = 1591, $\upsilon_{C\text{-}S}$ = 1149, $\upsilon_{C=S}$ = 853. Anal. Calc. for $C_{38}H_{38}N_4P_2PtS_4$: C 48.76, H 4.09, N 5.99, S 13.70. Found: C 49.21, H 2.98, N 5.81, S 14.01%.

*4.3.2.23. Synthesis of bis-(indazolyl-1-dithiocarbamato)-bis-(diphenylphosphino)ethaneplatinum(II) (**29**)*

L7 (0.07 g, 0.3 mmol); [$PtCl_2$(dppe)] (0.1 g, 0.15 mmol). Yield = 0.1 g (67%). ^{1}HNMR ($CDCl_3$): δ 9.14 (s, 1H, Ha); 8.17 (s, 1H, Hb); 7.74 (m, 8H, $\underline{Ph_2}P(CH_2)_2P\underline{Ph_2}$); 7.52 (m, 12H, $Ph_2P(C\underline{H_2})_2PPh_2$); 7.67 (d, 1H, $^3J_{HH}$ = 8.4 Hz, He); 7.78 (1H, Hd); 7.43 (t, 1H, $^4J_{HH}$ = 15 Hz, Hc); 3.11 (qt, 4H, $^2J_{P\text{-}H}$ + $^3J_{P\text{-}H}$ = 18.9 Hz, $Ph_2P(C\underline{H_2})_2PPh_2$). $^{31}P\{^1H\}$ NMR ($CDCl_3$): δ 44.3 (2P, $J_{Pt\text{-}P}$ = 3761 Hz, $Ph_2\underline{P}(CH_2)_2\underline{P}Ph_2$). IR (KBr, cm^{-1}): $\upsilon_{C=N}$ = 1634, $\upsilon_{C\text{-}S}$ = 1187, $\upsilon_{C=S}$ = 849. Anal. Calc. for $C_{42}H_{34}N_4P_2PtS_4$: C 51.47, H 3.50, N 5.72 %. Found: C 50.82, H 4.01, N 5.19%.

*4.3.2.24. Synthesis of bis-(pyrazol-1-yl-dithiocarbamato)-bis(diphenylphosphino)ethane nickel(II) (**30**)*

L5(0.06 g, 0.3 mmol); [$NiCl_2$(dppe)] (0.08 g, 0.15 mmol). Yield = 0.06 g (55%). Yield = 0.13 g (93%). $^{31}P\{^1H\}$ NMR ($CDCl_3$): δ 33.8. IR (KBr, cm^{-1}): $\upsilon_{C=N}$ = 1617, $\upsilon_{C\text{-}S}$ = 1183, $\upsilon_{C=S}$ = 835. Anal. Calc. for $C_{34}H_{30}N_4NiP_2S_4$: C 54.92, H 4.07, N 7.54, S 17.25. Found: C 54.81, H 4.02, N 7.61, S 17.14%.

*4.3.2.25. Synthesis of bis(pyrazolyl-1-dithiocarbamato)platinum(II) (**31**)*

To a solution of **L5** (0.09 g, 0.48 mmol) in deionised water (10 mL) was added $K_2[PtCl_4]$ (0.1 g, 0.24 mmol) in deionised water (10 mL). The solution mixture was stirred at room temperature for 2 h upon which a colour change of the solution, from yellow to deep red, was observed. A brown solid was isolated as the product by filtration. Yield = 0.07 g (58%). ^{1}H

NMR ($CDCl_3$): δ 8.62, 8.51 (s, 2H, 5-pz); 8.16, 8.02 (s, 2H, 3-pz); 6.69, 6.50 (s, 2H, 4-pz). IR (KBr, cm^{-1}): $\upsilon_{C=N}$ = 1518, υ_{C-S} = 1110, $\upsilon_{C=S}$ = 855.

Synthesis of compounds **32** and **33** were prepared using the procedure described for **31** above, but using the reagents indicated for each compound.

*4.3.2.26. Synthesis of bis(3,5-dimethylpyrazolyl-1-dithiocarbamato)platinum(II) (**32**)*

L6 (0.11 g, 0.52 mmol); $K_2[PtCl_4]$ (0.11 g, 0.26 mmol). Yield = 0.08 g (54%). ^1H NMR ($CDCl_3$): δ 6.23, 6.16 (s, 2H, 4-pz); 2.83, 2.70 (s, 6H, 5-pz); 2.40, 2.33 (s, 6H, 3-pz). $^{13}C\{^1H\}$ NMR ($CDCl_3$): δ 226.8 (C(C=S)); 156.5 (C(5-pz)); 143.9 (C(3-pz); 115.3, 113.3 (C(4-pz)); 16.5, 15.3 (C($\underline{C}H_3$, 5-pz); 14.6, 14.0 (C($\underline{C}H_3$, 3-pz). IR (KBr, cm^{-1}): $\upsilon_{C=N}$ = 1580, υ_{C-S} = 1158, $\upsilon_{C=S}$ = 887. Anal. Calc. for $C_{12}H_{14}N_4PtS_4$: C 26.81, H 2.62, N 10.42. Found: C 26.81, H 2.20, N 10.42%.

*4.3.2.27. Synthesis of bis-(indazolyl-1-dithiocarbamato)platinum(II) (**33**)*

L7 (0.1 g, 0.43 mmol); $K_2[PtCl_4]$ (0.09 g, 0.22 mmol). Yield = 0.06 g (46%). ^1H NMR ($CDCl_3$): δ 9.53 (d, 2H, $^4J_{HH}$ = 8.4 Hz, (Ha)); 8.65 (d, 1H, $^3J_{HH}$ = 8.7 Hz, He); 8.43, 8.31 (s, 2H, Hb); 7.82 (t, 1H, $^4J_{HH}$ = 14.8 Hz, Hd); 7.50 (t, 1H, $^4J_{HH}$ = 15 Hz, Hc). IR (KBr, cm^{-1}): $\upsilon_{C=N}$ = 1606, υ_{C-S} = 1172, $\upsilon_{C=S}$ = 917.

4.3.3. X-ray crystallography

4.3.3.1. Data Collection

An orange crystal of [Au(**L7**)(PPh_3)] (**15**) with approximate dimensions 0.45 x 0.33 x 0.21 mm^3 was selected under oil under ambient conditions and attached to the tip of a Micromount©. The crystal was mounted in a stream of cold nitrogen at 105(2) K and centred in the X-ray beam by using a video camera. The crystal evaluation and data collection were performed on a Bruker CCD-1000 diffractometer with Mo K_α (λ = 0.71073 Å) radiation and the diffractometer to crystal distance of 4.9 cm.

The initial cell constants were obtained from three series of ω scans at different starting angles. Each series consisted of 20 frames collected at intervals of 0.3º in a 6º range about ω with the exposure time of 10 seconds per frame. A total of 131 reflections were obtained. The reflections were successfully indexed by an automated indexing routine built in the SMART program. The final cell constants were calculated from a set of 12116 strong reflections from the actual data collection.

The data were collected by using the full sphere data collection routine to survey the reciprocal space to the extent of a full sphere to a resolution of 0.80 Å. A total of 20998 data were harvested by collecting four sets of frames with 0.4º scans in ω and one set of frames with 0.5º scan in φ. These highly redundant datasets were corrected for Lorentz and

polarization effects. The absorption correction was based on fitting a function to the empirical transmission surface as sampled by multiple equivalent measurements.[52]

4.3.3.2. Structure solution and refinement

The systematic absences in the diffraction data were uniquely consistent for the space group $P2_1/n$ that yielded chemically reasonable and computationally stable results of refinement. A successful solution by the direct methods provided most non-hydrogen atoms from the *E*-map. The remaining non-hydrogen atoms were located in an alternating series of least-squares cycles and difference Fourier maps. All non-hydrogen atoms were refined with anisotropic displacement coefficients. All hydrogen atoms except those on the water molecule were included in the structure factor calculation at idealized positions and were allowed to ride on the neighboring atoms with relative isotropic displacement coefficients. There is also one solvated water molecule per Pd complex in the unit cell. The water molecules were refined with restraints. The final least-squares refinement of 172 parameters against 3166 data resulted in residuals *R* (based on F^2 for $I \geq 2\sigma$) and *wR* (based on F^2 for all data) of 0.0180 and 0.0504, respectively. The final difference Fourier map was featureless. The molecular diagram is drawn with 50% probability ellipsoids.

The solid state structures of $(pzCS_2)_2$ (**L9**), $(3,5\text{-}pzCS_2)_2$ (**L10**), $[Au_{18}S_8(dppe)_6]Cl_2$ (**17b**), [Au(**L7**)(dpph)] (**25**), [Pt(S_2CO)(dppe)] (**27**), and [Pt(**L2**)$_2$] (**32**) were determined in a similar manner such as described above for **15.**

[52] Bruker-AXS. (**2000-2003**) SADABS V.2.05, SAINT V.6.22, SHELXTL V.6.10 & SMART 5.622 Software Reference Manuals. Bruker-AXS, Madison, Wisconsin, USA.

4.4. Results and discussion

4.4.1. Synthesis of ligands and metal complexes

*4.4.1.1. Dithiocarbamate ligands **L5-L8**.*

The N-N- and N-heterocyclic dithiocarbamate ligands were synthesised as potassium salts by introducing a CS_2 group in positions 1 of pyrazole, 3,5-dimethylpyrazole, indazole and imidazole as shown in equation 4.1-4.3. The dithiocarbamate (dtc) salts were isolated as yellow powders in high yields and are readily soluble in water.

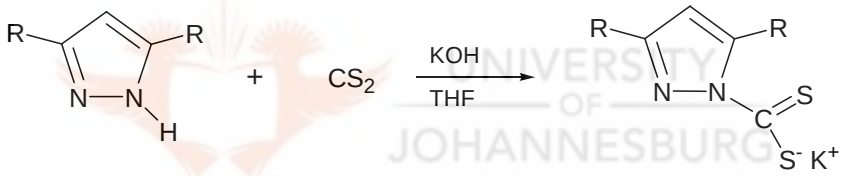

R = H (**L5**), Me (**L6**)

(**4.1**)

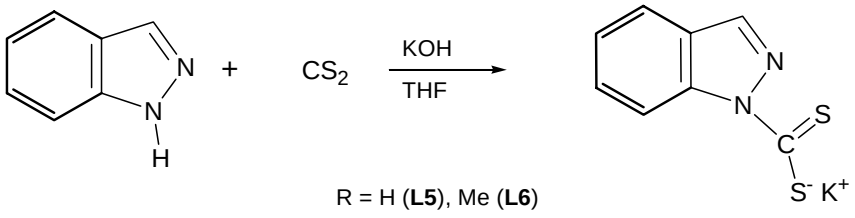

R = H (**L5**), Me (**L6**)

(**4.2**)

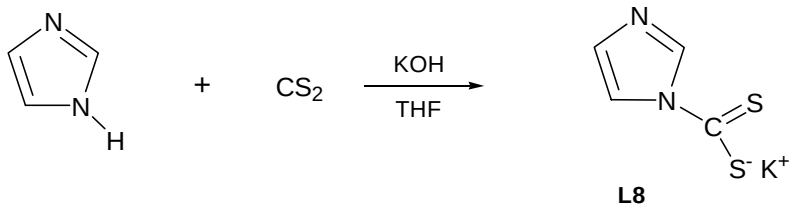

(**4.3**)

The ^{1}H NMR spectrum of **L7** showed peaks at 8.75 ppm (doublet), 7.89 ppm (singlet), 7.49 ppm (doublet), 7.24 ppm (triplet) and 7.01 ppm (triplet), which were assigned to He, Ha, Hb, Hd and Hc protons of the indazole ring, respectively (Fig. 4.11). The ^{13}C{^{1}H} NMR spectrum of **L7** shows the resonance of the diagnostic carbon (C=S) peak at 218.6 ppm. Similar NMR spectral patterns were observed for **L5**, **L6** and **L8**, but with different chemical shifts. Ligands **L5** and **L6** are known and are reported in the literature.[49] The spectroscopic and microanalysis data for **L5** and **L6** reported in this thesis are in agreement with those reported in the literature.

Subsequently, the dtc salts were reacted with [AuCl(PPh$_3$)], [Au$_2$Cl$_2$(dppe)], [Au$_2$Cl$_2$(dppp)], [Au$_2$Cl$_2$(dpph)], [PtCl$_2$(dppe)] or K$_2$[PtCl$_4$] to afford several gold(I) and platinum(II) complexes, respectively. The following sections reports on these new gold(I) and platinum(II) complexes.

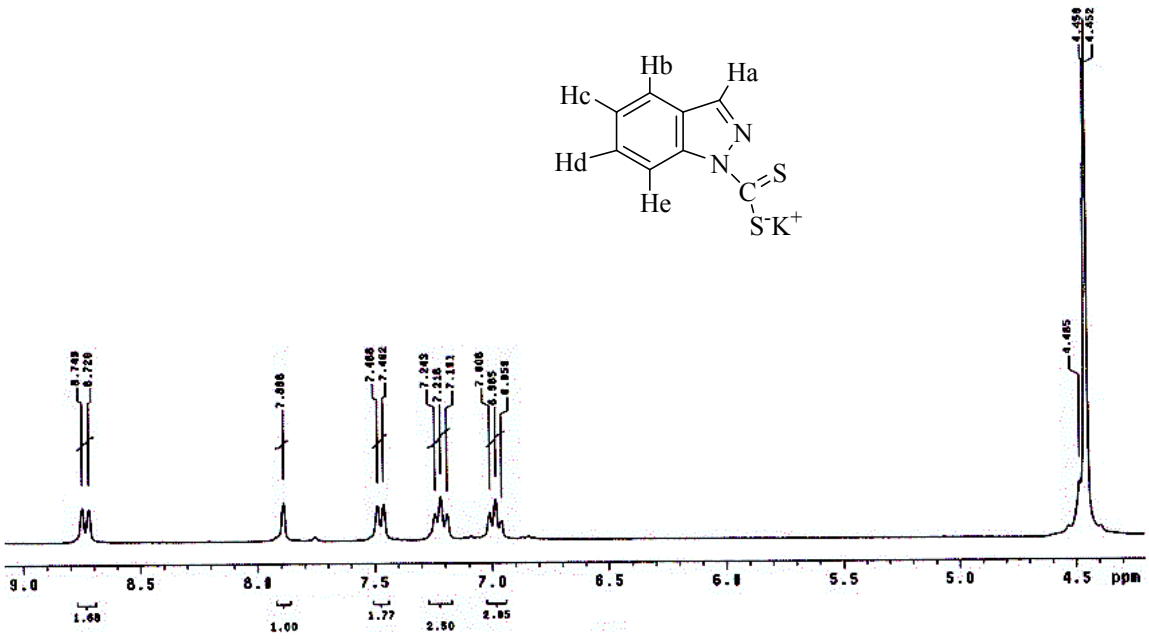

Figure 4.11. ^{1}H NMR spectrum of **L7**.

*4.5.1.2. Monophosphine gold(I) dithiocarbamato complexes **13-16**.*

Gold(I) complexes [Au(**L5**)(PPh_3)] (**13**), [Au(**L6**)(PPh_3)] (**14**), [Au(**L7**)(PPh_3)] (**15**) and [Au(**L8**)(PPh_3)] (**16**) obtained from reaction of [AuCl(PPh_3)] and dtc ligands, were isolated as orange-yellow solids as in Scheme 4.4. The complexes were characterised by a combination of spectroscopic, mass spectrometry, microanalysis, and in the case of complex **15**, X-ray crystallography techniques. For complex **13**, the significant upfield shift observed in the proton peaks of pyrazole indicated complexation. In the ^{1}H NMR spectrum of **13**, the 4-pz and 5-pz proton peaks appeared as singlets at 6.27 and 7.63 ppm, respectively, compared to 6.53 and 8.95 ppm for ligand **L5**. The $^{13}C\{^{1}H\}$ NMR spectrum of complex **13** showed peaks between 128 and 134 ppm, which were assigned to the phenyl carbons of PPh_3 ligand. There was no significant shifts of dithio-carbon (C=S) peak of the dtc ligand upon complexation. For instance, for complex **13**, it resonated at 213.4 ppm compared to that of

L5, which was at 218.6 ppm. Complexes **14**, **15** and **16** displayed similar NMR spectral patterns of downfield shifts, but with different chemical shift values as evident from the spectroscopic data (sec. 4.4.2).

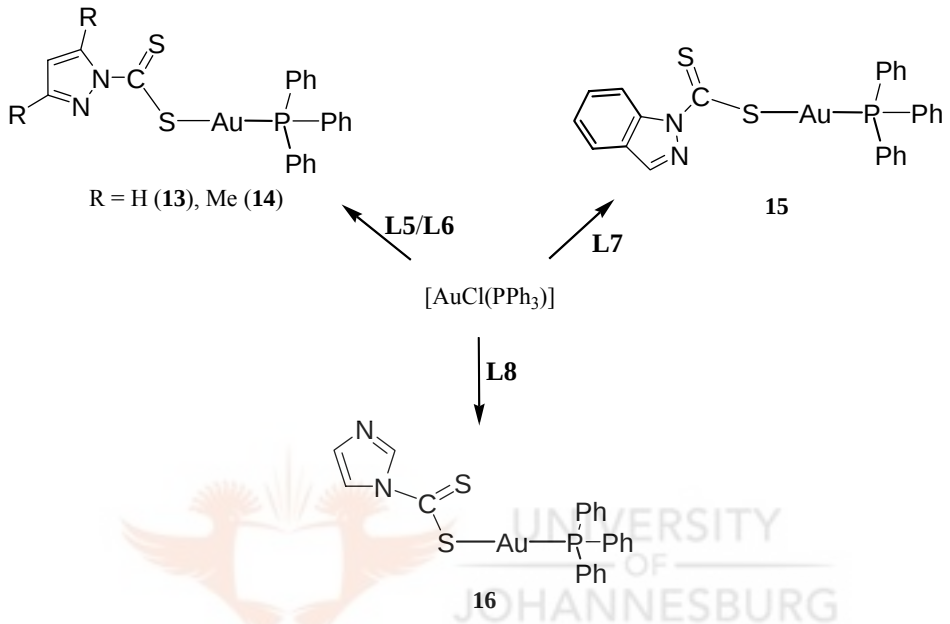

Scheme 4.4. Preparation of monophosphine gold(I) dithiocarbamato complexes **13-16**.

The $^{31}P\{^{1}H\}$ NMR spectra of complexes **13-16** displayed a broad signal in each case, which resonated between 29.9 and 36.3 ppm compared to a sharp peak of the starting material, $[AuCl(PPh_3)]$, at 33.8 ppm. The broad signal was attributed to fluxional behaviour of the complexes in solution that occurred at an intermediate rate on the NMR time scale. It was postulated that there was an interchange in the S atom coordinated to gold atom (eq. 4.4) due to the presence of the CS_2 moiety, which has delocalised electrons along S=C=S. Compounds related to complexes **13-16** include complexes $[AuX(PR_3)]$ (R = $(CF_3C_6H_4)$, $(3,5\text{-}(CF_3)_2C_6H_3)$; X = Cl, 1-thiophenolate (SPh), 1-thiopyridine (Spy)) reported by Nunokawa

and co-workers,[53] and [Au(2-mpa)(PPh_3)] (2-mpa = 2-mercaptopropionate)[54] where they exhibit pseudo linear geometries along P-Au-S bond. The geometry of complexes **13-16** was further established by solid state structure analysis of complex **15**.

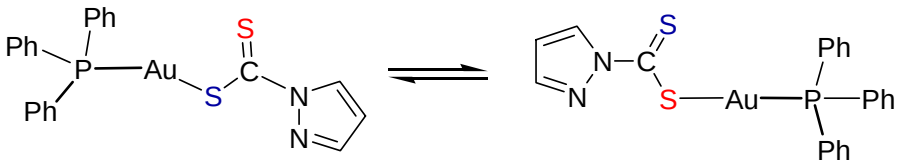

(**4.4**)

*4.4.1.3. Molecular structure of [Au(**L7**)(PPh_3)] (**15**).*

Orange crystals of complex **15** suitable for single-crystal X-ray analysis were obtained from a dichloromethane-hexane mixture. The molecular structure of the crystal is shown in Figure 4.12. The bond lengths Au(1)-S(1) = 2.3272(6), Au(1)-P(1) = 2.2533(6), and N(1)-C(1) = 1.399(3) Å are typical for linear phoshine gold-thiolate complexes.[36,37,55] The Au(I) centre has approximately linear P-Au-S geometry such that the P(1)-Au(1)-S(1) angle = 175.36(2)^o with a maximum deviation from linearity of 4.64^o. The S(1)-C(1) bond distance of 1.732(3) Å is substantially and statistically longer than 1.663(3) Å of S(2)-C(1) which has more double bond character (C=S). The ligand and the Au atom lies out of the plane as manifested in the torsional angle of -165.30(17)^o for Au(1)-S(1)-C(1)-N(1). The crystal structure determination of closely related complexes, e.g. [Au(PPh_3)(2-mba)] (2-mba = 2-

[53] Nunokawa K., Onaka S., Tatematsu T., Ito M., Sakai J., *Inorg. Chim. Acta*, **2001**, *322*, 56.
[54] Nomiya K., Yamamoto S., Noguchi R., Yokoyama H., Kasuga N. C., Ohyama K., Kato C., *J. Inorg. Biochem.*, **2003**, *95*, 208.

mercaptobenzoic acid) has been reported by de Vos *et al*. and the bond lengths and distances of **15** correspond to their reported data (Au-P(1) = 2.258(1) Å, Au-S(1) = 2.297(2) Å and P(1)-Au-S(2) = 177.9(1)^{o}). A molecular packing diagram of **15** viewed along the *c* axis is shown in Figure 4.13. It displays the formation of cage-like cuboids defined by repetitive P-Au-S motifs and the axial phenyl rings of the phosphine ligand. The packing is also enhanced by the π-π interactions between the indazolyl unit and the phenyl groups of the phosphine. The selected bond distances and angles with their estimated standard deviations are listed in Table 4.1. Crystal data, together with the data collection and refinement parameters are presented in Table 4.2.

Table 4.1. Selected bond lengths [Å] and angles [°] for **15**

Bond lengths (Å)		*Bond angles (°)*	
Au(1)-P(1)	2.2533(6)	P(1)-Au(1)-S(1)	175.36(2)
Au(1)-S(1)	2.3272(6)	C(1)-S(1)-Au(1)	100.04(9)
P(1)-C(9)	1.811(2)	C(9)-P(1)-Au(1)	118.20(8)
N(1)-C(1)	1.399(3)	S(2)-C(1)-S(1)	124.85(15)
S(1)-C(1)	1.732(3)		
S(2)-C(1)	1.663(3)		

[55] [a]Hunks J. W., Jennings C. M., Puddephatt R. J., *Inorg. Chim. Acta,* **2006**, *359*, 3605; [b]Li C. K., Lu X. X., Wong K. M. C., Chan C. L., Zhu N. Y., Yam V. W. W., *Inorg. Chem*., **2004**, *43*, 7421; [c]Balasubramanian R., Guo R., Mills A. J., Murray R. W., *J. Am. Chem. Soc*., **2005**, 127, 8126.

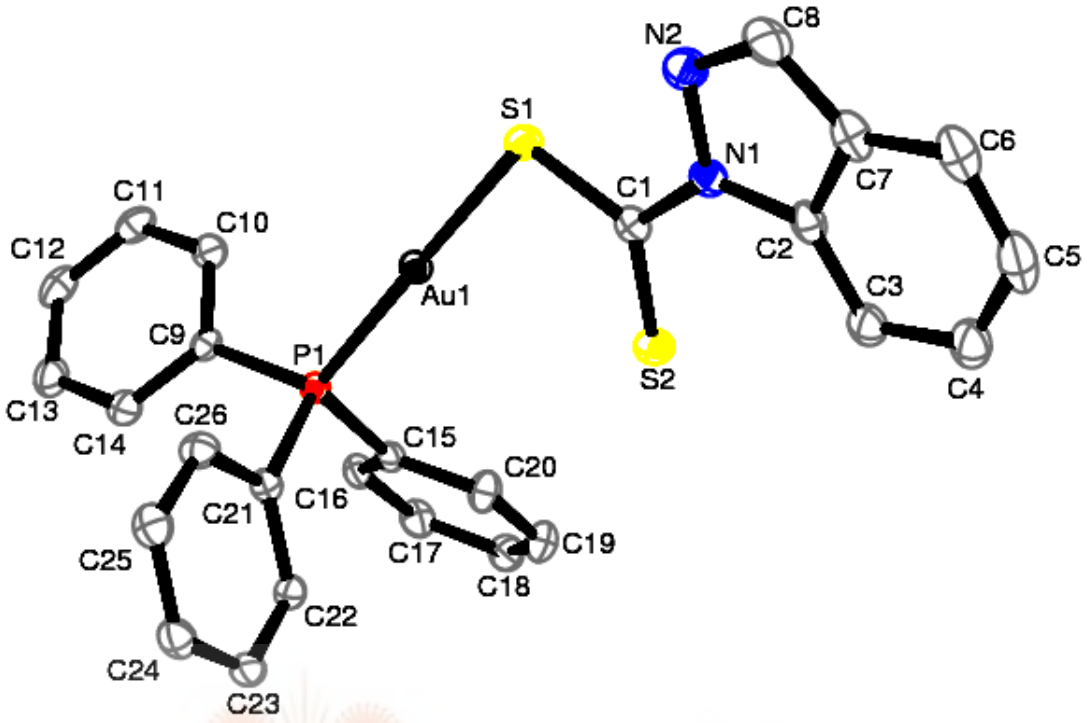

Figure 4.12. A molecular drawing of **15** drawn with 50% probability ellipsoids. H atoms omitted for clarity.

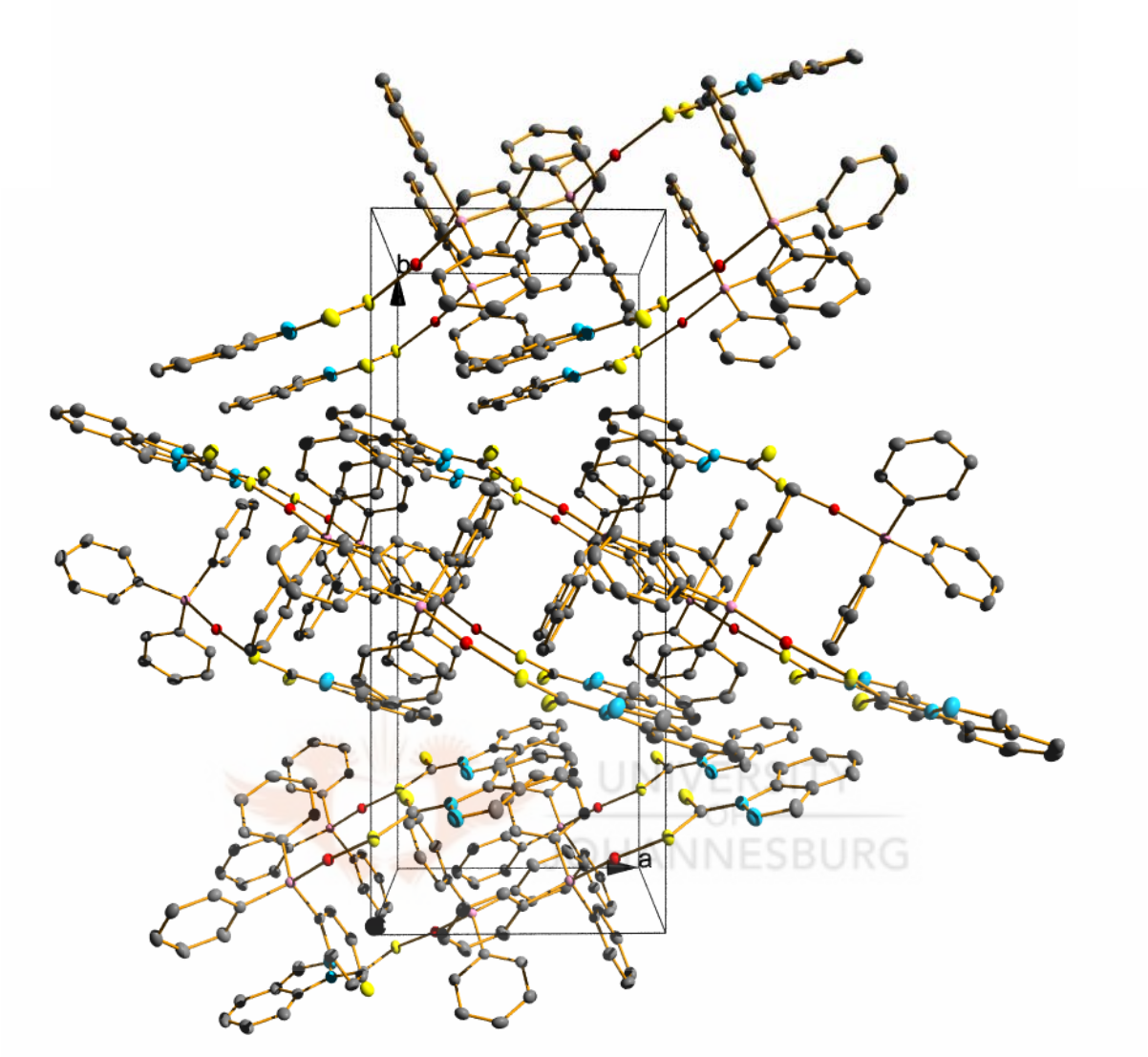

Figure 4.13. A molecular packing diagram of **15** viewed along the *c* axis**.** The hydrogen atoms omitted for clarity.

Table 4.2. Crystal data, data collection and refinement parameters of **15**

Parameter	**15**
Empirical formula	$C_{26}H_{20}AuN_2PS_2$
Formula weight	652.50
Temperature (K)	100(2)
Wavelength (Å)	0.71073
Crystal system	Monoclinic
Space group	$P2_1/n$
Unit cell dimensions	
a(Å)	9.1382(12)
b(Å)	22.487(3) Å
c(Å)	11.3760(14)
α	90°
β	91.541(2)°
γ	90°
Volume ($Å^{3)}$	2336.8(5)
Z	4
Density (calculated) (Mg/m^3)	1.855
Absorption coefficient (mm^{-1})	6.560
F(000)	1264
Final R indices (R1)	0.0587
Reflections collected	36929
Completeness to theta	99.3 %
Goodness of fit on F^2	1.188
Largest diff. peak & hole ($e.Å^{-3}$)	1.146 and -0.880

*4.4.1.4. Diphosphine gold(I) dithiocarbamato complexes **17a-19**.*

The preparation of diphosphine gold(I) complexes of **L5-L7** was pursued by employing bis(diphenylphosphino)alkanes. Binuclear gold(I) complexes $[Au_2(\mathbf{L5})_2(dppe)]$ (**17a**), $[Au_2(\mathbf{L6})_2(dppe)]$ (**18**) and $[Au_2(\mathbf{L7})_2(dppe)]$ (**19**) (dppe = bis(diphenylphosphino)ethane) were prepared by reacting $[Au_2Cl_2(dppe)]$ with two molar equivalents of the corresponding dithiocarbamates (Scheme 4.5).

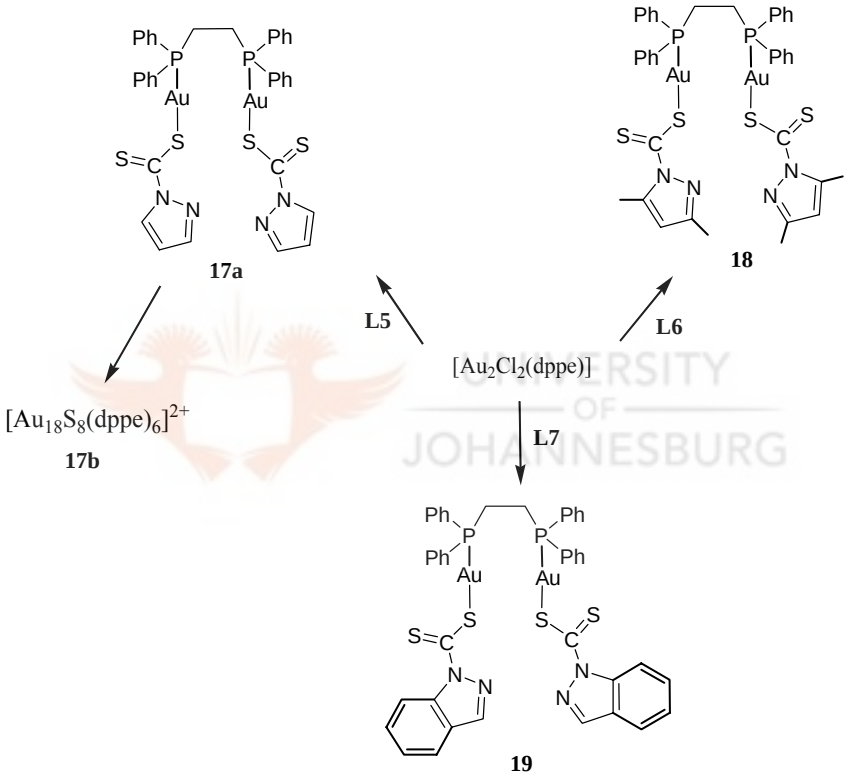

Scheme 4.5. Preparations of diphosphine gold(I) dithiocarbamato complexes **17a-19**.

Complexes **17a-19** were isolated as sticky orange materials and were readily soluble in chlorinated solvents. The ^{1}H NMR spectra displayed signals that corresponded to the protons of the diphosphine ligand plus those of the dithiocarbamates. There were no significant shifts in the NMR signals of the phenyl protons of dppe in complexes **17a-19** compared to those of

the starting material [Au_2Cl_2(dppe)]; but there was slight chemical shifts in the NMR peaks of the ethylene linker protons indicating formation of the desired products. For instance, in the ^{1}H NMR spectrum of **17a** (Fig. 4.14), the CH_2 protons in the diphosphine backbone appeared downfield as a broad singlet at 2.87 ppm compared to that of [Au_2Cl_2(dppe)] (2.76 ppm). The CH_2 protons of the dppe ligand appeared as a broad singlet probably due to unresolved ^{31}P-^{1}H coupling. The 5-pz protons (5H, 5H′) of the pyrazolyl ring in **17a** appeared as a doublet at 8.78 ppm, while the 3-pz protons (3H, 3H′) peak were masked by the phenyl protons of the dppe ligand (7.80 ppm). This is in contrast to that of **L5** where 3-pz and 5-pz protons appeared at 6.27 and 7.63, respectively.

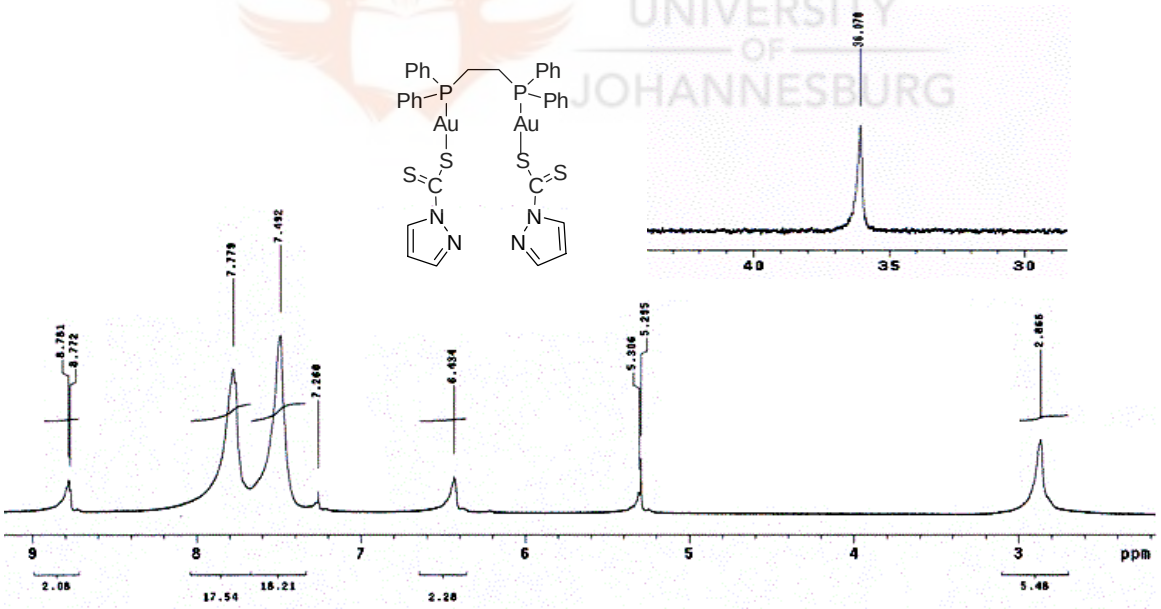

Figure 4.14. The ^{1}H NMR spectrum of **17a** ($CDCl_3$), with the ^{31}P{^{1}H} NMR spectrum of **17a** as inset.

As mentioned for complexes **13-16**, the ^{31}P{^{1}H} NMR spectrum of complex **17a** (inset, Fig. 4.14) showed one relatively broad singlet at 36.1 ppm, which is characteristic of compounds

with P-Au-S motif.[55a,56,57] Similar broad peaks were observed in the spectra of complexes **18** and **19** at 35.7 and 34.9 ppm, respectively. Complexes **17a-19** are comparable to diphosphine digold(I)-pyridine-2-thiolate complexes, $[(AuSN)_2(dppm)]$ and $[(AuSN)_2(dpph)]$ (HNS = pyridine-2-thiolate), reported by Tseng *et al*. that show ^{31}P NMR peaks in the range 32.7-35.9 ppm.

*4.4.1.5. Molecular structure of $[Au_{18}S_8(dppe)_6]2Cl$ (**17b**).*

Interestingly, attempts to crystallise complex **17a** in a dichloromethane/diethylether solution led to the isolation of the cationic gold(I) cluster, $[Au_{18}S_8(dppe)_6]^{2+}$ (**17b**) (Fig. 4.15 and 4.16) as confirmed by X-ray crystallography and microanalysis. The formation of complex **17b** is unique in the sense that, there are no reports on the use of dithiocarbamates to make gold(I) clusters. It appears that there is a similarity between dtc (RCS_2^-) and $Se(SiMe_3)_2$,[58] used by Fenske and co-workers, in that they both act as sources of S atoms.

The solid state structure of complex **17b** is shown in Figure 4.15 while its skeletal (Au, P, S) geometry is shown in Figure 4.16. The molecular structure has 18 gold atoms, 8 sulfur atoms and 6 dppe units. The counterions that should account for the +2 positive charge of the Au cluster could not be found in the difference map. The complex is isomorphous with the Se analogue reported by Fenske and co-workers[58] and therefore two chloride ions were assumed to be the anions. This is strongly supported by the macroanalysis data obtained. There were several partially occupied molecules of some solvent also present in the asymmetric unit.

[56] Chen J., Mohamed A. A., Abdou H. E., Krause Bauer J. A., Fackler J. P., Bruce A. E., Bruce M. R. M., *Chem. Commun*., **2005**, 1575.
[57] Tzeng B.-C., Liao J.-H., Lee G.-H., Peng S.-M., *Inorg. Chim. Acta*, **2004**, *357*, 1405.

Bond length restraints were applied to model the molecules but the resulting isotropic displacement coefficients suggested the molecules were mobile. Option SQUEEZE of program PLATON[59] was used to correct the diffraction data for diffuse scattering effects and to identify the solvate molecule. PLATON calculated the upper limit of volume that can be occupied by the solvent to be 3394 $Å^3$, or 19% of the unit cell volume. The program calculated 3364 electrons in the unit cell for the diffuse species, or 841 electrons in the asymmetric unit. This approximately corresponded to two chloride ions (36 electrons) and eight molecules of $CHCl_3$ (464 electrons) and eight molecules of CH_2Cl_2 (336 electrons) for a total of 836 electrons. It should be however noted that all derived results are based on the known contents with the exception of the chloride anions that were included in the formula. This data was corroborated by the microanalysis data obtained.

The structure of **17b** exhibits pseudo-threefold axis that runs through sulfur atoms S1 and S2. The S1, S2 and other sulfur atoms at the periphery act as μ_3 bridges between gold atoms, with each peripheral sulfur atoms displaying three short Au-S bonds (2.328(4)-2.374(3) Å). The Au···Au distances involving the central gold atom fall in the range of 2.9263(7)-3.1395(7) Å, which is indicative of a d^{10}-d^{10} closed shell metal interactions. Four different surroundings are observed for gold atoms in **17b**, *viz*. (i) sulfur bridged non-bonded Au···Au interactions; (ii) Au-Au non-bridged single bonds; (iii) Au···Au sulfur bridged single bonds; and (iv) Au···Au phosphine bridged single bonds. Similar to the $[Au_{18}Se_8(dppe)_6]^{2+}$ reported by Fenske, complex **17b** has two $[Au_9S_4(dppe)_3]^{2+}$ fragments that are interlocked in such a manner that a distorted Au_6S_2 heterocubane arrangement (Au(1)-Au(6), S(1), S(2)) arises in

[58] Fenske D., Langetepe T., Kappes M. M., Hampe O., Weis P., *Angew. Chem. Int. Ed*. **2000**, *39*, 1857.

the centre of the complex. Cluster **17b** features bond angles, S(2)-Au(1)-S(3) = 175.80(12)° and S(2)-Au(1)-Au(2) = 92.05(8)°. The other bond distances and angles are similar to those reported in literature.[56,60a,b] The selected bond distances and angles with their estimated standard deviations are listed in Table 4.3. Crystal data, together with the data collection and refinement parameters are presented in Table 4.4.

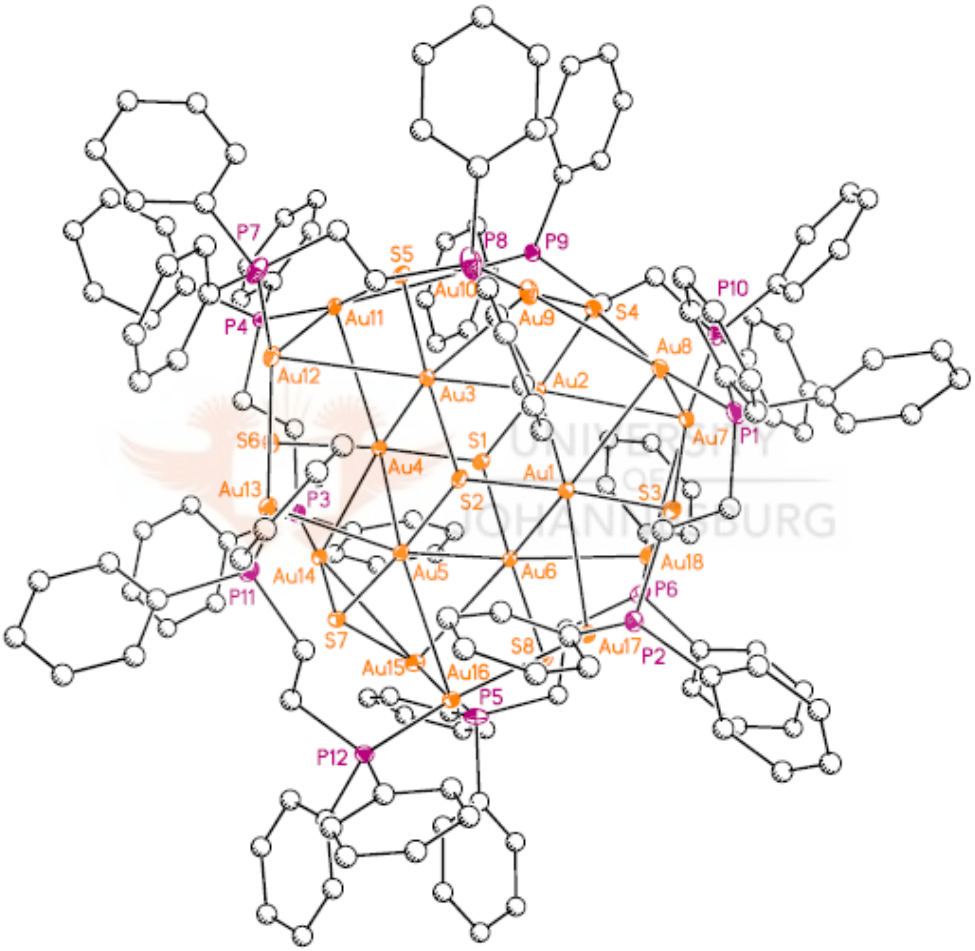

Figure 4.15. The molecular diagram of **17b** drawn with 30% probability ellipsoids. The hydrogen atoms omitted for clarity.

[59] Spek A. L., *Acta Cryst. Sect*. A., **1990**, *A46*, C34.
[60] [a]Canales F., Gimeno M. C., Jones P. G., Laguna A., *Angew. Chem*., **1994**, *106*, 811; [b]Huang S. P., Kanatzidis M. G., *Angew. Chem. Int. Ed*., **1992**, *31*, 787.

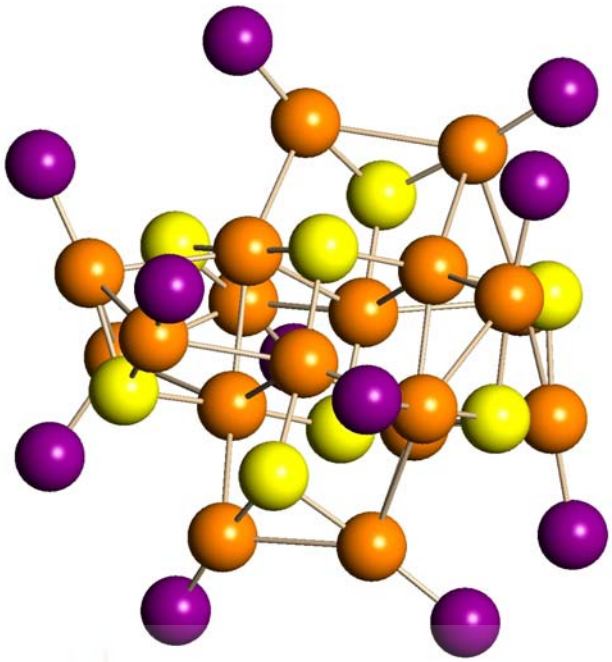

Figure 4.16. The skeletal (Au, P, S) geometry of **17b**.

Table 4.3. Selected bond lengths [Å] and angles [°] of **17b**

Bond lengths (Å)		*Bond angles (°)*	
Au(1)-S(2)	2.343(3)	S(2)-Au(1)-S(3)	175.80(12)
Au(1)-S(3)	2.368(4)	Au(10)-Au(2)-Au(3)	77.409(18)
Au(1)-Au(2)	2.9263(7)	S(2)-Au(1)-Au(2)	92.05(8)
Au(1)-Au(17)	2.9452(7)	S(1)-Au(2)-Au(7)	109.71(8)
Au(2)-Au(7)	3.1395(7)	P(8)-Au(9)-S(4)	172.85(14)
Au(7)-P(10)	2.268(4)		

Table 4.4. Crystal data, data collection and refinement parameters of **17b**

Parameter	**17b**
Empirical formula	$C_{156}H_{144}Au_{18}Cl_2P_{12}S_8$.x solvents
Formula weight	6263.13
Temperature (K)	105(2)
Wavelength (Å)	0.71073
Crystal system	Monoclinic
Space group	$P2_1/n$
Unit cell dimensions	
a(Å)	17.6854(7)
b(Å)	34.4361(14)
c(Å)	29.1894(12)
α	90°
β	92.4570(10)°
γ	90°
Volume ($Å^{3)}$	17760.5(12)
Z	4
Density (calculated) (Mg/m^3)	2.342
Absorption coefficient (mm^{-1})	15.077
F(000)	11376
Final R indices (R1)	0.0473
Reflections collected	188093
Completeness to theta	99.8 %
Goodness of fit on F^2	1.019
Largest diff. peak & hole ($e.Å^{-3}$)	2.135 and -1.443

The ease of dtcs formation and their wide ranging coordination chemistry has led to the formation of an array of novel and complex supramolecular architectures.[4] For gold compounds, the process of supramolecular formation seems to be assisted by aurophilicity. Aurophilicity is the weak gold-gold interactions observed in gold compounds.[61] Theoretical calculations by Pyykko *et al*. show that aurophilicity is amplified by electron correlation effect (electron interactions in a quantum system) and relativistic effects, which leads to length contraction between gold atoms. Furthermore, aurophilicity is augmented by soft ligands, e.g. sulfur, where thiolates compounds of general formula $[AuX(PPh_3)]$ (X = RS) display great aurophilic effects.[62] In addition, the observed aurophilicity is enhanced by use of diphosphines, such as in $[(Au\text{-}SPh)_2(\mu\text{-}trans\text{-dpen})]$ (*trans*-dpen = *trans*-1,2-bis(diphenylphosphino)ethylene).[63] It is therefore clear that due to close proximity of the P atoms in the dppe backbone, this property of aurophilicity coupled with the ease of cleavage of C-N bond in the dithiocarbamate in complex **17a**, expedited the process of self-assembly. It is believed that complex **17b** is the first (dppe)-gold(I) dithiocarbamate-generated complex of high nuclearity that incorporates a range of intramolecular Au···Au interactions.

*4.4.1.6. Diphosphine gold(I) dithiocarbamato complexes **20-25**.*

In order to further establish the phenomenon of cluster formation, the linker spanning between the two phosphine atoms were increased to $(CH_2)_3$ (dppp) and $(CH_2)_6$ (dpph). Complexes $[Au_2(\mathbf{L5})_2(dppp)]$ (**20**), $[Au_2(\mathbf{L6})_2(dppp)]$ (**21**), $[Au_2(\mathbf{L7})_2(dppp)]$ (**22**)

[61] Pyykkö P., Zhao Y., *Angew. Chem., Int. Ed. Engl*., **1991**, *30*, 604.
[62] Pyykkö P., Li J., Runeberg N., *Chem. Phys. Lett*., **1994**, *218*, 133.
[63] [a]Onaka S., Katsukawa Y., Shiotsuka M., Kanegawa O., Yamashita M., *Inorg. Chim. Acta*, **2001**, *312*, 100;

[Au_2(**L5**)$_2$(dpph)] (**23**), [Au_2(**L6**)$_2$(dpph)] (**24**), and [Au_2(**L7**)$_2$(dpph)] (**25**) were synthesised in the same manner as for complexes **17a-19** by reacting [Au_2Cl_2(dppp)] or [Au_2Cl_2(dpph)] with two molar equivalents of **L5, L6** and **L7**, respectively (Scheme 4.6). In the ^{1}H NMR spectra of **20-22** in $CDCl_3$, the CH_2 protons of the diphosphine ligand appeared upfield (1.88-2.93 ppm) as second order multiplets. The $^{13}C\{^1H\}$ NMR spectra of **20-22** showed peaks at *ca*. 215 and *ca*. 129.2-133.5 ppm, which were assigned to C(C=S) and the phenyl carbons, respectively. Moreover, the $^{13}C\{^1H\}$ NMR spectra of **20-22** displayed ^{31}P-^{13}C coupling, with J_{P-C} values between 58.4-64.2 Hz, due to P-CH_2. The $^{31}P\{^1H\}$ NMR spectrum of **22** showed one broad singlet at 29.2 ppm compared to that of the starting material, [Au_2Cl_2(dppp)], which resonated at 27.6 ppm signifying complexation. Broad phosphorous peaks were also observed for **20** and **21** at 32.8 ppm and 29.2 ppm, respectively.

Compounds **23-25** displayed similar NMR spectral patterns as those of **20-22**, with no significant shifts of the proton peaks in comparison to those of the starting materials ([(AuCl)$_2$(dpph)], **L5**, **L6** and **L7**). The only difference is that complexes **23-25** did not exhibit ^{31}P-^{13}C coupling observed for **20-22**. The $^{31}P\{^1H\}$ NMR spectra of **23-25** showed broad singlet peaks around 32 ppm. The general broadness of the ^{31}P NMR peaks for compounds **20-25** suggests fluxional behaviour of the complexes in solution.

---

[b]Pintado-Alba A., de la Riva H., Nieuwhuyzen M., Bautista D., Raithby P. R., Sparkes H. A., Teat S. J., López-de-Luzuriaga J. M., Lagunas M. C., *Dalton Trans*., **2004**, 3459.

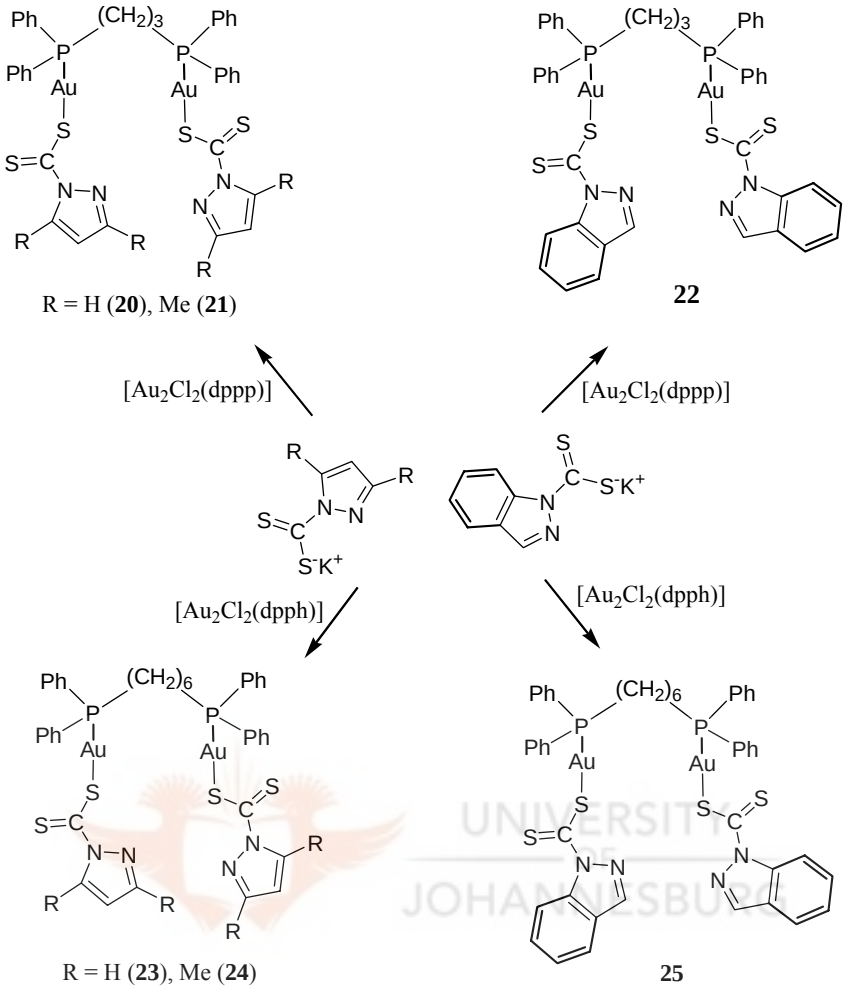

Scheme 4.6. Preparations of diphosphine gold(I) complexes **20**-**25**.

*4.4.1.7. Molecular structure of [Au$_2$(**L7**)$_2$(dpph)] (**25**).*

All the spectroscopic and microanalysis showed that complexes **20**-**25** were gold(I) binuclear complexes. This evidence was corroborated by the solid state structure obtained for **25** (Fig. 4.17). Orange crystals suitable for single-crystal X-ray analysis were obtained from a saturated dichloromethane solution of **25**. The bond lengths Au(1)-S(1) = 2.312(3), Au(1)-P(1) = 2.255(2), and N(1)-C(8) = 1.390(8) Å are typical for linear phosphine gold-thiolate complexes.[36,57] The gold dinuclear compound feature approximately linear gold atom

geometries defined by a P-Au-S angle of 173.4(6)^{o}. The S(2)-C(1) bond distance (1.656(6) Å) was considerably shorter than S(1)-C(1) (1.720(7) Å), which has a double bond character. The torsional angle of -15.7(4) ^{o} for Au(1)-S(1)-C(1)-S(2) signified that the gold atoms and the dithiocarbamate ligands lie out of the plane defined by the phosphine ligand. There are no intramolecular or intermolecular Au···Au interaction, probably because of the hexylene linker ($(CH_2)_6$) between the two P atoms keeping the gold atoms far apart. The bond angles and distances the complex **25** are similar to those reported in literature (P-Au-S ≈ 177^{o}, Au-P = 2.25 Å, Au-S = 2.3 Å)[64,65] and is similar to [dpph$(AuSSNH_2)_2$] ($NaSSNH_2$ = sodium-2-amino-5-mercapto-1,3,4-thiadiazolate) reported by Tzeng *et al*. The molecular packing diagram of **25** viewed along the *c* axis is shown in Figure 4.18. The packing of the complex appears to be governed by the stacking of phenyl groups of the neighbouring molecules with a combination of π- π contributions of the phenyl rings. At the centre of the unit cell, there is formation of a hollow cavity defined by two wedged-shapes conjoined with a quasi-circular one at the centre. The packing displays a dendrimer-like supramolecular spreading outwards (Fig. 4.18). The selected bond distances and angles with their estimated standard deviations are listed in Table 4.5. Crystal data, together with the data collection and refinement parameters are presented in Table 4.6.

[64] Tzeng B.-C., Huang Y.-C., Wu W.-M., Lee S. –Y., Lee G..-H., Peng S.-M., *Crystal Growth & Design*, **2004**, *4*,3457.
[65] Cookson P. D., Tiekink E. R. T., *J. Chem. Soc., Dalton Trans*., **1993**, 259.

Table 4.5. Selected bond lengths [Å] and angles [°] for **25**

Lengths (Å)		*Angles(°)*	
Au(1)-P(1)	2.255(2)	P(1)-Au(1)-S(1)	173.41(6)
Au(1)-S(1)	2.312(3)	C(1)-S(1)-Au(1)	100.9(2)
P(1)-C(9)	1.818(6)	C(15)-P(1)-Au(1)	112.6(8)
N(1)-C(8)	1.390(8)	S(2)-C(1)-S(1)	124.1(4)
S(1)-C(1)	1.720(7)		
S(2)-C(1)	1.656(6)		

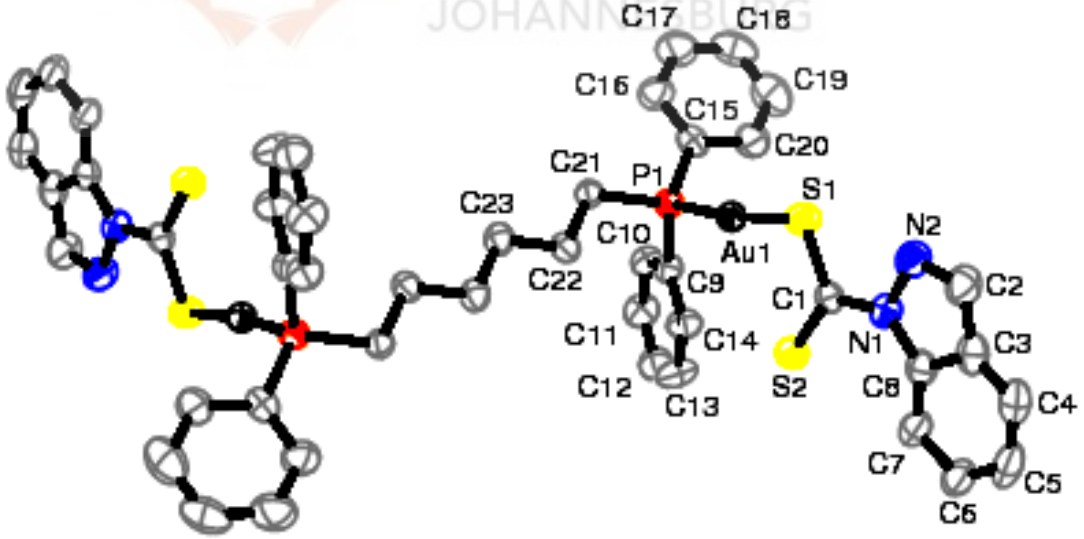

Figure 4.17. A molecular drawing of **25** drawn with 50% probability ellipsoids. The hydrogen atoms are omitted for clarity.

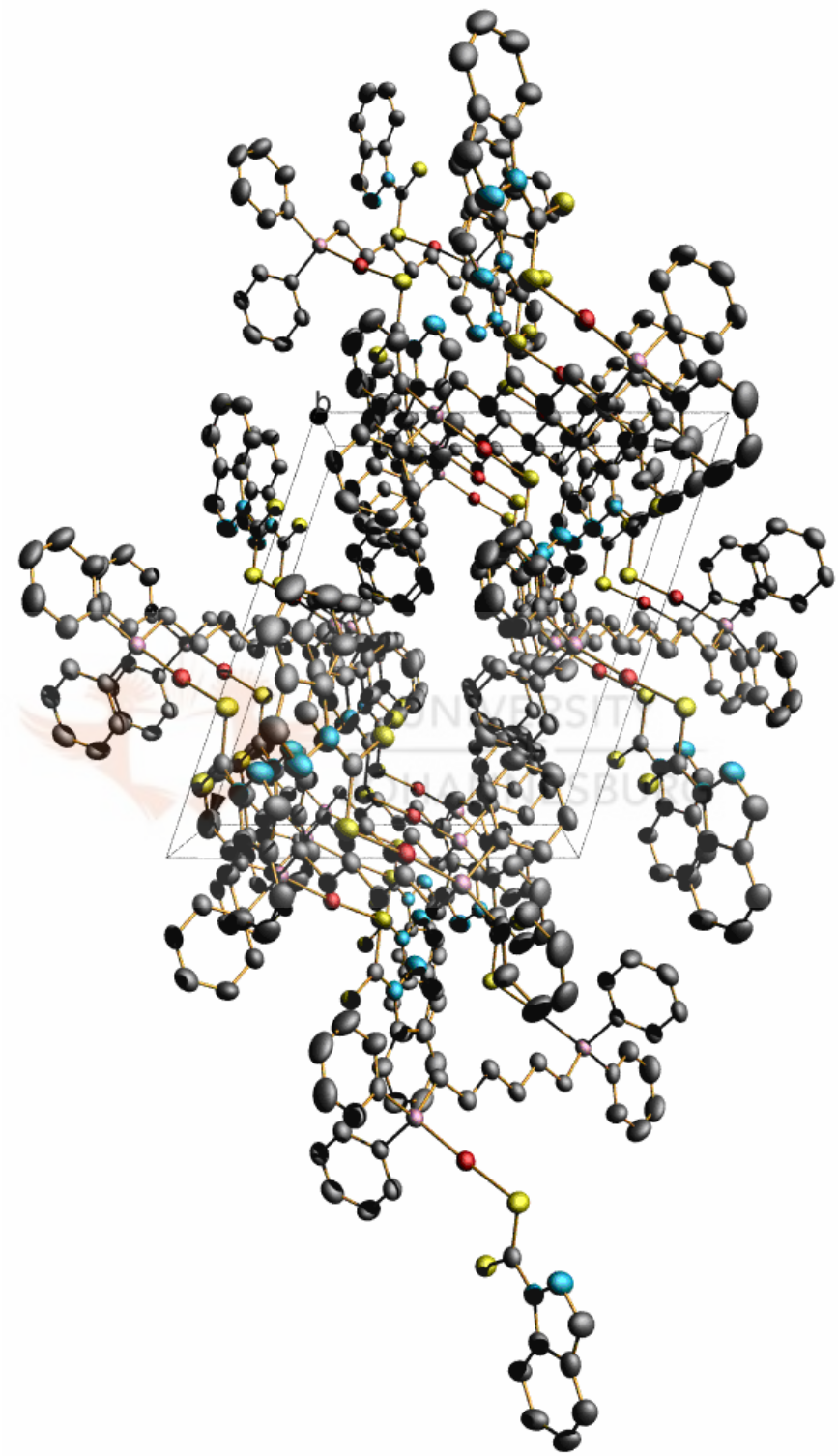

Figure 4.18. A molecular packing diagram of **25** viewed along the *c* axis, which forms a hollow cubane in the centre. The hydrogen atoms omitted for clarity.

Table 4.6. Crystal data, data collection and refinement parameters of **25**

Parameter	**25**
Empirical formula	$C_{46}H_{42}Au_2N_4P_2S_4$
Formula weight	1234.95
Temperature (K)	150(2)
Wavelength (Å)	0.77490
Crystal system	Monoclinic
Space group	$P2_1/n$
Unit cell dimensions	
a(Å)	13.499(11)
b(Å)	11.560(19)
c(Å)	15.396(15)
α	90°
β	108.60(6)°
γ	90°
Volume ($Å^{3)}$	2277(5)
Z	2
Density (calculated) (Mg/m^3)	1.801
Absorption coefficient (mm^{-1})	8.334
F(000)	1196
Final R indices (R1)	
	0.0404
Reflections collected	31033
Completeness to theta	99.2 %
Goodness of fit on F^2	1.021
Largest diff. peak & hole ($e.Å^{-3}$)	1.454 and -0.856

From the solid state structure obtained for complex **25**, it is clear that the length of the linker of the diphosphine ligand plays a crucial role in the formation of cluster compounds previously observed for complex **17b**. The X-ray structure obtained for **25,** which is a dpph derivative**,** indicates a binuclear gold(I) complex. As the length of the CH_2 linker increases, the two gold centres are kept far apart, hence the Au···Au interaction present in **17a**, which contributed in formation of **17b**, was absent in complexes **23-25**. Thus, rearrangement to obtain cluster was not observed for **25** or its analogues. Similarly, complexes **20-22,** which have a propane linker between the phosphine atoms, showed no cluster formation either. Time of flight ESI-MS data typified by the spectrum of complex **22** (Fig. 4.19) showed molecular ions corresponding to a binuclear complex. The molecular ion peak is at m/z 1190.88 (Fig. 4.19). However, the fragmentation pattern of **22** seemed complicated and thus could not be accounted for. Probably this is due to fast disintegration of the complex during mass spectrum analysis.

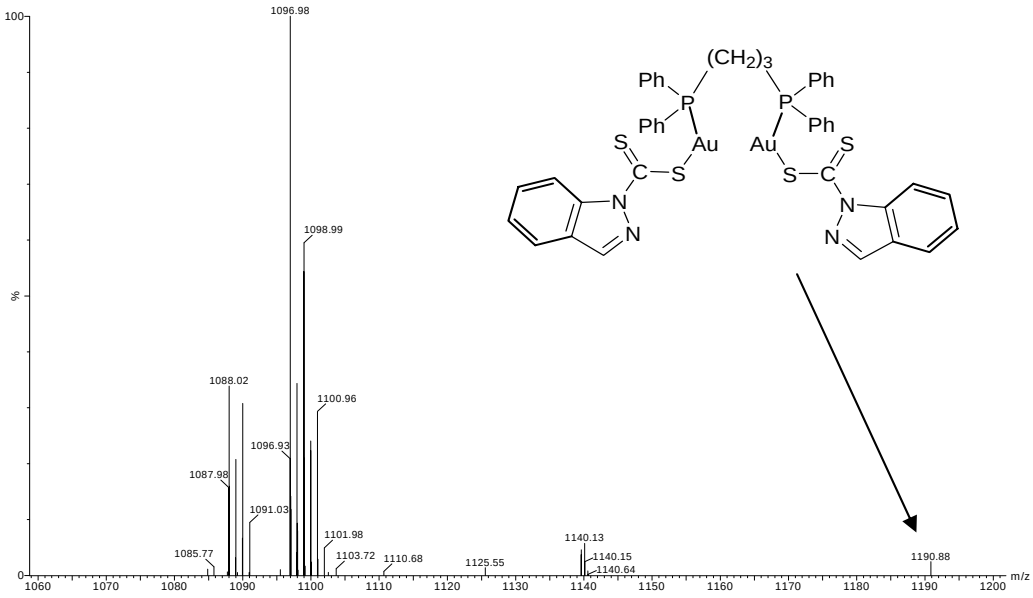

Figure 4.19. Time of flight ESI-MS spectrum of **22**.

*4.4.1.8. Diphosphine platinum(II) dithiocarbamato complexes **26**, **28** and **29**.*

Phosphine platinum(II) dithiocarbamate complexes related to gold(I) complexes discussed above, were also prepared. Reactions of ligands **L5-L7** with $[PtCl_2(dppe)]$ in dichloromethane/water mixture, gave complexes $[Pt(\mathbf{L5})_2(dppe)]$ (**26**), $[Pt(\mathbf{L6})_2(dppe)]$ (**28**) and $[Pt(\mathbf{L7})_2(dppe)]$ (**29**). However, in dichloromethane or chloroform solutions, these yellow complexes underwent facile transformation to green complexes at room temperature (Scheme 4.7). One possible reason for lack of stereochemical rigidity observed in solution is the thermal motion of the atoms in the ligands.[66] These could have been accelerated by rotation of the pyrazole rings, which would then force the diphosphine ligand to rearrange in order to minimise steric repulsions due to the bulky phenyl substituents. Nevertheless, initial ^1H and $^{31}P\{^1H\}$ NMR spectroscopic data acquired immediately upon isolation (yellow solution), indicate formation of the desired products which undergo changes in solution over time to give an identical green product, $[Pt(S_2CO)(dppe)]$ (**27**) (Scheme 4.7). The $^{31}P\{^1H\}$ NMR spectra of **26**, **28** and **29** showed only a single resonance, $J_{Pt\text{-}P}$, around 3800 Hz indicating *trans*-disposition geometries.

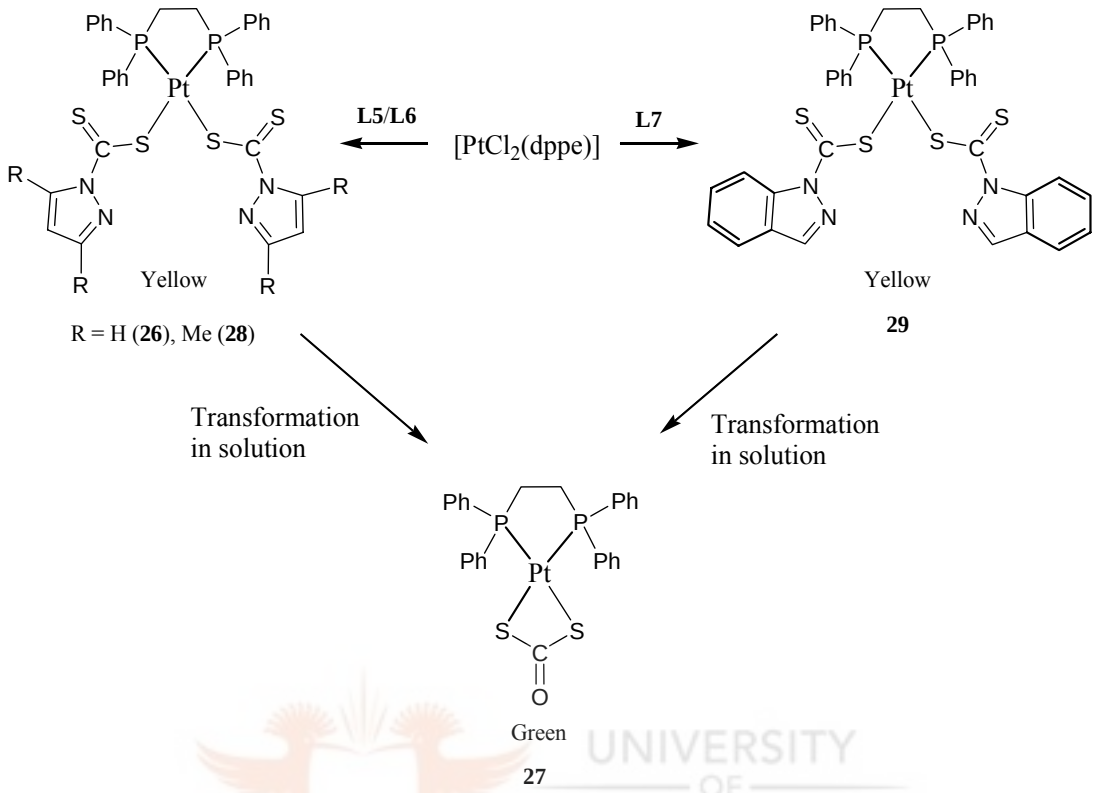

Scheme 4.7. A representation of the proposed mechanism for transformation of complexes **26**, **28** and **29** to identical product **27** in dichloromethane solution.

Structural investigation confirms that the complexes **26**, **28** and **29** were transformed from [Pt(**L**)$_2$(dppe)] (L = **L5**, **L6** and **L7**) to identical [Pt(S_2CO)(dppe)] (**27**) (Scheme 4.7, Fig. 4.21). Tenorio *et al.*[66] reported on a similar occurrence involving nickel-dialkyldithiocarbonate complexes. The IR spectrum of **26** exhibited a band at 1609 cm^{-1} (Fig. 4.20), which was attributed to the stretching frequency of C=N bonds. However, upon transformation (Scheme 4.7), the C=N motifs were lost and the emergence of C=O observed. This was evident in the IR spectrum of **27** (Fig. 4.20), with the C=O band at 1680 cm^{-1}, which is consistent with a bidentate chelating coordination mode of the dithiocarbamate unit

[66] Tenorio M. J., Puerta M. C., Valerga P., *J. Chem. Soc., Dalton Trans*., **1996**, 1935.

(Fig. 4.20).[67] The IR spectra of complexes **28** and **29** display similar pattern as that of complex **26**, with the stretching frequencies of C=N motifs at 1591 and 1634 cm^{-1}, respectively. Likewise to complex **26**, upon transformation, IR spectra of complexes **28** and **29** show the presence of identical C=O band at 1680 cm^{-1}.

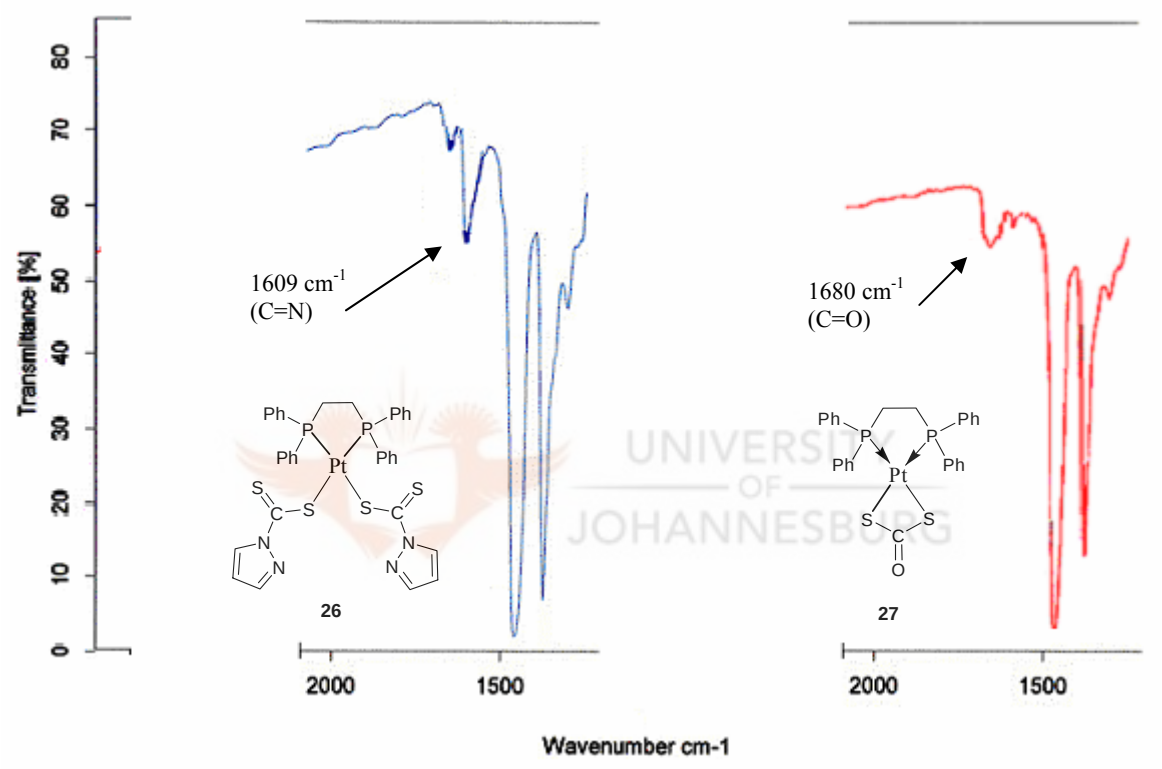

Figure 4.20. IR spectra of **26** and **27** depicting the stretching frequencies of υ(C=N) band (1609 cm^{-1}) in **26** and υ(C=O) band (1680 cm^{-1}) in **27**.

[67] Ruiz J., Rodriguez V., Vicente C., Perez J., Lopez G., Chaloner P. A., Hitchcock P. B., *Inorg. Chim. Acta,* **2003**, *351*, 114.

*4.4.1.9. Molecular structure of [Pt(S_2CO)(dppe)] (**27**).*

Single crystals of complex **27** were grown by slow evaporation of a neat chloroform solution of **26** at room temperature. The solid state structure of **27** is shown in Figure 4.21. It crystallised with one molecule of solvent in the crystal lattice. It displays a distorted square planar geometry as indicated by the angles P(4)-Pt(1)-P(1) = 86.17(1)^o, S(2)-Pt(1)-S(1) = 76.77(3)^o. The dithiocarbonate ligand is considerably more planar, with a mean deviation from the S_2CO plane of 0.001 Å and is closely related to those of bis(diphenylphosphine)-ligated Ni(II) compounds. The bond angles around C(1) are attributed to the sp^2 hybridisation for C(1) that is, S(2)-C(1)-S(1) = 108.12(18)^o, O(1)-C(1)-S(2) = 126.5(3)^o and O(1)-C(1)-S(1) = 125.3(3)^o. The selected bond distances and angles with their estimated standard deviations are listed in Table 4.7 Crystal data, together with the data collection and refinement parameters are presented in Table 4.8.

Table 4.7. Selected bond lengths [Å] and angles [°] for **27**

Lengths		*Angles*	
Pt(1)-P(4)	2.2482(8)	P(4)-Pt(1)-P(1)	86.17(3)
Pt(1)-P(1)	2.2532(7)	P(1)-Pt(1)-S(2)	177.48(3)
Pt(1)-S(2)	2.3353(7)	S(2)-Pt(1)-S(1)	76.77(3)
Pt(1)-S(1)	2.3425(7)	S(2)-C(1)-S(1)	108.12(18)
S(1)-C(1)	1.808(3)	O(1)-C(1)-S(1)	125.3(3)
S(2)-C(1)	1.779(4)	O(1)-C(1)-S(2)	126.5(3)

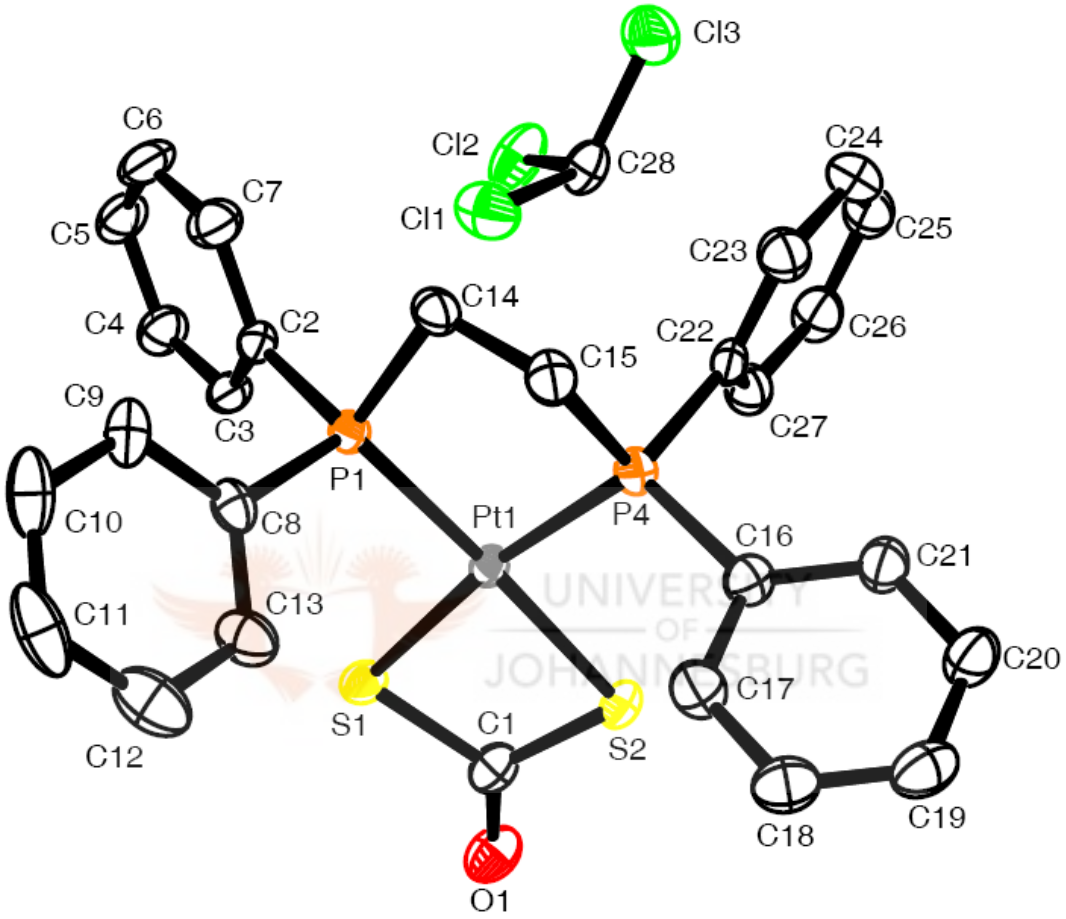

Figure 4.21. A molecular drawing of **27** with 50% probability ellipsoids. The hydrogen atoms are omitted for clarity.

Table 4.8. Crystal data, data collection and refinement parameters of **27**

Parameter	**27**
Empirical formula	$C_{28}H_{25}Cl_3OP_2PtS_2$
Formula weight	804.98
Temperature (K)	105(2)
Wavelength (Å)	0.71073
Crystal system	Orthorhombic
Space group	$P2_12_12_1$
Unit cell dimensions	
a(Å)	10.1025(5)
b(Å)	13.8660(6)
c(Å)	20.6850(9)
α	90°
β	90°
γ	90°
Volume ($Å^{3)}$	2897.6(2)
Z	4
Density (calculated) (Mg/m^3)	1.845
Absorption coefficient (mm^{-1})	5.396
F(000)	1568
Final R indices (R1)	0.0198
Reflections collected	38869
Completeness to theta	99.8 %
Goodness of fit on F^2	1.027
Largest diff. peak & hole ($e.Å^{-3}$)	1.518 and -0.406

*4.4.1.10. Transformation of complexes **26, 28** and **29** into **27** monitored by UV-Vis and $^{31}P\{^{1}H\}$ NMR spectroscopy.*

As mentioned earlier, keeping complexes **26**, **28** and **29** in solution (dichloromethane or chloroform) led to their transformation to one identical green product, **27**, [Pt(S_2CO)(dppe)] (Scheme 4.5). This transformation was followed in solution by acquiring UV-Vis and $^{31}P\{^{1}H\}$ NMR spectra at different intervals. Complex [Pt(**L5**)$_2$(dppe)] (**26**) was chosen as a representative complex for this study. The transformation of **26** was monitored for three days at room temperature. The UV-Vis spectra acquired showed spectral changes at λ_{max} 283 and 385 nm (Fig. 4.22). The $^{31}P\{^{1}H\}$ NMR spectral data shown in Figure 4.23 is indicative of the transformation process as described below.

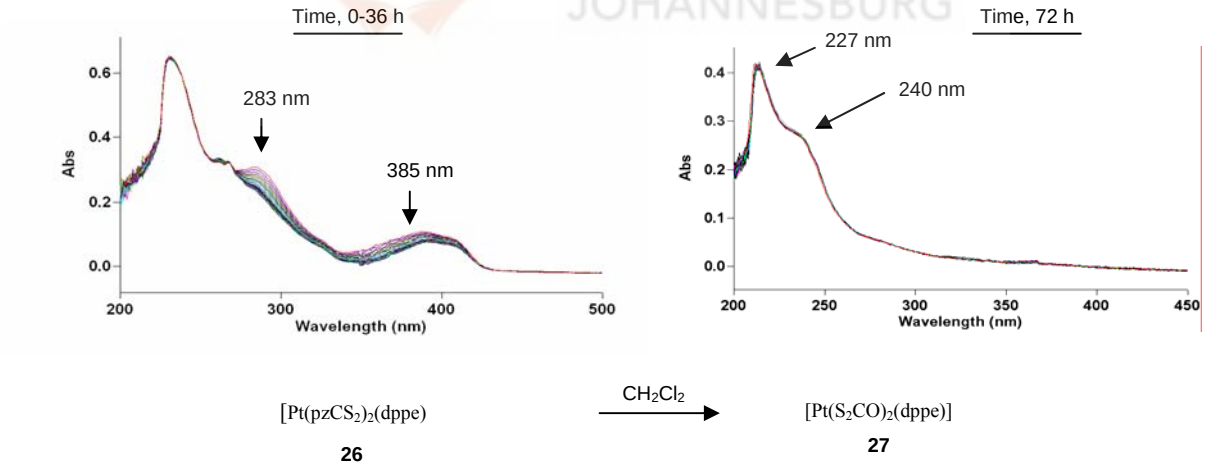

Figure 4.22. UV-Vis spectra of **26a** and the transformed product **26b**.

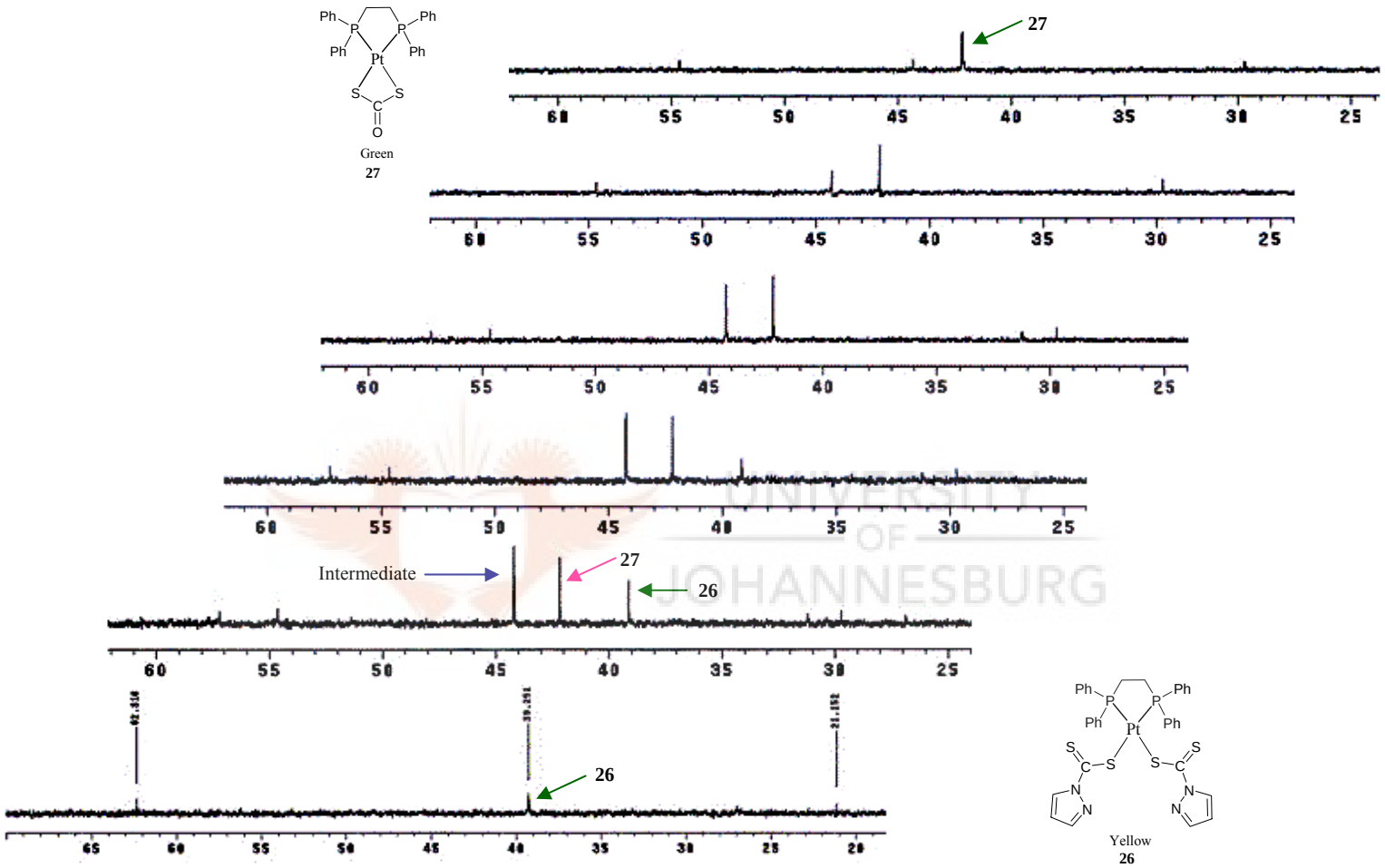

Figure 4.23. $^{31}P\{^{1}H\}$ NMR spectra showing the transformation of **26** to **27** over a period of 3 days, solvent = $CDCl_3$.

From the $^{31}P\{^{1}H\}$ NMR profile (Fig. 4.23), it was observed that after 1 h, there was an emergence of two additional peaks at 44.2 and 42.2 ppm. These peaks were attributed to the formation of an intermediate species and [Pt(S_2CO)(dppe)] (**27**), respectively. This indicated the onset of the transformation process proposed in Scheme 4.6. Between 4 and 34 h, a gradual disappearance of the product [Pt(**L5**)$_2$(dppe)] (**26**) peak at 39.1 ppm was observed. A similar profile of peak disappearance was observed for the intermediate species (44.2 ppm), even though it was much slower than that of **26**. Eventually, at 34 h, the peaks due to **26** and the intermediate species were diminished completely.

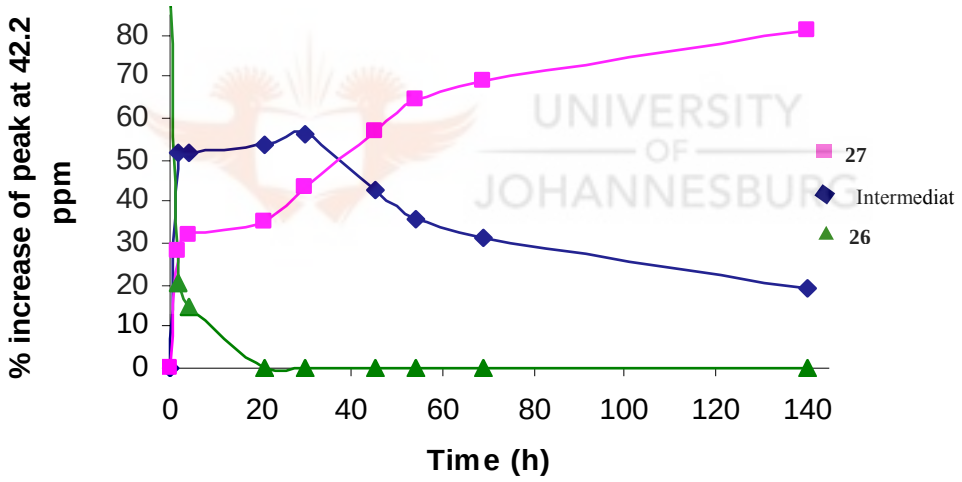

Figure 4.24. Kinetic plots of transformation of **26** to **27** followed by $^{31}P\ \{^{1}H\}$ NMR spectroscopy at 298 K.

The kinetic plots of the transformation process are shown in Figure 4.24. This process is characteristic of unimolecular reactions, involving transformation of compound **26** to **27**. For the purposes of establishing the reaction rate for this transformation process, the percentage (%) increase of the ^{31}P NMR peak at 44.2 ppm, which is due to [Pt(S_2CO)(dppe)] (**27**), was

monitored. It was arbitrarily assumed that 100% of compound **27** would be formed when the transformation is complete. Since the % increase in formation of **27** was proportional to time, the kinetic rate was determined by measuring the % values as a function of time. The various arbitrary % values (A) (Table 4.9) were obtained from the integration values of the peaks in the ^{31}P NMR spectra at different times. Subsequently, these values were used to calculate rate constant according to the equation 4.5 below. The parameter A represents integration value presumably after complete transformation (100%), whilst At represents integration value at time t.

$$\ln(A-At) = -kt \qquad \textbf{(4.5)}$$

Table 4.9. Manipulation of integration values

Time (h)	% value (A)	100%-A	ln(100%- A)
0	0	100	4.61
1	23.05	76.95	4.34
2	28.10	71.90	4.27
21	35.20	64.80	4.17
30	43.62	56.38	4.03
45	57.19	42.81	3.76
54	65.27	34.73	3.55
69	71.81	28.19	3.34
140	89.01	11.99	2.40

* A = Arbitrary NMR integration value.

A plot of ln(A-At) versus time (Fig. 4.25) gave a straight line from which the rate constant was obtained. The transformation process for the formation of [Pt(S_2CO)(dppe)] (**27**) was found to be pseudo-first-order, with a rate constant of 1.4 x 10^{-2} h^{-1}.

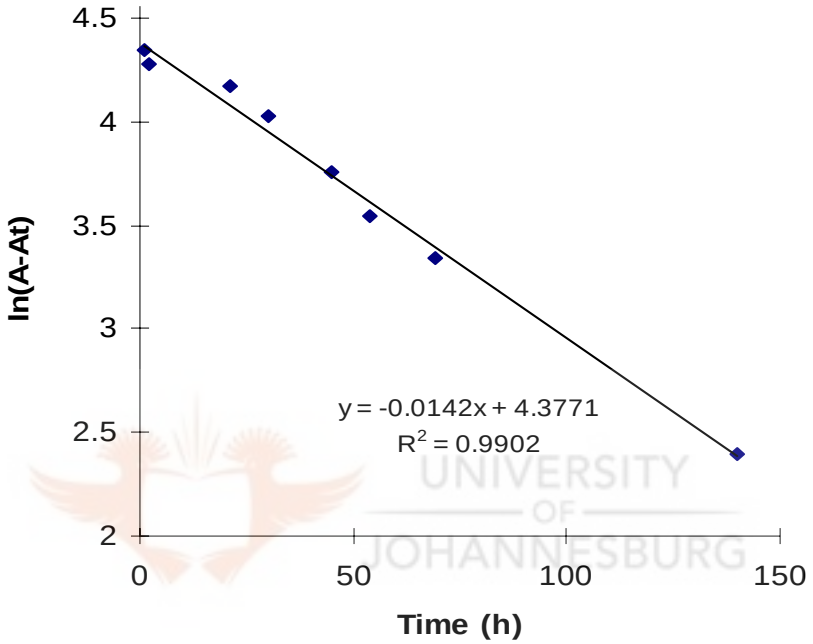

Figure 4.25. First order kinetics plot-determination of the pseudo-first order rate constant of transformation of **26** to **27**.

A postulated mechanism as to how complexes **26**, **28** and **29** transform into complex **27** is given in Scheme 4.8. It involves the intramolecular nucleophilic attack of the platinum(II) centre by the uncoordinated sulfur, and a subsequent displacement of one mole of dithiocarbamate ligand to give **b** (Scheme 4.8). A further nucleophilic attack by H_2O in **b** leads to an intermediate (**c**), which finally transforms to [Pt(S_2CO)(dppe)] (Scheme 4.8**d**). It is suggested that, (i) the rearrangement of the phosphine ligands to minimise steric hindrance

due to its phenyl groups and (ii) the ease with which **L5-L8** dissociate, accelerates the transformation to **27**.

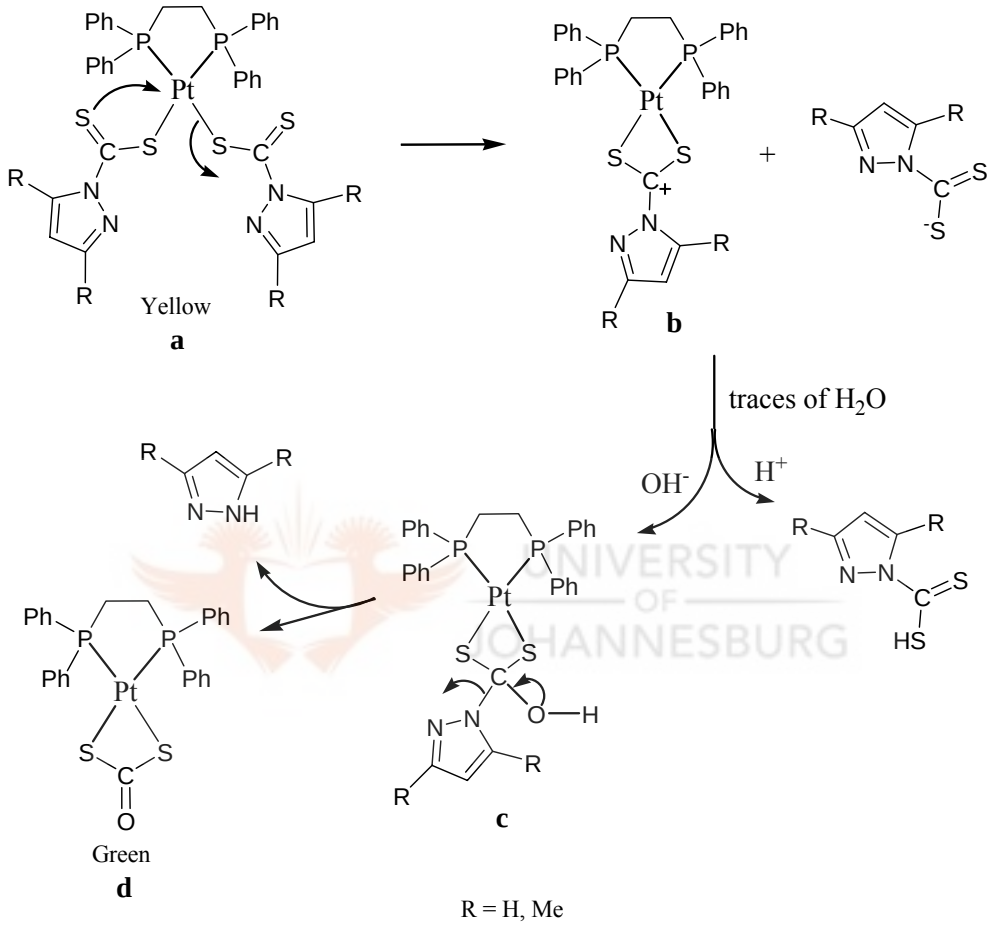

Scheme 4.8. Proposed mechanism of formation of **27** from **26**. This applies to complexes **28** and **29** as well.

Further investigations were pursued by using Ni(II), which gave analogous compounds to the Pt(II) complexes (**26**, **28** and **29**). [Ni(**L5**)$_2$(dppe)] (**30**) was isolated as brown powder by reacting [$NiCl_2$(dppe)] with two molar equivalents of **L5**. The $^{31}P\{^1H\}$ NMR data (Fig. 4.26) and microanalysis data were a confirmation of the formation of the proposed product.

Additionally, the IR spectrum displayed bands at 1617 cm^{-1}, 1183 cm^{-1} and 835 cm^{-1}, which are due to υ(C=N), υ(C-S), and υ(C=S), respectively. Crystallisation of **30** gave blue single crystals, which after X-ray analysis proved to be the known octahedral nickel pyrazole complex, $[NiCl_2(pzH)_4]$[68] shown in Figure 4.27. Despite the fact that [Ni(**L5**)$_2$(dppe)] never formed an analogous product to [Pt(S_2CO)(dppe)] (**27**), it was speculated that this process may have been exacerbated by the ease with which ligands **L5**-**L8** dissociate (*vide supra*).

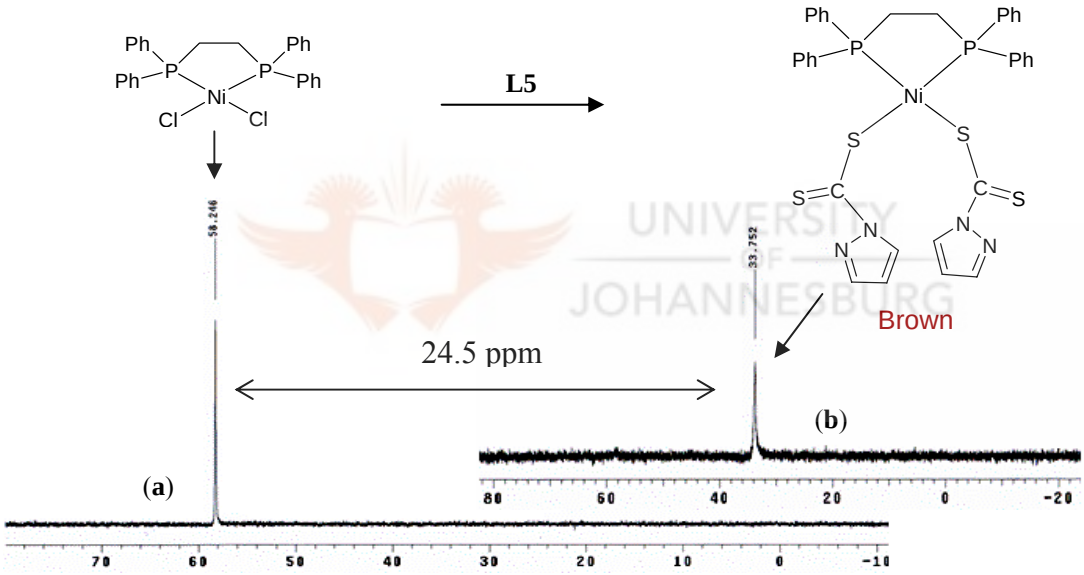

Figure 4.26. $^{31}P\{^1H\}$ NMR spectra of $[NiCl_2(dppe)]$ (spectrum (**a**)) and [Ni(**L5**)$_2$(dppe)] (spectrum (**b**)).

[68] Helmholdt R. B., Hinrichs W., Reedijk J., *Acta Crystallogr., Sect. C: Cryst. Struct. Commun.*, **1987**, *43*, 226.

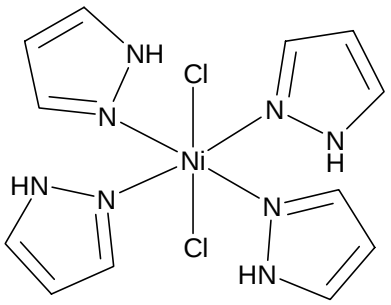

Figure 4.27. The structure of octahedral $[NiCl_2(pzH)_4]$ complex.

*4.4.1.11. Platinum(II) dithiocarbamato complexes **31-33**.*

Non-phosphine platinum(II) dithiocarbamato complexes **31-33** were also prepared. Complexes $[Pt(\mathbf{L5})_2]$ (**31**), $[Pt(\mathbf{L6})_2]$ (**32**) and $[Pt(\mathbf{L7})_2]$ (**33**) were isolated as microcrystalline reddish-brown solid materials in moderate yields by reacting $K_2[PtCl_4]$ in deionised water with **L5**, **L6** and **L7**, respectively (Scheme 4.9). The ^{1}H NMR spectrum of **32** showed protons that belong to the methyl groups of 3,5-dimethylpyrazolyl in four different chemical environments, hence resonated at four different frequencies, that is, at 2.83, 2.70, 2.40 and 2.33 ppm (Fig. 4.28). The $^{13}C\{^1H\}$ NMR spectrum of **32** showed a diagnostic peak at 226.8 ppm assignable to C(C=S), which was slightly more downfield than that the corresponding ligand **L6** (222.0 ppm). X-ray crystallography was used in the case of **32** to confirm the proposed formulation of the complex (Fig. 4.29). The structural features are discussed in detail in section 4.4.1.12 below.

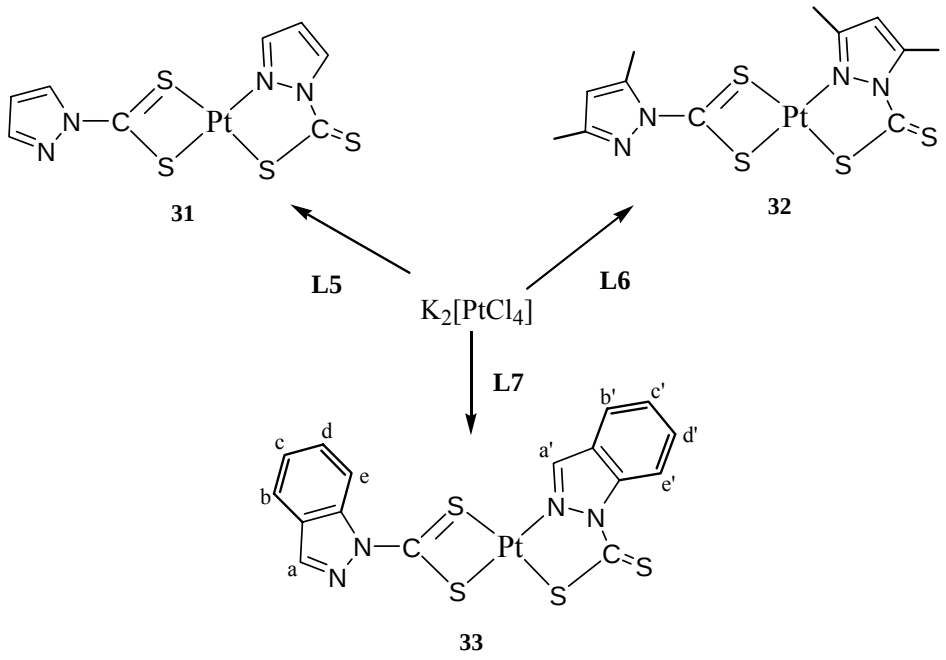

Scheme 4.9. Synthesis of platinum(II) dithiocarbamato complexes **31-33**.

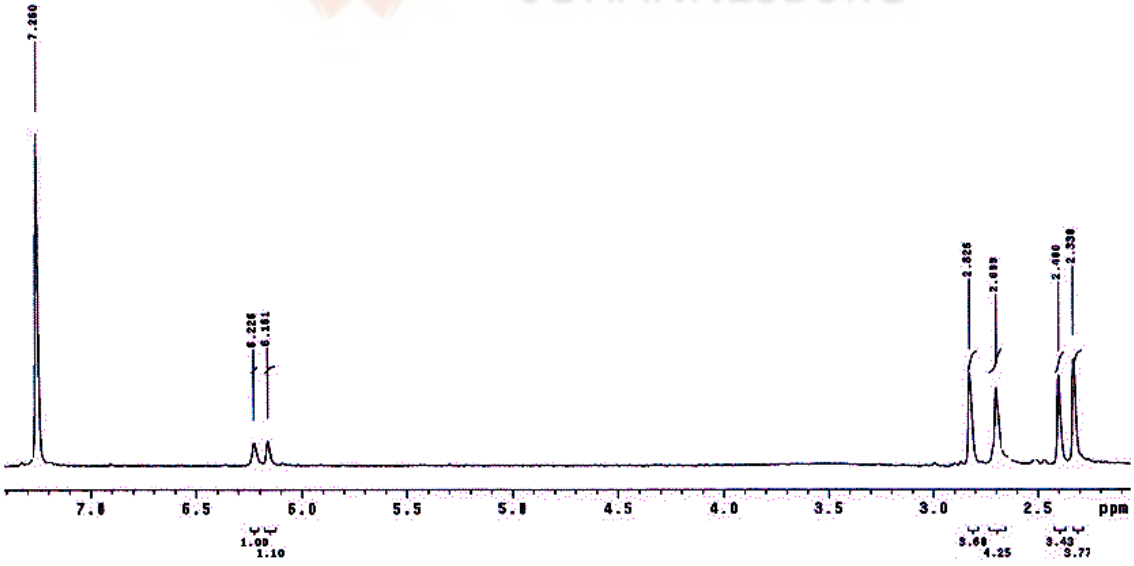

Figure 4.28. A ^{1}H NMR spectrum of **32**. The four methyl peaks resonate at different frequencies between 2.2 and 2.9 ppm indicating that they are in different chemical environments in solution.

The ^{1}H NMR spectra of **31** displayed a similar pattern to that **32**, with all the peaks resonating in pairs. The peaks due to 5H, 5H′ protons of the pyrazolyl unit appeared at 8.62 and 8.51 ppm. This was indicative of two **L5** ligands in different chemical environments. Other peaks were (3H, 3H′) at 8.16, 8.02 ppm and (4H, 4H′) at 6.69, 6.50 ppm. However, a similar pattern was not very pronounced in **33**. Except for the fact that Hb and H′b protons appeared as two different protons at 8.43 and 8.31 ppm, respectively, all the other peaks did not resonate in pairs as observed for complexes **31** and **32**. The ^{13}C{^{1}H} NMR spectra of **31** and **33** could not be obtained because of the poor solubility in common polar solvents, such as, $CDCl_3$, CD_2Cl_2 and DMSO-d_6. The similarity in the patterns of ^{1}H NMR spectra of compounds **31**-**33**, led to postulating that they have analogous structures.

The IR spectra of complexes **31**-**33** showed bands in the 1110-1172 cm^{-1} region assignable to $\upsilon(CS_2)$ vibration expected for a κ^2-S^S coordination of the dtc ligands. The insignificant shift of υ(C=S) band at *ca*. 843 cm^{-1} in the IR spectra of complexes **31**-**33** compared to the υ(C=S) band in the spectra of the free ligands **L5**-**L7**, indicated the presence of a non-coordinated C=S moiety.[69] The pyrazole ring vibrational frequencies for all the complexes occurred between 1518 and 1606 cm^{-1}, which were generally lower compared to those of the free ligands **L5**-**L7**. The spectroscopic as well as microanalysis data suggest that compounds **31**-**33** have similar structural features. X-ray crystallography was used in the case of **32**, to verify the proposed structures (cf. sec. 4.4.1.7 below).

[69] Mukhopadhyay S., Mukhopadhyay U., Mak T. C. W., Ray D., *Inorg. Chem*., **2001**, *40*, 1057.

*4.4.1.12. Molecular Structure of [Pt(**L6**)$_2$] (**32**).*

Orange crystals of complex **32** suitable for single-crystal X-ray analysis were obtained from a dichloromethane-heptane mixture. The molecular structure of the crystal is shown in Figure 4.29. The coordination properties of the ambidentate **L6** and its preferential formation of the five-membered N,S chelate ring led to the formation of PtS_2SN coordination similar to that observed for nickel(II) compounds reported in the literature. The Pt-S bond length is substantially longer than the Pt-N bond. In this case, Pt(1)-S(3) was found to be 2.2613Å and Pt(1)-N(4) to be 2.028(3) Å. Other bond distances are Pt(1)-S(1) (2.35 Å) and Pt(1)-S(2) (2.28 Å).

The interesting feature is the formation of a five-membered $PtSCN_2$ ring which is presumably stable than the rigid four-membered $PtCS_2$ ring. The bond angles, N(4)-Pt(1)-S(3) (82.88(9)°); S(2)-Pt(1)-Sl(1) (74.18(3)°); S(3)-Pt(1)-S(2) (97.67(3)°) and N(4)-Pt(1)-S(1) (105.25(9)°) indicate a distorted square-planar geometry with a PtS_2SN coordination sphere. Coordination around the metal is close to linearity along N(4)-Pt(1)-S(2) (179.31(9)°) and S(3)-Pt(1)-S(1) (171.32(3)°). Complex **32** is structurally comparable to complexes $[Pt(Me_2pipdt)_2](BF_4)_2$ and $[Pt(Me_2pipdt)_2][Pt(mnt)_2]_2$ (Me_2pipdt = *N,N'*-dimethyl-piperazine-2,3-dithione; mnt = maleonitrile-2,3-dithiolate) reported by Bigoli *et al*.[70] which possess four-membered $PtCS_2$ ring as in **32**. The selected bond distances and angles with their estimated standard deviations are listed in Table 4.10 below. Crystal data, together with the data collection and refinement parameters are presented in Table 4.11.

[70] (a) Bigoli F., Deplano P., Mercuri M. L., Pellinghelli M. A., Pilia L., Pintus G., Serpe A., Trogu E. F., *Inorg. Chem*., **2002**, *41*, 5241. (b) Bigoli F., Deplano P., Mercuri M. L., Marchio L., Pilia L., Serpe A., Concas G., Congiu F., Sanna S., *Chem. Phys. Lett*., **2006**, *421*, 361.

Table 4.10. Selected bond lengths [Å] and angles [°] for **32**

Bond lengths (Å)		*Bond angles (°)*	
Pt(1)-N(4)	2.028(3)	N(4)-Pt(1)-S(3)	82.88(9)
Pt(1)-S(3)	2.2613(10)	N(4)-Pt(1)-S(2)	179.31(9)
Pt(1)-S(2)	2.2861(10)	S(3)-Pt(1)-S(2)	97.67(3)
Pt(1)-S(1)	2.3557(10)	N(4)-Pt(1)-S(1)	105.25(9)
S(1)-C(1)	1.690(4)	S(3)-Pt(1)-S(1)	171.32(3)
S(2)-C(1)	1.690(4)	S(2)-Pt(1)-S(1)	74.18(3)
S(3)-C(7)	1.716(4)	C(1)-S(1)-Pt(1)	85.85(14)
S(4)-C(7)	1.648(4)	C(7)-S(3)-Pt(1)	102.56(13)
N(1)-C(1)	1.378(5)	S(2)-C(1)-S(1)	111.8(2)

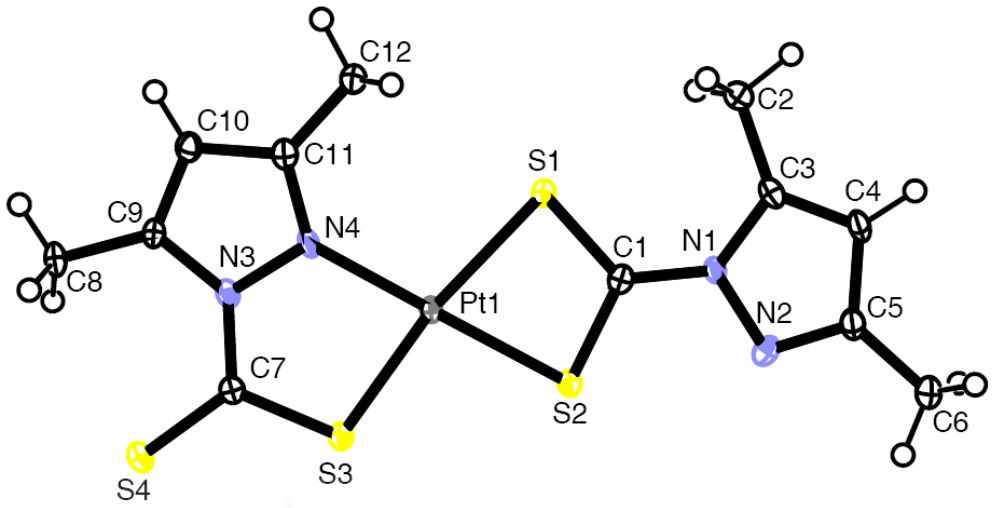

Figure 4.29. A molecular drawing of **32** drawn with 50% probability ellipsoids. The hydrogen atoms omitted for clarity.

Table 4.11. Crystal data, data collection and refinement parameters of **32**

Parameter	**32**
Empirical formula	$C_{12}H_{14}N_4PtS_4$
Formula weight	537.60
Temperature (K)	100(2)
Wavelength (Å)	0.71073
Crystal system	Triclinic
Space group	$P\bar{1}$
Unit cell dimensions	
a(Å)	8.1583(8)
b(Å)	8.6938(9)
c(Å)	11.5863(11)
α	75.211(2)°
β	85.768(2)°
γ	89.997(2)°
Volume ($Å^{3)}$	792.24(14)
Z	2
Density (calculated) (Mg/m^3)	2.254
Absorption coefficient (mm^{-1})	9.379
F(000)	512
Final R indices (R1)	0.0235
Reflections collected	12899
Completeness to theta	98.4 %
Goodness of fit on F^2	1.088
Largest diff. peak & hole ($e.Å^{-3}$)	1.534 and -1.216

4.4.2. Synthesis of new bis(dithiocarbamato)disulfide ligands

Three new bis(dithiocarbamato)disulfide ligands, **L9-L11**, were synthesised by oxidation of **L5-L7** using iodine in methanol (Scheme 4.10). Interest in preparing these ligands emanated from the fact that it has been reported that compounds with S-S moiety have some biological activity. For instance $Et_2NC(=S)S\text{-}SC(=S)NEt_2$ (disulfram) has shown anticancer activity.[71,72] The possible mechanism for biological activity of such compounds is discussed in detail in section 5.6.1. All the ligands were isolated as yellow powders in high yields. Except for **L11**, all the other ligands were readily soluble in chlorinated solvents.

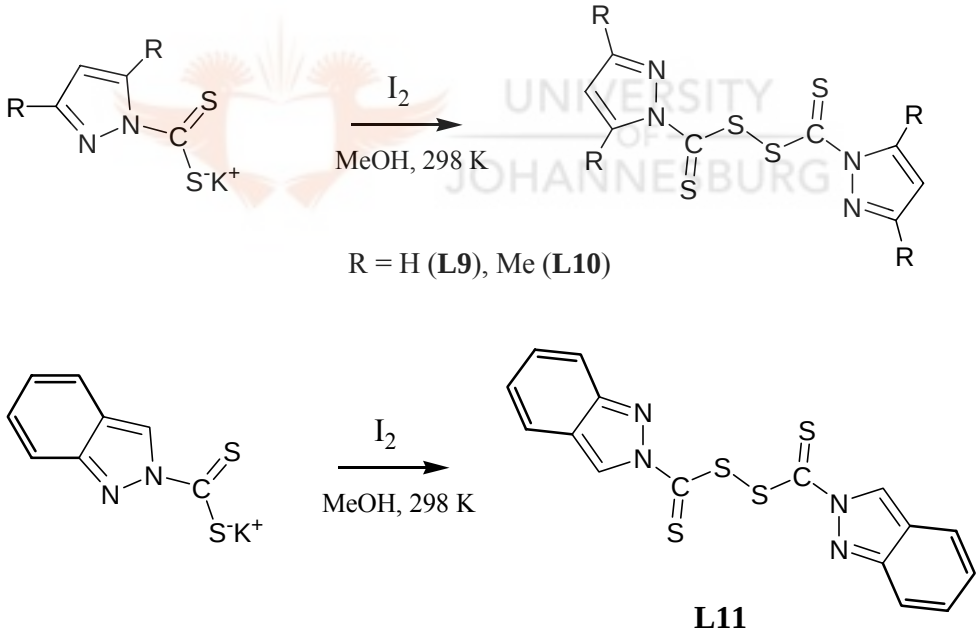

Scheme 4.10. Synthesis of pyrazole-based dithiocarbamato disulfide ligands.

[71] Ying T. S., Sarma D. S. R., Farber E., *Am. J. Pathol*., **1980**, *99,* 159.
[72] Spath A., Tempel K., *Chem.-Biol. Interactions*, **1987**, *64*, 151.

From the $^{13}C\{^{1}H\}$ NMR data acquired (Fig. 4.30), the C(C=S) peaks for **L9**-**L11** appeared at *ca*. 193 ppm compared to those of the respective starting material, **L5**, **L6** and **L7**, which appeared between 218.6 and 222.2 ppm. This provided evidence for the formation of these new bis(dithiocarbamato)disulfide ligands.

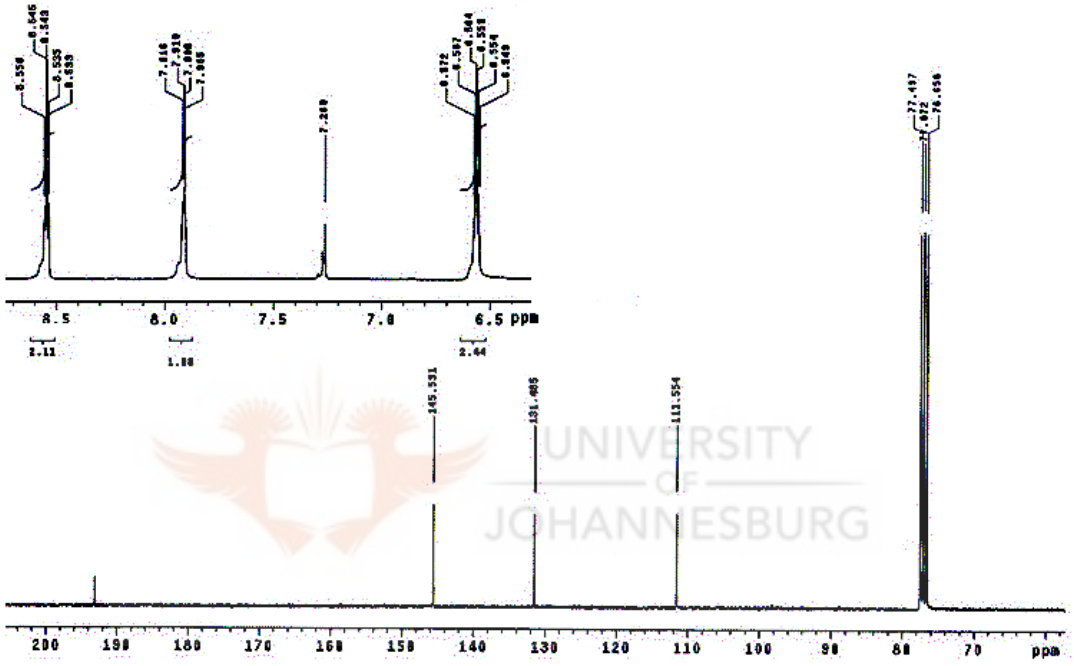

Figure 4.30. The $^{13}C\{^{1}H\}$ NMR spectrum of **L9** with a ^{1}H NMR spectrum (inset).

The IR spectra of the ligands showed bands assigned to the υ(C-S) and υ(C=S) vibration modes in the region of 1334-1254 cm^{-1} and 869-901 cm^{-1}, respectively. These ligands are closely related to the bis[(3,5-dimethylpyrazol-1-yl)ethyl]disulfide reported by Mills *et al.*[73] Structure elucidation of **L9** and **L10** was performed using single crystal X-ray analysis.

[73] Mills A. M., Chalbot M., Bouwman E., Spek A. L., *Acta Cryst. Sect. E.*, **2003**, E59, o258.

Orange crystals suitable for single crystal X-ray analysis were obtained from slow evaporation of THF solutions of **L9** and **L10**. The molecular structures of the crystals are shown in Figures 4.31 and 4.32. In **L9** and **L10**, the two pyrazolyl rings are connected *via* N(1) and N(1A) by a disulfide bridge and are in perpendicular planes. The bond lengths and angles (S(2)-S(2)#1 = 2.0309(6) Å, S(2)-C(6) = 1.7958(11) Å, C(6)-S(2)-S(2)#1 = 102.78(4)°) are consistent with those of disulfide compounds.[73,74] The molecular packing diagram of **L10** viewed along *c* axis is shown in Figure 4.33. There is formation of cuboids, which are defined by two ligand units and have no intermolecular interactions. The selected bond distances and angles with their estimated standard deviations, for **L9** and **L10**, are listed in Table 4.12, whilst the crystal data, together with the data collection and refinement parameters of **L9** and **L10** are presented in Table 4.13.

[74] Mullica D. F., Trawick M. L., Wu P. W. N., Sappenfield E. L., *J. Chem. Crystallogr*., **1998**, 28, 761.

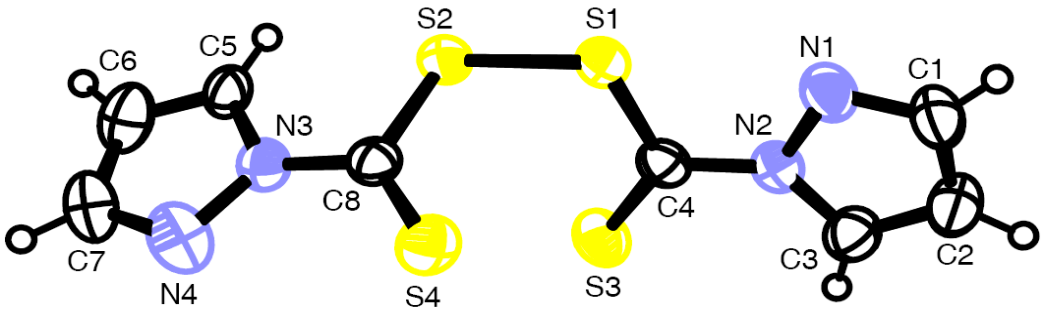

Figure 4.31. A molecular drawing of **L9** shown with 50% probability ellipsoids. The hydrogen atoms omitted for clarity.

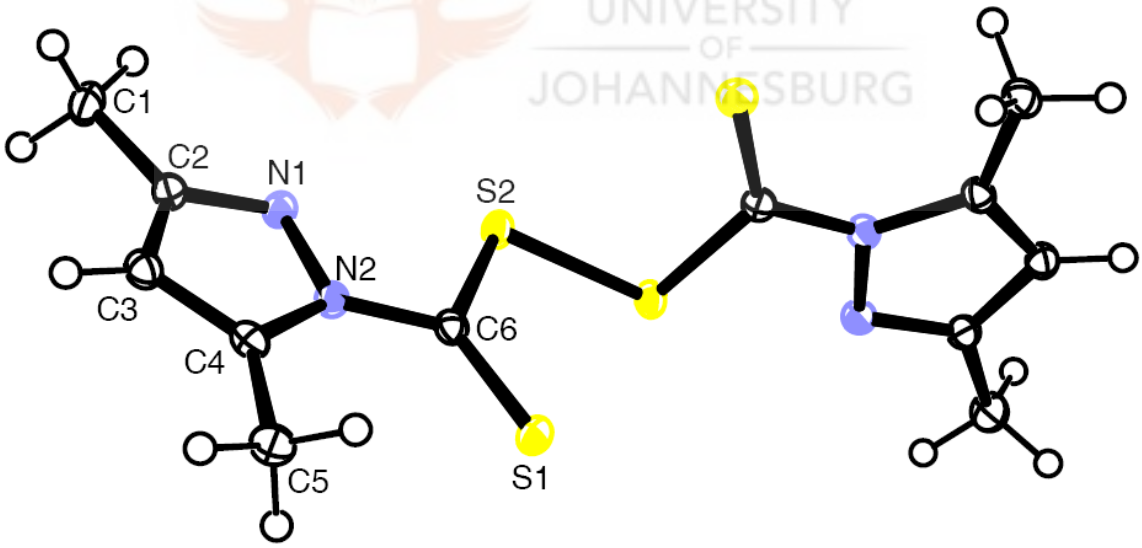

Figure 4.32. A molecular drawing of **L10** shown with 50% probability ellipsoids. The hydrogen atoms omitted for clarity.

Table 4.12. Selected bond lengths [Å] and angles [°] for **L9** and **L10**

	L9	**L10**
	Bond lengths (Å)	
S(1)-C(6)	1.621(2)	1.6294(11)
S(2)-C(6)	1.778(3)	1.7958(11)
S(2)-S(2)#1	2.0194(10)	2.0309(6)
N(1)-N(2)	1.370(3)	1.3884(12)
N(2)-C(6)	1.386(3)	1.3825(13)
	Bond angles (°)	
C(6)-S(2)-S(2)#1	102.49(9)	102.78(4)
C(2)-N(1)-N(2)	111.8(2)	105.28(9)
C(6)-N(2)-N(1)	104.1(2)	91.07(12)

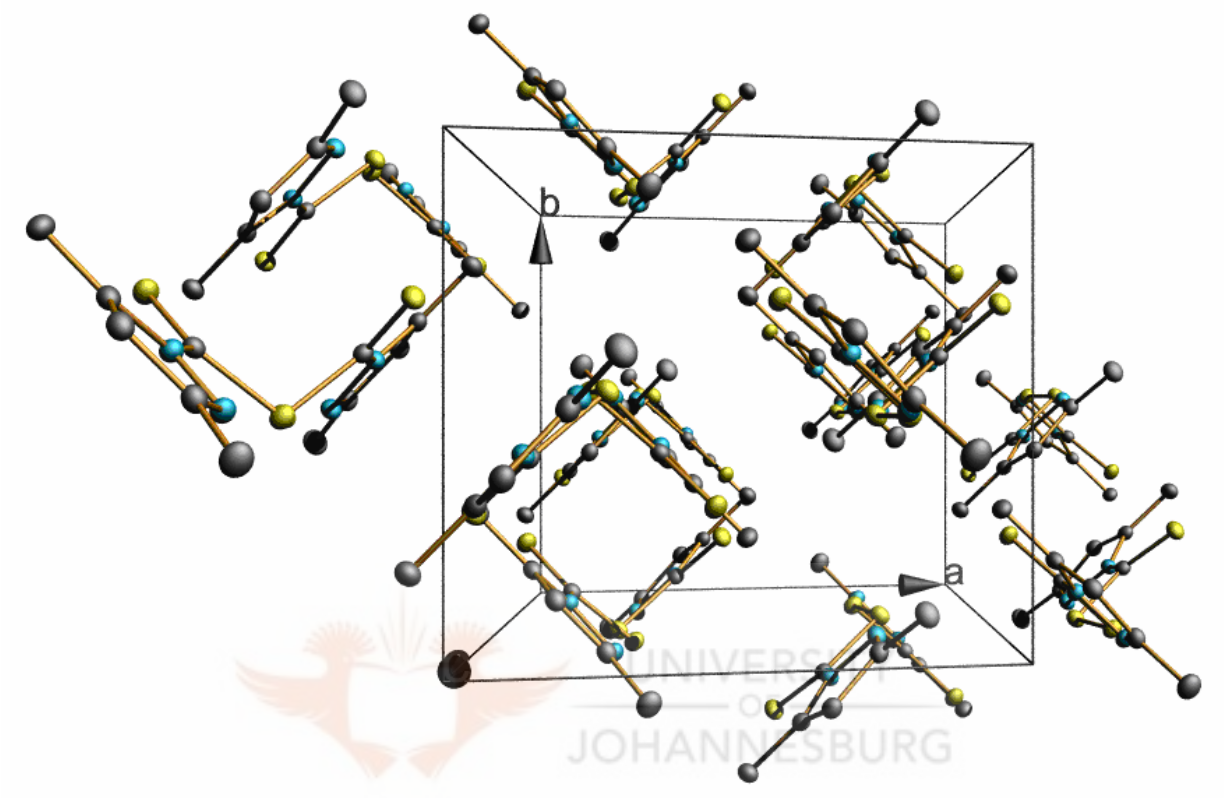

Figure 4.33. A molecular packing diagram of **L10** viewed along *c* axis. The hydrogen atoms omitted for clarity.

Table 4.13. Crystal data, data collection and refinement parameters of **L9** and **L10**

Parameter	**L9**	**L10**
Empirical formula	$C_8H_6N_4S_4$	$C_{12}H_{14}N_4S_4$
Formula weight	286.41	342.51
Temperature (K)	293(2)	100(2)
Wavelength (Å)	0.71073	0.71073
Crystal system	Triclinic	Monoclinic
Space group	$P\bar{1}$	I2/a
Unit cell dimensions		
a(Å)	5.43340(10)	10.6094(16)
b(Å)	31.3556(7)	9.4667(14)
c(Å)	7.2893(2)	15.156(2)
α	90°	90°
β	107.9860(10)°	101.760(2)°
γ	90°	90°
Volume ($Å^{3)}$	1181.17(5)	1490.2(4)
Z	4	4
Density (calculated) (Mg/m^3)	1.611	1.527
Absorption coefficient (mm^{-1})	0.780	0.632
F(000)	584	712
Final R indices (R1)	0.0416	0.0262
Reflections collected	20623	13011
Completeness to theta	100.0 %	98.5 %
Goodness of fit on F^2	1.116	1.062
Largest diff. peak & hole ($e.Å^{-3}$)	0.664 and -0.617	0.483 and -0.251

*4.4.3. Attempted complexation of ligands **L9-L11**.*

Attempts were made to form gold(I) complexes using the bis(dithiocarbamato)disulfide ligands **L9-L11.** Reactions of **L9-L11** with [AuCl(tht)] gave unstable products at 25 ^{o}C and -78 ^{o}C. Thus, a second approach involving reaction of **L9-L11** with $[(Ph_3P)Au]^+$ salts, was pursued. The starting material, $[(Ph_3P)Au(NCMe)]BF_4$ salt, was generated *in situ* from the reaction of $[(Ph_3P)AuCl]$ with $AgBF_4$ at -78 ^{o}C. The $^{31}P\{^1H\}$ NMR spectrum of compound $[(Ph_3P)Au(NCMe)]BF_4$ displayed one peak at 45.5 ppm. Consequently, the $^{31}P\{^1H\}$ NMR spectrum of products isolated from reaction of **L9** and $[(Ph_3P)Au(NCMe)]BF_4$, showed three peaks (Fig. 4.34). The peak at 47.2 ppm was assigned to $[(Ph_3P)Au(PPh_3)]^+$. This is informed by the fact that the ^{31}P NMR studies of closely related species, $[Au\{P(C_6H_{11})Ph_2\}_2]^+$[75] and $[Au(PPhMe_2)_2]^+$,[76] showed phosphorous peaks at around 54.0 and 62.0 ppm, respectively. Thus, the peak at 34.1 ppm was tentatively assigned to $[Au_2(PPh_3)_2(\mathbf{L9})].2BF_4$. Furthermore, $[Au_2(PPh_3)_2(\mathbf{L9})].2BF_4$ have S-containing ligand (**L9**) that increase the electron density in the compound; hence it is more shielded and the phosphorus peak would appear upfield (34.1 ppm). The ^{31}P NMR spectra acquired over a period of 24 h indicated that the predominant species in solution were $[Au_2(PPh_3)_2(\mathbf{L9})]2BF_4$ and $[(Ph_3P)Au(PPh_3)]BF_4$ (Fig. 4.34). However, no further efforts were made to isolate $[Au_2(PPh_3)_2(\mathbf{L9})]2BF_4$ as the purification processes were not successful.

[75] Parish (´Dick´) R. V., Parry O., McAuliffe C. A., *J. Chem. Soc., Dalton Trans*., **1981**, 2098.
[76] Al-Saady A. K. H., McAuliffe C. A., Moss K., Parish (´Dick´) R. V., Fields R., *J. Chem. Soc., Dalton Trans*., **1984**, 491.

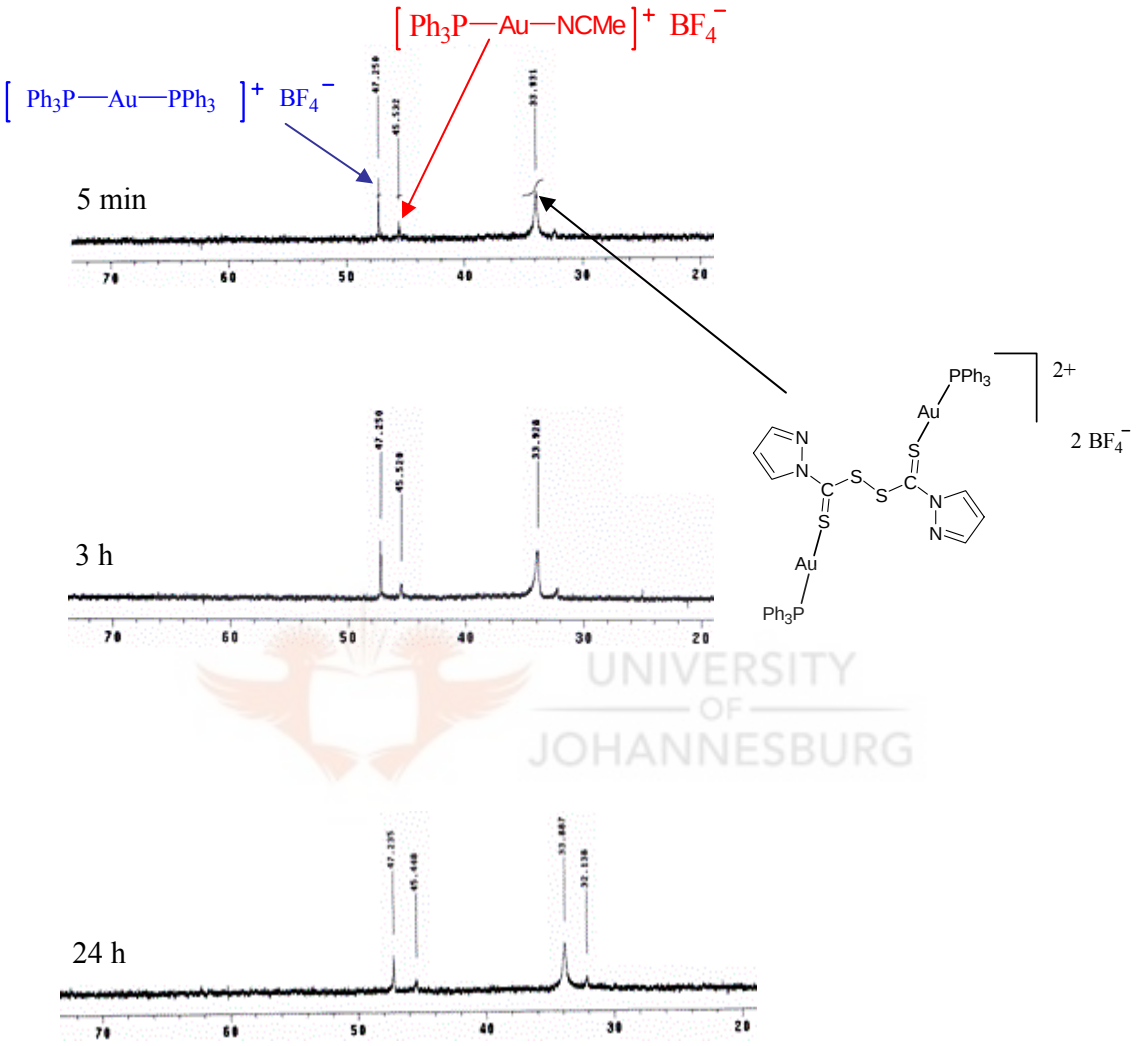

Figure 4.34. A $^{31}P\{^{1}H\}$ NMR profile showing a mixture of desired product $[Au_2(PPh_3)_2(\mathbf{L9})]2BF_4$, $[(Ph_3P)\text{-}Au\text{-}(PPh_3)]^+$ and $[Ph_3P\text{-}Au\text{-}NCMe]^+$.

4.5. Conclusions

The reaction of dithiocarbamate ligands **L5-L8** with [AuCl(PPh_3)], [Au_2Cl_2(dppp)] and [Au_2Cl_2(dpph)] led to successful isolation of mononuclear and binuclear gold(I) complexes. This was confirmed from the spectroscopic and microanalysis data. Furthermore, the molecular structure of [Au(**L7**)(PPh_3)] (**15**) and [(Au**L7**)$_2$(dpph)] (**25**) which features approximately linear gold atom geometry, is a further confirmation of existence of complexes **13-25**. Notably, attempts to crystallise complex [(Au**L5**)$_2$(dppe)] (**17a**) led to the formation of gold(I) cluster compound, $[Au_{18}S_8(dppe)_6]Cl_2$ (**17b**). The span between the P atoms of the dppe ligand in **17a** seems to play a role in the formation of **17b**. The close proximity of the P atoms in dppe back bone, allows for the gold atoms coordinated to them to have aurophilic interactions. The presence of these interactions would bring the two gold centres closer, thus contributing to cluster formation; but it is not clear how this leads to the re-arrangement and formation of **17b**. The X-ray structure of **17b** displays Au···Au interactions (2.9263(7)-3.1395(7) Å).

Reaction of ligands **L5-L7** with $K_2[PtCl_4]$ gave bis-chelated complexes (**31-33**) having three sulfur atoms and one nitrogen atom coordinated to the platinum metal, leaving one uncoordinated sulfur. These complexes have distorted square-planar geometries as revealed from the solid state structure of **32**. Ligand **L6** coordinated to platinum atom to form a five-membered N,S chelate ring (PtS_2SN). On the other hand, reactions of [$PtCl_2$(dppe)] with **L5-L7** gave complexes **26, 28** and **29** with a general formula [Pt(**L**)$_2$(dppe)]. These yellow complexes were found to be unstable in solution and transformed to an identical green product, [Pt(S_2CO)(dppe)] (**27**), at room temperature. This has been clearly demonstrated

from the UV-Vis and $^{31}P\{^{1}H\}$ NMR spectroscopic studies. A pseudo-first-order transformation process was proposed, with a rate constant of 1.4 x 10^{-2} h^{-1}. A further conformation of this transformation was the solid state structure of **27**. Once again the ease with which **L5-L7** disintegrate is speculated to be the cause for this occurrence. Moreover, there is no doubt that the rearrangement of the phenyl rings in the diphosphine ligands causes the compound to be rather unstable in solution. Experiments utilising various diphosphine ligands would help prove this concept.

Isolation of new bis(dithiocarbamato)disulfide ligands (**L9-L11**) was indicative of how **L5-L7** can undergo easy oxidation. The solid state structures of **L9** and **L10** is a confirmation of the oxidation products. Strategies to isolate gold(I) complexes of bis(dithiocarbamato)disulfide ligands **L9-L11** were unsuccessful as they led to formation of very unstable products. Just as dithiocarbamate ligands **L5-L7** undergo oxidation easily, the resultant disulfides (**L9-L11**) can also be easily reduced back to **L5-L7**. Thus, it is possible that the unstable nature of gold products from **L9-L11** is due to reduction of the disulfide ligands. No further efforts were made to isolate $[(PPh_3)_2\mathbf{L}].2BF_4$ because of purification problems.

The major findings are:

1. dithiocarbamate ligands (**L5-L8**) could act as sources of sulfur for the isolation of gold(I) cluster compounds. This is clearly demonstrated from the isolation of the cluster compound $[Au_{18}S_8(dppe)_6]^{2+}$ (**17b**). This inference is drawn from the fact that the analogous $[Au_{18}Se_8(dppe)_6]^{2+}$ was prepared by reacting $[(AuCl)_2(dppe)]$ with $Se(SiMe_3)_2$. However, the isolation of **17b** from **L5** is unique as there are no reports of gold(I) cluster obtained from dithiocarbamates.

2. that while the biphasic synthetic procedure for the monophopshine and diphosphine gold(I) dithiocarbamato complexes works, it is not ideal for the synthesis of the analogous diphosphine platinum(II) dithiocarbamato complexes. The slightest traces of water could lead to transformation of the desired compounds. Thus for synthesis of diphosphine platinum(II) dithiocarbamato compounds, a dry solvent synthetic procedure is advised.

CHAPTER 5

ANTI-TUMOUR ACTIVITY OF LIGANDS, PLATINUM(II) AND GOLD(I) DITHIOCARBAMATO COMPLEXES AGAINST HELA CELLS AND LUMINESCENCE STUDIES

Screening of the complexes for their in vitro anticancer activities were performed by Mrs. Nell of Pretoria University (SA), whilst the photoluminescence experiments were performed by Ms. Sumitra of University of North Texas. The interpretation and discussion of the results is by the candidate.

5.0. Introduction

The biochemistry of gold has developed primarily in response to the extensive use of gold compounds in treating rheumatoid arthritis and in response to efforts to develop complexes with antitumour, and to some extent, anti-HIV activity.[1] These efforts are as a result of the realisation of the activity of 2,3,4,6-tetra-O-acetylglucopyranosato-S-(triethyl-phosphine)gold(I) (auranofin) as an antiarthritic agent.[2] Thus, gold(I) coordination compounds are receiving considerable attention because of their potential applications in medicine, particularly as antitumour agents.[3] For instance, auranofin, although an antiarthritic agent, has also been found to be an effective agent against P388 lymphocytic leukemia.[4] This led to the examination of the antitumour activity of

[1] *Gold Progress in Chemistry, Biochemistry and Technology*. Shaw III C. F., Ed. Schmidbaur H., John Wiley & Sons, Chichester, England, **1999**, 260.
[2] Sutton B. M., McGusty E., Walz D. T., DiMartino M. J., *J. Med. Chem.*, **1972**, 15, 1095.
[3] Kostova I., *Anti-cancer Agents Med. Chem.*, **2006**, *6*, 19.

phosphine gold(I) thiolate complexes containing the P-Au-S motif found in auranofin.[5] This has been achieved by using various phosphines and S-containing ligands.

Researchers have also sought to understand the mechanism(s) by which phosphine gold(I) thiolate complexes exhibit their antitumour activities. This is informed by the fact that, unlike platinum complexes, DNA is not the primary target. It has been shown that the mitochondria act as a potential target of anticancer drugs.[6,7,8,9,10] The mitochondria are also known to play a decisive role in apoptosis or programmed cell death. Apoptosis is a distinct form of cell death that proceeds along a genetically determined execution program.

Several studies now show that mitochondria and thioredoxin reductase, which is a homodimeric selenoenzyme, are the targets for the phosphine gold(I) compounds.[7,11,12,13] The mechanism is believed to involve the binding of Au(I) to the selenocysteine (Cys-SeCsy) residue in the mitochondrial enzyme thioredoxin reductase.[7,14] From discussions

---

[4] [a]Simon T. M., Kinishima D. H., Vilbert G. J., Lorber A., *Cancer Res*., **1981**, *41*, 94; [b]Mirabelli C. K., Johnson R. K., Sung C., Faucette L. F., Muirhead K., Crooke S. T., *Cancer Res*., **1985**, *45*, 32.

[5] Mirabelli C. K., Johnson R. K., Hill D. T., Faucette L. F., Girard G. R., Kuo G. Y., Sung C., Crooke S. T., *J. Med. Chem*., **1986**, *29*, 218.

[6] McKeage M. J., Maharaj L., Berners-Price S. J., *Coord. Chem. Rev*., **2002**, *232*, 127.

[7] Barnard P. J., Berners-Price S. J., *Coord. Chem. Rev*., **2007**, *25*, 1889.

[8] Farrell N., *Coord. Chem. Rev*., **2002**, *232*, 1

[9] Bouchier-Hayes L., Lartigue L., Newmeyer D. D., *J. Clin. Invest*., **2005**, *11*, 240.

[10] Weissig V., Boddapati S. V., D'Souza G. G. M., Cheng S. M., *Drug Design Reviews*, **2004**, *1*, 15.

[11] [a]Bragadin M., Scutari G., Folda A., Bindoli A., Rigobello M. P., *Ann. N. Y. Acad. Sci*., **2004**, *1030*, 348; [b]Rigobello M. P., Folda A., Dani B., Menabo R., Scutari G., Bindoli A., *Eur. J. Pharmacol*., **2008**, *582*, 26.

[12] [a]Rigobello M. P., Scutari G., Folda A., Bindoli A., *Biochem. Pharmacol*., **2004**, *67*, 689; [b]Rigobello M. P., Scutari G., Boscolo R., Bindoli A., *Br. J. Pharmacol*., **2002**, *136*, 1162.

[13] Hill K. E., McCollum G. W., Boeglin M. E., Burk R. F., *Biochem.Biophys. Res. Commun.,* **1997**, *234*, 293.

[14] Gromer S., Arscot L. D., Williams Jr. C. H.,Schirmer R. H., Becker K., *J. Biol. Chem*., **1998**, *273*, 20096.

in chapter 4, it is clear that any attempts to prepare new gold(I) anticancer agents could make use of a phosphine-gold motif in its design. This is what this project took advantage of and the biological activities are reported in this chapter.

5.1. Luminescent gold(I) complexes

Apart from the biological activities of gold(I) thiolate complexes, their photophysical and photochemical properties have potential applications as luminescent materials.[15] Luminescence originates from the valence orbitals of free gold(I) ion, which are the filled 5d orbitals, empty 6s and 6p orbitals.[16] Since Au(I) is oxidising as well as reducing, LMCT and MLCT transitions (Fig. 5.1) could occur at reasonable energies. Low-energy MLCT absorptions for gold(I) complexes with π-acceptor ligands is dominant; thus, Au(I) complexes with simple π-acceptor ligands, such as phosphines and isocyanides, display MLCT absorptions in their electronic spectra.

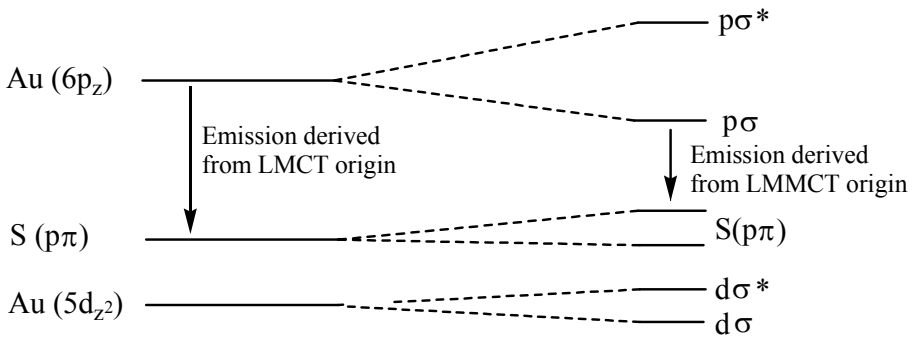

Figure 5.1. Schematic representations of orbital splitting of gold(I) thiolate compounds (Taken from ref. 18).

[15] Yam V. W. W., Lo K. K. W., *Chem. Soc. Rev*., **1999**, *28*, 323.
[16] Vogler A., Kunkely H., *Coord. Chem. Rev*., **2001**, *219*, 489.

Even though complete knowledge of the nature of luminescence in gold(I) compounds is lacking, a variety of different excited states suggests that they are emissive. It is assumed that the lowest-energy excited state, which is populated in absorption, is the emissive state.[16,17] For instance, for mononuclear gold(I) thiolate complexes like $[Au(SR')(PR_3)]$ (R = Et, Ph; R′ = Ph), solid-state emissions occur at 77 K over a wide energy range of 413-702 nm.[18] The origin of the emission has been ascribed to a LMCT (S→Au) triplet state. Other examples include complexes $[Au_2(SR')_2(Ph_2PN(R)PPh_2)]$ (R′ = C_6H_4Cl-*p* > C_6H_4F-*p* > C_6H_4Me-*p*; R = hexyl) (Fig 5.2), which shows absorption energy trend in line with the σ-donating ability of the thiolate ligands.[19] This low-energy absorption band has been assigned to a thiolate-to-gold LMCT transition. The high energy absorptions of $[Au_2(SR')_2(Ph_2PN(R)PPh_2)]$ at *ca*. 262-305 nm were tentatively assigned as intraligand transitions characteristic of the diphosphine ligands. Excitation of solids and fluid $CHCl_3$ solutions of $[Au_2(SR')_2(Ph_2PN(R)PPh_2)]$ complexes are dominated by broad and intense blue-green emission, typical of a metal perturbed ligand-centred emission of the phosphine ligand.

[17] Kunkely H., Vogler A., *Naturforsch*., **1996**, *51b*, 1067.
[18] Yam V. W., Chan C., Li C., Wong K. M., *Coord. Chem. Rev*., **2001**, *216*, 173.
[19] Yam V. W, Chan C. L., Cheung K. K., *J. Chem. Soc., Dalton Trans*., **1996**, 4019.

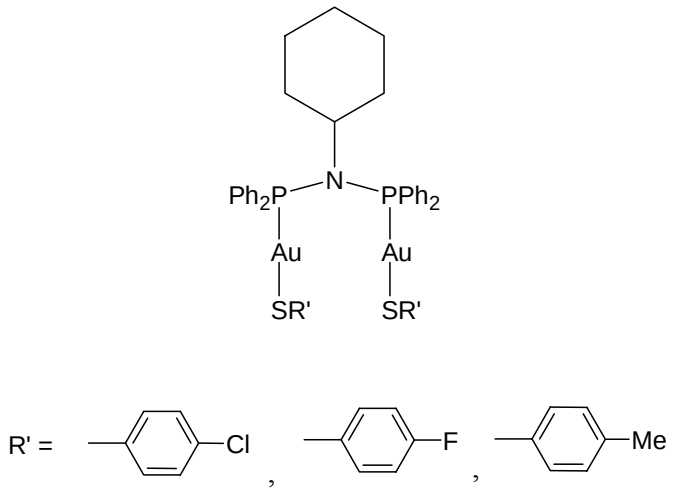

Figure 5.2. Structures of $[Au_2(SR')_2(Ph_2PN(R)PPh_2)]$.

The low energy emissions of $[Au_2(SR')_2(Ph_2PN(R)PPh_2)]$ complexes observed at *ca*. 600 nm originate from emissive states derived from thiolate-to-gold LMCT transitions. The large Stokes shifts (difference between the λ_{max} of the absorption spectrum and λ_{max} of the emission spectrum) and the observed lifetimes in microseconds range are suggestive of a triplet parentage (^{3}LMCT).[19,20] There is also a relationship between the luminescence properties and the extent of Au···Au association in the compounds concerned.[21] The excited state for those complexes with short Au···Au contacts has been suggested to show ligand-to-metal-metal charge-transfer (LMMCT) (Fig. 5.1).

In this project, the new phosphine gold(I) complexes and platinum(II) complexes were investigated for their anticancer activities against human cervix epithelial carcinoma (HeLa) cells. Some of the gold compounds were further investigated for luminescence. The results are presented in the following sections.

[20] Lebedkin S., Langetepe T., Sevillano P., Dieter F., Kappes M. M., *J. Phys. Chem. B*, **2002**, *106*, 9019.
[21] A. G., Staples R. J., Fackler J. P., Jr, *Inorg. Chem.*, **1995**, *34*, 75.

5.2. Experimental

5.2.1 Biological reagents and instrumentation

All commercial reagents were used as received. Phosphate Buffered Saline (PBS), Eagle's RPMI-1640 medium, 3-(4,5-dimethylthiazol-2-yl)-2,5-diphenyltetrazolium bromide (MTT) kit, phytohemagglutinin-protein form (PHA-P) and the 96-well flat-bottomed culture plates were all purchased from BD Biosciences Ltd. Cisplatin was purchased from Sigma Aldrich. Eagle's medium with 0.1 mM non-essential amino acids was prepared by adding 2 mM L-glutamine, 1.0 mM sodium pyruvate and 5% bovine fetal calf serum to the pure Eagle's RPMI-1640 medium. Twenty compounds, **L5-L11** (Scheme 5.1), **13-16** (Scheme 5.2), **20-25** (Scheme 5.3) and **31-33** (Scheme 5.4) were screened for their antitumour activities against human cervix epithelial carcinoma (HeLa) cells. HeLa cells and human lymphocytes (PBMCs) from preservative free heparinised peripheral blood were obtained from the Department of Pharmacology and Pretoria Medical Hospital, University of Pretoria, South Africa. The absorbance values were recorded on a Whittaker Microplate Reader 2001 spectrophotometer at 570 nm and the reference wavelength of 630 nm.

5.2.2. Cell culture and drug treatment

HeLa cells were cultured in Eagle's medium with 0.1 mM non-essential amino acids, 2 mM L-glutamine, 1.0 mM sodium pyruvate and 5% bovine fetal calf serum, at 37 ^{o}C in an atmosphere of 5% CO_2. Cells were plated in 96-well sterile plates at a density of 1 x

10^4 cells/well in 100 μL of medium, and incubated for 1 h. Subsequently, compounds were added with concentrations from 0 to 50 μM. Cytotoxicity was determined by using MTT to stain treated HeLa cells after 7 days according to literature methods[22]. MTT dye is reduced by living cells to yield a soluble formazan product that can be assayed colourimetrically. A 20 μL volume of freshly prepared MTT (5 mg/mL) was added to each well and the cells incubated for another 4 h. Cell survival was evaluated by measuring absorbance at 570 nm, using a Whittaker Microplate Reader 2001. The IC_{50} values were calculated with the Graphpad programme. All experiments were performed in triplicate.

The inhibition of the growth of normal cells by the complexes tested was also measured by employing human lymphocytes (PBMC) cells. The same procedure described above was used, except for the fact that the treated PBMC cells were incubated for 3 days as opposed to 7 days for HeLa cells. The aim of testing these compounds on normal cells was to determine whether the compounds could target the cancerous (HeLa) cells specifically and not the normal cells. While that was the primary objective, it also allowed investigation into whether there was any relationship between the observed activities and the growth rate of the cells. In performing these experiments, the lymphocytes were divided into two namely; (i) normal cells that were stimulated using PHA-P so as to increase their proliferation rate (stimulated lymphocytes) and (ii) un-stimulated normal cells (resting lymphocytes).

[22] Mossman T., *J. Immunol. Methods*, **1983**, *65*, 55.

NOTE: In all the cases, the compounds were tested in different batches and therefore the IC_{50} values for the reference compound (cisplatin) had to be established for every batch of compounds tested. The reader is advised to take note of this.

5.2.3. Electronic absorption and photoluminiscence spectra measurements

UV-Vis spectra of [Au(**L7**)(PPh_3)] (**15**), [(Au**L5**)$_2$(dppe)] (**17a**), [(Au**L5**)$_2$(dppp)] (**20)** and [(Au**L5**)$_2$(dpph)] (**23**) (Scheme 5.5) were recorded on a Perkin-Elmer Lambda 900 spectrophotometer at 298 K as dichloromethane solutions. Photoluminescence measurements were performed on both solid materials and frozen dichloromethane solutions of complexes [Au(**L7**)(PPh_3)] (**13**), [Au(**L7**)(PPh_3)] (**14**), **15**, [Au(**L7**)(PPh_3)] (**16**), **17a** and $[Au_{18}S_8(dppe)_6]2Cl$ (**17b**) (Scheme 5.6). Photoluminescence measurements were carried out at the University of Texas, USA, on a Spex Fluorolog-3 spectrometer equipped with a 450 W Xe-lamp and double grating monochromators in the excitation (λ_{exc} ~ 250-1000 nm) and two emission channels. Three photo-detectors R5108 Hamamatsu photomultiplier tubes (PMT) and a liquid nitrogen-cooled germanium photodiode (Edinburgh Instruments) covered the emission ranges of λ_{em} ~ 400-800 (UV-Vis emission channel). All emission spectra were corrected for the wavelength-dependent instrumental response. The latter was determined using a standard calibration lamp (Oriel) and a two-inch Spectralon intergrating sphere (Labsphere) installed in the sample chamber of the Fluorolog-3 spectrometer.

5.3. Biological results

Twenty compounds, dithiocarbamate and disulfide ligands (Scheme 5.1), ten gold(I) complexes (Scheme 5.2 and 5.3) and three platinum(II) dithiocarbamato complexes (Scheme 5.4), were investigated for their ability to inhibit cell growth on tumour cells *in vitro*. The human cervical epitheloid carcinoma (HeLa) cell-line was chosen in this case. All data were acquired in triplicate and the final values recorded as averages. Tables 5.1-5.5 list the dose values that caused 50% inhibition of cell growth (IC_{50}). The syntheses of the ligands, gold(I) and platinum(II) complexes tested are reported in chapter 4. The biological results are discussed in the following sections systematically starting with the activities of the ligands, the gold(I) compounds, and finally platinum(II) compounds.

5.3.1. Dithiocarbamate and bis(pyrazolyldithiocarbamate)disulfide ligands

In order to establish the activities of phosphine gold(I) complexes **20**-**25** and platinum(II) complexes **31**-**33**, it was important to establish the activities of the ligands first. This was paramount as it helped in determining whether activities of the metal complexes could be due to the presence of the dithiocarbamate ligands. Thus, the dithiocarbamate ligands **L5**-**L8** (Scheme 5.1) were tested for their antitumour activities against cancerous HeLa cells. They were all found to be inactive against HeLa cells (Table 5.1). However, the new disulfide ligands **L9**-**L11** (Scheme 5.1), derivatised from **L5**-**L7**, showed antitumour activities against HeLa cells. Ligand **L9** had an IC_{50} value of 3.7 μM (Fig. 5.3, Table 5.1), which was comparable to that of cisplatin (1.1 μM), while that of **L10** was *ca*. 16 times less active than cisplatin (17.8 μM).

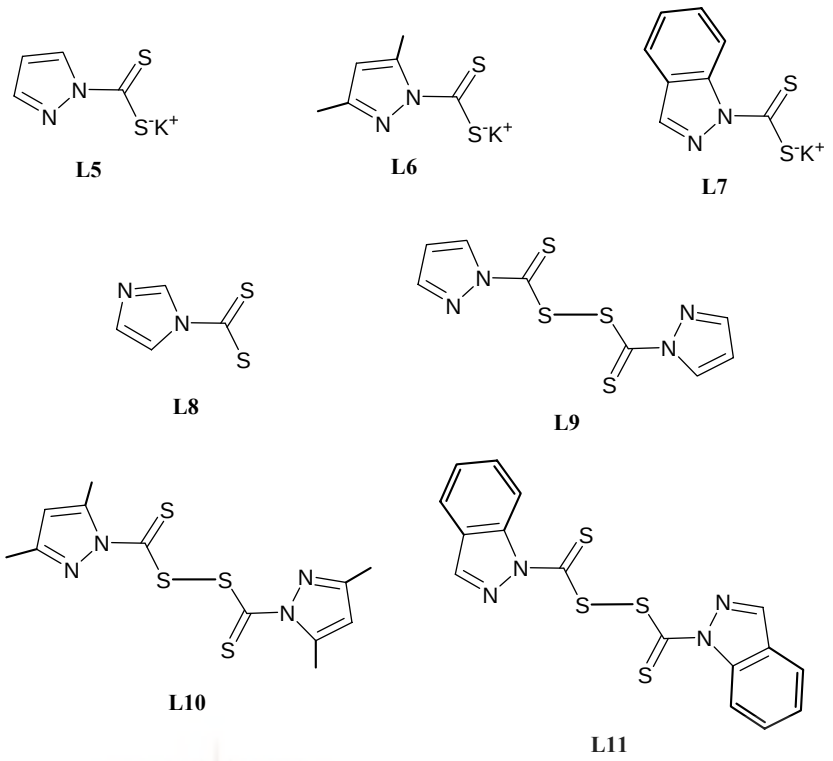

Scheme 5.1. Dithiocarbamate salts and their disulfide analogues.

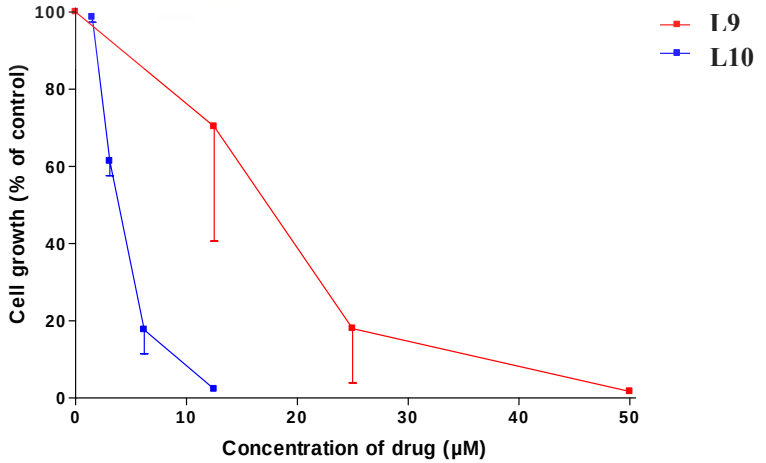

Figure 5.3. Growth inhibition profile of HeLa cells by **L9** and **L10**.

Table 5.1. Growth inhibition values of compounds **L5-L11** tested against HeLa cells.

Drug	IC_{50}	Drug	IC_{50}
L5	>50	**L9**	3.7 ± 0.2
L6	>50	**L10**	17.8 ± 4.2
L7	>50	**L11**	Nd
L8	>50		
Cisplatin	1.1 ± 0.2		

IC_{50} is the concentration of drug required to inhibit cell growth by 50%. Nd = Not done.

Compound **L9** was further tested to probe its antitumour specificity. This was achieved by comparing its activity against cancerous HeLa cells and normal cells (human lymphocytes). The IC_{50} values registered for resting and stimulated lymphocytes were 34.0 and 36.4 μM (Table 5.2), respectively as opposed to 3.7 μM displayed by the same ligand against HeLa cells. From these results, the tumour specificity factor (TS) was calculated according to equation 5.1 below.

$$TS = \frac{\text{Mean } IC_{50} \text{ of the normal cells (stimulated + resting Lymphocytes)}}{\text{Mean } IC_{50} \text{ of the cancer cells}} \quad \textbf{(5.1)}$$

The TS factor was found to be 9.6 (Table 5.2). The implication of this result is that cancerous HeLa cells were 9.6 times more sensitive to the cytotoxic action of **L9** compared to normal cells (resting and the stimulated lymphocytes). Notably, the IC_{50} values of resting (IC_{50} = 34.0 μM) and stimulated lymphocytes (IC_{50} = 36.4 μM) were

comparable. This suggests that increased growth rate of cells in stimulated lymphocytes, did not reduce the activity of **L9** significantly (36.4 μM). From this result, it was concluded that the growth rate of cells in this instance had little influence in the observed activities.

Ligand **L9** is similar to $Et_2NC(=S)S\text{-}SC(=S)NEt_2$ (disulfram), which has anticancer activity.[23,24,25,26] Many proposals have been given for the mechanism of action of disulfram, which ranges from inhibiting DNA topoisomerase,[27] to reducing angiogenesis[28] and also inhibiting proteasome signalling pathways.[29] Even though there are no clear structural activity relationships of disulfram, the anticancer activity of disulfram has been suggested to be due its disulfide nature (S-S moiety), which allows for the formation of diethyldithiocarbamate that react with sulfhydryl groups of several enzymes.[30,31] Compound **L9** could be acting in a similar manner as disulfram.

Table 5.2. Tumour Specificity of **L9**.

Drug	HeLa IC_{50} (μM)	Lymph (resting) IC_{50} (μM)	Lymph (stimulated) IC_{50} (μM)	Tumour Specificity
L9	3.7	34.0	36.4	9.6

IC_{50} is the concentration of drug required to inhibit cell growth by 50%.

[23] Spath A., Tempel K., *Chem.-Biol. Interactions*, **1987**, *64*, 151.
[24] Grafstroem R., Greene F. E., *Biochem. Pharmacol*., **1980**, *29*, 1517.
[25] Sauna Z. E., Shukla S., Ambudkar S. V., Mol. BioSyst., **2005**, *1*, 127.
[26] Wickström M., Danielsson K., Rickardson L., Gullbo J., Nygren P., Isaksson A., Larsson R., Lövborg H., *Biochem. Pharmacol*., **2007**, *73*, 25.
[27] Yakisich J. S., Siden A., Eneroth P., Cruz M., *Biophys. Res. Commun*., **2001**, *289*, 586.
[28] Shiah S. G., Kao Y. R. Wu F. Y. H., Wu C. W., *Mol. Pharmacol*., **2003**, *64*, 1076.
[29] Lövborg H., Oberg F., Rickardson L., Gullbo J., Nygren P., Larsson R., *Int. J. Cancer*, **2006**, *118*, 1577.
[30] Hacker M. P., Ershler W. B., Newman R. A., Gamelli R. L., *Cancer Res*., **1982**, *42,* 4490.
[31] Neims A. H., Coffey D. S., Hellerman L., *J. Biol. Chem*., **1966**, *241*, 5941.

5.3.2 Gold(I) complexes

*5.3.2.1 Mononuclear gold(I) complexes **13-16***

The gold(I) complexes **13-16** (Scheme 5.2) were found to be very active against HeLa cells with good inhibitions at low concentrations (Table 5.3). The cytotoxicity results were comparable to those of the clinical reference, cisplatin (IC_{50} = 2.8 μM). At 1.5 μM, the activity of complex **13** was insignificant, inhibiting just 10% of the HeLa cells' growth (Fig. 5.4). However at 3.0 μM, complex **13** significantly inhibited the growth of HeLa cells up to *ca*. 90%. The analogous compounds **14**, **15** and **16** showed similar patterns of concentration dependent activities (Fig. 5.5, 5.6 and 5.7). The IC_{50} values of **13**, **14**, and **15** are the same, 2.6 μM, whilst that of **16** is 3.1 μM (Table 5.3). Given the fact that the respective ligands (**L5-L8**) were inactive, it was concluded that the observed activities of **13-16** were due to the P-Au fragments of the gold(I) compounds.

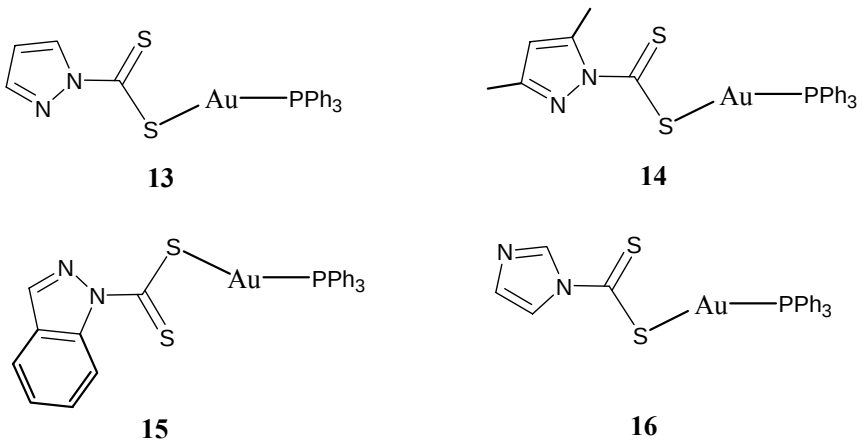

Scheme 5.2. Monophosphine gold(I) dithiocarbamate based complexes **13-16**.

From literature reports,[5,32,33] it seems that the thiolate ligands help in the formation of the active species from the phosphine gold(I) thiolates that act against cancer cells. It is possible that the dithiocarbamate ligands (**L5-L8**) could have aided in expediting the conversion of the gold(I) complexes (**13-16**) to active species. Literature reports also indicate that such transformations involve ligand substitution of the thiolate ligands by membrane-localised biological thiols to form intermediates with P-Au-S motifs.[34,35] A direct comparison of antitumour activity of [AuClPPh$_3$] with those of complexes **13-16** would have confirmed that P-Au-S motif is necessary for better activity as shown in literature. However, the antitumour activity of [AuClPPh$_3$] was not determined in this study. Nevertheless, from the literature, phosphine gold(I) thiolates are known to display better efficacies compared to their chloro phosphine gold(I) analogues.

Table 5.3. Growth inhibition values of compounds **13-16** tested against HeLa cells.

Drug	IC_{50} (μM)	Drug	IC_{50} (μM)
13	2.6 ± 0.1	**15**	2.6 ± 0.2
14	2.6 ± 0.1	**16**	3.1 ± 0.5
Cisplatin	2.8 ± 0.6		

IC_{50} is the concentration of drug required to inhibit cell growth by 50%.

[32] Tiekink E. R. T., *Bioinorg. Chem. Applns*., **2003**, *1*, 53.
[33] Mirabelli C. K., Jensen B. D., Mattern M. R., Sung C. M., Mong S. M., Hill D. T., Dean S. W., Schein P. S., Johnson R. K., Crooke S. T., *Anti-Cancer Drug Des*., **1986**, *1*, 223.
[34] Snyder R. M., Mirabelli C. K., Crooke S. T., *Biochem. Pharmacol*., **1986**, *35*, 923.
[35] Berners-Price S. J., Jarrett P. S., Sadler P. J., *Inorg. Chem*., **1987**, *26*, 3074.

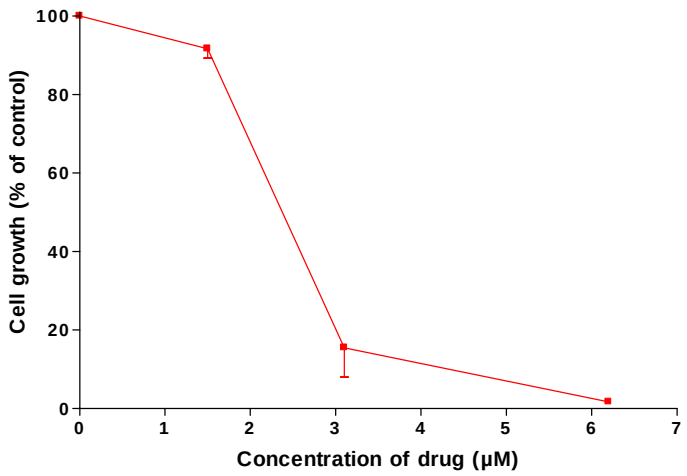

Figure 5.4. Growth inhibition profile of HeLa cells by gold(I) complex **13**.

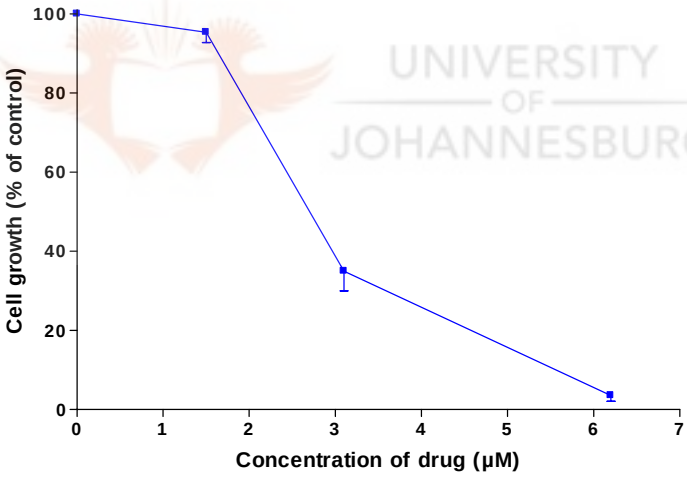

Figure 5.5. Growth inhibition profile of HeLa cells by gold(I) complex **14**.

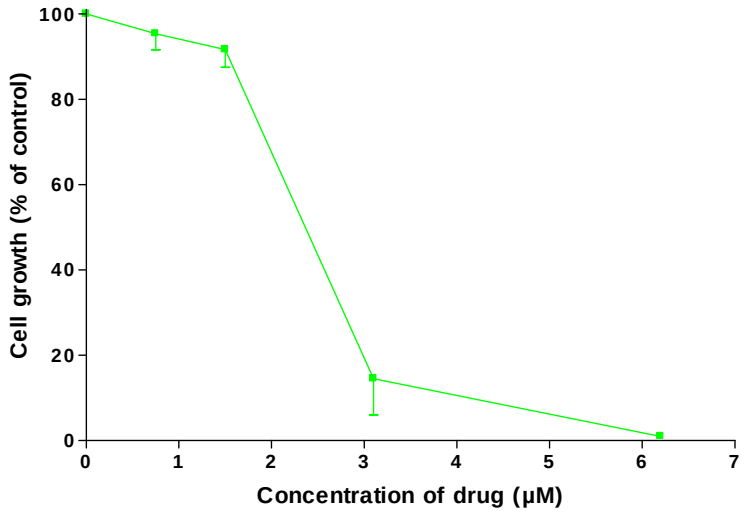

Figure 5.6. Growth inhibition profile of HeLa cells by gold(I) complex **15**.

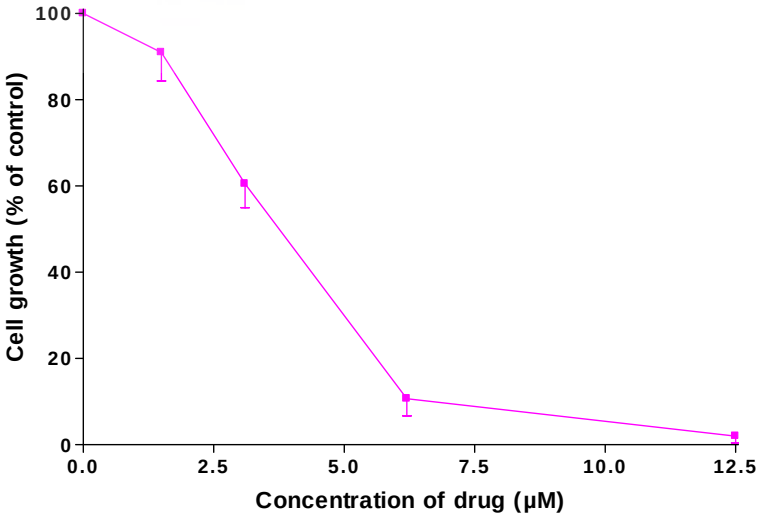

Figure 5.7. Growth inhibition profile of HeLa cells by gold(I) complex **16**.

The cytotoxicities of gold(I) complexes **13-16** (Scheme 5.2) against normal cells (human lymphocytes) were also investigated. This was one of the key objectives of the project; to establish whether these compounds were specific to killing tumour cells and not normal cells (tumour specificity). All the complexes displayed tumour specific activities. Complex **13** was cytotoxic against normal cells (resting and stimulated lymphocytes) with IC_{50} values 9.1 and 8.6 μM, respectively, compared to it activity against cancerous HeLa cells (2.6 μM). The tumour specificity values (TS) were obtained using equation 5.1. However, the TS values were not significantly high and were in the range 3.5-6.1 as given in Table 5.4.

Table 5.4. Tumour Specificity of **13-16**.

Drug	HeLa IC_{50} (μM)	Lymph (resting) IC_{50} (μM)	Lymph (stimulated) IC_{50} (μM)	Tumour Specificity
13	2.6	9.1	8.5	3.4
14	2.6	9.5	8.6	3.5
15	2.6	14.0	5.1	3.7
16	3.1	15.5	18.5	6.1
Cisplatin	2.8			

IC_{50} is the concentration of drug required to inhibit cell growth by 50%.

There was no clear trend between the activities of compounds **13-16** against stimulated and resting lymphocytes, contrary to the expectations that stimulated cells would be less susceptible to the compounds. A case in point is compound **15** with its activities against resting and stimulated lymphocytes being 14.0 μM and 5.1 μM, respectively. It is possible that phytohemagglutinin-protein (PHA-P), which was used to stimulate lymphocytes, could have made the cells more susceptible to these compounds. However,

it should be noted that this is an inference drawn from the observed activities and further experiments would be necessary to ascertain this point. Overall, the increased growth rate of stimulated cells as opposed to the resting cells did not play a significant role at all. It was then concluded that the activities observed were independent of the cells' growth rate. Complex **16** was found to show the highest TS factor of 6.1, which meant **16** inhibited tumour cells six times more specifically than it inhibited normal cells. As for complexes **13**, **14** and **15**, the low TS factors suggested that these compounds killed both tumour and normal cells indiscriminately.

It is clear that gold(I) compounds **13-16** exhibit good antitumour activity against HeLa cells. However, there was no clear trend on the dependence of the activities on the bulkiness of the compounds, i.e. in the order of imidazole, pyrazole, 3,5-dimethylpyrazole, indazole. It is possible that the dithiocarbamate ligands (**L5-L8**) are readily substituted in solution irrespective of their bulkiness. Further stability studies of complexes **13-16**, in solution, should shed some light on this matter.

*5.3.2.2 Dinuclear gold(I) complexes **20-25***

Binuclear gold(I) complexes **20-25** (Scheme 5.3) were also investigated for their antitumour activities against cancerous HeLa cells. The IC_{50} results are given in Table 5.5 below. Of all the six diphosphine gold(I) complexes (**20-25**) tested, the dpph-based gold(I) compounds **23-25** were the most active (Scheme 5.3, Fig. 5.11-5.13) with complex **24** showing the highest activity against HeLa cells (IC_{50} = 0.1 μM). In the growth inhibition profile of **24** (Fig. 5.12), there was no significant inhibition of the cells'

growth (*ca*. 20%) at 0.05 μM, but at 0.18 μM, a 80% growth inhibition was registered. A similar profile was observed for **23** with an IC_{50} of 0.4 μM. The activities of **24** (IC_{50} = 0.1 μM) and **23** (IC_{50} = 0.4 μM) were comparable to that of the reference compound cisplatin (IC_{50} = 0.5 μM). However, complex **25** was about seven times less active (IC_{50} = 3.7 μM) than the reference compound cisplatin. As for the dppp-based gold(I) compounds **20**-**22**, their IC_{50} values were 2.2, 7.0 and 3.4 μM for **20**, **21** and **22**, respectively (Table 5.5, Fig. 5.8-5.10).

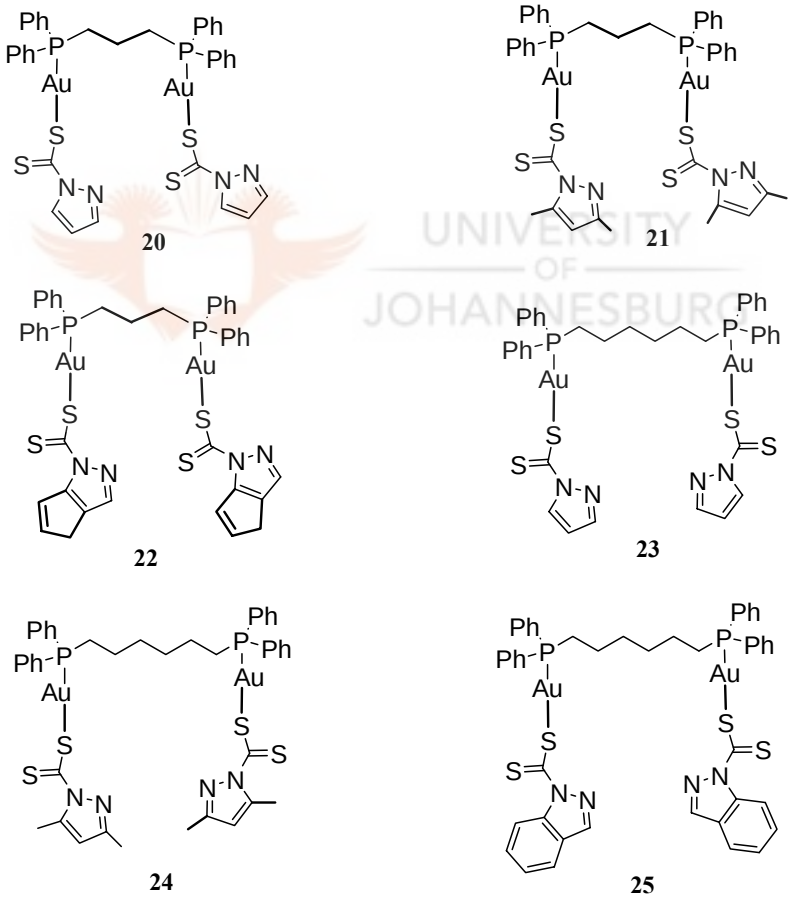

Scheme 5.3. Diphosphine gold(I) dithiocarbamate based complexes **20**-**25**, screened for their anti-tumour activities against HeLa cells.

Table 5.5. Growth inhibition values of compounds **20-25** tested against HeLa cells.

dppp derivatives		dpph derivatives	
Drug	**IC_{50} (µM)**	**Drug**	**IC_{50} (µM)**
20	2.2 ± 0.5	**23**	0.4 ± 0.1
21	7.0 ± 0.5	**24**	0.1 ± 0.01
22	3.4 ± 0.3	**25**	3.7 ± 0.5
Cisplatin	0.5 ± 0.1		

IC_{50} is the concentration of drug required to inhibit cell growth by 50%.

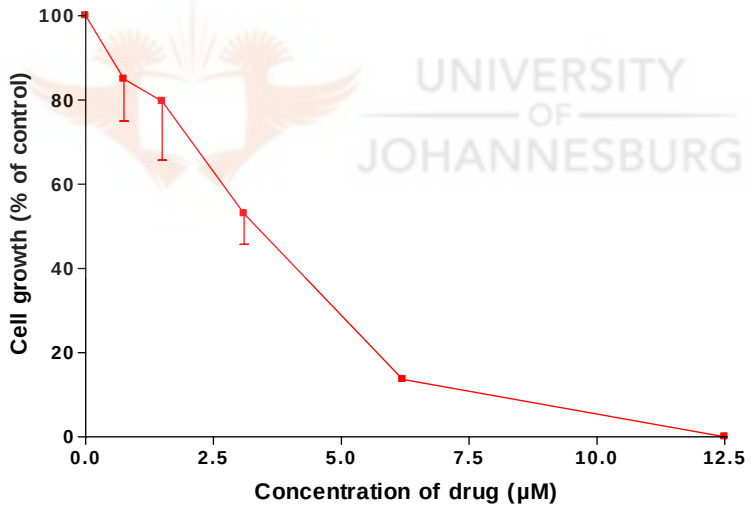

Figure 5.8. Growth inhibition profiles of HeLa cells by complex **20.**

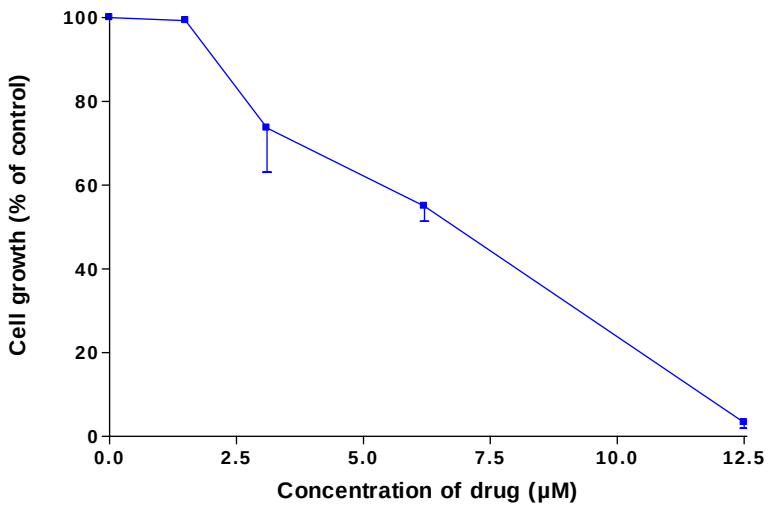

Figure 5.9. Growth inhibition profiles of HeLa cells by complex **21.**

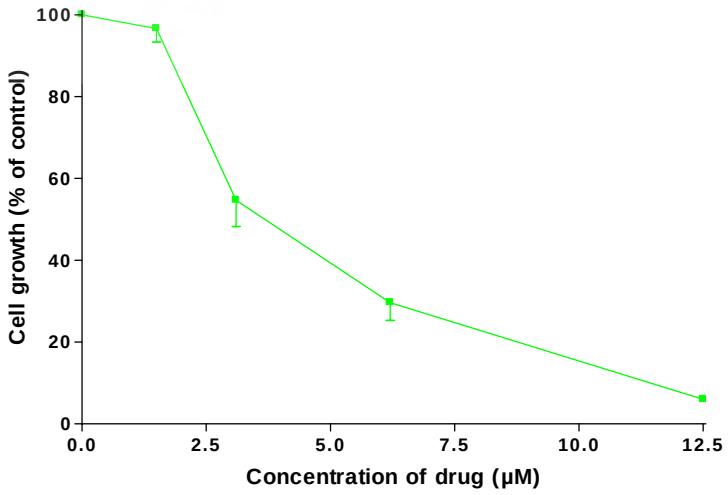

Figure 5.10. Growth inhibition profiles of HeLa cells by complex **22.**

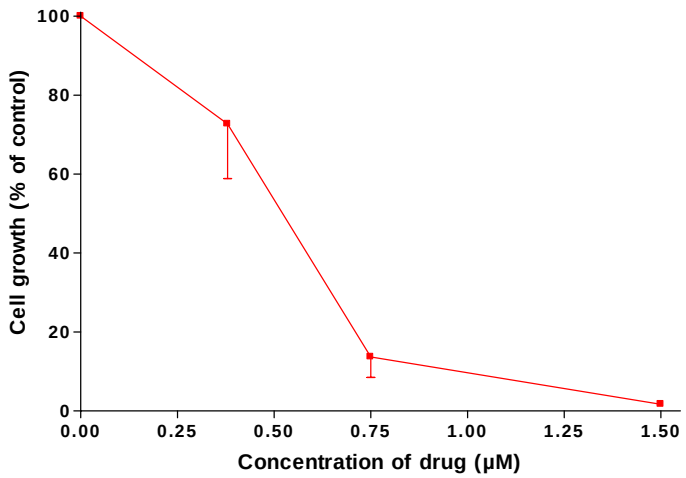

Figure 5.11. Growth inhibition profiles of HeLa cells by complex **23.**

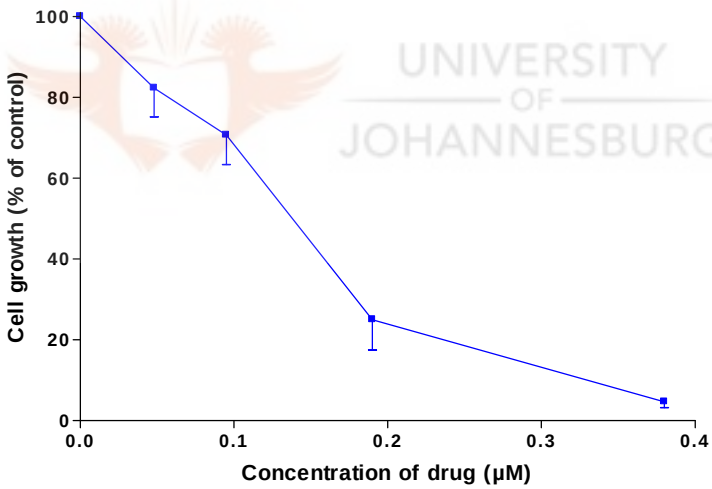

Figure 5.12. Growth inhibition profiles of HeLa cells by complex **24.**

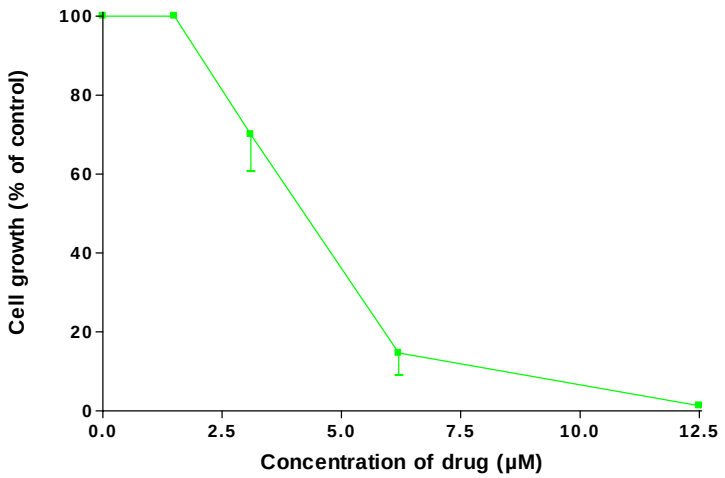

Figure 5.13. Growth inhibition profiles of HeLa cells by complex **25.**

It is evident that the dpph gold(I) compounds are more active than the dppp derivatives (Table 5.5). This observation is attributed to the difference in the diphosphine ligands, given the fact that the dithiocarbamate ligands of complexes **20**-**22** and **23**-**25** are the same (**L5**-**L7**) and were inactive. It is possible that the action of complexes **20**-**22** is through the formation of 6-membered bis-chelated compound, $[Au(dppp)_2]^+$, as the active species. This is informed by studies involving dppe gold(I) complexes, where the active species is $[Au(dppe)_2]^+$. Furthermore, bis(diphenylphosphino)propane gold(I) compounds have been shown to form stable $[Au(P\text{-}P)_2]^+$ species that exhibit antitumour activity.[36] As for complexes **23**-**25**, which feature bis(diphenylphosphino)hexane, the length of hexylene linker suggests that the 9-membered bis-chelated $[Au(dpph)_2]^+$ might be unattainable. Thus, the active metabolites for complexes **23**-**25** may not necessarily be similar to that of complexes **20**-**22** ($[Au(dppp)_2]^+$. However, further experiments are necessary to confirm the above postulations.

[36] [a]Berners-Price S. J., Sadler P. J., *Inorg. Chem.*, **1986**, *25*, 3822; [b]Berners-Price S. J., Johnson R. K., Giovenella A. J., Faucette L. F., Mirabelli C. K., Sadler P. J., *J. Inorg. Biochem.*, **1988**, *33*, 285.

The tumour specificity of complexes **20**-**25** was also investigated. From the results obtained, dppp derived complexes (**20**-**22**) not only killed HeLa cells but also killed normal cells at comparable concentrations. For example, compound **21** killed HeLa cells at 7 μM and resting lymphocytes at 6.1 μM. It is noteworthy that the same complex had an activity of IC_{50} = 2.9 μM against stimulated lymphocytes. There was no specific trend derived from these results apart from the fact that the IC_{50} values registered for compounds **20**-**22** against stimulated lymphocytes were generally lower compared to the respective IC_{50} values against resting lymphocytes (Table 5.6). Similar observations were made for complexes **23**-**25**. Notably, the registered IC_{50} values for **23**-**25** against stimulated lymphocytes are significantly lower than the registered IC_{50} values against resting lymphocytes (Table 5.6). For instance, the activity of **24** against stimulated lymphocytes (1.4 μM) is thirteen times higher than its activity against resting lymphocytes (18.2 μM). At the moment, there are no facts to explain this phenomenon.

Table 5.6. Tumour Specificity of complexes **20**-**25**.

Drug	HeLa IC_{50} (μM)	Lymph (resting) IC_{50} (μM)	Lymph (stimulated) IC_{50} (μM)	Tumour Specificity
		dppp derivatives		
20	2.2	7.1	5.0	2.8
21	7.0	6.1	2.9	0.6
22	3.4	18.5	8.2	3.8
		dpph derivatives		
23	0.4	18.9	6.7	31.0
24	0.1	18.2	1.4	70.5
25	3.7	37.7	30.3	9.2
Cisplatin	0.5			

IC_{50} is the concentration of drug required to inhibit cell growth by 50%.

Similar to **13-16**, it is possible that the stimulant used, PHA-P, could have had an influence in the activities observed. This is a mere postulation at the moment and mechanistic studies involving reaction of PHA-P and compounds **20-25** would be necessary to confirm or negate this argument.

Tumour specificity (TS) factors were also calculated for complexes **20-25** using equation 5.1 (cf. sec. 5.5.1). The results are presented in Table 5.6 above. In this batch of compounds, complexes **23** and **24** were found to be more specific in inhibiting the growth of tumour cells than in normal cells, with TS factors being 31.0 and 70.5, respectively. The significance of this result is that **23** and **24** are very specific to inhibiting HeLa cancer cells and not normal cells.

While the analogous dppe gold(I) complexes **17a-19** were synthesised, their biological activities were, however, not evaluated. This was because of the observed self-aggregation of the dinuclear complex **17a** in solution to form the cluster **17b** as reported in chapter 4.

*5.3.3. Platinum(II) complexes **31-33***

The dithiocarbamato platinum(II) complexes **31-33** (Scheme 5.4) were also investigated for their antitumour activities. Compounds **32** and **33** showed insignificant inhibition activities towards HeLa cells, whilst **31** was not tested because of its limited solubility. The IC_{50} values of **32** and **33** were greater than 50 μM.

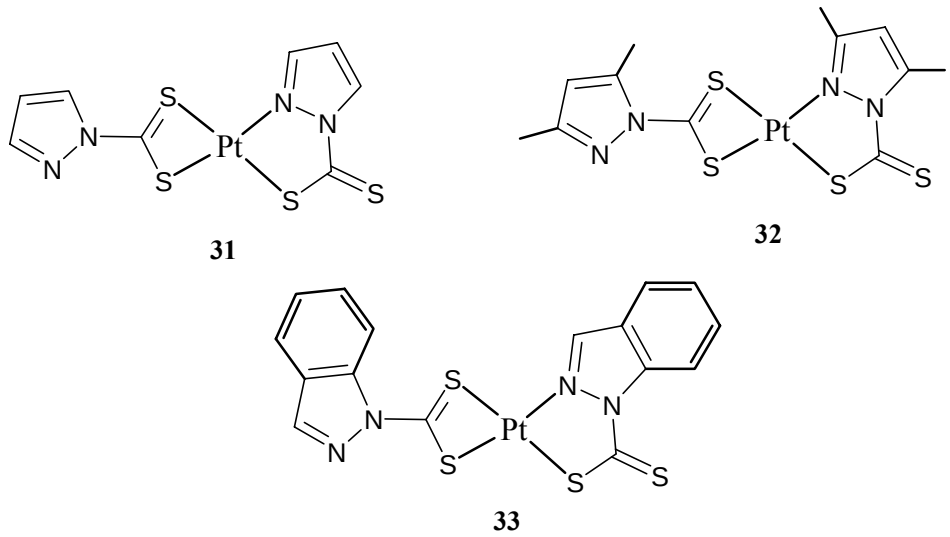

31 **32** **33**

Scheme 5.4. Platinum(II) dithiocarbamate complexes **31**-**33**.

5.4. Electronic absorption and photoluminescence results

5.4.1. Absorption spectra

The electronic absorption measurements were performed for four complexes (Scheme 5.5). The UV-Vis absorption spectra of dichloromethane solutions of the complexes were acquired at 298 K. For the mononuclear gold(I) complexes, [Au(**L7**)(PPh_3)] (**15**) was chosen as the representative sample. The absorption spectrum of **15** showed a broad band at 336 nm (ϵ = 12000 M^{-1} cm^{-1}), with a shoulder at 266 nm, and a sheer increase in absorbance below 250 nm; likely to be ligand based absorption (Fig. 5.14).

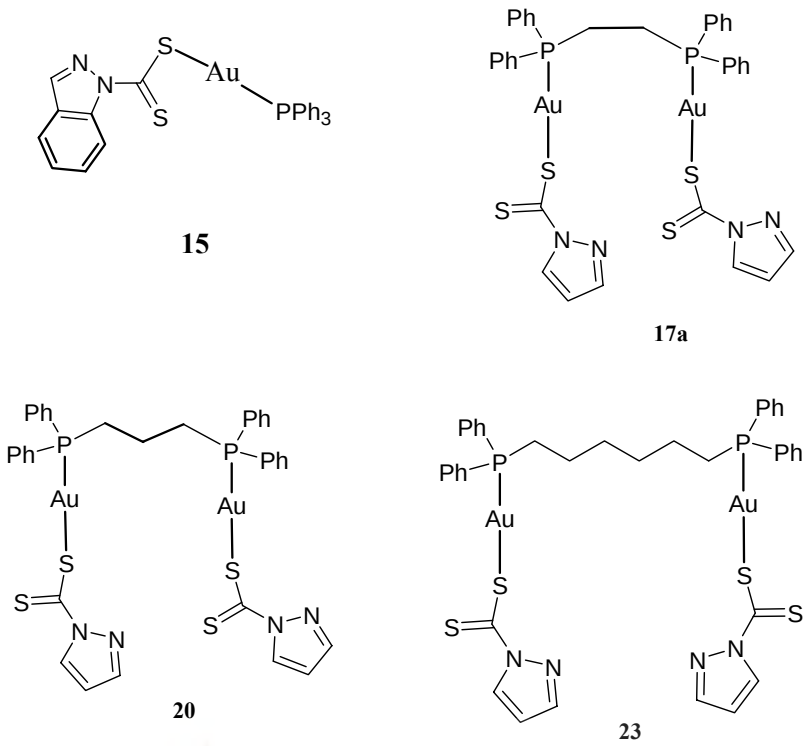

Scheme 5.5. Gold(I) complexes **15**, **17a**, **20** and **23**.

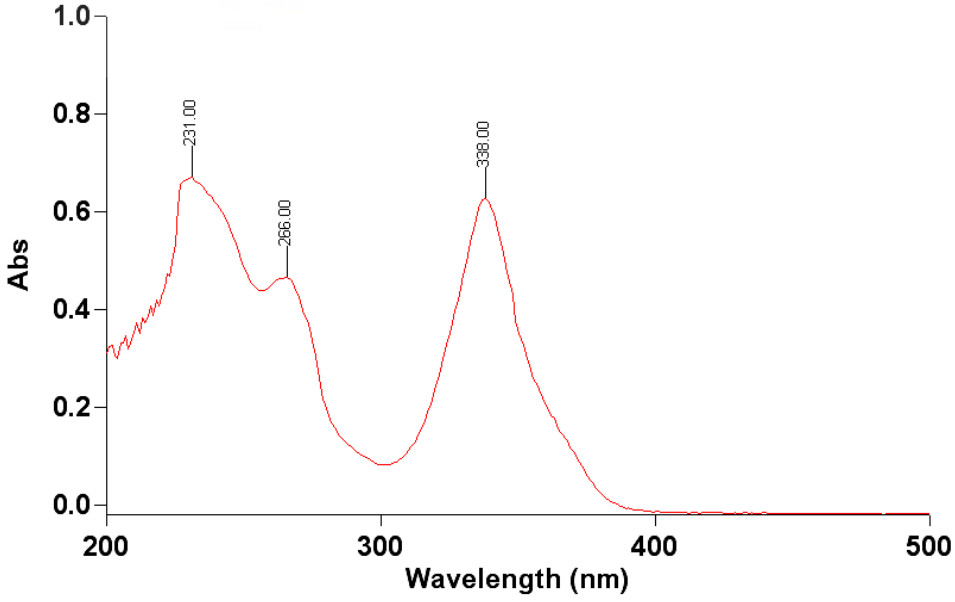

Figure 5.14. UV-Vis spectrum of **15** in CH_2Cl_2 at 298 K. Concentration = 5 x 10^{-5} M.

The intense low-energy absorption band observed for **15** at 336 nm was attributed to metal-to-ligand charge transfer (MLCT) transition from the mixed Au(d)/π**L7** HOMO and a dithiocarbamate (**L7**) based π* orbital.[37] The large molar extinction coefficient (12000 M^{-1} cm^{-1}) of **15** closely resembles those of related dithiolato gold(I) complexes, in agreement with charge-transfer transitions.[38]

Similarly, UV-Vis spectra of the analogous digold(I) complexes of **15**, i.e. [(Au**L5**)$_2$(dppe)] (**17a**), [(Au**L5**)$_2$(dppp)] (**20**) and [(Au**L5**)$_2$(dpph)] (**23**) (Scheme 5.5) were also acquired. The absorption spectra of dichloromethane solutions of **17a** (Fig. 5.15), **20** (Fig. 5.16) and **23** (Fig. 5.17) had the same profile, but slightly different from that of the mononuclear gold(I) **15** (Fig. 5.14). This difference is attributed to **15** being a gold(I) mononuclear complex, while **17a**, **20** and **23** are dinuclear gold(I) complexes (Scheme 5.5). As depicted in the respective Figures 5.15-5.17, complexes **17a**, **20** and **23** showed three absorption bands at *ca*. 229, 303 and 370 nm, respectively. The intense bands at *ca*. 229 nm are due to the phenyl rings of the phosphine ligands, which exhibit π-π* intraligand transitions. The broad low energy bands at *ca*. 303 and 370 nm were attributed to MLCT charge transfer transition from the gold ion to the dithiocarbamate ligand (**L5**), as observed for **15**.

[37] Cummings S. D., Eisenberg R., *Inorg. Chim. Acta*, **1996**, *242*, 225.
[38] Vicente J., Gonzalez-Herrero P., Perez-Cadenas M., *Inorg. Chem.*, **2007**, *45*, 4718.

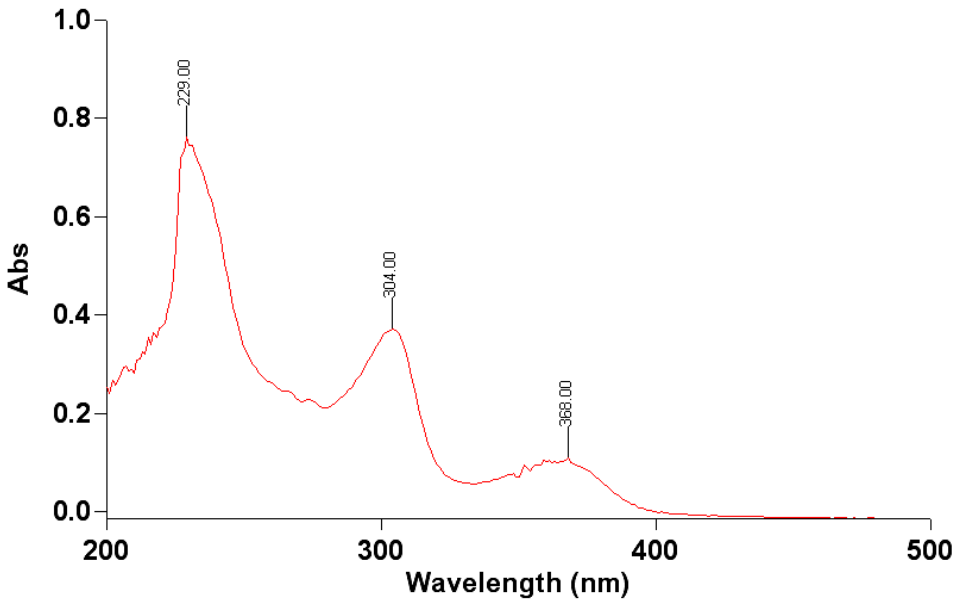

Figure 5.15. UV-Vis spectrum of **17a** in CH_2Cl_2 at 298 K. [**17a**] = 5 x 10^{-5} M.

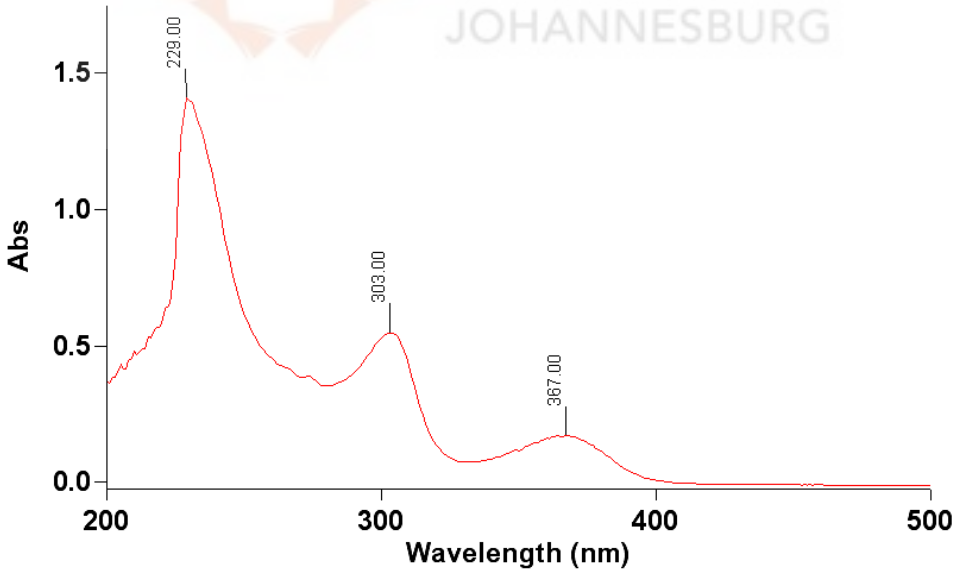

Figure 5.16. UV-Vis spectrum of **20** in CH_2Cl_2 at 298 K. [**20**] = 5 x 10^{-5} M.

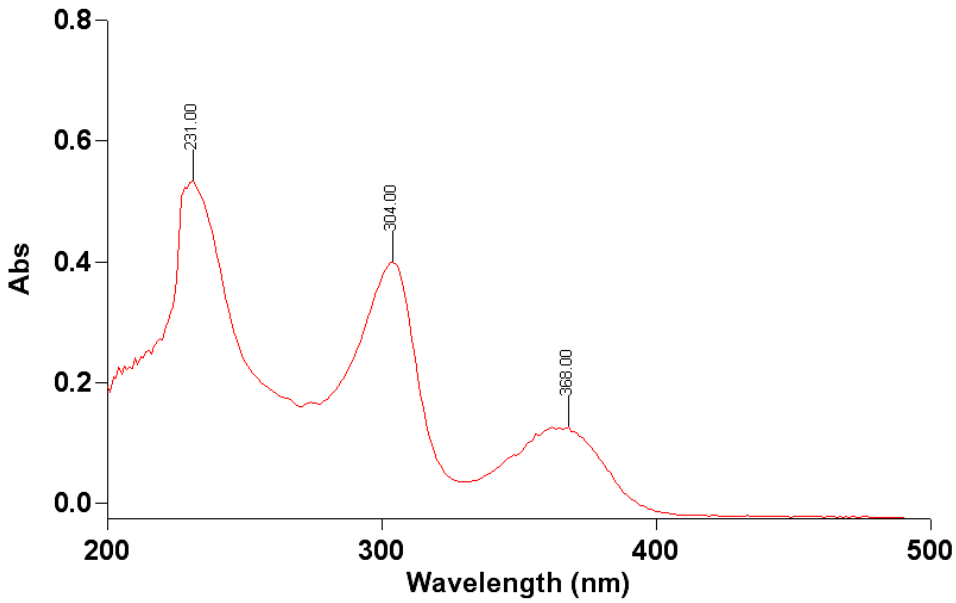

Figure 5.17. UV-Vis spectrum of **23** in CH_2Cl_2 at 298 K. [**23**] = 5 x 10^{-5} M.

5.4.2. Photoluminescence spectra

The ability of the gold(I) complexes reported in this study to luminesce was also investigated. Complexes **13**, **14**, **15**, **16**, **17a** and **17b** (Scheme 5.6) were the representative complexes tested for photoluminescence. It is worth mentioning that **17b** is the gold cluster, $[Au_{18}S_8(dppe)_6]^{2+}$, obtained from crystallisation of **17a** (see chapter 4).

The excitation of solid materials and solutions of **13**, **14**, **15**, **17a** and **17b** at room temperature resulted in weak yellow emission, whereas that of **16** showed a light blue emission. The excitation of solutions of **13**, **14**, **16**, **17a** and **17b** were enhanced by lowering the temperature to 77 K. The UV-Vis irradiation of mononuclear gold(I) complexes **13**, **14** and **16** at 250-800 nm and complexes **17a** and **17b** at 250-500 nm, gave weak visible luminescence. Complexes **13**, **14** and **16** showed broad band

photoluminescence with λ_{maxes} of ~500 and 650 nm in the frozen solution at 77 K, whereas **17a** and **17b** exhibited broad double-band photoluminescence, but with a λ_{max} of ~520 nm at the same conditions. The spectra of photoluminescence of **13**, **14**, **16**, **17a** and **17b** are shown in Figures 5.19, 5.20, 5.21, 5.22 and 5.23, respectively (*vide infra*). The results of the measurements are summarised in Table 5.7. The microsecond decay components suggest formally a triplet character of the luminescent excited electronic state(s) of **17a** and **17b** (Fig. 5.18), and indicates phosphorescence as opposed to fluorescence. Neither solids nor the solution of **15** at 77 K showed luminescence.

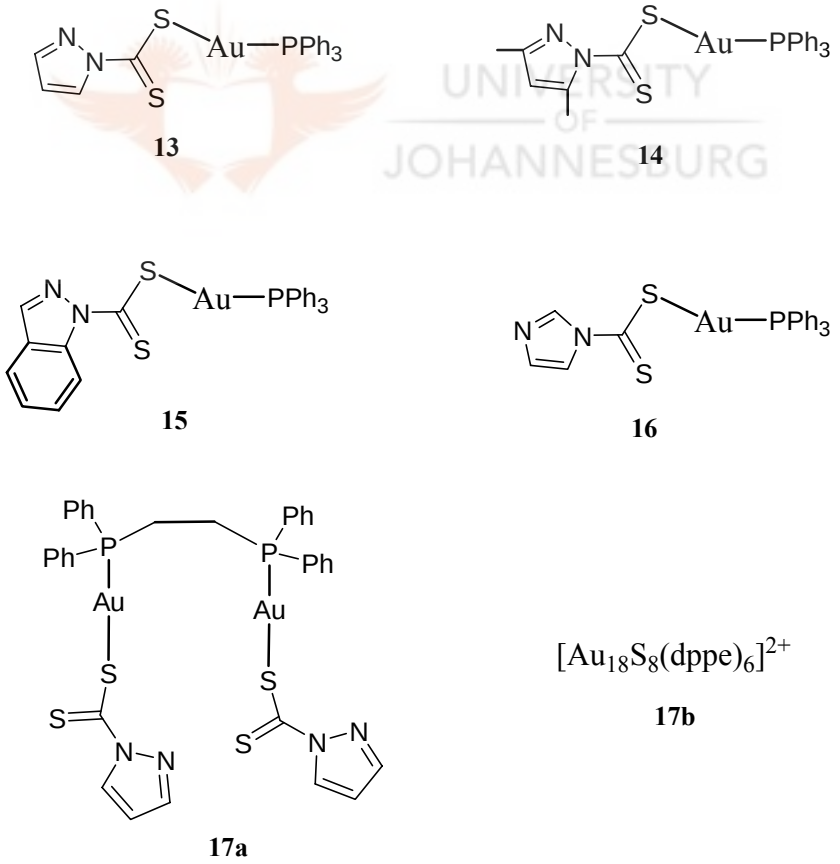

Scheme 5.6. Gold(I) complexes **13**, **14**, **15**, **16**, **17a** and gold(I) cluster **17b**.

Table 5.7. Excitation and emission data for **13**, **14**, **15**, **16**, **17a** and **17b**.

Complexes	Solid colour (298 K)	Solution Colour (298 K)	λ_{exc} (nm)	λ_{em} (nm)	Luminescence/ Colour (298 K)	Luminescence/ Colour (77 K)	τ (µs)
13	Yellow	Light Yellow	485	400	-	Light orange	-
			650	320			
14	Yellow	Yellow	650	375	-	Orange	-
15	Orange	Orange	-	-	-	No	-
16	Yellow	Light Yellow	480	320	Light blue	Intense orange	-
			650	-			
17a	Yellow	Yellow	470	520	-	Yellow/Green	117.6
17b	Yellow	Yellow	471	522	-	Yellow/Green	127.6

The features of the photoluminescence of gold(I) complexes **13**, **14**, **16**, **17a** and **17b** (Fig.5.19-5.23) are similar in all respects despite their different chemical compositions. The similarity of the emissions of these compounds suggests an emitting state of common origin. Literature reports indicate that the absorption and emission bands of neutral phosphine gold(I) thiolate complexes originate from sulfur-to-gold(I) charge transfer (S→Au CT).[39,40,41] From these reports, the origin of emissions at ~650 nm for complexes **13**, **14** and **16** and ~ 525 nm for both **17a** and **17b** were attributed to LMCT in character (S→Au CT), with contributions from metal centred states (Figs. 5.2 and 5.19). The shoulders observed in the emission spectra of **13**, **14**, **16, 17a** and **17b** were postulated to be as a result of intraligand transition from π-orbitals associated with the diphosphine ligands.[16,42]

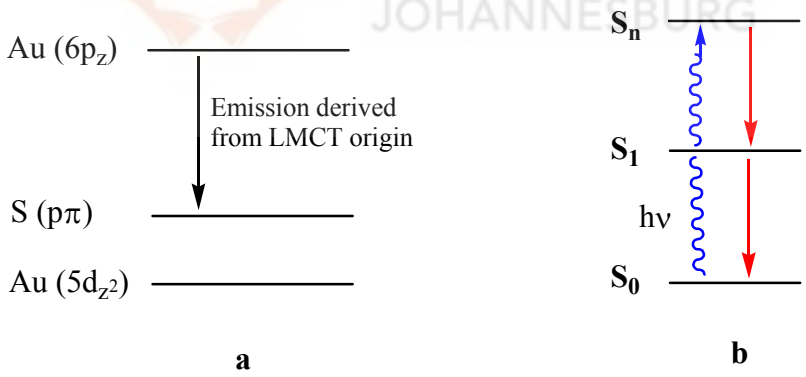

Figure 5.18. Schematic representations of (**a**) orbital splitting and (**b**) energy diagram of **17a** and **17b**. Photoexcitation into higher excited singlet-like electronic states S_n is followed by rapid relaxation to S_1.

[39] Yam V. W., Cheng E. C., Cheung K. K., *Angew. Chem. Int. Ed.*, **1999**, *38*, 197.
[40] Yam V. W., Cheng E. C., Zhu N., *Angew. Chem. Int. Ed.*, **2001**, *40*, 1763.
[41] Pintado-Alba A., De la Riva H., Nieuwhuyzen M., Bautista D., Raithby P. R., Sparkes H. A., Teat S. J., Lopez-de-Luzuriaga J. M., Lagunas M. C., *J. Chem. Soc., Dalton Trans.*, **2004**, 3459.
[42] Foley J. B., Bruce A. E., Bruce M. R. M., *J. Am. Chem. Soc.*, **1995**, *117*, 9595.

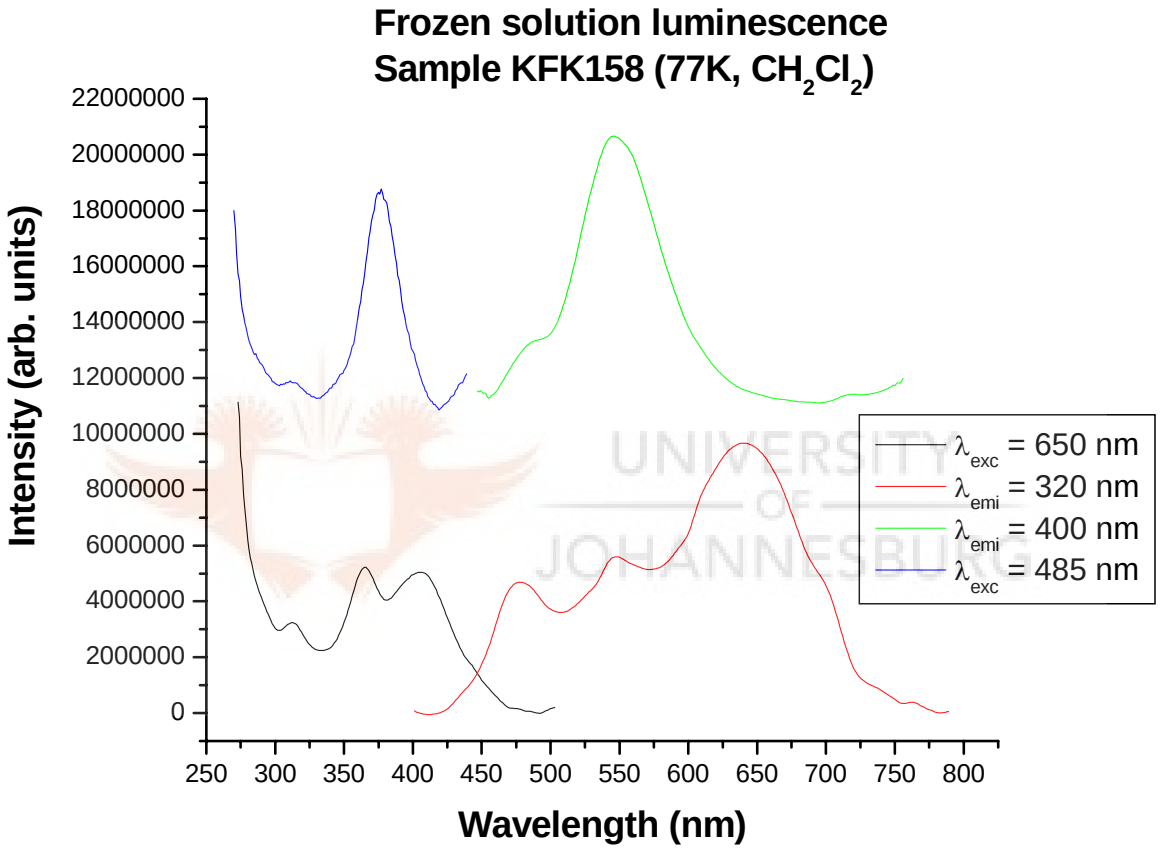

Figure 5.19. Excitation and emission spectra of a frozen solution of **13** in dichloromethane at 77 K.

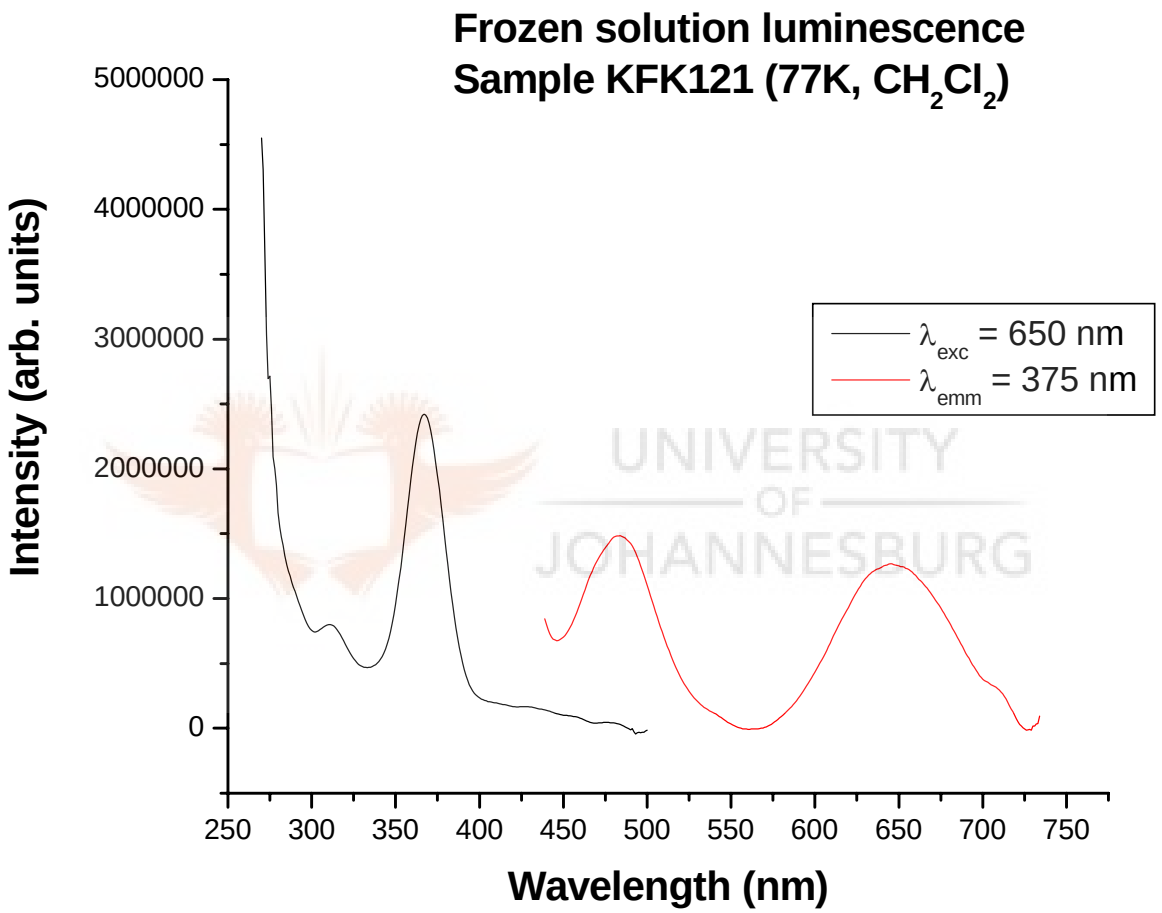

Figure 5.20. Excitation and emission spectra of a frozen solution of **14** in dichloromethane at 77 K.

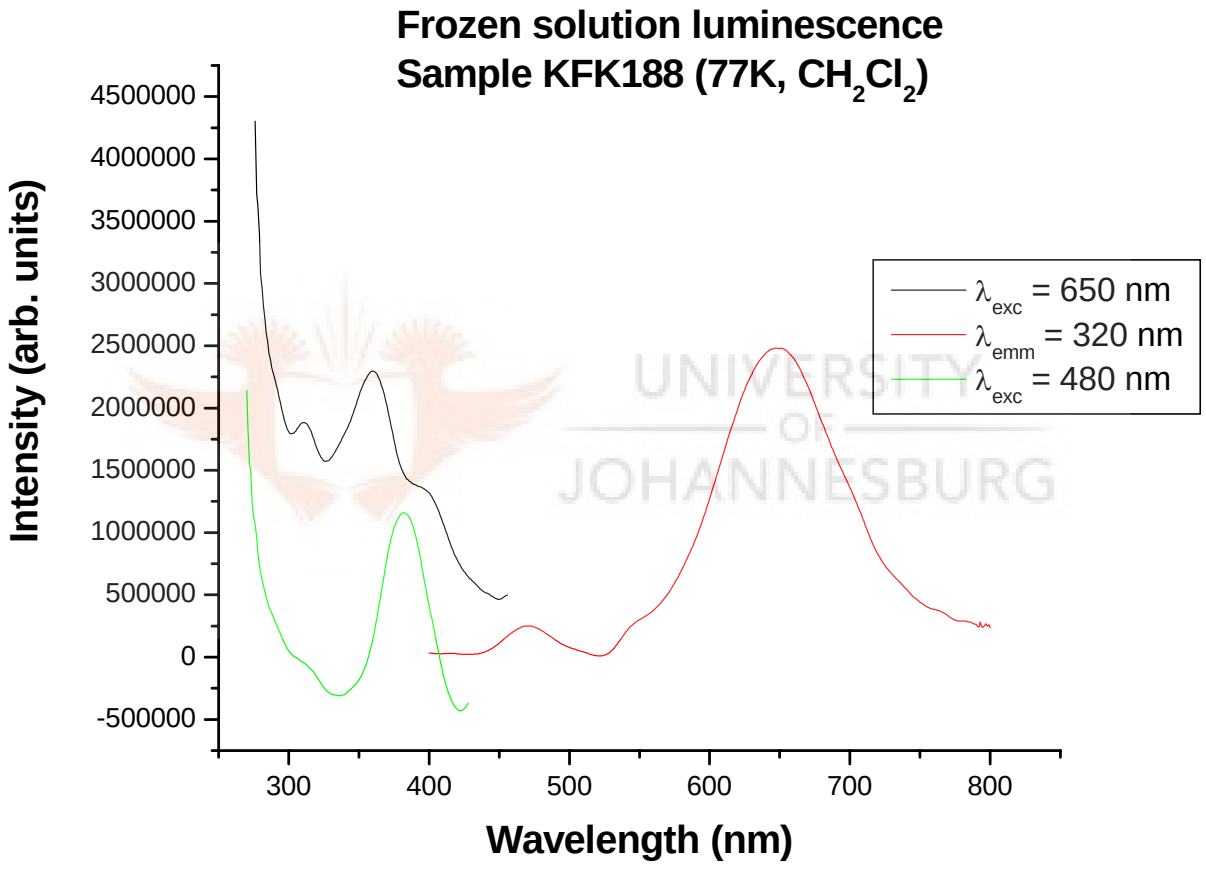

Figure 5.21. Excitation and emission spectra of a frozen solution of **16** in dichloromethane at 77 K.

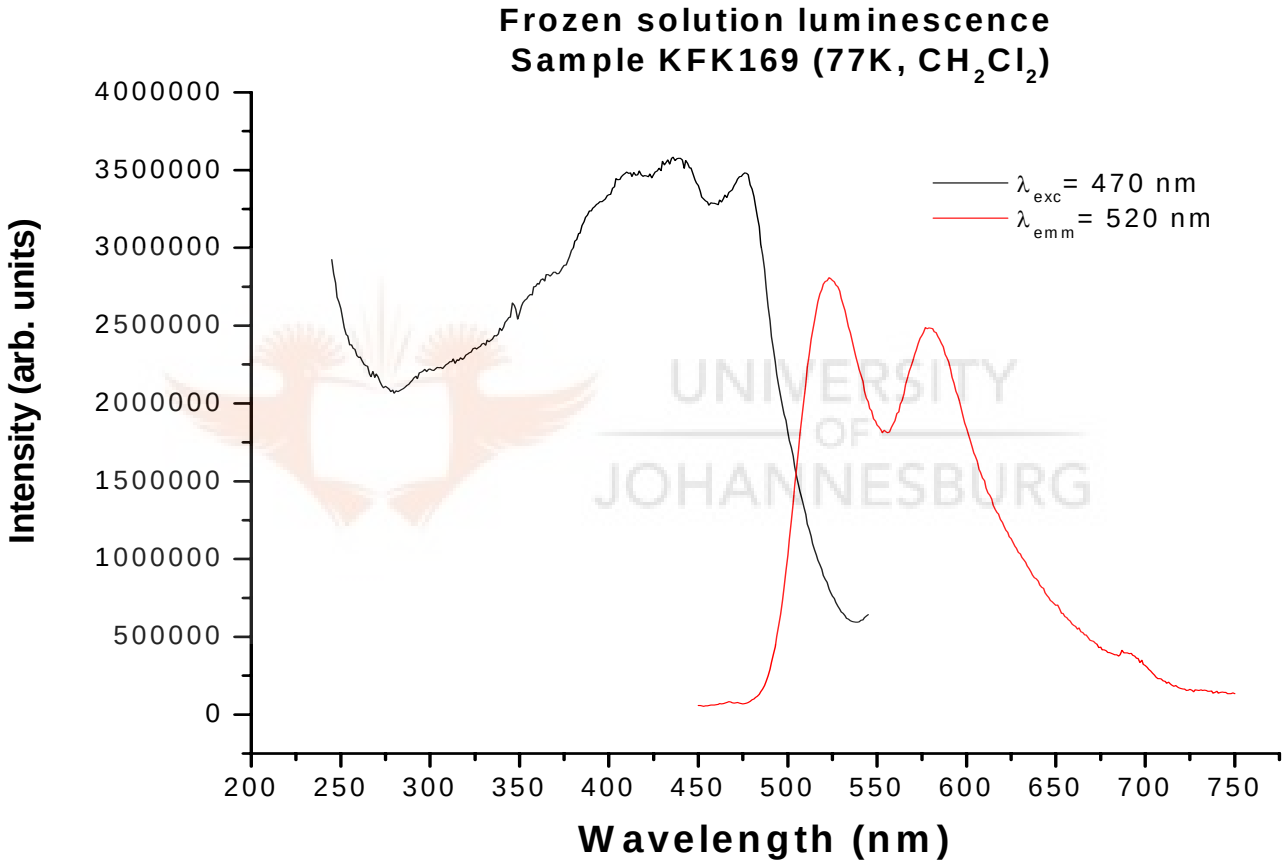

Figure 5.22. Excitation and emission spectra of a frozen solution of **17a** in dichloromethane at 77 K.

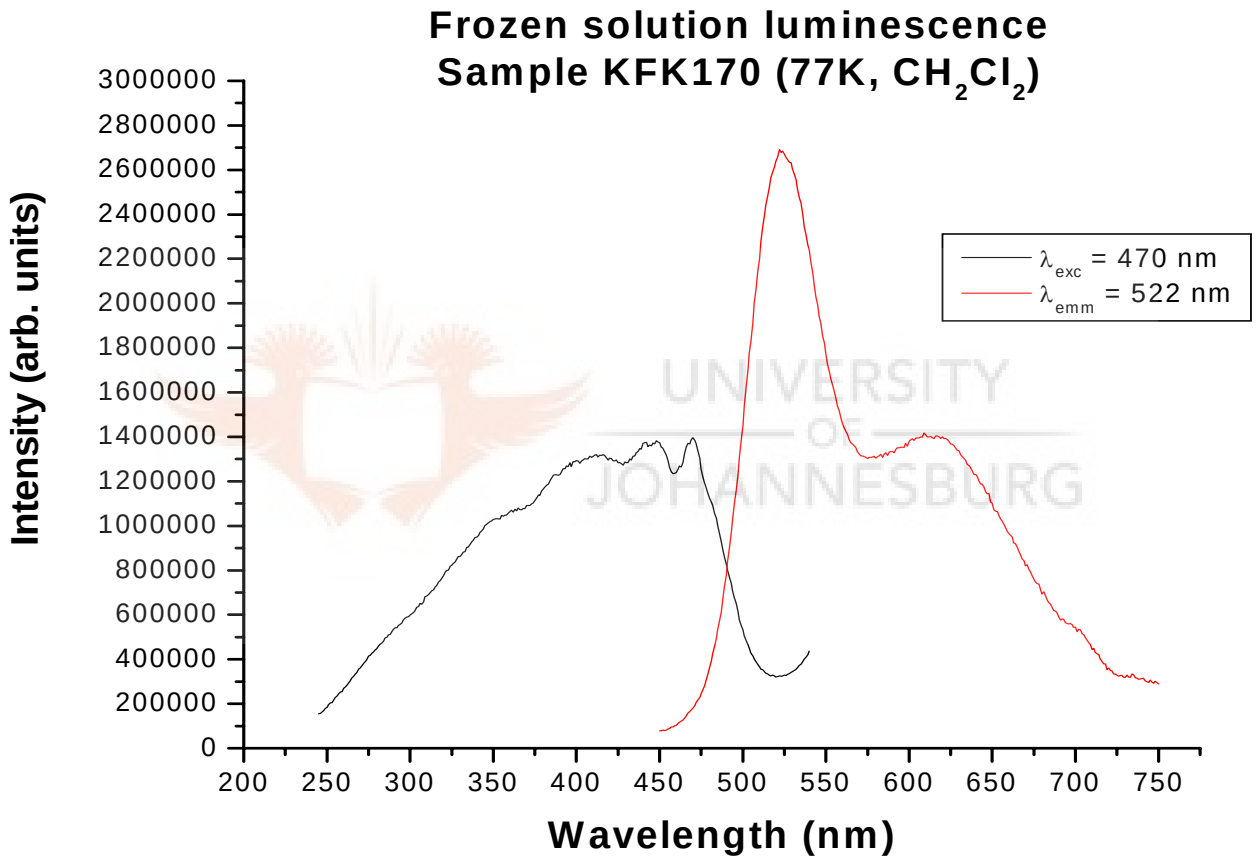

Figure 5.23. Excitation and emission spectra of a frozen solution of **17b** in dichloromethane at 77 K.

5.5. Conclusions

The biological screening of ligands **L5-L11**, gold(I) complexes **13-16, 20-25** and platinum(II) complexes **31-33** for their *in vitro* anticancer activity were performed on HeLa cells. Compounds **31-33** were inactive. Whereas ligands **L5-L8** and **L11** showed no inhibition against HeLa cells, **L9** and **L10** showed activity, with **L9** being the most active (IC_{50} = 3.7 ± 0.2 μM, TS = 9.6). It is seems that **L9** exert it activity in the same way as disulfram, by reducing *in vivo* to pyrazolyldithiocabarmic acid species, which would react with several enzymes and cause apoptosis. But judging from the various mechanisms of action reported for disulfram, various mechanistic studies involving **L9** are needed to confirm its exact mechanism of action.

The obtained biological data of the gold(I) complexes indicated their appreciable activities against HeLa cells. Mononuclear gold(I) complexes **13-16** had good antitumour activities. It was worth mentioning that the activities for **13**, **14** and **15** were the same (IC_{50} ≈ 2.6 μM). This suggests that the ligands used (**L5-L7**) are readily substituted in solution by other biological thiols and thus their bulkiness do not necessarily contribute in regulating the metabolic rates for conversion of these complexes to active species. Similarly, the dinuclear gold(I) complexes **20-25** showed appreciable growth inhibitions against HeLa cells. The dpph based gold compounds **23-25** were the most active, with **24** showing the highest activity against HeLa cells (IC_{50} = 0.1 ± 0.01 μM). The difference in activities of complexes **20-22** and **23-25** was attributed to the nature of diphosphine ligands. While it is necessary to perform further experiments to establish the active metabolites of **20-25**, it is possible to postulate what the active metabolites could be

based on literature reports (in chapter 4); that the dppp-based complexes **20**-**22** would easily form the possible 6-membered bis-chelated active species, $[Au(dppp)_2]^+$; but the formation of a 9-membered bis-chelated $[Au(dpph)_2]^+$ species from dpph-based compounds **23**-**25**, is highly unlikely. Thus, it appears that the above structural postulation could be the basis for the difference in the anticancer activities of **20**-**22** and **23**-**25**.

By testing the potency of gold(I) complexes **13**-**16**, **20**-**22** and **23**-**25** on normal cells (resting and stimulated lymphocytes), the tumour specificity values (TS) were obtained. Complexes **23** and **24** had the highest TS factors, 31.0 and 70.5, respectively. This means these two complexes were more specific in inhibiting the growth of tumour cells and not normal cells.

Two fundamental observations were made from experiments involving normal cells (resting and stimulated lymphocytes) namely; (i) the growth rate of cells did not hamper the antitumour activities of these complexes. This is evident from the registered activities of these gold(I) complexes against stimulated and resting lymphocytes, where there was a general susceptibility of stimulated lymphocytes to the test compounds compared to un-stimulated (resting) lymphocytes. This negated the anticipation that stimulated lymphocytes should have been less susceptible to the gold(I) compounds. (ii) It is possible that the PHA-P, used to stimulate the growth of normal cells, had an influence on the observed activities of the gold(I) complexes. It is proposed that PHA-P may have

made the cells more susceptible to the compounds. Further studies are needed to probe this possibility and forms part of the future work.

Electronic absorption measurements were performed in four gold(I) complexes **15**, **17a**, **20** and **23**. The intense lowest-energy absorption band observed for these complexes at *ca*. 304, 338 and 368 nm were attributed to the metal-to-ligand charge transfer (MLCT) transition. The intense bands at *ca*. 229 nm are due to the phenyl rings of the phosphine ligands, which feature π intraligand interactions. The broad low energy bands at *ca*. 303 and 370 nm are attributed to charge transfer transition from gold to the dithiocarbamate ligand (**L5**). The excitation of solid materials and solutions of **13**, **14**, **15**, **17a** and **17b** at room temperature resulted in weak yellow emission, whereas that of **16** showed a light blue emission. Generally, the visible luminescence of complexes **13**, **14**, **16**, **17a** and **17b** were weak characterised by broad bands photoluminescence. The double-band photoluminescence for **17a** and **17b** suggests that the LMCT emissions observed is influenced by gold-gold interactions (aurophilicity). Overall, the emissions of the complexes are proposed to originate from a MLCT triplet state, indicating phosphorescence.

APPENDIX

Manuscript 1

Bis(pyrazolyl) Palladium(II), Platinum(II) and Gold(III) Complexes: Syntheses, Molecular Structures and Substitution Reactions with L-cysteine.

Frankline K. Keter[a], Stephen O. Ojwach[a], Olayinka A. Oyetunji[b], Ilia A. Guzei[c] James Darkwa[a]

[a]Department of Chemistry, University of Johannesburg, P.O. Box 524 Auckland Park 2006, South Africa

[b]Department of Chemistry, University of Botswana, Private Bag UB 00704, Gaborone, Botswana

[c]Department of Chemistry, University of Wisconsin-Madison, 1101 University Avenue, Madison, WI 53706, USA.

(*Submitted to Inorganica Chimica Acta*)

Abstract

The reactivity of L-cysteine with pyrazolyl gold(III), platinum(II) and palladium(II) complexes, $[AuCl_2(3,5\text{-}R_2bpza)]Cl$ {R = H (**1**)}, $[PtCl_2(3,5\text{-}R_2bpza)]$ {R = H (**2**)}, $[PdCl_2(3,5\text{-}R_2bpza)]$ {R = H (**3**), R = Me (**4**)} (bpza = bis-pyrazolyl acetic acid), was investigated at 20 – 40 ^oC in an aqueous medium with an ionic strength of 0.1 M, between pH 2.92 and 3.72, using conventional UV-Vis and stopped-flow spectrophotometry. The reactions were performed with the pre-activated species, $[Au(OH_2)_2(3,5\text{-}R_2bpza)]Cl$ {R = H (**5**)}, $[Pt(OH_2)_2(3,5\text{-}R_2bpza)]$ {R = H (**6**)} and $[Pd(OH_2)_2(3,5\text{-}R_2bpza)]$ {R = H (**7**), R = Me (**8**)} and L-cysteine. These substitution reactions followed the second-order rate law $d[M^{n+}]/dt = k[Cys][M^{n+}]$ (n = 2, 3), where k is a pH-independent rate constant. The entropies of activation obtained are largely negative (-52.7 and -174 J $mol^{-1}K^{-1}$), except for **8**, which is +18.4 kJ mol^{-1}. Further reduction of the gold(III) complex (**1**) to gold(I) species was observed with an entropy change of -183 J $mol^{-1}K^{-1}$. The substitution reactions take place in two steps, involving two incoming cysteine molecules in a sequential manner, with a rapid process second step. The reactivity of complexes **5** – **8** towards L-cysteine, under pseudo-first-order conditions, showed that reactions of L-cysteine with **7** and **8** are 10^3 and 10^6 times faster than those of **5** and **6** respectively. Mass spectrometry was used to confirm reaction product of **8** with L-cysteine and found to be $[Pd(Cys)_2(3,5\text{-}Me_2bpza)]$.

Key words: Kinetics and mechanism; Substitution; L-cysteine; Palladium; Platinum; Gold; Complexes.

Manuscript 2

Dichloro-bis(3,5-dimethylpyrazolyl)Palladium(II) complex. A DMSO-*d6* solvated complex

Frankline K. Keter, Bernard O. Omondi, James Darkwa

[a]Department of Chemistry, University of Johannesburg, P.O. Box 524 Auckland Park 2006, South Africa

(*Submitted to Journal of Molecular Structures*)